DEVELOPMENT OF AN IMPROVED DESIGN PROCEDURE FOR UNBONDED CONCRETE OVERLAYS

TPF-5(269)

Task 2 Report
Interlayer Characterization, Field Performance Assessment,
and Guidelines on Drainage

Prepared by:

Julie Vandenbossche
Steven Sachs
Kevin Alland

Department of Civil and Environmental Engineering
University of Pittsburgh

Mark Snyder

Project Consultant

Lev Khazanovich
Derek Tompkins
Kyle Hoegh
Abbas Booshehrian

Department of Civil, Environmental, and Geo-Engineering
University of Minnesota

October 2015

CONTENTS

1. PERFORM LABORATORY STUDY

The primary focus of Task 2 was a laboratory investigation of the effects of the interlayer on the response of the pavement structure under load. Beam specimens were tested to evaluate three different mechanisms. Both hot mix asphalt and nonwoven geotextile fabric interlayer systems were considered. The objective of Task 2 was to establish parameters for these interlayers that can be used to develop structural models, which in turn can be used to develop a mechanistic-empirical design procedure for unbonded concrete overlays. The laboratory work considers four physical mechanisms at the interlayer:

1. Deflection characteristics of the interlayer
2. Friction developed along the interface between the interlayer and the overlay
3. Ability of the interlayer to prevent reflective cracking
4. Bond strength at the interfaces of the interlayer

Details on modifications to the general setups, methodology, and test results to characterize each of the four behaviors are contained in each of their corresponding sections below (Sections 1.2 through 1.5). The data from the tests described below will later be analyzed and applied in the work of Task 3. To begin, details on the materials used in the laboratory study are included in Section 1.1.

1.1. Remarks on PCC materials and interlayer fabrics

The following subsections describe the materials used in the laboratory study described in the following sections. Note that any mention of named products in this report is not an endorsement of that product.

1.1.1. Interlayers

The nonwoven geotextile fabrics used for this study were manufactured by Propex and consisted of a thick and a thin fabric. The thick fabric weighed 15 oz/yd^2 and was dark in color. The thinner white colored fabric, called Reflectex, was made specifically for this study and weighed 10 oz/yd.^{2} In this report, the fabrics will be called F15 and F10 for the thick and the thin fabrics, respectively. These fabrics can be seen in Figure 1. For this study, the fabrics are attached to the existing concrete beams according to two methods:

- Pins: Fabric interlayers were pinned to the existing concrete using a gas powered gun to attach 2 fasteners to each beam approximately 6 inches from the edge. This approximates methods used in the field.
- Glue: Fabric interlayers were glued to the existing concrete using a geotextile glue made by 3M called Scotch-Weld HoldFast 70 Adhesive.

Figure 1. F15 on the Left and F10 on the Right

The specimens with asphalt interlayers were sawed from in service pavements to ensure that mixture proportioning and density of the asphalt interlayers are typical of those found in the field. These asphalt-concrete composite beams were obtained from the Minnesota and Michigan Departments of Transportation (MNDOT and MIDOT, respectively).

- MIDOT provided beams with dense graded asphalt interlayers as well as beams with open graded asphalt mix interlayers. The dense graded asphalt interlayer is approximately 1 inch thick and the open graded interlayer is approximately 2 inches thick.
- MNDOT provided specimens from a concrete pavement that had previously been overlaid with asphalt. Some of the beams were cut prior to milling the dense graded asphalt overlay and the others were cut after some of the asphalt had been milled. MNDOT also provided beams cut immediately after an open graded asphalt was placed on a distressed existing pavement.

A summary of asphalt specimen sources, ages, and average asphalt thicknesses is provided in Table 1. For each of the beam specimens, sand patch testing (ASTM E965) was performed and dimensions were measured. This information is summarized in Appendix A.

Table 1. Sources of Asphalt Samples Collected

Roadway	Asphalt Description	Ave. Asphalt Thickness
US-131, MI	Old, dense graded	1 in
US-131, MI	Old, open-graded	2 in
I-94, MnROAD	Old, dense graded, milled	0.875 in
I-94, MnROAD	Old, dense graded, unmilled	2.75 in
US-169, MN	New, open graded (PASSRC)	1.75 in

1.1.2. Specimen Designation

All specimens consisted of a bottom beam representing the existing concrete being overlaid, an interlayer, and a concrete beam on the top of the interlayer representing the overlay. The specimens with the fabric interlayers were made by first casting the bottom beam using a high strength mix representative of concrete properties for a 30-year old paving mix. Next, the fabric

interlayer was either glued or pinned to the top surface of the bottom beam. Finally, a beam was cast on top of the fabric using a PCC paving mix specified in Section 1.1.3. For the specimens with the asphalt interlayer, the top beam was cast using the same PCC paving mix used for casting the top beam of the fabric layer specimens.

Each finished specimen had its own code identifying when each layer was cast (if it was not obtained in the field) and a description of the interlayer. The nomenclature is shown in Figure 2. From left to right, the first four numbers represent the month and date of cast, the middle letters and numbers are the interlayer designation, and the last letter indicates the batch number for the day of casting. The labeling designating each asphalt interlayer is defined as follows:

- MIDAU: unmilled, aged dense graded asphalt from Michigan
- MIOAU: unmilled, aged open graded asphalt from Michigan
- MNDAU: unmilled, aged dense graded asphalt from Minnesota
- MNDAM: milled, aged dense graded asphalt from Minnesota
- MNONU: unmilled, new open graded asphalt from Minnesota

For the fabric interlayer specimens, the letter following the fabric designation indicated whether the concrete layer represented an existing pavement or an overlay, as both had to be cast for each fabric specimen.

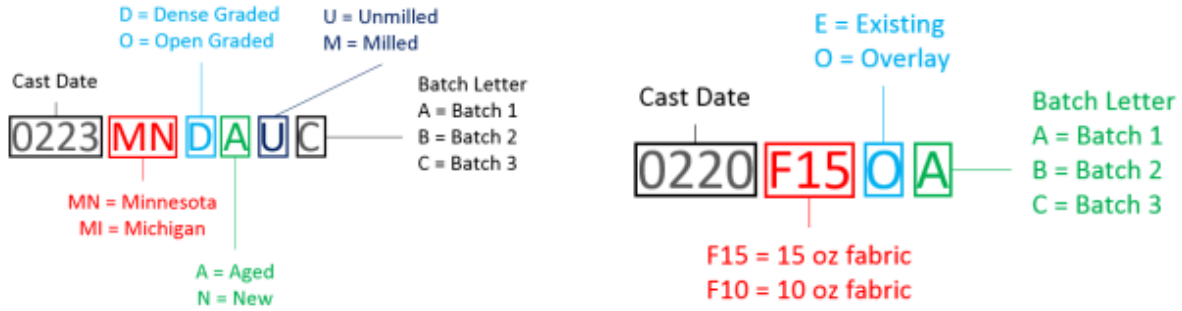

Figure 2. Asphalt Specimen Designation (Left) and Fabric Specimen Designation (Right)

1.1.3. PCC Mix Design

The concrete mixture design for the lower beam of the specimens with the fabric interlayer has a water to cementitious material ratio (w/cm) of 0.36 and a target flexural strength of approximately 850 psi. The overlay (top beam) mixture design for all specimens has a w/cm of 0.42 and a target flexural strength of 650 psi. The bottom beam flexural strength is higher than the overlay flexural strength to simulate aged concrete being overlaid with a traditional overlay mix. Table 2 summarizes the final mixture design information for the two mixes. All material test data (including compressive strengths, elastic modulus, and modulus of rupture) are summarized in Appendix A. All specimens were made and cured according to ASTM C192.

Finally, an important note to the mix designs is that, due to a calibration error in the air meter used during the first four cast days, the overlay mix had a high air content and therefore reduced strengths. Once this error was noted and the air meter was recalibrated, the volume of air entraining admixture was adjusted and the desired strengths were achieved. All overlay beams tested at 28 days and cast between 2/20/15 and 3/3/15 had a high air content. All

specimens tested for reflective cracking with the high air mixture were replicated using the corrected mix.

Table 2. Target Mixture Design

Mixture Design for Casting Beams Representative of the Existing Slab			
Material	Weight (lb/cy)	Volume (cft/cy)	Volume fraction
Coarse aggregate, Limestone	1918	11.34	0.42
Fine aggregate	1163	6.98	0.26
Cement, Cemex Type I	650	3.31	0.12
Water	234	3.75	0.14
Air content	-	1.62	0.06
Superplasticizer, Sikament SPMN	17 oz per 100 lbs of cement		
Air entrainer, Sika AIR-360	3 oz per 100 lbs of cement		
Mixture Design for Casting Beams Representative of the Overlay			
Material	Weight (lb/cy)	Volume (cft/cy)	Volume fraction
Coarse aggregate Limestone	2053	12.15	0.45
Fine aggregate	1023	6.14	0.23
Cement, Cemex Type I	600	3.05	0.11
Water	252	4.04	0.15
Air content	-	1.62	0.06
Air entrainer, Sika AIR-360	2 oz per 100 lbs of cement		

1.2. Deflection characterization

The deflection characteristics of the interlayer were established using the setup shown in Figure 3.

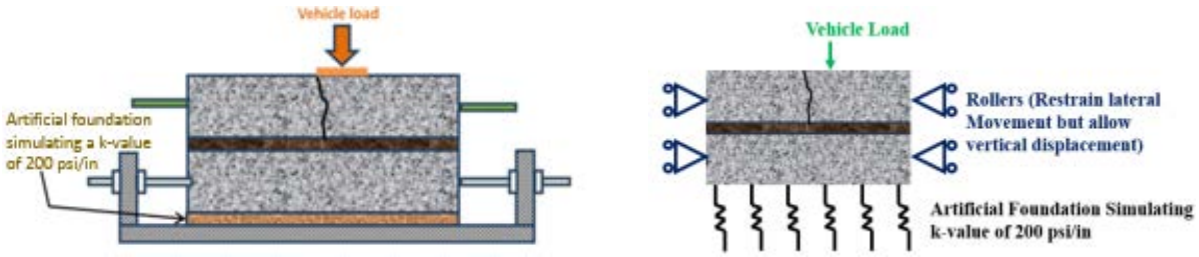

Figure 3. At left, .a schematic of Deflection Characteristic Test Setup; at right, the boundary Conditions of Test Setup

The composite section consists of a beam representing the existing slab (in strength and stiffness), the interlayer system, and a beam representing the overlay (in strength and stiffness). A load is applied to one side of a joint sawed in the overlay and deflections in the overlay and existing beams are measured by linear variable displacement transducers (LVDTs). A brief discussion of the finite element modeling performed to insure the beam test is representative of the response (deflection and rotation) of the pavement structure is provided. This is followed by a discussion of the hardware used in the setup, the loading regime, and the material properties for the beams tested.

1.2.1. Initial test planning

Finite element analysis software was used to establish and confirm an appropriate setup and boundary conditions for the specimens. The goal of the finite element modeling was to establish

the specimen length, boundary conditions, and load magnitude and location required to create deflections and rotations representative of those in an overlay loaded by a 9,000 lb design load.

In the computational model, all components were assumed to be elastic solids, no load transfer was provided across the joint, and the three contact conditions between the layers were assumed. Contact conditions included fully bonded, unbonded, and an intermediate level of bond where some shear transfer was allowed. The contact for both interfaces at the interlayer was modified such that every reasonable permutation of contact conditions at the interfaces was considered.

Before any analyses were conducted, it was determined that that rods would be cast into the ends of the beams so they could be connected to the testing frame to provide restraint in the transverse directions. This restraint helps the short beam respond in a more similar nature to a longer slab. At the start of modelling, a few elementary analyses were conducted to determine how to restrain the beam specimen so that it remained in contact with the support layer when a dynamic load was applied. It was eventually determined from a number of analyses that bearings would need to be placed through the overlay beam when testing for deflection at the interface. Mechanism 1 consists of a joint in the overlay and the load placed to one side of the beam to determine deflection characteristics as well as load transfer as seen in Figure 3. Also, a roller bearing was applied to create a pinned condition for facilitating rotation.

Next, the required length of the beam was determined. Three lengths were considered: 24 inches, 30 inches, and 36 inches. Since a modulus of rupture beam is 24 inches long, this was chosen as the minimum value. Due to the considerable depth (slightly over one foot since the depth of both the overlay and existing are 6 inches) of the two beam high structure, it was thought that the length of the overlay specimen should be increased to maintain a length to height ratio similar to a modulus of rupture beam. However, the length should remain as short as possible due to the significant increase in the weight of the stacked beam structure that would have to be moved on and off of the testing frame for each test. Neglecting the interlayer, the specimens would weight approximately 150 and 225 pounds for the 24 and 36 inch long specimens, respectively. All three beam lengths (24, 30, and 36 inches) were considered in the finite element analyses, and it was found that the beam had to be at least 30 inches long to maintain deflection and rotation characteristics similar to those of a slab. Therefore, it was decided to make each overlay specimen 30 inches long.

1.2.2. Final test setup

Figure 4 shows a specimen in the testing frame used to isolate the deflection at the interface.

Figure 4. Test setup used to characterize deflection at the interface

The loading head contains a ball joint and is the same loading head used for testing the modulus of rupture beams. The foundation support provided by the lower layers under the concrete slab in an in-service pavement was replicated by an artificial foundation of two layers of neoprene pads, known as Fabcel 25. Figure 5 shows the Fabcel 25 waffle-shaped neoprene pads.

Figure 5. Neoprene pads used to simulate support conditions

The stiffness of the two combined Fabcel layers was determined by conducting a plate load test (ASTM D1195/D1195M), and was found as 200 psi/in. The bearing assembly used to initiate points of rotation can be seen in Figure 6.

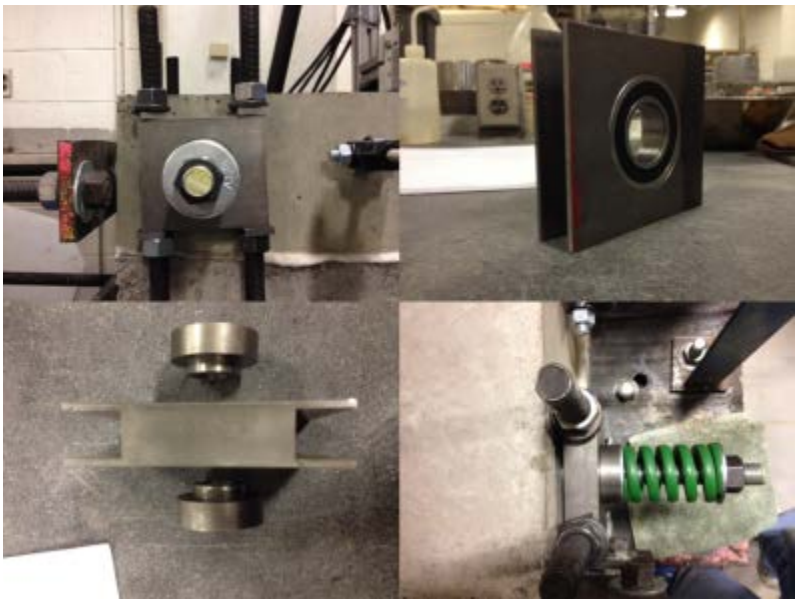

Figure 6. Bearing assembly

The green spring is used in conjunction with a torque wrench to apply the same compression every time. A torque of 40 inch-pounds was applied to the bearings for all specimens. Additional restraint was provided by vertical rollers on both the loaded and unloaded sides of the beam on the front and back to prevent horizontal displacement of the specimen. Figure 7 shows the components of this assembly.

Figure 7. Roller assembly

Displacement in this configuration is measured using eight LVDTs. The LVDT locations are as shown in Figure 8.

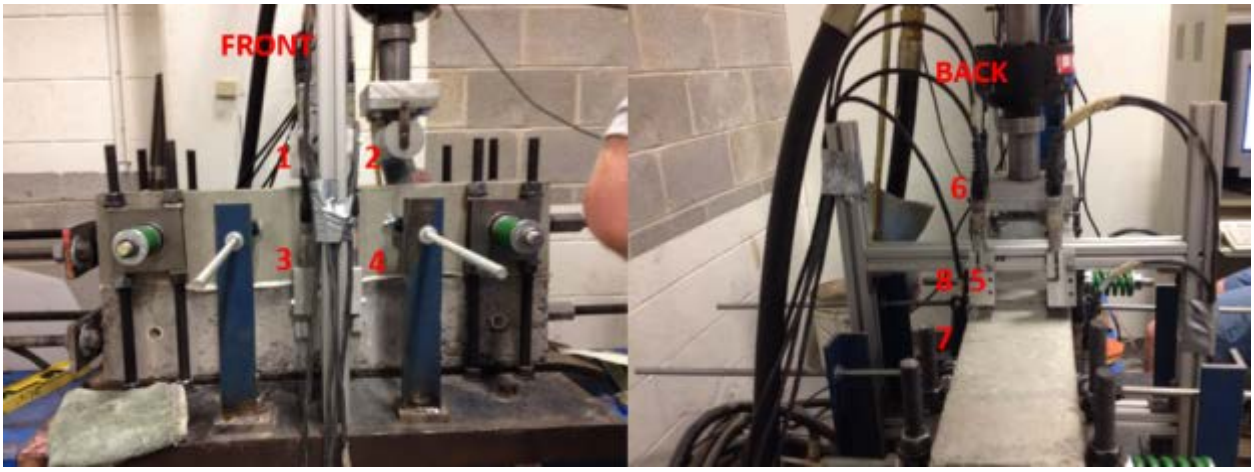

Figure 8. LVDT locations in deflection test setup

Displacement is measured at 1.5 inches from the center saw cut joint on the top of the overlay beam and at mid depth of the lower beam representing the slab being overlaid. The locations of LVDTs 5, 6, 7, and 8 are opposite of 1, 2, 3, and 4. Therefore, displacements measured by LVDTs 2 and 6 are averaged to obtain the overlay loaded (OL) deflection, 1 and 5 are averaged to obtain the overlay unloaded (OU) deflection, 3 and 7 are averaged to obtain the existing unloaded (EU) deflection, and 4 and 8 are averaged to obtain the existing loaded deflection (EL).

1.2.3. Test protocol, loading conditions, and specimens

The dynamic load applied to the specimen to test Mechanism 1 is intended to simulate a vehicle traveling 65 mph over 10 inches and the specimen is loaded at a rate of 7 Hz. 7 Hz was chosen as the loading frequency as it enables testing of specimens to occur in a reasonable time while still allowing for data to be sampled and show a clear time history of load and displacement. A constant 25 pound minimum load is maintained for a 0.134 second rest period. A haversine load which approximates the stress pulse of a moving vehicle is applied over a 0.0087 second duration with a peak load of 600 pounds.

Testing was carried out for at least 300,000 cycles for each specimen. A static sweep from the seat load of 25 pounds to 600 pounds is conducted at 50, 100, 500, 1000, 2000, 5000, 10k, 20k, and every 10k loading cycles afterwards. The 600 pound load induced a similar deflection and angular rotation in the beam to that of a 9-kip falling weight deflectometer load applied to an overlay in the field.

A total of 16 specimens were tested using the setup and loading described above. Table 3 provides summary information about each Mechanism 1 specimen. Displacement vs. load cycle, interlayer compression vs. load cycle, and LTE vs. load cycle plots for each specimen can be found in Appendix A.

Table 3. Summary Information for Specimens used in deflection testing

Specimen	Test Date	Overlay Elastic Modulus and Compressive Strength	Temp and Rel Humidity @ Test Time
0211F15EA 0220F150A	3/20/15	E = 3.11 million psi f'_c = 2666 psi	69.4ºF (51%)
0302F15EA 0303F150A	4/1/15	E = 3.04 million psi f'_c = 2156 psi	70.2ºF (51%)

Specimen	Test Date	Overlay Elastic Modulus and Compressive Strength	Temp and Rel Humidity @ Test Time
0312F10EA 0330F10OB	4/8/15	E = 3.81 million psi f'_c = 3881 psi	71.5ºF (52%)
0316F10EB 0402F10OB	4/9/15	E = 3.88 million psi f'_c = 4512 psi	71.9ºF (51%)
0223MNDAUA	3/25/15	E = 3.28 million psi	69.8ºF (48%)
0417MNDAUC	4/23/15	E = 3.88 million psi	70.8ºF (47%)
0319MNDAMA	4/2/15	E = 4.94 million psi	71.7ºF (49%)
0422MNDAMA	4/28/15	E = 4.3 million psi	71.4ºF (45%)
0226MNONUA	3/27/15	E = 3.11 million psi	70.7ºF (59%)
0522MNONUA	5/27/15	E = 4.65 million psi	72.2ºF (51%)
0424MIDAUB	4/29/15	E = 4.23 million psi	72.6ºF (41%)
0515MIDAUC	5/20/15	E = 4.78 million psi	71.3ºF (36%)
0513MIOAUB	5/19/15	E = 4.71 million psi	72.3ºF (58%)
0520MIOAUA	5/26/15	E = 4.62 million psi	72.6ºF (53%)

1.2.4. Summary of interlayer deflection test results

As can be seen from the plots for both the 10 and 15 oz/yd^2 fabrics (F10 and F15) in Appendix A, the response of specimens with fabric interlayers remains relatively constant throughout the duration of the test and are therefore more consistent in time than the HMA specimens. F15 and F10 deflect approximately 6 and 4 mils respectively on the loaded side of the overlay. The LTE and interlayer compression (as defined in Appendix A) for F15 remains around 15% and 4 - 5 mils, respectively. For F10, LTE fluctuates between 20 and 40% while the interlayer compression is consistently around 3 mils. F10 is thinner than F15, so it does not compress as much.

For the specimens with an HMA interlayer, permanent compression developed in the HMA over time. The open graded asphalt interlayer from Minnesota had a LTE of 50 - 60% for first specimen and 60 - 75% for the second. Interlayer compression at the end of the test was approximately 19 mils and 13 mils for the first and second specimens, respectively. These high values of interlayer compression indicate that either damage or displacement occurred within the interlayer.

For the specimens with the unmilled dense graded HMA interlayer from Minnesota, LTE began at approximately 40% to 50% and decreased to approximately zero over the test and interlayer compression increased from approximately 2 mils to 8 mils. For the specimens with the milled dense graded HMA interlayer from Minnesota, LTE decreased from approximately 75% to 40% and interlayer compression increased from approximately 4 mils to 6 mils. The difference in thickness between the thicker unmilled and the thinner milled HMA could be part of the reason for the difference.

The specimens with the dense graded asphalt interlayer from Michigan had LTEs that fluctuated between 60% to 80% and peak interlayer compression was approximately 4 mils. The specimens with the open graded HMA interlayer from Michigan had basically constant LTEs of approximately 70% for first specimen and 60% for the second. Additionally, the final interlayer compression was approximately 4 mils for both specimens.

1.3. Interlayer Friction Characterization

Shear transfer at the interlayer is a critical parameter in the design of unbonded overlays because the interlayer system must be able to provide a slip plane to allow the overlay to move freely with respect to the existing pavement. On the other hand, field observations have indicated that some interlayer systems do not provide sufficient restraint to allow for joint deployment. This can lead to high curling stresses, and the joints that actually do crack are wide. Therefore, an unbonded overlay interlayer system must both have sufficient slip to allow free movement of the overlay and provide sufficient restraint for joint deployment.

Interaction between a concrete slab and a granular or stabilized base layer is traditionally characterized using the Push-Off Test (Maitra, Reddy, and Ramachandra, 2009; Ruiz, Kim, Schindler, and Rasmussen, 2001; Rasmussen and Rozycki, 2001). In this test, a small section of pavement is cast a short distance away from a paved lane. The paved lane acts as a rigid support and a hydraulic jack or actuator is used to displace the test section. The displacement of the test section is measured using a displacement measurement device rigidly fixed to the subgrade. The resistance to sliding is reported either as a force per unit area of interface or as a friction coefficient. The friction coefficient is the frictional force divided by the weight of the slab. When a chemical bond exists between the slab and the base, the sliding resistance will not be proportional to the slab weight, therefore it is more logical to report the force per unit area than the friction coefficient.

1.3.1. Initial test planning and test setup

In order to characterize the resistance to sliding of each interlayer system, a modified push-off test was performed in the laboratory. In this test, a joint is sawn in the overlay of a 30-inch beam. The bottom beam is not sawn, and both ends of this beam are restrained to prevent translational displacement. One side of the overlay is also restrained against displacement. The other side of the overlay is attached to a threaded rod instrumented with strain gauges to record force. Two LVDTs attached to the loading frame are used to measure displacement of the loaded section. A thrust bearing attached to the vertical actuator is placed on the top of the loaded section of the overlay beam near the joint to prevent vertical displacement. The actuator is used in a displacement control mode to ensure no vertical displacement of the test block occurs near the joint during a test. The variable force provided by the actuator prevents rotation of the loaded half of the overlay and subsequent tensile debonding failure near the joint. A schematic of the test setup can be seen in Figure 9, and the test setup in the laboratory is shown in Figure 10.

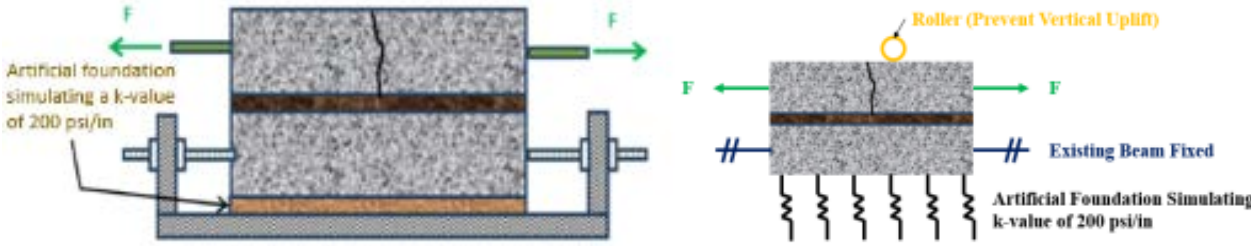

Figure 9. At left, Schematic of Modified Push Off Test Setup; At right, Boundary Conditions of Modified Push Off Test

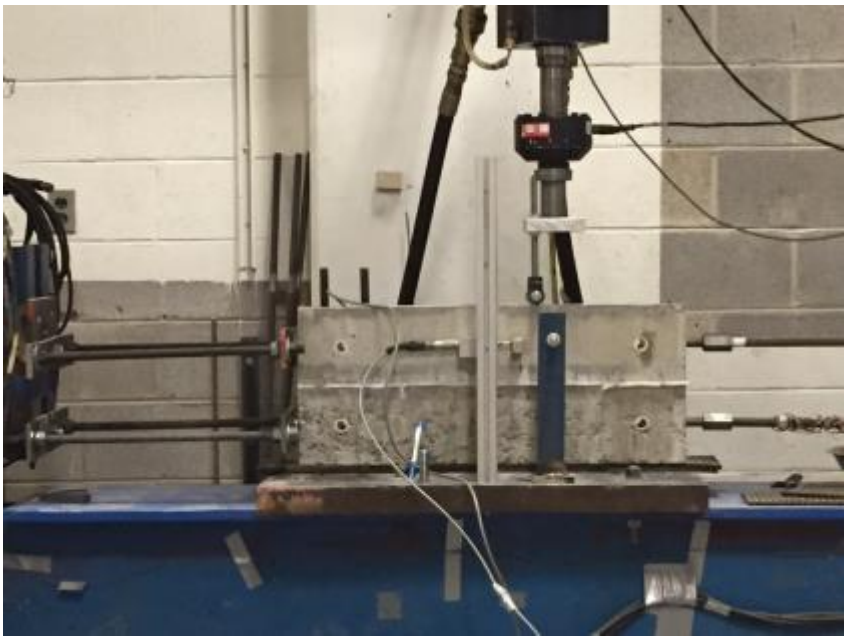

Figure 10. Laboratory setup for the modified push-off test

1.3.2. Test loading conditions and specimens

The horizontal push-off load is applied by manually tightening the instrumented threaded rod. The modified push-off test has two phases. Phase 1 is the cyclic loading phase. In this phase, load is applied until the loaded portion of overlay reaches approximately 80 mils of displacement. The 80 mil displacement corresponds to a 100 degree Fahrenheit drop in temperature for a 12 foot slab cast of concrete with a thermal coefficient of expansion of 5.3 microstrain per degree F. The load is then held constant to observe the relaxation of the interlayer system until the force is relatively constant over time. The load is then removed from the rod. To account for non-elastic displacement, a load is applied in the opposite direction of the initial load until the overlay section returns to its initial position. This position is then held until the force is relatively constant over time. The load, relaxation, opposite load cycle is repeated between 6 to 8 times for each test. Phase 2 is the ultimate loading phase. In this phase, load is applied until the interlayer system fails, or very large displacements (over one inch) are observed.

The modified push-off test was performed on nine different interlayer systems. The details of these systems are shown in Table 4. The attachment to the existing concrete sample taken from the field could be an either an “asphaltic bond” or a “cementitious bond”:

- For an asphaltic bond, the HMA was placed on hardened concrete.
- For a cementitious bond, the wet concrete was placed directly onto the asphalt.

The test date, elastic modulus for the concrete overlay, and temperature and relative humidity at the time of testing for each specimen are recorded in Table 5.

Table 4. Summary of Interlayers Tested in Modified Push-off Test

Label	Source	Grading	Surface	Age	Fabric Weight	Attachment to Existing Concrete
F15-Glued	Propex	n/a	n/a	n/a	15 lb/yd^2	Glued
F15-Pinned	Propex	n/a	n/a	n/a	15 lb/yd^2	Pinned[1]
F10-Glued	Propex	n/a	n/a	n/a	10 lb/yd^2	Glued
F10-Pinned	Propex	n/a	n/a	n/a	10 lb/yd^2	Pinned[1]
MNDAU	MnDOT	Dense	Unmilled	Aged	n/a	Asphaltic Bond
MNDAM	MnDOT	Dense	Milled	Aged	n/a	Asphaltic Bond
MNONU	MnDOT	Open	Unmilled	New	n/a	Asphaltic Bond
MIDAU	MDOT	Dense	Unmilled	Aged	n/a	Cementitious Bond
MIOAU	MDOT	Open	Unmilled	Aged	n/a	Cementitious Bond

Table 5. Summary Information for Modified Push-off Test Beams

Corresponding Beam Nomenclature	Test Date (Time)	Overlay Elastic Modulus and Compressive Strength	Temp and Rel Humidity @ Test Time
0211F15EB 0220F150 (Glued)	3/20/15 (12:15 PM)	E = 3.11 million psi f'$_c$ = 2666 psi	69.6^{o}F (51%)
0302F15EB 0303F10B (Glued)	4/1/15 (9:15 AM)	E = 3.04 million psi f'$_c$ = 2156 psi	70.0^{o}F (51%)
0413F15EA 0506F15OA (Pinned)	5/11/15 (5:00 PM)	E = 4. 63 million psi f'$_c$ = 5334 psi	71.4^{o}F (56%)
0413F15EB 0506F15OB (Pinned)	5/12/15 (12:15 PM)	E = 4. 63 million psi f'$_c$ = 5334 psi	71.8^{o}F (54%)
0312F10EB 0330F10OC (Glued)	4/10/15 1:30 PM	E = 3.81 million psi f'$_c$ = 3881 psi	71.7^{o}F (52%)
0316F10EB 0402F10OC (Glued)	4/10/15 (2:45 PM)	E = 3.88 million psi f'$_c$ = 4512 psi	71.7^{o}F (52%)
0406F10EB 0506F10OB (Pinned)	5/11/15 (3:30 PM)	E = 4.63 million psi f'$_c$ = 5334 psi	71.9^{o}F (55%)
0223MNDAUB	3/24/15 (1:30 PM)	E = 3.28 million psi f'$_c$ = 2326 psi	69.6^{o}F (48%)
0417MNDAUB	4/23/15 (3:00 PM)	E = 3.88 million psi f'$_c$ = 4590 psi	70.9^{o}F (47%)
0319MNDAMB	4/3/15 (11:00 AM)	E = 4.94 million psi f'$_c$ = 6833 psi	71.8^{o}F (50%)
0422MNDAMB	4/27/15 (1:00 PM)	E = 4.3 million psi f'$_c$ = 4696 psi	71.2^{o}F (45%)
0226MNONUB	3/30/15 (10:30 AM)	E = 3.11 million psi f'$_c$ = 2237 psi	70.2^{o}F (59%)

Corresponding Beam Nomenclature	Test Date (Time)	Overlay Elastic Modulus and Compressive Strength	Temp and Rel Humidity @ Test Time
0522MNONUB	5/26/15 (4:30 PM)	E = 4.65 million psi f'_c = 5131 psi	71.1°F (55%)
0424MIDAUA	4/29/15 (12:00 PM)	E = 4.23 million psi f'_c = 4694 psi	72.5°F (42%)
0515MIDAUA	5/20/15 (3:30 PM)	E = 4.78 million psi f'_c = 5357 psi	70.6°F (37%)
0513MIOAUB	5/18/15 (4:45 PM)	E = 4.71 million psi f'_c = 5013 psi	71.0°F (59%)
0520MIOAUA	5/26/15 (2:40 PM)	E = 4.62 million psi f'_c = 5073 psi	71.0°F (56%)

1.3.3. Test protocol and response measurement

The first cycle of each test provided information on the material properties relevant in determining when and where joints in the overlay would deploy. The average stiffness of the interlayer system for the first load cycle was calculated as the force over displacement at a displacement of 80 mils. If the first cycle did not reach 80 mils displacement, the stiffness was calculated using the maximum displacement. The average initial stiffness of each interlayer system is provided in Table 6.

During testing it was determined that the interlayer system stiffness stabilized between 5 and 8 load cycles. This stiffness is relevant when calculating the stress in the overlay caused by the interlayer resisting uniform volume changes due to a decrease in temperature and/or moisture. An overly stiff unbonded overlay system can prevent true debonding, cause high stresses to develop in the overlay, and prevent proper joint deployment. The average final stiffness for each interlayer is summarized in Table 6. The definition of the initial and final stiffness is shown in Figure 11.

Finally, the ultimate strength of each interlayer system was tested to establish the ultimate resistance to sliding for each interlayer system. The average ultimate resistance is provided in Table 6 for each specimen. When reviewing Table 6, note that for one of the tests on the F10-Glued interlayer, a delay in the initial loading cycle caused the first load cycle to appear less stiff than several subsequent load cycles. For this test, the initial stiffness was estimated using the second load cycle. Data for each modified push-off beam are plotted in Appendix A.

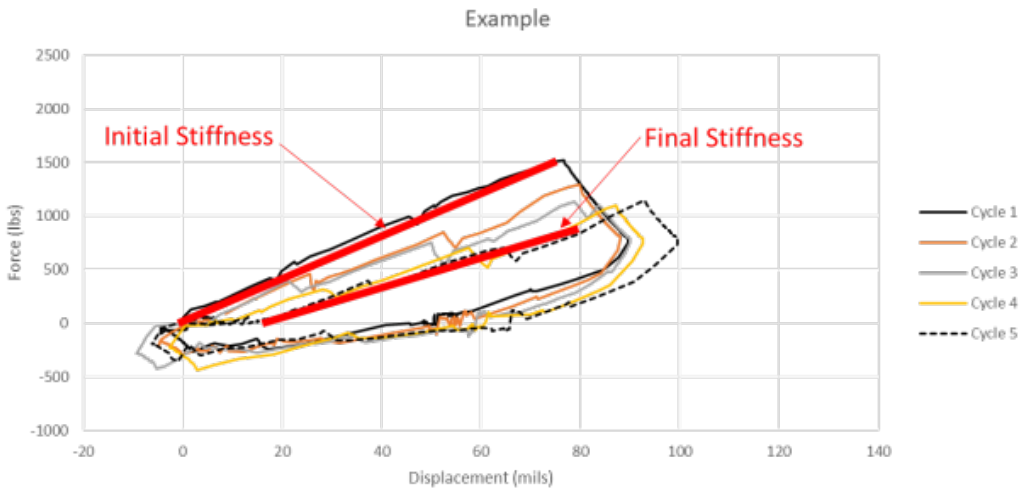

Figure 11. Example of Initial and Final Stiffness determination

Table 6. Summary Results from Modified Push-Off Test

Interlayer (Code)	Interlayer & interlayer thickness	Initial Stiffness (psi/in)	Final Stiffness (psi/in)	Ultimate Resistance (psi)
F15-Glued	Fabric (15 oz/yd^2)	61	37	13
F15-Pinned	Fabric (15 oz/yd^2)	50	40	26
F10-Glued	Fabric (10 oz/yd^2)	104	87	22
F10-Pinned	Fabric (10 oz/yd^2)	98	29	21
MNDAU	HMA (2.75 in)	234	167	39
MNDAM	HMA (0.875 in)	333	263	59
MIDAU	HMA (1 in)	336	317	>62
MNONU	HMA (1.75 in)	217	55	16
MIOAU	HMA (2 in)	169	136	63

1.3.4. Summary of interlayer friction test results

Results in Table 6 show that specimens with a fabric interlayer have a lower stiffness than the specimens with an HMA interlayer. Within the fabric specimens, the F10 specimens had a higher stiffness than the F15 specimens. This is most likely due to the smaller thickness of F10 that limits in-plane deformation of the interlayer (the thickness being smaller than that of F15).

The specimens with the milled interlayer from Minnesota have a higher initial and final stiffness than the specimens with the unmilled interlayer. It can also be seen that the ultimate resistance of the specimens with the milled interlayer was much greater that for the specimens with the unmilled interlayer. This is possibly due to the decreased thickness of the milled specimens. The largest reduction in stiffness among asphalt specimens occurs with the open graded asphalt interlayer from Minnesota which was visibly distressed during testing and had a very small ultimate resistance.

The specimens with the open and dense graded asphalt interlayers from Michigan exhibited the smallest decreases in stiffness and also had the largest ultimate resistance. The ultimate resistance for the thicker asphalt interlayers was lower with the exception of the open graded interlayer for the specimens from Minnesota, which damaged due to the lower strength.

In general, with the exception of the specimens with the open graded HMA interlayer from Minnesota, the fabric interlayers provide less restraint than the asphalt layers.

1.4. Reflective Cracking

1.4.1. Test setup

Reflective cracking is a potential concern for unbonded overlays. The reflective cracking test setup is designed to assess the ability of the interlayer system in deterring cracks in the existing pavement from reflecting up into the overlay. For this test setup, a saw cut is made in the lower beam at midspan to represent a joint or crack in the existing concrete. The beam was loaded directly above the sawed joint in the middle of the 30 inch beam using the same loading head used for the deflection test setup. Figure 12 below illustrates the schematic used in the planning of the reflective cracking test setup, while Figure 13 illustrates the as-built apparatus in the laboratory.

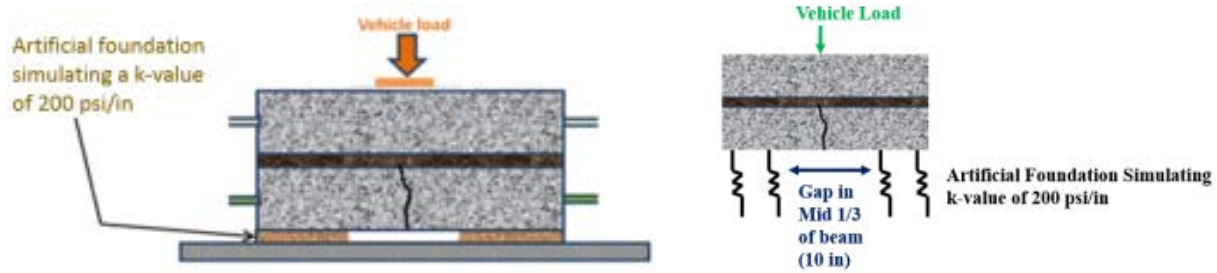

Figure 12. At left, Schematic of Reflective Cracking Test Setup; at right, Boundary Conditions of Reflective Cracking Test Setup

Figure 13. Final test apparatus for reflective cracking

1.4.2. Test loading conditions and specimens

The load in the test configuration is applied at a constant rate until a reflective crack is generated in the overlay beam. The load rate was chosen to be 30 pounds per second, which is the loading rate specified when performing modulus of rupture testing for concrete beams (ASTM C78).

LVDTs record the displacement at the front and back of the beam on the overlay and existing beams. The LVDTs are located 3.5 inches to the left of the applied load.

Shakedown testing for reflective cracking was performed using a specimen with the 15 oz/yd2 nonwoven fabric, and the bottom of the beam was fully supported with two layers of Fabcel 25. Three specimens were tested and a reflective crack could not be generated. The overlay cracked from the top-down – as opposed to bottom-up, as would be expected. This indicates that the failure was due to the stress concentration and crushing under the loading head and not due to a crack reflecting up from the underlying cracked beam.

In order to overcome this problem, a gap was created under the central 10 inches of the beam by removing the Fabcel so there was no support in this area. This gap under the center of the beam is intended to simulate a void under the joint of an existing pavement. Figure 14 shows the gap in the Fabcel measured with plywood and centered with a plumb bob. With the gap under the beam, subsequent shakedown tests generated reflective cracking which propagated from the bottom-up.

Figure 14. 10-inch Gap in Fabcel with Plumb Bob to Center the Gap

Table 7 summarizes information relating to each specimen tested using the reflective cracking test setup. This includes the ultimate load and modulus of rupture (MOR) of the overlay beam. Force vs displacement plots for each reflective cracking specimen are provided in Appendix A.

Table 7. Summary Information for Reflective Cracking Specimens

Specimen	Break Load (lbs)	Test Date (Time)	MOR of the Overlay Beam (psi)	Temp and Rel Humidity @ Test Time
0406F15EB 0429F15OB	6,218	5/4/15 (9:20 AM)	610	71.8ºF (50%)
0406F15EC 0429F15OC	6,605	5/4/15 (10:00 AM)	644	71.9ºF (51%)
0302F15EB 0701F15OD	7,508	7/6/15 (1:10 PM)	682	72.4ºF (61%)

Specimen	Break Load (lbs)	Test Date (Time)	MOR of the Overlay Beam (psi)	Temp and Rel Humidity @ Test Time
0316F10EC 0402F10OA	6,565	4/7/15 (2:40 PM)	628	71.7ºF (57%)
0409F10EA 0501F10OA	6,984	5/6/15 (11:15 AM)	641	70.8ºF (56%)
0316F10EB 0709F10OC	7,517	7/14/15 (11:35 AM)	701	72.3ºF (60%)
0417MNDAUA	5,562	4/22/15 (11:20 AM)	590	71.7ºF (46%)
0507MNDAUA	6,345	5/12/15 (3:00 PM)	738	70.7ºF (51%)
0701MNDAUA	6,052	7/6/15 (12:00 PM)	658	70.3ºF (62%)
0422MNDAMC	5,923	4/27/15 (12:40 PM)	623	71.1ºF (44%)
0507MNDAMB	6,638	5/12/15 (4:00 PM)	690	72.1ºF (49%)
0709MNDAMB	5,912	7/14/15 (11:10 AM)	649	72.2ºF (60%)
0507MNONUC	6,414	5/12/15 (5:00 PM)	694	71.9ºF (47%)
0522MNONUC	6,678	5/27/15 (9:30 AM)	724	72.1ºF (58%)
0701MNONUB	6,460	7/6/15 (12:30 PM)	636	72.1ºF (61%)
0424MIDAUC	5,777	4/29/15 (11:10 AM)	652	72.4ºF (42%)
0515MIDAUB	6,438	5/20/15 (11:15 AM)	717	72.2ºF (35%)
0701MIDAUC	5,896	7/6/15 (1:10 PM)	663	72.4ºF (59%)
0513MIOAUC	6,957	5/18/15 (12:20 PM)	697	70.1ºF (60%)
0520MIOAUC	7,129	5/25/15 (10:35 AM)	711	72.2ºF (48%)
0709MIOAUA	6,471	7/14/15 (10:40 AM)	698	72.3ºF (60%)

1.4.3. Summary of reflective cracking test results

Reflective cracking is cracking which occurs in the overlay directly over a joint or cracking in the existing pavement. It is also possible to have reflective distress over a region of reduced support. This could occur over a severely deteriorated joint or crack where the stiffness is smaller in a short region where the distress in the existing pavement is located. As discussed in the section on Mechanism 3 setup, it is important to note that reflective cracking could not be generated from the bottom up when the specimen is fully supported. This suggests that the potential for reflective cracking in the concrete overlay is extremely low unless a void is present in the vicinity of the crack or joint. A summary of the results from Mechanism 3 testing is provided in Table 8, where the "Load Ratio" refers to the Reflective Crack Load normalized by the Failure Load for the Overlay MOR Beam.

Table 8. Reflective Cracking Beam Summary

UBOL Specimen	Reflective Crack Load (lbs)	MOR for the Overlay Mixture (psi)	Failure Load for Overlay MOR Beam (lbs)	Load Ratio	Average Load Ratio for Each Interlayer
F15	6218	610	7417	0.838	0.842
	6605	644	7980	0.828	
	7508	682	8730	0.860	
F10	6565	628	7707	0.852	0.869
	6984	641	7920	0.882	
	7517	701	8620	0.872	
MNDAU	5562	590	7480	0.744	0.725
	6345	738	9217	0.688	
	6052	658	8155	0.742	
MNDAM	5923	623	7767	0.763	0.753
	6638	690	8730	0.760	
	5912	649	8020	0.737	
MNONU	6414	694	8594	0.746	0.767
	6678	724	8925	0.748	
	6460	636	8015	0.806	
MIDAU	5777	652	8140	0.710	0.711
	6438	717	8874	0.725	
	5896	663	8460	0.697	
MIOAU	6957	697	8675	0.802	0.787
	7129	711	8798	0.810	
	6471	698	8637	0.749	

The load required to induce a reflective crack into the overlay beam is provided in the second column. The load required to fail a modulus of rupture beam cast with the same mixture as the overlay is provide in column 4. The reflective crack load (column 2) is divided by the failure load for the overlay modulus of rupture beam (column 4) to obtain the load ratio (column 6). The failure load of the overlay modulus of rupture beam is the maximum load sustained by the modulus of rupture beam according to ASTM C78. These load ratios were then averaged for each interlayer type.

The average load ratio has a range of 0.73 to 0.87. The fabric specimens are at the upper end this range, which may indicate that they are more resistant to the development of reflective cracking as compared to the specimens with an HMA interlayer. All of the HMA interlayer specimens performed roughly comparable to one another. The open graded HMA interlayer from Michigan yielding the highest average load ratio of 0.79. This is similar to that achieved by the F15 interlayer specimens.

1.5. Bond Strength Characterization

1.5.1. Test setup

Bond strength of interlayers was evaluated by measuring the vertical force-displacement relationship as the concrete layers of the unbonded overlay structure are loaded in direct tension, as shown in Figure 15. This test is intended to provide insight into how debonding between the existing and overlay concrete layers develops in the field and to determine if curling can result in debonding between the interlayer and the concrete layers.

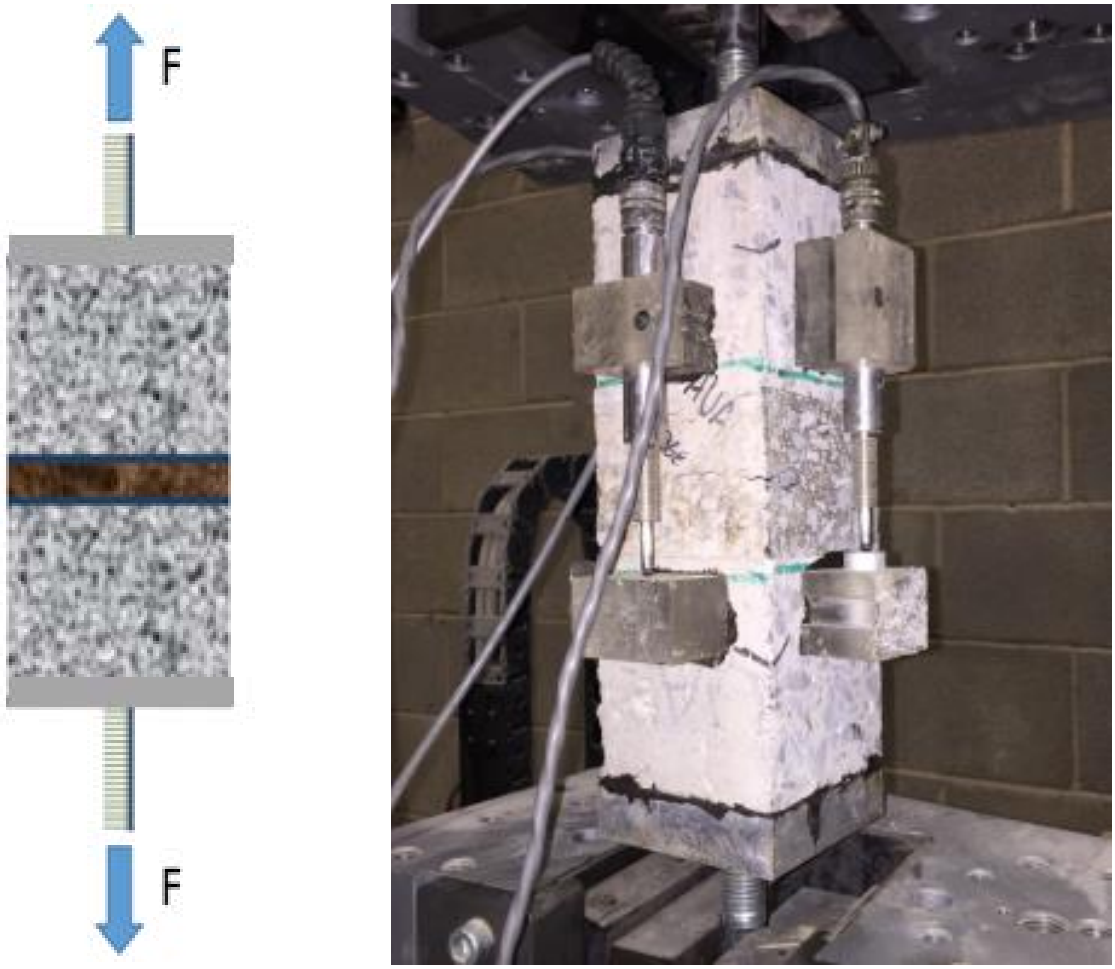

Figure 15. Schematic of direct tension test; at right, laboratory direct tension test on specimen with HMA interlayer

1.5.2. Notes on extraction of specimens from beams

Each direct tension specimen was either cut from one of the already tested Mechanism 3 specimens (asphalt interlayers) or cast in cylindrical molds (fabric interlayers). It was assumed that little to no damage was experienced where the direct tension specimens were sawn from the Mechanism 3 specimens and would therefore not affect the results of the direct tension test. The direct tension specimens required very precise preparation. The location of the specimens in the direct tension beams is provided in Figure 16.

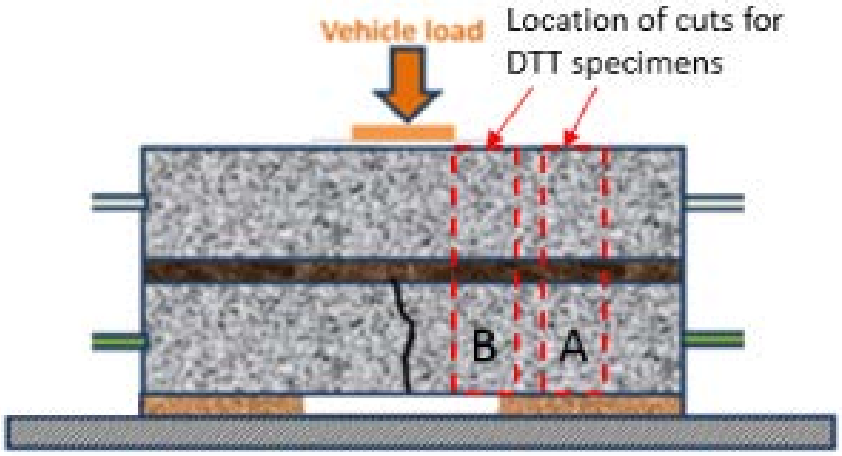

Figure 16. Location of asphalt direct tension specimens

A rig was used to provide compression while metal blocks were epoxied to the top and bottom of the specimens to ensure that the steel rods used in the testing apparatus were perfectly straight and in line with one another.

1.5.3. Test specimens and loading conditions

The asphalt interlayer specimens were 4-inches on each side and approximately 12 inches tall (an asphalt interlayer direct tension specimen is shown in Figure A-16 in the Appendix). The fabric interlayer specimens were 4-inch diameter and approximately 8 inches tall cylinders. The fabric specimens were made in two steps. First, the bottom of the specimen was cast using a 0.36 w/cm. Next, the fabric was glued to the top of the specimen bottom and the top of the specimen was cast using a 0.42 w/cm overlay mixture.

An Instron loading machine was used to apply a direct tensile load. A photo of the test setup is shown in Figure 15. The test is run in displacement control mode at a rate of 1 mil/sec and the force is recorded by the load machine. Displacement is also recorded with two LVDTs attached to opposite sides of the specimen. The relative displacement between the concrete above and below the fabric is measured, which can be seen in Figure 15. Table 9 summarizes the specimens tested and the peak load and displacement at the peak load. Force vs displacement for each direct tension specimens is plotted in Appendix A.

Table 9. Summary of Specimens Tested for Bond Strength

Code	Replicate	Location	Peak Load (#)	Displacement at Peak Load (mils)	Location of Break
F15	1	N/A	18	64	Glued Interface
F15	2	N/A	16	61	Glued Interface
F10	1	N/A	31	139	Glued Interface
F10	2	N/A	38	120	Glued Interface
MNDAU	1	A	255	33	Middle of HMA
MNDAU	2	B	251	42	Middle of HMA
MNDAM	1	A	262	10	Bond w/ Existing Concrete (into HMA)
MNDAM	2	B	392	13	Both interfaces and into HMA

Code	Replicate	Location	Peak Load (#)	Displacement at Peak Load (mils)	Location of Break
MNONU	1	A	169	12	Middle of HMA
MNONU	2	B	208	12	Bond w/ Existing Concrete (into HMA)
MIDAU	1	A	586	22	Bond w/ Overlay Concrete
MIDAU	2	B	411	13	Bond w/ Overlay Concrete
MIOAU	1	A	206	4	Bond w/ Existing Concrete (into HMA)
MIOAU	2	B	142	6	Bond w/ Existing Concrete

1.5.4. Summary of bond strength test results

As shown in Table 9, both fabrics tested had comparable values of peak force and displacement at peak force. The F10 specimens resulted in a peak load of 30 - 40 pounds at a displacement ranging between 120 mils to 140 mils and the F15 specimens maintained a peak load of 15 to 20 pounds at a displacement of approximately 60 mils. The variation observed between fabric specimens can be partly attributed to the quality and quantity of geotextile adhesive placed at the glued interface. Overall, these results indicate that the fabrics would provide insignificant resistance to upward curl of the concrete overlay. Greater variability was observed with the HMA interlayers than the fabric interlayer specimens. Additionally, higher strength and smaller displacements at the peak load for the HMA specimens was observed as compared to the fabric specimens as one would expect. The magnitude of the peak load varied with the location of the failure within the inter layer system. Both the Minnesota and Michigan open graded asphalts produced the smallest peak loads, followed by Minnesota dense unmilled, Minnesota dense milled, and Michigan dense unmilled which had the greatest peak load.

2. ASSESS IN-FIELD PAVEMENTS TO COLLECT FIELD DATA

2.1. Dynamic backcalculation using FWD data from LTPP GPS-9 test sections

Another portion of the Task 2 research was an attempt to understand the behavior of UCOCP by analyzing FWD deflection basins obtained from various LTPP test sections and in-service pavements. To this end, the research team obtained the time histories of FWD deflections collected under GPS 9 ("Unbonded PCC Overlay of PCC Pavement (PCC/PCC)" under the LTPP study (FHWA, 2015). The available time histories of the FWD deflections of existing pavements with overlays are:

- 14 sections of overlaid jointed plain concrete pavement (JPCP) with 63 visits
- 8 sections of overlaid jointed reinforced concrete pavement (JRCP) with 45 visits
- 4 sections of continuously reinforced concrete pavement (CRCP) with 21 visits

A majority of the FWD visits are related to years before year 2000. The quality of the recorded data after the year 2000 is relatively better because of the longer recorded time history (60 ms vs 30 ms) and the shorter time steps (0.1 ms vs 0.2 ms). Therefore, the research team focused on FWD data collected after 2000.

The research team performed close investigations of four specific LTPP sections and their associated basins. Some criteria considered in selecting the four sections were: A) the presence of a very thin HMA interlayer, B) JPCP design (as they are more likely to agree with principles in the plate-on-a-foundation model), and C) proximity to panel members' states. Those four cases are described in more detail in Table 10.

Table 10. LTPP test sections from the GPS-9 experiment considered for dynamic backcalculation study (missing or unavailable data is indicated as "n/a")

Location	ID	OL Layer / Thickness (in)	Interlayer / Thickness (in)	Original PCC / Thickness (in)	Base layer / Thickness (in)	Subbase layer / Thickness (in)	Subgrade Type
California	06-9048	JPCP / 6.4	Chip Seal / 0.2	JPCP / 8.1	n/a	n/a	Coarse-Grained Soil: Silty Sand with Gravel
Kansas	20-9037	JPCP / 5.8	Open Graded Asphalt / 2.0	JRCP / 8.8	Unbound Granular Sand / 4.0	n/a	Fine-Grained Soils: Lean Clay with Sand
Minnesota	27-9075	JPCP / 5.9	Open Graded Asphalt / 0.8	JPCP / 7.8	n/a	n/a	Fine-Grained Soils: Sandy Lean Clay
Michigan	26-9029	JRCP / 7.3	Open Graded Asphalt / 0.8	CRCP / 8.0	Unbound Granular Gravel / 4.0	Unbound Granular Sand / 9.5	Fine-Grained Soils: Sandy Lean Clay

Using the basins associated with the sections in Table 10, the research team performed dynamic backcalculation based on the generalized plate on a foundation model proposed by Khazanovich and Boosheherian (2015).

In comparing the results of the dynamic backcalculation using the four sections investigated during the task work, a few observations are:

- The existing PCC contributes to the overlay slab rigidity and increases the elastic modulus of the plate in the plate-on-a-foundation model. However, the exact amount of contribution of the existing PCC to the structural capacity of the plate and subgrade is not identifiable yet.
- Performing the dynamic backcalculation at different load levels on the same location resulted in very similar structural parameters. This shows that sections under study are not constructed with stress dependent materials (at least for the typical stress ranges applied by FWD).
- The structural integrity of a road pavement changes at different locations; this can be observed in varied maximum deflections under identical applied FWD loads. The research attempted to determine a trend based on the changes in maximum deflections and the backcalculated pavement parameters. In spite of observing connections between the deflections and the pavement parameters for each individual road section, these connections were not consistent for other pavement sections constructed with different materials and exposed to different climatic conditions. Therefore, no generalization could be made in this regard.

Overall, the research team concludes that the generalized plate-on-a-foundation model is capable of capturing the behavior of UCOCP constructed with JPCP and JRCP.

2.2. Using ultrasound testing to determine bond integrity and uniformity

During Task 2 the research team performed non-destructive tests on four unbonded overlay sections at the MnROAD test facility using both ultrasonic and ground penetrating radar methods. The designs of these test cells in cross-section is provided in Figure 17. Naturally these tests can be used to assess overlay thickness, however an additional objective was to relate these tests to unbonded slabs and determine if they can be used to assess bond condition.

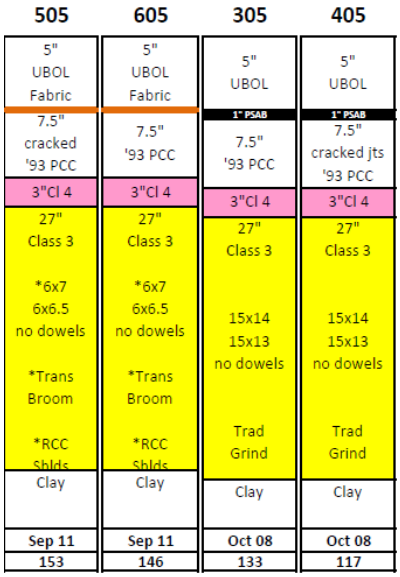

Figure 17. Structural designs for four unbonded overlay test sections at MnROAD

Figure 18 illustrates the results of ultrasonic testing on the MnROAD unbonded overlay cells. Consider the hypothesis that greater measured thicknesses may be interpreted in some cases as the result of stronger bond between the overlay and the interlayer. If this is the case, then it is possible that Cell 405 has a better bond than Cell 305 with the HMA interlayer, given the number of local instances in the plot of Cell 405 where its thickness measurements are six inches or greater. Likewise, one might assume that Cell 505 prior to station 112680 has a better, more uniform bond than Cell 605 over the same distance, whereas for the last 50-60 feet of both cells Cell 605's bond is superior to Cell 505.

One complication of the MnROAD study, however, is that any attempt to compare the influence of HMA interlayer (Cells 305 and 405) and fabric interlayer (Cells 505 and 605) on overlay-interlayer bond is confounded by overlay age. (Note the construction dates in the next to last row of Figure 17.) Thus it is difficult to interpret in-field performance of interlayers in terms of bond.

Finally, a recent NDT technology that MnDOT has pursued for QA/QC on its infrastructure is three-dimensional ground penetrating radar (henceforth "3D radar"). This technology is being explored given that, when compared with other ultrasonic or GPR technologies, 3D radar offers much higher productivity and greater coverage. That is, for the same amount of testing in hours, more data can be extracted in those hours using 3D radar to assess the pavement system. Figure 19 illustrates the results of 3D radar testing on the four test unbonded overlay cells at MnROAD. Again, it is assumed that in many instances, greater thicknesses as measured by 3D radar are not due to actual variance in overlay paving but rather a different level of bond condition at the overlay-interlayer interface.

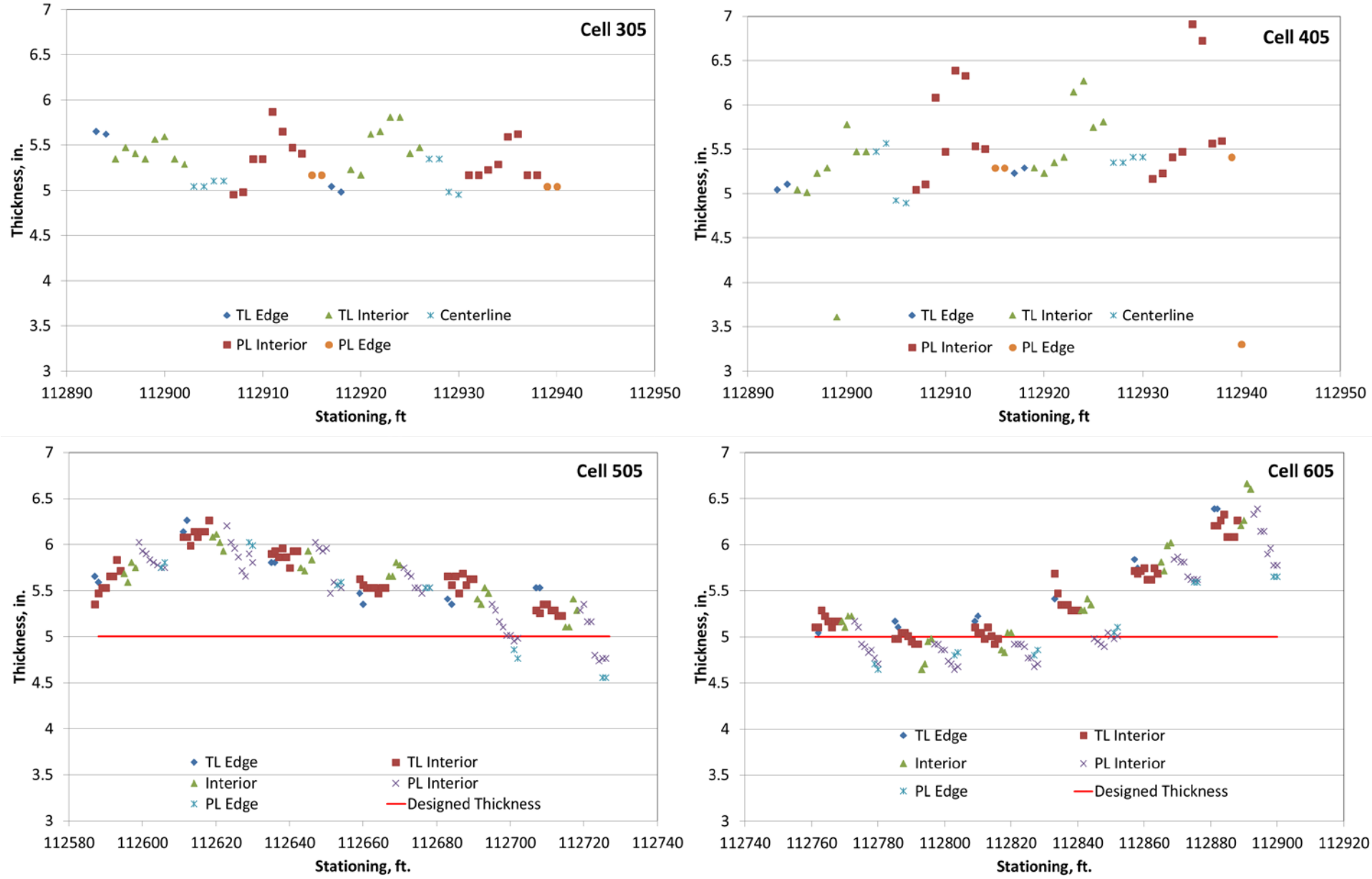

Figure 18. Thickness plots from ultrasonic testing of MnROAD Cells 305 & 405 (HMA interlayer) and 505 & 605 (fabric)

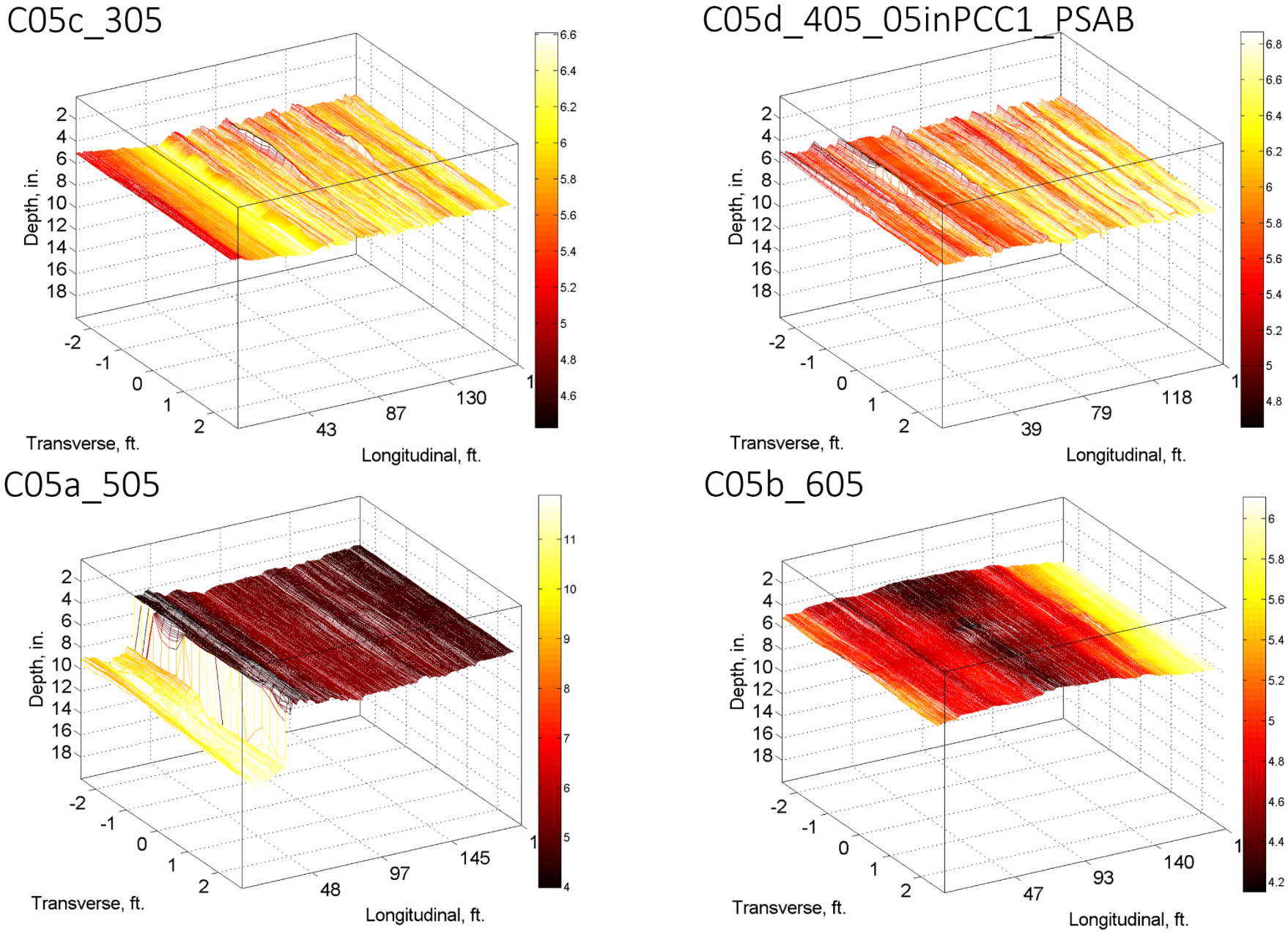

Figure 19. Tomographic plots from 3D ground penetrating radar testing of MnROAD Cells 305, 405, 505, and 605

2.3. Surveys of in-field pavements

2.3.1. Unbonded overlays in Michigan

Members of the research team surveyed in-field sections of unbonded concrete overlays in Michigan with the cooperation of the Michigan Department of Transportation (MIDOT). A summary of these in-field pavements is provided in Table 11.

Table 11. Unbonded overlays surveyed in Michigan for Task 2

Road	Location	CMS	Year Constructed	Age	Interlayer
US-131	Plainwell	3111	1998	16	1 in dense graded HMA
US-23		47014	1999	15	1 in dense graded HMA
I-69	North of I-94	13074	1999	15	1 in dense graded HMA
I-69	Charlotte	13074 & 23061	2000	14	1 in dense graded HMA
US-131	Rockford	41132 & 41133	2000	14	1.25-1.75 in open graded HMA
US-23		47014	2001	13	1 in dense graded HMA
I-75 NB	West Branch	65041	2003	11	1 in open graded HMA
US-131	Kalamazoo	39014 & 03111	2004	10	1 in dense graded HMA
I-96	Coopersville	70063	2004	10	1 in open graded HMA
I-75		25032 & 73171	2004 & 2005	10/9	Existing HMA from composite pavement
I-94		77111	2006	8	1 in open graded HMA
I-96	Walker	70063 & 41026	2006 & 2007	8/7	1 in open graded HMA

The oldest in-service UBOLs in Michigan were built in 1984. Their designs consist of between 6 to 8 inch jointed plain concrete pavements overlays with conventional joint spacing and between 1 to 1.75 inches of either dense or open graded hot mix asphalt (HMA) interlayers. Please note that in 1995 and prior the overlay was constructed as a jointed reinforce concreted pavement (JRCP) with either, 27 ft, 41ft, or a random joint spacing. After viewing 13 different UBOLs in Michigan in August 2014 and 8 additional sections in September 2015, the following observations, discussed in terms of relevant distresses or issues, were made.

2.3.1.1 Longitudinal cracking

The predominant distress in these pavements was longitudinal cracking. Three separate mechanisms are believed to contribute the development of each of the three different types of longitudinal cracks.

Erosion longitudinal cracks. A contributing cause to the development of some of the longitudinal cracks is erosion of the interlayer between the lane shoulder joint and the wheelpath, as shown in Figure 20.

Figure 20. Longitudinal cracking due to erosion of the HMA interlayer in surveyed Michigan sections

These longitudinal cracks tend to gradually meander towards the lane/shoulder joint. For example, on I-96, drainage was not included as part of the overlay. This resulted in water build up in the interlayer and longitudinal cracking in the overlay. MIDOT has found that ensuring adequate drainage as well as maintaining edge drains is therefore significantly important to these structures where the interlayer is susceptible to erosion. If the drainage system backs up, then water will remain trapped in the interlayer, as shown in Figure 21.

Figure 21. Plugged edge drain near surveyed Michigan sections

Longitudinal cracks in the wheel path. Longitudinal fatigue cracking can also develop along the wheel path. This may propagate from one transverse joint to the next along the wheel path or begin propagating along a diagonal to the lane/shoulder joint, as illustrated in Figure 22.

Figure 22. Longitudinal (or diagonal) cracking in the wheelpath in sections surveyed in Michigan

A gap created due to consolidation of the HMA interlayer or localized erosion at the intersection of the wheel path and the transverse joint might contribute to the initiation of these longitudinal/diagonal cracks. Once the crack has propagated along one side of the transverse joint, it will tend to propagate on the other as well as since high shear stresses can develop as the wheel moves off the crack slab on to the uncracked slab on the opposing side of the joint.

Midslab longitudinal cracks. Midslab longitudinal cracking was also observed, as shown in Figure 23. This appears to be top-down cracking related to fatigue. The shorter joint spacings of 10 or 12 ft can result in fatigue cracking preferentially occurring in the longitudinal direction in lieu of the transverse direction.

Figure 23. Midslab longitudinal cracking in surveyed Michigan sections

2.3.1.2. Wide working joints

In some sections every fifth or sixth joint was wider than the others indicating that they were the working joints. Distress frequently developed at these wider joints and consisted of longitudinal cracks propagating from the transverse joint. Possible causes of this include:

1. Not all joints deployed initially (observed for both open and dense graded interlayers) and/or
2. The use of dowel bar inserters could have contributed to joint lock-up.

One of these wider distressed working joint is shown in Figure 24.

Figure 24. Wider working joint exhibiting distress in Michigan sections surveyed for Task 2

2.3.1.3. Corner breaks

Corner breaks were also observed in many sections. A few instances of the corner breaks observed are illustrated in Figure 25. The observed corner breaks could be the result of drainage issues. If water only enters on part of the lane, and becomes trapped at the edge, a corner break may develop. This water will cause an asphalt interlayer to strip and ravel, leading to loss of support. MIDOT now installs edge drain systems when constructing unbonded overlays.

Figure 25. Corner breaks observed in Michigan

2.3.1.4. Transverse cracking

Transversely cracked slabs can be classed according to the following subdistresses.

Fatigue cracking. This is not a commonly observed distress even for relatively thin structures (6-8 in) on heavily trafficked roadways. This is most likely due to the shorter transverse joint spacing of 10 or 12 ft that is typically used.

Reflective distress. A transverse crack in the overlay can develop as the result of a region of reduced support in the existing pavement such as a severely distressed region. On US-131 in Plainwell, transverse cracking was more prevalent than in any other section. The existing PCC pavement was severely distressed and no pre-overlay repairs were performed. The interlayer is 1 in dense graded HMA. The cause of this transverse cracking is therefore most likely reflective distress from the existing PCC pavement up into the overlay. A confirmed case of reflective distress was on I-96 near Portland where a tight mid-slab transverse crack was cored. The core revealed that the crack was above a distressed region in the existing pavement.

Reflective cracking. Reflective cracking is a transverse crack in the overlay directly above a well-defined joint or crack in the existing pavement. The laboratory study revealed that a discrete joint or crack in the existing pavement will tend to not reflect up into the overlay under normal wheel loads if the existing pavement is fully supported. However, when a void is simulated under the discontinuity in the existing pavement a reflective crack is possible. No instances of reflective cracking were observed in Michigan.

Transverse cracking near joints. Transverse cracking just on the leave side of the joint also appears to be common and does not appear to be a reflective crack. Examples of this can be seen in Figure 26. Further investigation is needed to determine the cause of these cracks.

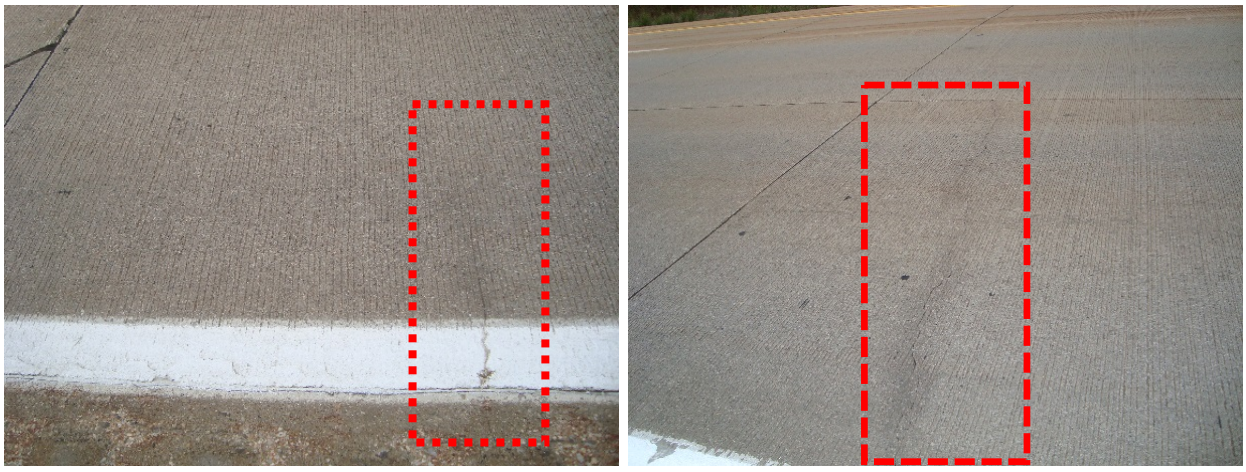

Figure 26. Transverse cracking on leave side of joint

2.3.1.5. Joint faulting

Joint faulting is a distress also observed in UBOLs in Michigan. Faulting data was examined and between 0.3 and 1.3 inches/mile of faulting were recorded on the sections in which faulting

data was available. This indicates that faulting can develop due to pumping of the HMA interlayer resulting in a loss of support due to interlayer material breakdown and must be accounted for in the design process.

2.3.1.6. Observations of section using interlayer fabric

One nonwoven geotextile fabric was constructed in Michigan as part of a test section within a project where an UBOL was constructed with a 1 in open graded HMA interlayer. This project is along US 10 near Coleman. The structure is a 6 in doweled JPCP with a 12 ft joint spacing and a tied shoulder. Early age longitudinal cracking was observed near the location where the fabric meets the asphalt. This could be due to a backup of water at the interface of the two interlayers leading to the crack initiation. The water could become trapped at the interface between the fabric and HMA resulting in a buildup of pressure resulting in the observed cracking. Additionally, the abrupt change in support condition between the asphalt and fabric could have resulted in additional stresses leading to the crack development. This longitudinal crack continued to develop in adjacent panels down the roadway, as would be expected without isolating the adjacent panels. Figures depicting this cracking are shown in Figure 27 below.

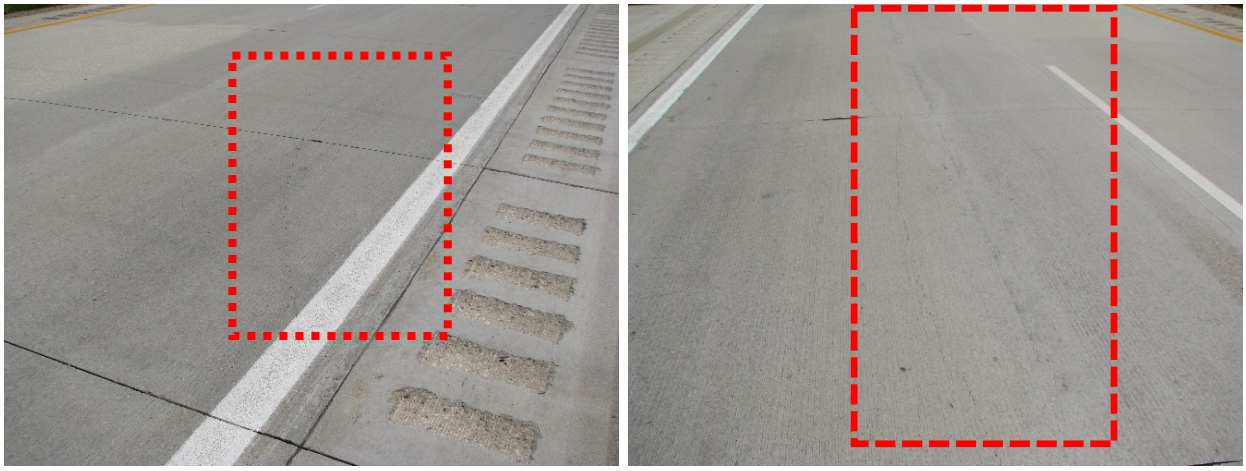

Figure 27. Longitudinal cracks on US-10 near Coleman, MI

3. PROVIDE GUIDELINES ON THE NEED FOR DRAINAGE

3.1 Introduction

Unbonded concrete overlays (UBOLs) typically include the use of a separation layer between the original concrete pavement and the new concrete overlay. The separation layer material has typically been either 1 inch (sometimes up to 2 inches) of asphaltic concrete or a relatively thin (less than 1/8 in under load) nonwoven geotextile fabric (Harrington and Fick, 2014).

The separation layer typically performs one or more of three functions: 1) isolation of the overlay from the underlying pavement to prevent the transmission or "reflection" of cracking and other defects in the underlying pavement through the overlay; 2) provision of a lower modulus "cushion" or "bedding" layer, which reduces load- and environment-related stresses in the overlay (compared to what these stresses would be if the overlay were constructed on a rigid foundation); and 3) provision of a path to allow the escape of infiltrated moisture. The design and function of this separation layer design are key factors that affect the performance of unbonded concrete overlays on concrete pavements.

This chapter considers research and practices concerning the need for and provision of drainage within the UBOL separation layer.

3.2 The Need for Drainage

Water can enter a pavement from either the top or the bottom through one or more of several mechanisms, including the following:

- The entry of surface water through joints and cracks (particularly longitudinal joints);
- High water table or interception of flow from "perched" water sources;
- Capillary moisture rise; and
- Ditches and/or subdrain systems that do not drain properly.

The infiltration of surface water through joints and cracks is generally considered to be the potential source of greatest relevance for UBOL interlayer systems, although other sources can significantly impact the overall pavement structure. Infiltrated surface water can be retained in the UBOL system, particularly in the presence of a dense-graded subbase and/or slow-draining subgrade material (e.g., fat clay).

The presence of water at the interface between the overlay and underlying concrete can contribute to many distress mechanisms in UBOL systems. For example, moisture-driven materials-related distresses, such as freeze-thaw damage and alkali-aggregate reactions, often increase in severity and rate of development with increased presence of water. In addition, the build-up of hydraulic pressure under traffic can result in stripping and erosion of asphalt concrete interlayer materials. These pressures can even cause erosion in cement-based materials, as was found on the A5 in Germany in 1981 when pulverized fines and voids were found between the concrete pavement and cementious base materials, which were constructed without using an interlayer, resulting in many cracked slabs. It was this experience that led the Germans to develop the use of nonwoven geotextile fabric interlayers to provide drainage at this interface (Rasmussen and Garber, 2009).

U.S. anecdotal evidence and the German experience suggest that moisture-related deterioration of the interlayer and/or base (e.g., stripping and erosion) may be best avoided by providing an interlayer material with adequate capacity for moisture egress (e.g., through the use

of a properly selected fabric and/or a drainable layer of asphalt concrete) and by ensuring that the interlayer material itself is resistant to the effects of moisture in the presence of dynamic loads (i.e., stripping, erosion or other degradation). If geotextile or drainable interlayer is used, then that material must be a part of a system that provides positive drainage from the interlayer (e.,. through connection to a drainage system or by "daylighting" the layer to some point (often near the shoulder edge) where the moisture can drain away freely and harmlessly as surface water).

This section of the report deals primarily with the requirements for a drainable interlayer (i.e., drainage paths, required drainage capacity, etc.) and not with issues of material durability (e.g., the use of anti-strip agents in asphalt interlayers), although it is recognized that material durability considerations are also important for the long-term performance potential of the interlayer system.

3.3 Current Guidance

When unbonded concrete overlays are constructed in arid climates, the separation layer may not need significant drainage capacity. However, when UBOLs are constructed anywhere that moisture may reach the interlayer either through surface infiltration or from beneath the pavement, it is recommended that a positive drainage path be provided from all infiltration points to allow moisture to exit the interlayer. Drainable separation layer material options include nonwoven geotextiles that meets certain transmissivity requirements, as well as open-graded or drainable hot-mix asphalt (HMA) materials. In either case, an outlet system must be provided and properly maintained to allow water to escape the pavement system. Details of typical drainage outlet systems for UBOL interlayers are provided in Harrington and Fick (2014). A discussion of current guidance concerning the drainage requirements for asphalt and geotextile separator layer systems is presented below.

3.3.1 Asphalt Separation Layers.

Asphalt-based materials have been used as UBOL separation layers for many years. Asphalt stripping problems have occasionally developed within these interlayers under repetitive heavy loading in the presence of water, typically over the course of several years, causing a loss of support for the unbonded concrete overlay (see Figure 28). This loss of overlay support has led to the premature failure of some UBOLs. This type of problem may be more likely with relatively thin concrete overlays where higher load-related slab deflections are more likely to induce stripping, erosion and asphalt deformation problems.

Figure 28. Photo of asphalt stripping/raveling under concrete overlay (left) and overlay damage resulting from loss of support (right)

Solutions to these potential problems include the use of anti-strip additives in the asphalt mix and the use and maintenance of joint seals in the concrete overlay and along the lane-shoulder longitudinal joint. However, some engineers believe that a more reliable approach is to provide for the rapid removal of water from the interlayer through the use of a drainable/permeable asphalt material and/or a nonwoven geotextile fabric interlayer with acceptable permeability characteristics (as are described in the next subsection). The use of drainable asphalt or geotextile materials requires that the interlayer is "daylighted" or connected to a drainage conduit to carry water from the pavement system.

The development of a drainable (but structurally stable) asphalt-based interlayer can be accomplished by decreasing the amount of fine aggregate and increasing the amount of 3/8" aggregate in the mixture. An example aggregate gradation for a drainable asphalt interlayer is given in Table 12, and a photo of an asphalt concrete interlayer that uses this specification is shown in Figure 29.

Table 12. Michigan DOT Aggregate Gradation for Drainable Asphalt Interlayer (Harrington and Fick, 2014)

Sieve Size	Percent Passing
½ inch	100
⅜ inch	85–100
No. 4	22–38
No. 8	19–32
No. 16	15–24
No. 30	11–18
No. 50	8–14
No. 100	5–10
No. 200	4–7

Figure 29. Photo of Michigan DOT Drainable HMA Separation Layer

3.3.2 Geotextile Fabric Separation Layers

The ability of geotextiles to function as a drainage layer can be described as follows: water infiltrates the pavement surface (or other sources) and becomes trapped within the interlayer; the water then migrates within the material across the pavement cross-slope; water within the interlayer egresses along the edges of the material ("daylighting") or into a subdrain water collection system. This drainage function reduces the potential for water ingress to penetrate supporting layers and cause loss of support and premature overlay failure (Garber and Rasmussen, 2010).

The ability of the geotextile fabric to allow moisture transport is a function of the permeability and transmissivity of the material after it has been installed in the constructed pavement system and is partially compressed by the weight of the layers placed above it. Rasmussen and Garber (2010) presented the following recommendations for geotextile fabric permeability and transmissivity based on guidance provided in German design publications and the result of numerous discussions with German practitioners:

- Water permeability in normal direction under load:
  - ≥3.3E-4 ft/s at 2.9 psi pressure
  - (tested in accordance with DIN 60500-4 [modified ASTM D 5493 or ASTM D 4491]).
- In-plane water permeability (transmissivity) under load:
  - [a] ≥1.6E-3 ft/s at 2.9 psi pressure; or
  - [b] ≥6.6E-4 ft/s at 29 psi pressure
  - (tested in accordance with ISO 12958 [modified ASTM D 6574 or ASTM D 4716])

The values given above (among other physical and mechanical property requirements for nonwoven geotextile fabric) were considered to be a starting point for the development of specifications for these materials in the U.S. The ASTM test standards cited are the result of an effort to find standards commonly used in the U.S., but it was recommended that the original ISO and DIN tests be considered standard in the U.S. until full equivalency can be established

between the U.S. and European tests (Rasmussen and Garber, 2010). A list of accredited laboratory facilities capable of conducting these tests can be found on The Geosynthetic Institute web site (www.geosynthetic-institute.org).

It should be noted that the movement of water through the fabric is also affected by dynamic loading effects, as researched by Lederle et al (2013) and described in Section 3.4 of this report.

3.3.3 Construction Details Affecting Separation Layer Drainage

All UBOL separator layer materials (both drainable and impervious) must allow water to leave the system to avoid trapping water in the system, which can be very damaging. Interlayer drainage must channel infiltrated water along the pavement cross-slope to the pavement drainage system (subdrain) or to the pavement edge to allow water to flow away from the pavement structure. This is consistent with German practice, which requires that geotextile interlayers either terminate next to a drainage layer or be daylighted (allowing egress of water) (Rasmussen and Garber, 2009).

Garber and Rasmussen (2010) recommend that the free edge of geotextile fabric interlayers should extend beyond the edge of the new concrete overlay at least 4 inches to a location that facilitates drainage (i.e., "daylighted" or into an open-graded base material). Similar practice should be observed for drainable asphalt-based interlayer materials as well. Harrington and Fick (2014) present several schematic drawings of drainage outlet arrangements for various separation layers.

Existing pavement drainage needs and capabilities should be evaluated prior to design of the overlay project to determine the need for any steps required to ensure adequate drainage of the unbonded concrete overlay system (e.g., installation of retrofit edge drains, the need to "daylight" existing subbase materials, etc.). When existing underdrains are present, they should be inspected, cleaned, and repaired (if necessary) prior to construction of the overlay (Harrington and Fick, 2014).

Additional aspects of the pavement structure that should be considered in the design of the UBOL interlayer drainage system are the pavement geometrics (i.e., profile, cross-slope and joint layout) and the details of the overlay joint system, which vary widely with state practices. For example, a change in profile and/or cross-slope can be designed in the overlay so that water is more readily shed from the pavement surface with less infiltration of joints. Overlay joints can be designed to resist excessive ingress of water by constructing them with a narrow, single saw cut and/or filling or sealing them appropriately (Harrington and Fick, 2014). Some states are convinced that pavement joints, in general, (and UBOL joints, in particular) must be sealed, while others believe that the joints should be cut narrow and remain unsealed. Whether the joints are sealed or unsealed, the UBOL interlayer drainage system should be designed to remove any water collected in the pavement structure.

3.4 Recent Research Concerning Interlayer Drainage

A recent study at the University of Minnesota led by members of the research team examined the measured flow rate and velocity of water draining through an interlayer fabric in a UBOL under static and dynamic loading conditions using a laboratory-based full-scale accelerated pavement loading test stand. The objective of this work was to characterize the drainage provided by a nonwoven geotextile fabric interlayer in an unbonded concrete overlay system (Lederle et al, 2012). Figure 30 presents a schematic of the test set-up used in this study.

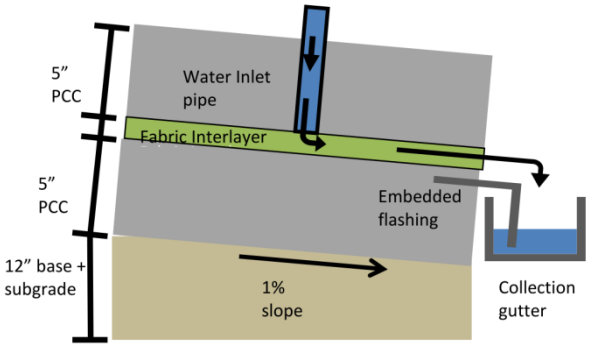

Figure 30. Schematic of apparatus used to test the effects of static and dynamic loads on the flow of water through a geotextile fabric interlayer in an unbonded concrete overlay of concrete pavement (Lederle et al, 2012)

Results of this study found that the drainage provided by the fabric interlayer exceeded the previously stated in-plane requirements for transmissivity during both static and dynamic loading. It is worth noting that the researchers found that the fabric interlayer drained more quickly during the dynamic load test than during the static load test. This was attributed to the fact that dynamic loading induced a pumping action that engaged a larger area of the fabric in carrying the infiltrated water (Lederle et al, 2012).

3.5 Considerations for Future Separation Layer Drainage Design Guidance

There appears to be little evidence of widespread interlayer drainage-related failures of UBOLs when current recommendations for separation layer material properties and construction are followed, so current recommendations may be sufficiently conservative that modifications are not needed to prevent moisture-related distress in UBOLs. However, it must be kept in mind that the oldest UBOLs constructed in the U.S. using nonwoven geotextile fabric interlayers are currently less than 6 years old, so long-term performance trends are not yet available. In any event, it is worth considering the potential impacts of newly developed transmissivity trends from the research of Lederle et al (2012) on interlayer design, and it is noted that well-established pavement drainage design analyses may be useful for evaluating the drainage requirements of UBOL separation layers.

3.5.1 Dynamic Transmissivity

Lederle et al (2013) found that the average rate of flow of water through a dynamically loaded geotextile fabric interlayer was approximately three times higher than the average flow rate observed for static loading conditions. Therefore, it is reasonable to assume that an increase in functional flow rate or transmissivity (beyond that measured by the ISO, DIN and ASTM tests cited previously) will be observed under field service loading conditions. Future permeability requirements for geotextile fabrics should reflect these benefits. Since the dynamic testing performed by Lederle et al was done at a constant load rate of 2 Hz, it is likely that the observed increases in flow rate are different from those that would be observed under service loads that are applied at different frequencies. Additional research will be required to better quantify this effect and to develop guidelines for considering the effect in interlayer drainage design.

Lederle et al did not examine the effects of dynamic loading on the flow rate (and effective transmissivity) of drainable asphalt interlayer materials. This is another area that

should be researched to determine whether the effects are significant and worthy of consideration in separation layer design.

3.5.2 Determination of Interlayer Drainage Requirements Based on Net Inflow

The technical rationale for the selection of the currently recommended geotextile permeability and transmissivity requirements described by Garber and Rasmussen (2010) are not readily apparent in the literature. Similarly, the role of interlayer drainage is not currently a consideration in determining the thickness or required transmissivity of asphalt-based interlayers. Two approaches to considering drainage requirements in UBOL interlayer design are possible through the application of the principles of highway drainage design that were set forth by Moulton (1980).

In the first approach, the drainage layer (or, in this case, interlayer) is designed with a combination of thickness and permeability to allow the removal of the net infiltrated water flow, q_n (steady state). Several potential sources of water inflow can be considered, but the most significant for UBOL interlayer design are the surface infiltration water (through cracks, joints and general pavement permeability), q_i, and the vertical outflow through the layer beneath the drainage layer (in this case, the pavement being overlaid), q_v, which reduces the flow of water that must be carried by the interlayer.

Moulton provides typical design inputs and design charts for determining q_i and q_v based on many factors, including joint patterns, surface permeability, pavement cross-slope and profile, etc. Once q_n has been determined (as $q_i - q_v$), it is a relatively simple matter to determine the thickness and permeability of the drainage layer (H_d and k_d, respectively) to carry the net inflow to an outlet (subdrain or daylight). Both parameters could be varied for asphalt-based separator layers to "optimize" the design of the layer. For geotextile interlayers, the statically compressed layer thickness would probably need to be limited to avoid excessive pavement deflections under dynamic loading, so this approach would yield only the required geotextile in-plane and vertical permeability values for a given thickness of material.

3.5.3 Determination of Interlayer Drainage Requirements Based on Time To Drain

Moulton (1980) recognized that it might not always be practical to develop drainage layer requirements based on net inflow because the required layer thickness or permeability might be unreasonably high. He also recognized that the amount of water that actually infiltrates the pavement is directly related to the ability of the drainage layer to remove that water; in other words, a drainage layer that is unable to carry the design net inflow of water will simply become saturated and the actual inflow will be limited by the ability of the drainage layer to remove it. Water that cannot infiltrate the pavement will run off the pavement surface and, assuming it does not create a hydroplaning hazard, will be of little concern.

If it is accepted that the interlayer (drainage layer) will become saturated and if it is acknowledged that the presence of excess moisture in the interlayer may reduce pavement life through durability, potential erosion and other mechanisms, then the goal in interlayer design can become one of limiting the time during which the interlayer is critically saturated to a relatively short time period after each saturating event.

Moulton (1980) presents a well-accepted method for estimating the time-dependent drainage characteristics of a saturated drainage layer. The analysis considers the permeability, thickness, slope and effective width of the drainage layer. For granular drainage layers, it has often been suggested that saturation levels should drop to 85% or less within 5 – 10 hours to

prevent unacceptable base layer deformations and loss of support. Similar guidance concerning both critical saturation levels and the acceptable time required to achieve those levels would need to be developed for UBOL interlayer applications. It is likely that these values would be different for geotextile interlayers than for asphalt-based interlayers, and that the allowable times-to-drain for either of these relatively durable materials would be significantly longer than those that have been adopted for granular base materials. The development of these criteria is a subject for future study.

3.6 Recommended Guidelines for UBOL Separation Layer Drainage

As was noted previously, there is no evidence of widespread interlayer drainage-related failures of UBOLs when current recommendations for separation layer material properties and construction are followed, although it is noted that the oldest UBOLs constructed in the U.S. using nonwoven geotextile fabric interlayers are currently less than 6 years old, so long-term performance trends are not yet available. Based on this premise, the following guidelines for UBOL separation layer drainage are offered:

- The potential for damage to the proposed interlayer material and supporting layers must be thoroughly evaluated (through field experience and/or laboratory testing) and considered in determining the need for providing a drainable interlayer. UBOLs constructed in areas with relatively low incidence of precipitation, light traffic, and/or with conventional pavement thickness and using erosion- and strip-resistant base materials may not require drainable interlayer materials. It should be borne in mind that German studies found erosion of cement-treated base materials under relatively thick concrete pavement sections when geotextile fabrics were not used (Rasmussen and Garber, 2009).
- The degree of need for (and potential benefits of) a drainable interlayer material must sometimes be weighed against construction staging, economics and other considerations. Examples might include:
    - when considering the use of existing HMA overlay material as a separation layer vs complete removal of that material and placement of a new interlayer material; and
    - when staging construction in a manner such that requires the interlayer to be subjected to construction or service traffic.
- When dense-graded or non-drainable HMA interlayers are used, the use of an effective anti-strip additive (proven in preconstruction testing and accepted by the specifying agency) is highly recommended.
- Current guidance for the physical and mechanical properties of geotextile fabric separator layers and drainable asphalt concrete interlayers appears to be adequate and their continued use is recommended until more refined requirements are developed.
- Positive drainage systems must be provided (and maintained) in conjunction with the use of any drainable separator layer materials to allow the egress and removal of intercepted water. Such systems may include the use of adequate pavement cross-slope in combination with pavement subdrain systems or egress through “daylighted” interlayer construction. Failure to properly maintain these drainage systems may result in the

storage of water in the interlayer and lower level of overlay performance than would have resulted from using an undrained interlayer material.

3.7 Recommendations for Future Research and Development

The following is a summary of research needs related to the improvement of guidelines for UBOL separation layer drainage, as mentioned previously in this report or as suggested by project technical advisors:

- Conduct laboratory and field performance studies to more precisely determine the combinations of climatic and loading conditions that do not require interlayer drainage for specific overlay design parameters (thickness and joint design/layout) and interlayer material properties.
- Determine and document the source and justification for current geotextile fabric transmissivity requirements and, if necessary or potentially beneficial, develop improved guidance for these requirements based on dynamic loading effects for saturated interlayer materials on various underlying layers (e.g., drainable vs. relatively impervious concrete and asphalt materials).
- Determine appropriate time-to-drain criteria for geotextile and drainable asphalt materials to prevent asphalt stripping and/or erosion of underlying support layers,
- Expand the research performed by Lederle et al (2013) to better determine the effects of dynamic loading on the effective transmissivity of both geotextile and drainable asphalt concrete interlayer materials.
- Consider the development of new U.S. Standard Tests (ASTM or AASHTO) that are fully equivalent to the DIN and ISO tests upon which current geotextile fabric interlayer qualifications are based.
- Continue to evaluate the impact of joint sealing and seal maintenance practices on the performance of UBOLs.
- Determine the relative stripping resistance of dense-graded asphalt concrete vs. drainable asphalt concrete when other factors are held constant.
- Determine “optimal” properties for geotextile fabric and drainable asphalt concrete. For drainable asphalt concrete, this should reflect consideration of both stability and drainability, as well as the impact of creep or secondary consolidation on reduced drainage characteristics.

REFERENCES

ASTM International. (2005). Standard Test Method for Compressive Strength of Cylindrical Concrete Specimens. ASTM Standard C 39. West Conshocken, PA.

ASTM International. (2009). Standard Test Method for Repetitive Static Plate Load Tests of Soils and Flexible Pavement Components, for Use in Evaluation and Design of Airport and Highway Pavements. ASTM Standard D1195/D1195M. West Conshocken, PA.

ASTM International. (2013). Standard Practice for Making and Curing Concrete Test Specimens in the Laboratory. ASTM Standard C 192. West Conshocken, PA.

ASTM International. (2014). Standard Test Method for Static Modulus of Elasticity and Poisson's Ratio of Concrete in Compression. ASTM Standard C 469. West Conshocken, PA.

ASTM International. (2015). Standard Test Method for Flexural Strength of Concrete (Using Simple Beam with Third-Point Loading). ASTM Standard C 78. West Conshocken, PA.

ASTM International. (2015). Standard Test Method for Measuring Pavement Macrotexture Depth Using a Volumetric Technique. ASTM Standard E 965. West Conshocken, PA.

CP Tech Center. 2009. "Use of Nonwoven Geotextiles as Interlayers in Concrete Pavements Systems." MAP Brief 7-1. National Concrete Pavement Technology Center, Iowa State University. Ames, IA.

Federal Highway Association (2015). Long-Term Pavement Performance Data Online. http://www.infopave.com/. Accessed September 17, 2015.

Garber, S. and R. Rasmussen (2010). "Nonwoven Geotextile Interlayers in Concrete Pavements." Transportation Research Record: Journal of the Transportation Research Board, Issue No. 2152: Construction 2010, Volume 2. Transportation Research Board. Washington, D.C. pp. 11-15.

Harrington, D. (2008). *Guide to Concrete Overlays: Sustainable Solutions for Resurfacing and Rehabilitating Existing Pavements*. 2nd Edition. Report No. TB021.02P, American Concrete Pavement Association, Rosemont, IL.

Harrington, D. and G. Fick (2014). Guide to Concrete Overlays: Sustainable Solutions for Resurfacing and Rehabilitating Existing Pavements (Third Edition). ACPA Publication TB021.03P. National Concrete Pavement Technology Center, Iowa State University. Ames, IA.

Khazanovich, L., and A. Booshehrian (2015). "Dynamic visco-elastic analysis of falling weight deflectometer deflections for rigid and flexible pavements." Accepted for publication in *Transportation Research Record: Journal of the Transportation Research Board*.

Lederle, R. E., K. Hoegh, T. Burnham, and L. Khazanovich (2013). "Drainage Capabilities of a Nonwoven Fabric Interlayer in an Unbonded Concrete Overlay." Paper No. 13-4107 in *TRB 92nd Annual Meeting Compendium of Papers*, Transportation Research Board 92nd Annual Meeting, January 13-17, 2013, Transportation Research Board, Washington D.C.

Maitra, S. R., Reddy, K. S., and L.S. Ramachandra. (2009). Experimental Evaluation of Interface Friction and Study of Its Influence on Concrete Pavement Response. *Journal of Transportation Engineering*, 135(8), 563–572.

Moulton, L.K. (1980). Highway Subsurface Design. FHWA-TS-80-224. Federal Highway Administration. Washington, D.C.

Rasmussen, R. and S. Garber (2009). Nonwoven Geotextile Interlayers for Separating Cementitious Pavement Layers: German Practice and U.S. Field Trials. Federal Highway Administration. Washington, D.C.

Rasmussen, R. O., and D.K. Rozycki. (2001). Characterization and modeling of axial slab-support restraint. *Transportation Research Record: Journal of the Transportation Research Board*, 1778(1), 26–32.

Ruiz, J. M., Kim, P. J., Schindler, A. K., and R.O. Rasmussen. Validation of HIPERPAV for Prediction of Early-Age Jointed Concrete Pavement. *Transportation Research Record: Journal of the Transportation Research Board*, 1778(1), 17–25.

Smith, K. D., H. T. Yu, and D. G. Peshkin (2002). Portland Cement Concrete Overlays: State of the Technology Synthesis. Report No. FHWA-IF-02-045. Federal Highway Administration, U.S. Department of Transportation, Washington D.C

APPENDIX A. EXTENDED LABORATORY REPORTING

Appendix disclaimer and acknowledgements

Mentions of named products in this report are not endorsements of these products. The authors gratefully acknowledge the assistance provided by Andrew Bennett and John Staton of the Michigan Department of Transportation, Thomas Burnham, Robert Strommen, and Jack Herndon at the MnROAD Research Facility, Derek Tompkins of the University of Minnesota, Rob Golish from the Minnesota Department of Transportation and the C. S. McCrossan Company for their assistance in obtaining field samples. Retrieving these samples was a great challenge but imperative to the success of this task. Additionally, the supply of the nonwoven geotextile fabrics and technical expertise provided by Eric Littel from Propex is also greatly appreciated.

Introduction

An unbonded concrete overlay of an existing concrete pavement is a Portland cement concrete (PCC) overlay separated from the existing concrete slab by an interlayer (Smith, Yu, & Peshkin 2002). The purpose of the interlayer is to reduce stress transferbetween the existing concrete layer and the overlay. Interlayers commonly consist of hot mix asphalt (HMA) or nonwoven geotextile fabric. Unbonded concrete overlay systems are becoming increasingly popular pavement rehabilitation techniques. This is due to the fact that they are durable, mitigate reflective cracking, require minimal pre-overlay repairs and preparation, and can be placed with traditional concrete pavement paving methods. Additionally, unbonded overlays have performed very well over the last 30 years (Harrington, Degraaf, & Riley, 2007).

In this study, a laboratory investigation is employed to examine the effects of the interlayer on the response of the pavement structure under load. Beam specimens are tested to evaluate three different mechanisms. Both hot mix asphalt and nonwoven geotextile fabric interlayer systems are considered. The objective of this study is to establish parameters for these interlayers that can be used to develop structural models, which, in turn can be used to develop a mechanistic-empirical design procedure for unbonded concrete overlays.

Four mechanisms are being examined using four separate test setups. The mechanisms considered are:

1. Deflection characteristics of the interlayer
2. Friction developed along the interface between the interlayer and the overlay
3. Ability of the interlayer to prevent reflective cracking
4. Bond strength at the interfaces of the interlayer

The specimens for evaluating mechanisms 1 through 3 consist of an overlay beam cast on top of the interlayer and existing concrete beam. The depth and width of both the overlay and the existing beams was chosen to be 6 inches. The measured deflection characteristics and interface

friction will be used to establish stiffness and shear transfer for validating the structural models. The results from mechanism 3 testing will be used to assess the potential for reflective cracking and, if necessary, to develop a reflective cracking model. The test setup for mechanism 4 will allow the research team to obtain an understanding as to how debonding between the existing and overlay concrete layers may occur in the field and if generated curling stresses are significant enough to cause the separation observed from this testing

Interlayers

The nonwoven geotextile fabrics used for this study were manufactured by Propex and consisted of a thick and a thin fabric. The thick fabric weighed 15 oz/yd^2 and was dark in color. The thinner white colored fabric, called Reflectex, was made specifically for this study and weighed 10 oz/yd^2 In this report, the fabrics will be called F15 and F10 for the thick and the thin fabrics, respectively. These fabrics can be seen in Figure A-1. For this study, the fabrics are attached to the existing concrete beams with a geotextile glue made by 3M called Scotch-Weld HoldFast 70 Adhesive.

Figure A-1. F15 on the Left and F10 on the Right

The specimens with asphalt interlayers were sawed from in service pavements to ensure that mixture proportioning and density of the asphalt interlayers are typical of those found in the field. These asphalt-concrete composite beams were obtained from the Minnesota and Michigan Departments of Transportation (DOT)'s. The Michigan DOT provided beams with dense graded asphalt interlayers as well as beams with open graded asphalt mix interlayers. The dense graded asphalt interlayer is approximately 1 inch thick and the open graded interlayer is approximately 2 inches thick. The Minnesota DOT provided specimens from a concrete pavement that had previously been overlaid with asphalt. Some of the beams were cut prior to milling the dense graded asphalt overlay and the others were cut after some of the asphalt had been milled. The Minnesota DOT also provided beams cut immediately after an open graded asphalt was placed on a distressed existing pavement. A summary of asphalt specimen sources, ages, and average asphalt thicknesses is provided in Table A-1. For each of the beam specimens,

sand patch testing (ASTM E965) was performed and dimensions were measured. This information is summarized in Appendix 6.

Table A-1. Sources of Asphalt Samples Collected

Roadway	Asphalt Description	Ave. Asphalt Thickness
US-131, MI	Old, dense graded	1 in
US-131, MI	Old, open-graded	2 in
I-94, MnROAD	Old, dense graded, milled	0.875 in
I-94, MnROAD	Old, dense graded, unmilled	2.75 in
US-169, MN	New, open graded (PASSRC)	1.75 in

Specimen Designation

All specimens consisted of a bottom beam representing the existing concrete being overlaid, an interlayer, and a concrete beam on the top of the interlayer representing the overlay. The specimens with the fabric interlayers were made by first casting the bottom beam using a high strength mix representative of concrete properties for a 30-year old paving mix. Next, the fabric interlayer was glued to the top surface of the bottom beam. Finally, a beam was cast on top of the fabric using a standard paving mix. For the specimens with the asphalt interlayer, the top beam was cast using the same standard paving mix used for casting the top beam of the fabric layer specimens.

Each finished specimen has its own code identifying when each layer was cast (if it was not obtained in the field) and a description of the interlayer. The nomenclature is shown in Figure A-2. From left to right, the first four numbers represent the month and date of cast, the middle letters and numbers are the interlayer designation, and the last letter indicates the batch number for the day of casting. The labeling designating each asphalt interlayer is defined as follows:

- unmilled, dense graded asphalt from Michigan = MIDAU
- unmilled, open graded asphalt from Michigan = MIOAU
- unmilled, dense graded asphalt from Minnesota = MNDAU
- milled, dense graded asphalt from Minnesota = MNDAM
- unmilled, open graded asphalt from Minnesota = MNONU

For the fabric interlayer specimens, the letter following the fabric designation would indicate whether the concrete layer is an existing or overlay beam as both had to be cast for each fabric specimen.

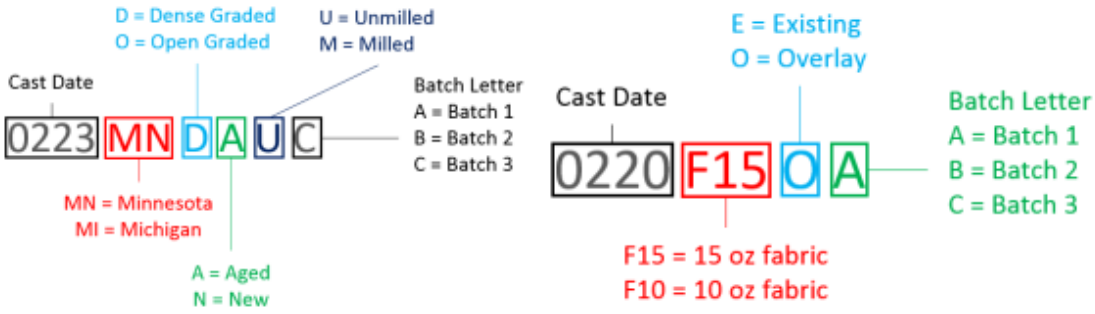

Figure A-2. Asphalt Specimen Designation (Left) and Fabric Specimen Designation (Right)

Mixture Design

The concrete mixture design for the lower beam of the specimens with the fabric interlayer has a water to cementicious material ratio (w/cm) of 0.36 and a target flexural strength of approximately 850 psi. The overlay (top beam) mixture design for all specimens has a w/cm of 0.42 and a target flexural strength of 650 psi. The bottom beam flexural strength is higher than

the overlay flexural strength to simulate aged concrete being overlaid with a traditional overlay mix. Table A-2 summarizes the final mixture design information for the two mixes. All material test data (including compressive strengths, elastic modulus, and modulus of rupture) are summarized in Appendix 1. All specimens were made and cured according to ASTM C192.

Table A-2. Target Mixture Design

Mixture Design for Casting Beams Representative of the Existing Slab			
Material	Weight (lb/cy)	Volume (cft/cy)	Volume fraction
Coarse aggregate, Limestone	1918	11.34	0.42
Fine aggregate	1163	6.98	0.26
Cement, Cemex Type I	650	3.31	0.12
Water	234	3.75	0.14
Air content	-	1.62	0.06
Superplasticizer, Sikament SPMN	17 oz per 100 lbs of cement		
Air entrainer, Sika AIR-360	3 oz per 100 lbs of cement		
Mixture Design for Casting Beams Representative of the Overlay			
Material	Weight (lb/cy)	Volume (cft/cy)	Volume fraction
Coarse aggregate Limestone	2053	12.15	0.45
Fine aggregate	1023	6.14	0.23
Cement, Cemex Type I	600	3.05	0.11
Water	252	4.04	0.15
Air content	-	1.62	0.06
Air entrainer, Sika AIR-360	2 oz per 100 lbs of cement		

NOTE: Due to a calibration error in the air meter, the first four cast days with the overlay mix resulted in a high air content and therefore reduced strengths. Once this error was noted, the air meter was recalibrated, the volume of air entraining admixture was adjusted, and the desired strengths were achieved. All overlay beams tested at 28 days and cast between 2/20/15 and 3/3/15 had a high air content. All specimens tested for reflective cracking with the high air mixture were replicated using the corrected mix.

Mechanism 1: Deflection Characteristics

The deflection characteristics of the interlayer were established using the setup shown in Figure A-3. The composite section consists of a beam representing the existing slab (in strength and stiffness), the interlayer system, and a beam representing the overlay (in strength and stiffness). A load is applied to one side of a joint sawed in the overlay and deflections in the overlay and existing beams are measured by linear variable displacement transducers (LVDTs). A brief discussion of the finite element modeling performed to insure the beam test is representative of the response (deflection and rotation) of the pavement structure is provided. This is followed by a discussion of the hardware used in the setup, the loading regime, and the material properties for the beams tested.

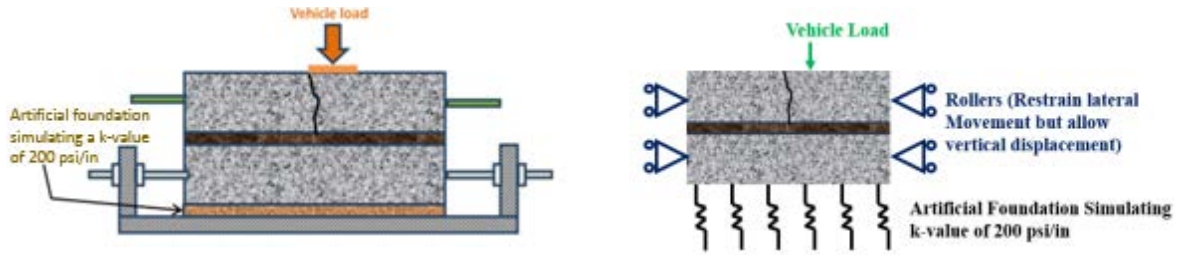

a. b.

Figure A-3. a. Schematic of Deflection Characteristic Test Setup
b. Boundary Conditions of Test Setup

Finite Element Modeling

In order to establish and confirm an appropriate setup and boundary conditions for the specimens, a finite element analysis was employed through the commercially available software ABAQUS™. The goal of the modeling was to establish the specimen length, boundary conditions, and load magnitude and location required to create deflections and rotations representative of those in an overlay loaded by a 9,000 lb design load.

In the computational model, all components were assumed to be elastic solids, no load transfer was provided across the joint, and the three contact conditions between the layers were assumed. Contact conditions included fully bonded, unbonded, and an intermediate level of bond where some shear transfer was allowed. The contact for both interfaces at the interlayer was modified such that every reasonable permutation of contact conditions at the interfaces was considered.

Before any analyses were conducted, it was determined that that rods would be cast into the ends of the beams so they could be connected to the testing frame to provide restraint in the transverse directions. This restraint helps the short beam respond in a more similar nature to a longer slab. At the start of modelling, a few elementary analyses were conducted to determine how to restrain the beam specimen so that it remained in contact with the support layer when a dynamic load was applied. It was eventually determined from a number of analyses that bearings would need to be placed through the overlay beam when testing Mechanism 1. Mechanism 1 consists of a joint in the overlay and the load placed to one side of the beam to determine deflection characteristics as well as load transfer as seen in Figure A-3. Also, a roller bearing was applied to create a pinned condition for facilitating rotation.

Next, the required length of the beam was determined. Three lengths were considered: 24 inches, 30 inches, and 36 inches. Since a modulus of rupture beam is 24 inches long, this was chosen as the minimum value. Due to the considerable depth (slightly over one foot since the depth of both the overlay and existing are 6 inches) of the two beam high structure, it was thought that the length of the overlay specimen should be increased to maintain a length to height ratio similar to a modulus of rupture beam. However, the length should remain as short as possible due to the significant increase in the weight of the stacked beam structure that would have to be moved on and off of the testing frame for each test. Neglecting the interlayer, the specimens would weight approximately 150 and 225 pounds for the 24 and 36 inch long

specimens, respectively. All three beam lengths (24, 30, and 36 inches) were considered in the finite element analyses, and it was found that the beam had to be at least 30 inches long to maintain deflection and rotation characteristics similar to those of a slab. Therefore, it was decided to make each overlay specimen 30 inches long.

Setup

Figure A-4 shows a specimen in the testing frame for Mechanism 1. The loading head contains a ball joint and is the same loading head used for testing the modulus of rupture beams. The foundation support provided by the lower layers under the concrete slab in an in-service pavement was replicated by an artificial foundation of two layers of neoprene pads, known as Fabcel 25 (http://www.fabreeka.com/Products &productId=24). Figure A-5 shows the Fabcel 25 waffle-shaped neoprene pads. The stiffness of the two combined Fabcel layers was determined by conducting a plate load test (ASTM D1195/D1195M), and was found as 200 psi/in. The bearing assembly used to initiate points of rotation can be seen in Figure A-6. The green spring is used in conjunction with a torque wrench to apply the same compression every time. A torque of 40 inch-pounds was applied to the bearings for all specimens. Additional restraint was provided by vertical rollers on both the loaded and unloaded sides of the beam on the front and back to prevent horizontal displacement of the specimen. Figure A-7 shows the components of this assembly.

Figure A-4. Mechanism 1 Setup

Figure A-5. Neoprene Fabcel 25

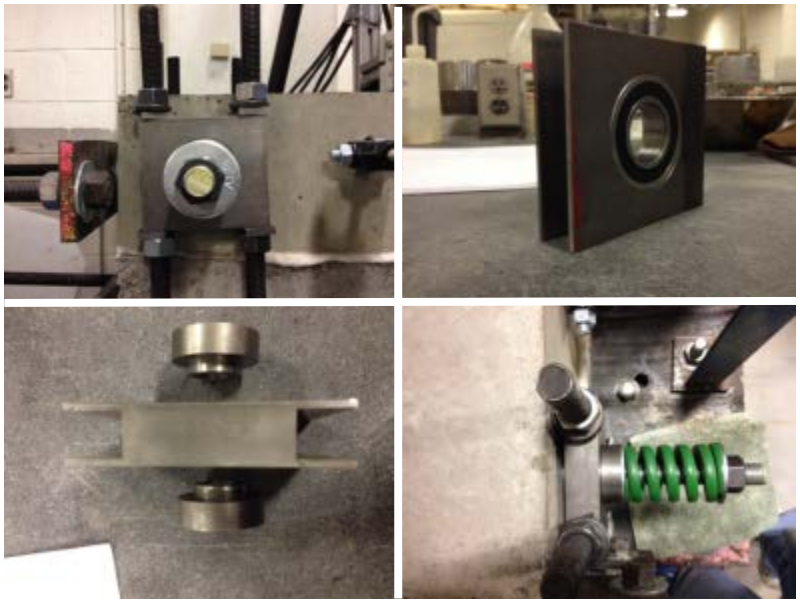

Figure A-6. Bearing Assembly

Figure A-7. Roller Assembly

Displacement is measured using eight LVDTs. The LVDT locations are as shown in Figure A-8. Displacement is measured at 1.5 inches from the center saw cut joint on the top of the overlay beam and at mid depth of the lower beam representing the slab being overlaid. The locations of LVDTs 5, 6, 7, and 8 are opposite of 1, 2, 3, and 4. Therefore, displacements measured by LVDTs 2 and 6 are averaged to obtain the overlay loaded (OL) deflection, 1 and 5 are averaged to obtain the overlay unloaded (OU) deflection, 3 and 7 are averaged to obtain the existing unloaded (EU) deflection, and 4 and 8 are averaged to obtain the existing loaded deflection (EL).

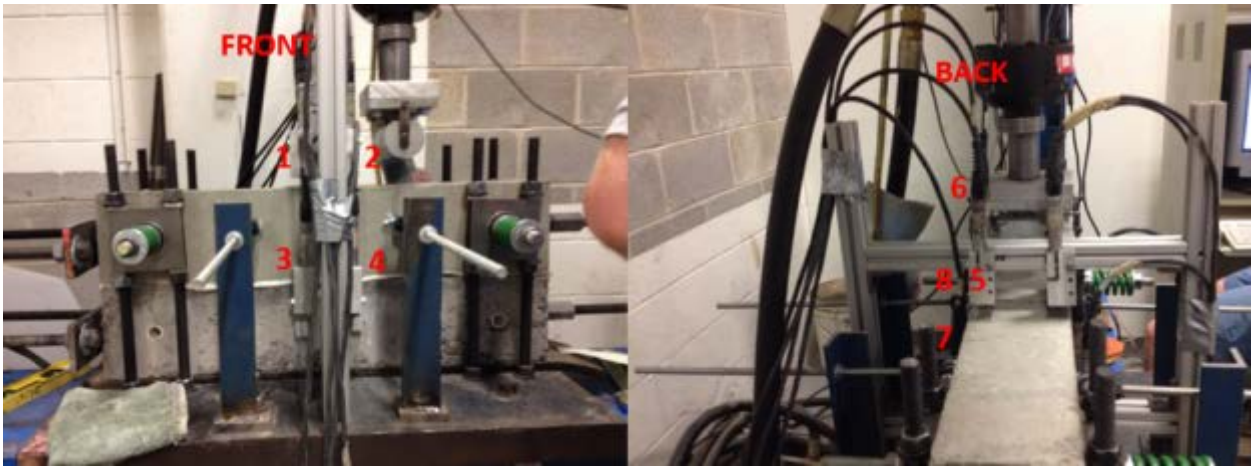

Figure A-8. LVDT Locations

Loading

The dynamic load applied to the specimen to test Mechanism 1 is intended to simulate a vehicle traveling 65 mph over 10 inches and the specimen is loaded at a rate of 7 Hz. 7 Hz was chosen as the loading frequency as it enables testing of specimens to occur in a reasonable time while still allowing for data to be sampled and show a clear time history of load and displacement. A constant 25 pound minimum load is maintained for a 0.134 second rest period. A haversine load which approximates the stress pulse of a moving vehicle is applied over a 0.0087 second duration with a peak load of 600 pounds. Testing was carried out for at least 300,000 cycles for each specimen. A static sweep from the seat load of 25 pounds to 600 pounds is conducted at 50, 100, 500, 1000, 2000, 5000, 10k, 20k, and every 10k loading cycles afterwards. The 600 pound load induced a similar deflection and angular rotation in the beam to that of a 9-kip falling weight deflectometer load applied to an overlay in the field.

A total of 16 specimens were tested using the Mechanism 1 setup and loading. Table A-3 provides summary information about each Mechanism 1 specimen. Displacement vs. load cycle, interlayer compression vs. load cycle, and LTE vs. load cycle plots for each specimen can be found in Appendix 2.

Table A-3. Summary Information for Mechanism 1 Specimens

Specimen	Test Date	Overlay Elastic Modulus and Compressive Strength	Temp and Rel Humidity @ Test Time
0211F15EA 0220F150A	3/20/15	E = 3.11 million psi f'_c = 2666 psi	69.4ºF (51%)
0302F15EA 0303F150A	4/1/15	E = 3.04 million psi f'_c = 2156 psi	70.2ºF (51%)
0312F10EA 0330F10OB	4/8/15	E = 3.81 million psi f'_c = 3881 psi	71.5ºF (52%)
0316F10EB 0402F10OB	4/9/15	E = 3.88 million psi f'_c = 4512 psi	71.9ºF (51%)
0223MNDAUA	3/25/15	E = 3.28 million psi f'_c = 2326 psi	69.8ºF (48%)
0417MNDAUC	4/23/15	E = 3.88 million psi f'_c = 4590 psi	70.8ºF (47%)
0319MNDAMA	4/2/15	E = 4.94 million psi f'_c = 6833 psi	71.7ºF (49%)
0422MNDAMA	4/28/15	E = 4.3 million psi f'_c = 4696 psi	71.4ºF (45%)
0226MNONUA	3/27/15	E = 3.11 million psi f'_c = 2237 psi	70.7ºF (59%)
0522MNONUA	5/27/15	E = 4.65 million psi f'_c = 5131 psi	72.2ºF (51%)
0424MIDAUB	4/29/15	E = 4.23 million psi f'_c = 4694 psi	72.6ºF (41%)
0515MIDAUC	5/20/15	E = 4.78 million psi f'_c = 5357 psi	71.3ºF (36%)
0513MIOAUB	5/19/15	E = 4.71 million psi f'_c = 5013 psi	72.3ºF (58%)
0520MIOAUA	5/26/15	E = 4.62 million psi f'_c = 5073 psi	72.6ºF (53%)

Mechanism 2: Modified Push-Off

Shear transfer at the interlayer is a critical parameter in the design of unbonded overlays because the interlayer system must be able to provide a slip plane to allow the overlay to move freely

with respect to the existing pavement. On the other hand, field observations have indicated that some interlayer systems do not provide sufficient restraint to allow for joint deployment. This can lead to high curling stresses, and the joints that actually do crack are wide. Therefore, an unbonded overlay interlayer system must both have sufficient slip to allow free movement of the overlay and provide sufficient restraint for joint deployment.

Interaction between a concrete slab and a granular or stabilized base layer is traditionally characterized using the Push-Off Test (Maitra, Reddy, & Ramachandra, 2009)(Ruiz, Kim, Schindler, & Rasmussen, 2001)(Rasmussen and Rozycki 2001). In this test, a small section of pavement is cast a short distance away from a paved lane. The paved lane acts as a rigid support and a hydraulic jack or actuator is used to displace the test section. The displacement of the test section is measured using a displacement measurement device rigidly fixed to the subgrade. The resistance to sliding is reported either as a force per unit area of interface or as a friction coefficient. The friction coefficient is the frictional force divided by the weight of the slab. When a chemical bond exists between the slab and the base, the sliding resistance will not be proportional to the slab weight, therefore it is more logical to report the force per unit area than the friction coefficient.

In order to characterize the resistance to sliding of each interlayer system, a modified push-off test was performed in the laboratory. In this test, a joint is sawn in the overlay of a 30-inch beam. The bottom beam is not sawn, and both ends of this beam are restrained to prevent translational displacement. One side of the overlay is also restrained against displacement. The other side of the overlay is attached to a threaded rod instrumented with strain gauges to record force. Two LVDTs attached to the loading frame are used to measure displacement of the loaded section. A thrust bearing attached to the vertical actuator is placed on the top of the loaded section of the overlay beam near the joint to prevent vertical displacement. The actuator is used in a displacement control mode to ensure no vertical displacement of the test block occurs near the joint during a test. The variable force provided by the actuator prevents rotation of the loaded half of the overlay and subsequent tensile debonding failure near the joint. A schematic of the test setup can be seen in Figure A-9, and a picture of the test setup can be seen in Figure A-10.

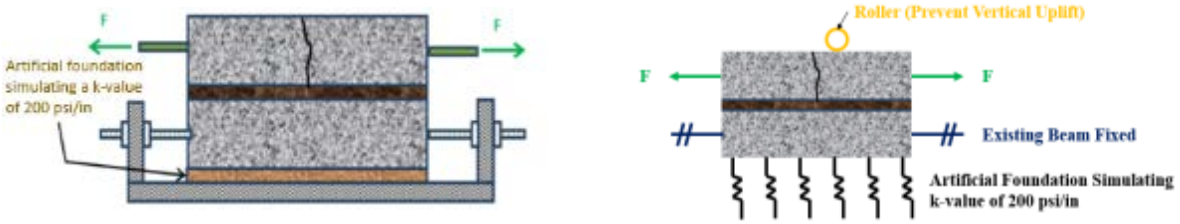

a. b.

Figure A-9. a. Schematic of Modified Push Off Test Setup
b. Boundary Conditions of Modified Push Off Test Setup

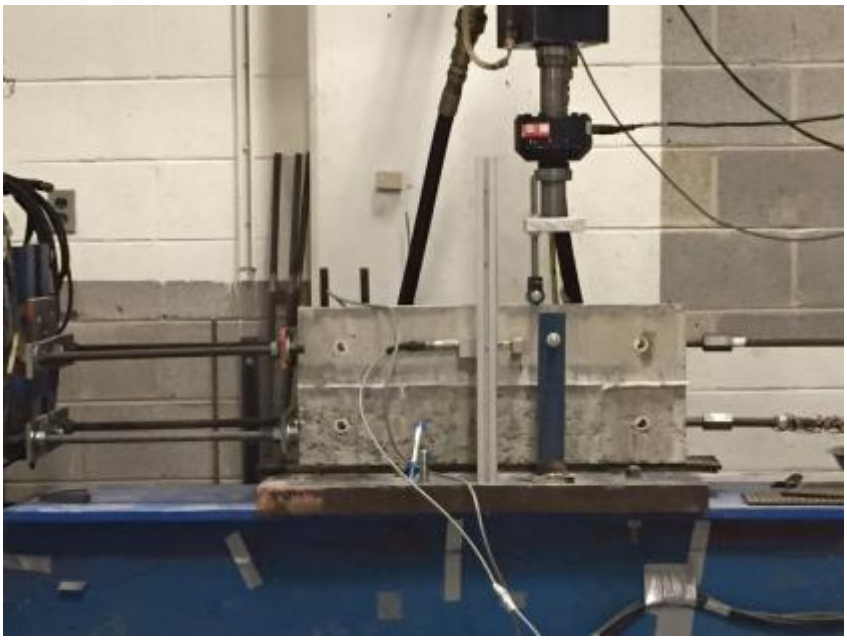

Figure A-10. Picture of Mechanism 2 Test Setup

The horizontal push-off load is applied by manually tightening the instrumented threaded rod. The modified push-off test has two phases. Phase 1 is the cyclic loading phase. In this phase, load is applied until the loaded portion of overlay reaches approximately 80 mils of displacement. The 80 mil displacement corresponds to a 100 degree Fahrenheit drop in temperature for a 12 foot slab cast of concrete with a thermal coefficient of expansion of 5.3 microstrain per degree F. The load is then held constant to observe the relaxation of the interlayer system until the force is relatively constant over time. The load is then removed from the rod. To account for non-elastic displacement, a load is applied in the opposite direction of the initial load until the overlay section returns to its initial position. This position is then held until the force is relatively constant over time. The load, relaxation, opposite load cycle is repeated between 6 to 8 times for each test. Phase 2 is the ultimate loading phase. In this phase, load is applied until the interlayer system fails, or very large displacements (over one inch) are observed.

The modified push-off test was performed on nine different interlayer systems. The details of these systems are shown in Table A-4. Please note that the attachment to the existing concrete taken from the field could be an asphaltic or cementitious bond. If it is an asphaltic bond then the HMA was placed on hardened concrete. If it is a cementitious bond then the concrete was placed wet onto the asphalt. The test date, elastic modulus for the concrete overlay, and temperature and relative humidity at the time of testing for each specimen are shown in Table A-5.

Table A-4. Summary of Interlayers Tested

Label	Source	Grading	Surface	Age	Fabric Weight	Attachment to Existing Concrete
F15-Glued	Propex	n/a	n/a	n/a	15 lb/yd^2	Glued
F15-Pinned	Propex	n/a	n/a	n/a	15 lb/yd^2	Pinned[1]
F10-Glued	Propex	n/a	n/a	n/a	10 lb/yd^2	Glued
F10-Pinned	Propex	n/a	n/a	n/a	10 lb/yd^2	Pinned[1]
MNDAU	MnDOT	Dense	Unmilled	Aged	n/a	Asphaltic Bond
MNDAM	MnDOT	Dense	Milled	Aged	n/a	Asphaltic Bond
MNONU	MnDOT	Open	Unmilled	New	n/a	Asphaltic Bond
MIDAU	MDOT	Dense	Unmilled	Aged	n/a	Cementitious Bond
MIOAU	MDOT	Open	Unmilled	Aged	n/a	Cementitious Bond

[1]Note: Fabric was pinned to existing concrete using gas powered gun to attach 2 fasteners to each beam approximately 6 inches from the edge. This is how the fabric would be pinned in the field.

Table A-5. Summary Information for Mechanism 2 Beams

Corresponding Beam Nomenclature	Test Date (Time)	Overlay Elastic Modulus and Compressive Strength	Temp and Rel Humidity @ Test Time
0211F15EB 0220F150B (Glued)	3/20/15 (12:15 PM)	E = 3.11 million psi f'_c = 2666 psi	69.6^{o}F (51%)
0302F15EB 0303F10B (Glued)	4/1/15 (9:15 AM)	E = 3.04 million psi f'_c = 2156 psi	70.0^{o}F (51%)
0413F15EA 0506F15OA (Pinned)	5/11/15 (5:00 PM)	E = 4. 63 million psi f'_c = 5334 psi	71.4^{o}F (56%)
0413F15EB 0506F15OB (Pinned)	5/12/15 (12:15 PM)	E = 4. 63 million psi f'_c = 5334 psi	71.8^{o}F (54%)
0312F10EB 0330F10OC (Glued)	4/10/15 1:30 PM	E = 3.81 million psi f'_c = 3881 psi	71.7^{o}F (52%)
0316F10EB 0402F10OC (Glued)	4/10/15 (2:45 PM)	E = 3.88 million psi f'_c = 4512 psi	71.7^{o}F (52%)

Corresponding beam nomenclature	Test Date (Time)	Overlay Elastic Modulus and Compressive Strength	Temp and Rel Humidity @ Test time
0406F10EB 0506F10OB (Pinned)	5/11/15 (3:30 PM)	E = 4.63 million psi f'_c = 5334 psi	71.9°F (55%)
0223MNDAUB	3/24/15 (1:30 PM)	E = 3.28 million psi f'_c = 2326 psi	69.6°F (48%)
0417MNDAUB	4/23/15 (3:00 PM)	E = 3.88 million psi f'_c = 4590 psi	70.9°F (47%)
0319MNDAMB	4/3/15 (11:00 AM)	E = 4.94 million psi f'_c = 6833 psi	71.8°F (50%)
0422MNDAMB	4/27/15 (1:00 PM)	E = 4.3 million psi f'_c = 4696 psi	71.2°F (45%)
0226MNONUB	3/30/15 (10:30 AM)	E = 3.11 million psi f'_c = 2237 psi	70.2°F (59%)
0522MNONUB	5/26/15 (4:30 PM)	E = 4.65 million psi f'_c = 5131 psi	71.1°F (55%)
0424MIDAUA	4/29/15 (12:00 PM)	E = 4.23 million psi f'_c = 4694 psi	72.5°F (42%)
0515MIDAUA	5/20/15 (3:30 PM)	E = 4.78 million psi f'_c = 5357 psi	70.6°F (37%)
0513MIOAUB	5/18/15 (4:45 PM)	E = 4.71 million psi f'_c = 5013 psi	71.0°F (59%)
0520MIOAUA	5/26/15 (2:40 PM)	E = 4.62 million psi f'_c = 5073 psi	71.0°F (56%)

The first cycle of each test provided information on the material properties relevant in determining when and where joints in the overlay would deploy. The average stiffness of the interlayer system for the first load cycle was calculated as the force over displacement at a displacement of 80 mils. If the first cycle did not reach 80 mils displacement, the stiffness was calculated using the maximum displacement. The average initial stiffness of each interlayer system is provided in Table A-5.

During testing it was determined that the interlayer system stiffness stabilized between 5 and 8 load cycles. This stiffness is relevant when calculating the stress in the overlay caused by the interlayer resisting uniform volume changes due to a decrease in temperature and/or moisture. An overly stiff unbonded overlay system can prevent true debonding, cause high stresses to

develop in the overlay, and prevent proper joint deployment. The average final stiffness for each interlayer is summarized in Table A-5. The definition of the initial and final stiffness is shown in Figure A-11.

Finally, the ultimate strength of each interlayer system was tested to establish the ultimate resistance to sliding for each interlayer system. The average ultimate resistance is provided in Table A-6 for each specimen.

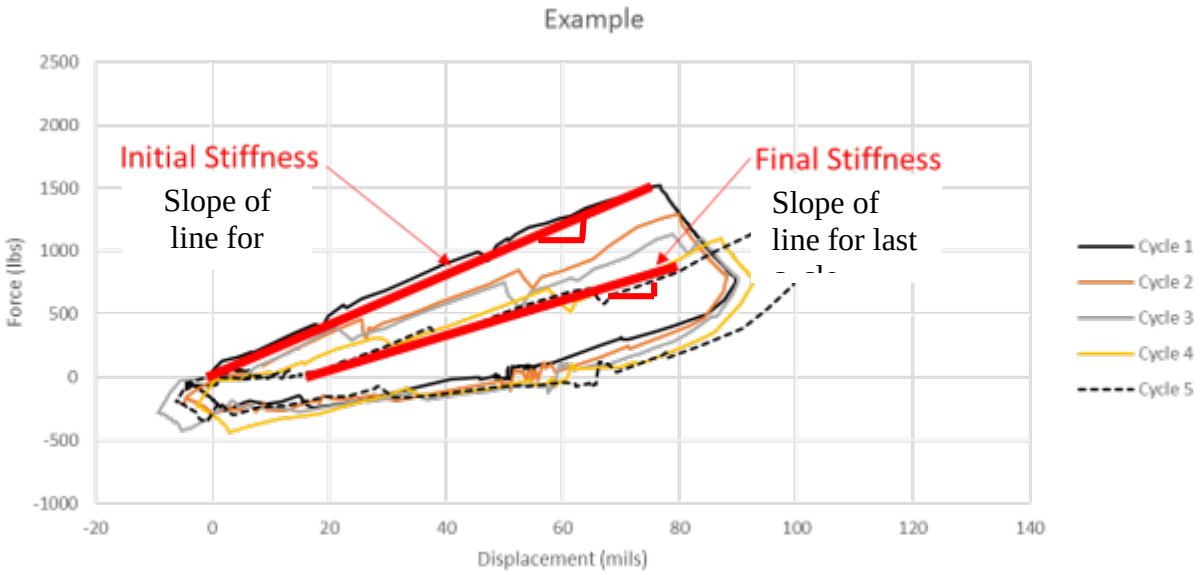

Figure A-11. Example of how Initial and Final Stiffness are Defined

Table A-6. Summary Results from Modified Push-Off Test

Interlayer (Code)	Initial Stiffness (psi/in)	Final Stiffness (psi/in)	Ultimate Resistance (psi)
F15-Glued	61	37	13
F15-Pinned	50	40	26
F10-Glued	104	87	22
F10-Pinned	98	29	21
MNDAU	234	167	39
MNDAM	333	263	59
MIDAU	336	317	>62
MNONU	217	55	16
MIOAU	169	136	63

Note: For one of the tests on the F10-Glued interlayer, a delay in the initial loading cycle caused the first load cycle to appear less stiff than several subsequent load cycles. For this test, the

initial stiffness was estimated using the second load cycle. Data for each Mechanism 2 beam is plotted in Appendix 3.

Mechanism 3: Reflective Cracking

Reflective cracking is a potential concern for unbonded overlays. The Mechanism 3 test setup is designed to assess the ability of the interlayer system in deterring cracks in the existing pavement from reflecting up into the overlay. For this test setup, a saw cut is made in the lower beam at midspan to represent a joint or crack in the existing concrete. The beam was loaded directly above the sawed joint in the middle of the 30 inch beam using the same loading head used for the Mechanism 1 test setup. See Figure A-11 below for an illustration of the Mechanism 3 test setup.

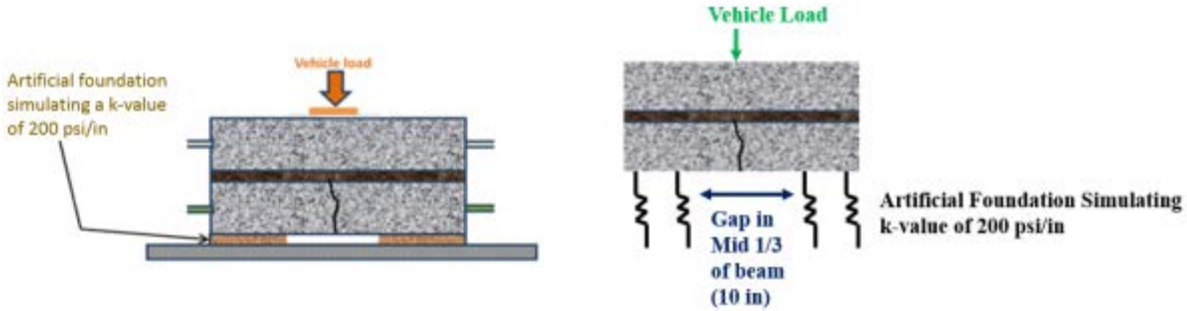

Figure A-11. a. Schematic of Reflective Cracking Test Setup
b. Boundary Conditions of Reflective Cracking Test Setup

Load is applied at a constant rate until a reflective crack is generated in the overlay beam. The load rate was chosen to be 30 pounds per second, which is the loading rate specified when performing modulus of rupture testing for concrete beams (ASTM C78). LVDTs record the displacement at the front and back of the beam on the overlay and existing beams. The LVDTs are located 3.5 inches to the left of the applied load. Figure A-12 provides a photo of a specimen in the Mechanism 3 test frame.

Figure A-12. Specimen in Mechanism 3 Test Frame for Assessing Reflective Cracking

Shakedown testing for Mechanism 3 was performed using a specimen with the 15 oz/yd^2 nonwoven fabric, and the bottom of the beam was fully supported with two layers of Fabcel 25. Three specimens were tested and a reflective crack could not be generated. The overlay cracked from the top down instead of bottom up as would be expected. This indicates that the failure was due to the stress concentration and crushing under the loading head and not due to a crack reflecting up from the underlying cracked beam. In order to overcome this problem, a gap was created under the central 10 inches of the beam by removing the Fabcel so there was no support in this area. This gap under the center of the beam is intended to simulate a void under the joint of an existing pavement. Figure A-13 shows the gap in the Fabcel measured with plywood and centered with a plumb bob. With the gap under the beam, subsequent shakedown tests generated reflective cracking which propagated from the bottom up.

Figure A-13. 10 inch Gap in Fabcel with Plumb Bob to Center the Gap

Table A-7 summarizes information relating to each specimen tested using the Mechanism 3 test setup. This includes the ultimate load and modulus of rupture (MOR) of the overlay beam. Force vs displacement plots for each Mechanism 3 specimen are provided in Appendix 4.

Table A-7. Summary Information for Mechanism 3 Specimens

Specimen	Break Load (lbs)	Test Date (Time)	MOR of the Overlay Beam (psi)	Temp and Rel Humidity @ Test Time
0406F15EB 0429F15OB	6,218	5/4/15 (9:20 AM)	643	71.8^{o}F (50%)

0406F15EC 0429F15OC	6,605	5/4/15 (10:00 AM)	643	71.9°F (51%)
0302F15EB 0701F15OD	7,508	7/6/15 (1:10 PM)	682	72.4°F (61%)
Specimen	**Break Load (lbs)**	**Test Date (Time)**	**MOR of the Overlay Beam (psi)**	**Temp and Rel Humidity @ Test Time**
0316F10EC 0402F10OA	6,565	4/7/15 (2:40 PM)	613	71.7°F (57%)
0409F10EA 0501F10OA	6,984	5/6/15 (11:15 AM)	645	70.8°F (56%)
0316F10EB 0709F10OC	7,517	7/14/15 (11:35 AM)	701	72.3°F (60%)
0417MNDAUA	5,562	4/22/15 (11:20 AM)	617	71.7°F (46%)
0507MNDAUA	6,345	5/12/15 (3:00 PM)	707	70.7°F (51%)
0701MNDAUA	6,052	7/6/15 (12:00 PM)	658	70.3°F (62%)
0422MNDAMC	5,923	4/27/15 (12:40 PM)	642	71.1°F (44%)
0507MNDAMB	6,638	5/12/15 (4:00 PM)	707	72.1°F (49%)
0709MNDAMB	5,912	7/14/15 (11:10 AM)	649	72.2°F (60%)
0507MNONUC	6,414	5/12/15 (5:00 PM)	707	71.9°F (47%)
0522MNONUC	6,678	5/27/15 (9:30 AM)	708	72.1°F (58%)
0701MNONUB	6,460	7/6/15 (12:30 PM)	636	72.1°F (61%)
0424MIDAUC	5,777	4/29/15 (11:10 AM)	643	72.4°F (42%)
0515MIDAUB	6,438	5/20/15 (11:15 AM)	719	72.2°F (35%)

0701MIDAUC	5,896	7/6/15 (1:10 PM)	663	72.4°F (59%)
0513MIOAUC	6,957	5/18/15 (12:20 PM)	695	70.1°F (60%)
Specimen	**Break Load (lbs)**	**Test Date (Time)**	**MOR of the Overlay Beam (psi)**	**Temp and Rel Humidity @ Test Time**
0520MIOAUC	7,129	5/25/15 (10:35 AM)	725	72.2°F (48%)
0709MIOAUA	6,471	7/14/15 (10:40 AM)	698	72.3°F (60%)

Mechanism 4: Direct Tension Test

Mechanism 4 was evaluated by measuring the vertical force-displacement relationship as the concrete layers of the unbonded overlay structure are loaded in tension, as shown in Figure A-14. This test is intended to provide insight into how debonding between the existing and overlay concrete layers develops in the field and to determine if curling can result in debonding between the interlayer and the concrete layers.

Figure A-14. Schematic of the Direct Tension Test

Each direct tension specimen was either cut from one of the already tested Mechanism 3 specimens (asphalt interlayers) or cast in cylindrical molds (fabric interlayers). It was assumed that little to no damage was experienced where the direct tension specimens were sawn from the

Mechanism 3 specimens and would therefore not affect the results of the direct tension test. The direct tension specimens required very precise preparation. The location of where the specimens were taken from the Mechanism 3 beams is provided in Figure A-15. A rig was used to provide compression while metal blocks were epoxied to the top and bottom of the specimens to ensure that the steel rods used in the testing apparatus were perfectly straight and in line with one another.

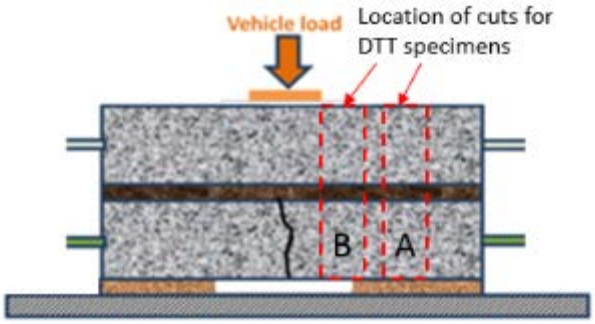

Figure A-15. Location of asphalt direct tension speicmens

The asphalt interlayer specimens were 4-inches on each side and approximately 12 inches tall. An asphalt interlayer direct tension specimen is shown in Figure A-16. The fabric interlayer specimens were 4-inch diameter and approximately 8 inches tall cylinders. The fabric specimens were made in two steps. First, the bottom of the specimen was cast using a 0.36 w/cm. Next, the fabric was glued to the top of the specimen bottom and the top of the specimen was cast using a 0.42 w/cm overlay mixture.

Figure A-16. Direct Tension Specimen with Asphalt Interlayer

An Instron loading machine was used to apply a direct tensile load. A photo of the test setup is shown in Figure A-17. The test is run in displacement control mode at a rate of 1 mil/sec and the force is recorded by the load machine. Displacement is also recorded with two LVDTs attached to opposite sides of the specimen. The relative displacement between the concrete above and below the fabric is measured, which can be seen in Figure A-17. Table A-8 summarizes the specimens tested and the peak load and displacement at the peak load. Force vs displacement for each Mechanism 4 specimen is plotted in Appendix 5.

Figure A-17. Mechanism 4 Test Setup (HMA interlayer)

Table A-8. Summary of Specimens Tested for Mechanism 4

Code	Replicate	Location	Peak Load (#)	Displacement at Peak Load (mils)	Location of Break
F15	1	N/A	18	64	Glued Interface
F15	2	N/A	16	61	Glued Interface
F10	1	N/A	31	139	Glued Interface
F10	2	N/A	38	120	Glued Interface
MNDAU	1	A	255	33	Middle of HMA
MNDAU	2	B	251	42	Middle of HMA
Code	**Replicate**	**Location**	**Peak Load (#)**	**Displacement at Peak Load (mils)**	**Location of Break**
MNDAM	1	A	262	10	Bond w/ Existing Concrete (into HMA)
MNDAM	2	B	392	13	Both interfaces and into HMA
MNONU	1	A	169	12	Middle of HMA

MNONU	2	B	208	12	Bond w/ Existing Concrete (into HMA)
MIDAU	1	A	586	22	Bond w/ Overlay Concrete
MIDAU	2	B	411	13	Bond w/ Overlay Concrete
MIOAU	1	A	206	4	Bond w/ Existing Concrete (into HMA)
MIOAU	2	B	142	6	Bond w/ Existing Concrete

Summary of Findings

Mechanism 1: Deflection Characteristics

As can be seen from the plots for both the 10 and 15 oz/yd^2 fabrics (F10 and F15) in Appendix 2, the response of specimens with fabric interlayers remains relatively constant throughout the duration of the test and are therefore more consistent in time than the HMA specimens. F1and F10 deflect approximately 6 and 4 mils respectively on the loaded side of the overlay. The LTE and interlayer compression (as defined in Appendix 2) for F15 remains around 15% and 4 - 5 mils, respectively. For F10, LTE fluctuates between 20 and 40% while the interlayer compression is consistently around 3 mils. F10is thinner than F15, so it does not compress as much.

For the specimens with an HMA interlayer, permanent compression developed in the HMA over time. The open graded asphalt interlayer from Minnesota had a LTE of 50 - 60% for first specimen and 60 - 75% for the second. Interlayer compression at the end of the test was approximately 19 mils and 13 mils for the first and second specimens, respectively. These high values of interlayer compression indicated damage or also displacement occurred within the interlayer.

For the specimens with the unmilled dense graded HMA interlayer from Minnesota, LTE began at approximately 40% to 50% and decreased to approximately zero over the test and interlayer compression increased from approximately 2 mils to 8 mils. For the specimens with the milled dense graded HMA interlayer from Minnesota, LTE decreased from approximately 75% to 40% and interlayer compression increased from approximately 4 mils to 6 mils. The difference in thickness between the thicker unmilled and the thinner milled HMA could be part of the reason for the difference.

The specimens with the dense graded asphalt interlayer from Michigan had LTEs that fluctuated between 60% to 80% and peak interlayer compression was approximately 4 mils. The specimens with the open graded HMA interlayer from Michigan had basically constant LTEs of approximately 70% for first specimen and 60% for the second. Additionally, the final interlayer compression was approximately 4 mils for both specimens.

Mechanism 2: Modified Push-Off

Results presented in Table A-5 show that specimens with a fabric interlayer have a lower stiffness than the specimens with an HMA interlayer. Within the fabric specimens, the F10 specimens had a higher stiffness than the F15 specimens. This is most likely due to the smaller thickness of F10 compared to F15 that limits in-plane deformation of the interlayer.

The specimens with the milled interlayer from Minnesota have a higher initial and final stiffness than the specimens with the unmilled interlayer. It can also be seen that the ultimate resistance of the specimens with the milled interlayer was much greater that for the specimens with the unmilled interlayer. This is possibly due to the decreased thickness of the milled specimens. The largest reduction in stiffness among asphalt specimens occurs with the open graded asphalt interlayer from Minnesota which was visibly distressed during testing and had a very small ultimate resistance.

The specimens with the open and dense graded asphalt interlayers from Michigan exhibited the smallest decreases in stiffness and also had the largest ultimate resistance. The ultimate resistance for the thicker asphalt interlayers was lower with the exception of the open graded interlayer for the specimens from Minnesota, which damaged due to the lower strength. In general, with the exception of the specimens with the open graded HMA interlayer from Minnesota, the fabric interlayers provide less restraint than the asphalt layers.

Mechanism 3: Reflective Cracking

Reflective cracking is cracking which occurs in the overlay directly over a joint or cracking in the existing pavement. It is also possible to have reflective distress over a region of reduced support. This could occur over a severely deteriorated joint or crack where the stiffness is smaller in a short region where the distress in the existing pavement is located. As discussed in the section on Mechanism 3 setup, it is important to note that reflective cracking could not be generated from the bottom up when the specimen is fully supported. This suggests that the potential for reflective cracking in the concrete overlay is extremely low unless a void is present in the vicinity of the crack or joint. A summary of the results from Mechanism 3 testing is provided in Table A-8. The load required to induce a reflective crack into the overlay beam is provided in the second column. The load required to fail a modulus of rupture beam cast with the same mixture as the overlay is provide in column 3. The reflective crack load (column 2) is divided by the failure load for the overlay modulus of rupture beam (column 3) to obtain the load ratio (column 4). The failure load of the overlay modulus of rupture beam is the maximum load sustained by the modulus of rupture beam according to ASTM C78. These load ratios were then averaged for each interlayer type.

The average load ratio has a range of 0.73 to 0.87. The fabric specimens are at the upper end this range, which may indicate that they are more resistant to the development of reflective cracking as compared to the specimens with an HMA interlayer. All of the HMA interlayer specimens performed roughly comparable to one another. The open graded HMA interlayer from Michigan

yielding the highest average load ratio of 0.79. This is similar to that achieved by the F15 interlayer specimens.

Table A-8. Reflective Cracking Beam Summary

UBOL Specimen[1]	Reflective Crack Load (lbs)	MOR for the Overlay Mixture (psi)	Failure Load for Overlay MOR Beam (lbs)	Load Ratio	Average Load Ratio for Each Interlayer
F15	6218	610	7417	0.838	0.842
	6605	644	7980	0.828	
	7508	682	8730	0.860	
F10	6565	628	7707	0.852	0.869
	6984	641	7920	0.882	
	7517	701	8620	0.872	
MNDAU	5562	590	7480	0.744	0.725
	6345	738	9217	0.688	
	6052	658	8155	0.742	
MNDAM	5923	623	7767	0.763	0.753
	6638	690	8730	0.760	
	5912	649	8020	0.737	
MNONU	6414	694	8594	0.746	0.767
	6678	724	8925	0.748	
	6460	636	8015	0.806	
MIDAU	5777	652	8140	0.710	0.711
	6438	717	8874	0.725	
	5896	663	8460	0.697	
MIOAU	6957	697	8675	0.802	0.787
	7129	711	8798	0.810	
	6471	698	8637	0.749	

*Load Ratio is Reflective Crack Load normalized by the Failure Load for the Overlay MOR Beam

Mechanism 4: Direct Tension Test

As shown in Table A-7, both fabrics tested had comparable values of peak force and displacement at peak force. The F10 specimens resulted in a peak load of 30 - 40 pounds at a displacement ranging between 120 mils to 140 mils and the F15 specimens maintained a peak load of 15 to 20 pounds at a displacement of approximately 60 mils. The variation observed between fabric specimens can be partly attributed to the quality and quantity of geotextile adhesive placed at the glued interface. Overall, these results indicate that the fabrics would provide insignificant resistance to upward curl of the concrete overlay. Greater variability was observed with the HMA interlayers than the fabric interlayer specimens. Additionally, higher strength and smaller displacements at the peak load for the HMA specimens was observed as compared to the fabric specimens as one would expect. The magnitude of the peak load varied with the location of the failure within the inter layer system. Both the Minnesota and Michigan open graded asphalts produced the smallest peak loads, followed by Minnesota dense unmilled, Minnesota dense milled, and Michigan dense unmilled which had the greatest peak load.

Conclusions

The four test setups described in this report provided significant insight into the response of different interlayer systems by restricting the response to a 2-dimensional system. The information gained coupled with field performance data can aid in determining and confirming what distress mechanisms must be designed against for UBOL structures. A design procedure for UBOL should first examine the damage in the interlayer (due to loading, temperature, etc.). Then damage should be accumulated for the JPCP overlay at each corresponding time step.

Appendix 1: Material Test Data

The following tables contain all material test data from the study, including averages and standard deviations for each test date and concrete age at testing. Elastic modulus, compressive strength, and modulus of rupture tests were conducted according to ASTM C469, ASTM C39, and ASTM C78, respectively.

	Elastic Modulus			
	14 Day		28 Day	
Cast Date	Avg	Std Dev	Avg	Std Dev
Lower Beam Mixture				
2/11/2015	5.24E+06	90000	5.34E+06	47000
2/19/2015	4.53E+06	13000	4.92E+06	81000
3/2/2015			4.80E+06	63000
3/12/2015	4.77E+06	67000	4.83E+06	109000
3/16/2015			5.03E+06	149000
	29 Day		31 Day	
4/6/2015			4.64E+06	111000
4/9/2015	4.60E+06	171000		
	14 Day		28 Day	
4/13/2015			4.83E+06	171000
Upper Beam Mixture				
	14 Day		28 Day	
2/20/2015	2.81E+06	14000	3.11E+06	50000
2/22/2015	3.11E+06	69000	3.24E+06	64000
2/23/2015			3.28E+06	112000
2/26/2015			3.11E+06	251000
3/3/2015			3.04E+06	49000
	5 Day		7 Day	
Cast Date	Avg	Std Dev	Avg	Std Dev
3/30/2015			3.81E+06	315000
4/2/2015			3.88E+06	187000
4/17/2015			3.88E+06	339000
4/22/2015			4.30E+06	142000
4/24/2015			4.23E+06	43000
	5 Day		6 Day	
4/29/2015			4.28E+06	155000
5/1/2015			4.17E+06	88000
5/6/2015	4.36E+06	258000		
5/7/2015	4.48E+06	218000		
5/13/2015			4.71E+06	47000
5/15/2015			4.79E+06	54000
5/20/2015			4.62E+06	88000
5/22/2015			4.65E+06	89000
7/1/2015	4.43E+06	165000		
7/9/2015	4.49E+06	112000		

Cast Date	Compressive Strength			
	14 Day		28 Day	
	Avg	Std Dev	Avg	Std Dev
Lower Beam Mixture				
2/11/2015	7610	533	7411	271
2/19/2015	6232	61	6471	96
3/2/2015	6196	160	6991	129
3/12/2015	6325	170	7059	263
3/16/2015	6443	298	7093	459
	29 Day		31 Day	
4/6/2015			6982	170
4/9/2015	6806	303		
	14 Day		28 Day	
4/13/2015			6847	177
Upper Beam Mixture				
	14 Day		28 Day	
2/20/2015	1977	199	2666	61
2/22/2015	2608	31	2905	242
2/23/2015	2352	129	2326	119
2/26/2015	2140	168	2237	32
3/3/2015	2242	24	2156	303
	5 Day		7 Day	
Cast Date	Avg	Std Dev	Avg	Std Dev
3/30/2015			3881	262
4/2/2015			4512	247
4/17/2015			4590	285
4/22/2015			4696	267
4/24/2015			4694	100
	5 Day		6 Day	
4/29/2015			5059	64
5/1/2015			5069	184
5/6/2015	5334	310		
5/7/2015	5106	225		
5/13/2015			5013	353
5/15/2015			5357	275
5/20/2015			5073	186
5/22/2015			5131	195
7/1/2015	4632	279		

7/9/2015	4732	235		

	Modulus of Rupture			
	14 Day		28 Day	
Cast Date	Avg	Std Dev	Avg	Std Dev
Lower Beam Mixture				
2/11/2015			932	86
2/19/2015			878	17.5
3/2/2015				
3/12/2015	838	20		
3/16/2015				
	29 Day		31 Day	
4/6/2015			884	3
4/9/2015	863	12		
	14 Day		28 Day	
4/13/2015			905	55
Upper Beam Mixture				
	14 Day		28 Day	
2/20/2015			584	13
2/22/2015			573	-
2/23/2015				
2/26/2015				
3/3/2015			552	-
	5 Day		7 Day	
Cast Date	Avg	Std Dev	Avg	Std Dev
3/30/2015			688	58
4/2/2015	613	18		
4/17/2015	617	31		
4/22/2015	642	30		
4/24/2015	643	8		
	5 Day		6 Day	
4/29/2015	643	47		
5/1/2015	645	23		
5/6/2015	685	53		
5/7/2015	707	27		
5/13/2015	695	10		
5/15/2015	719	6		
5/20/2015	725	27		
5/22/2015	708	18		

7/1/2015	660	19		
7/9/2015	683	29		

Cast Date	QC Data	
	Air	Avg. Slump
Lower Beam Mixture		
2/11/2015	*	2.5
2/19/2015	*	2.0
3/2/2015	*	1.3
3/12/2015	6.1	1.1
3/16/2015	6.1	1.1
4/6/2015	5.8	1.1
4/9/2015	5.5	1.3
4/13/2015	5.8	1.2
Upper Beam Mixture		
2/20/2015	*	4.0
2/23/2015	*	4.8
2/26/2015	*	4.2
3/3/2015	*	4.3
3/30/2015	6.3	3.5
4/2/2015	6.3	3.8
4/17/2015	6.5	2.5
4/22/2015	6.3	2.3
4/24/2015	6.3	2.1
4/29/2015	6.0	1.9
5/1/2015	5.9	1.9
5/6/2015	5.8	1.5
5/7/2015	6.0	1.6
5/13/2015	6.0	2.1
5/15/2015	6.2	1.7
5/20/2015	6.0	1.7
5/22/2015	6.4	2.1
7/1/2015	6.5	1.6
7/9/2015	6.3	1.5

*Not measured correctly due to air meter calibration issue

Appendix 2: Mechanism 1 Data

This appendix contains two types of plots for each specimen. The first plots type shows measured deflection at each of the four locations versus the cycle number. All deflection values correspond to the dynamic load at the peak of 600 pounds. All abbreviations are described below. Refer to Figure A-8 in the section on Mechanism 1 for the locations of the deflection measurements.

Note the following nomenclature:
OL = Overlay Loaded side
OU = Overlay Unloaded side
EL = Existing Loaded side
EU = Existing Unloaded side

The second plot type shows load transfer efficiency (LTE) and interlayer compression versus cycle number. Load Transfer Efficiency (LTE) is defined as the ratio of the deflection of the unloaded side to the loaded side of the joint in the overlay and is reported as a percent. Interlayer compression is the overlay loaded deflection minus the existing beam loaded deflection.

Interlayer Compression = OL – EL

Interlayer LTE = (OU – EU)/(OL – EL)*100

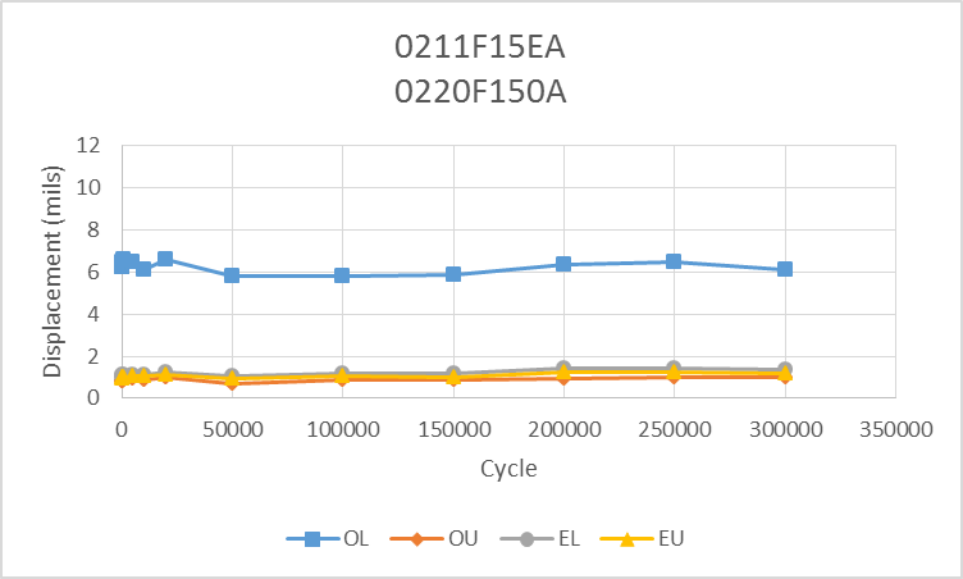

Figure A-A2.1. F15 Displacement vs. Load Cycle (Tested on 3/20/15)

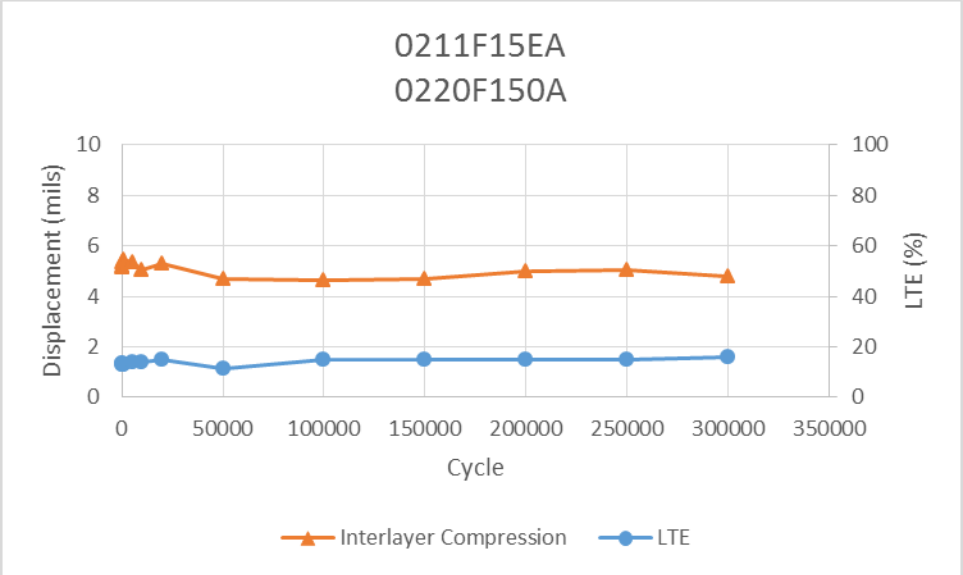

Figure A-A2.2. F15 Interlayer Compression and LTE vs. Load Cycle (Tested on 3/20/15)

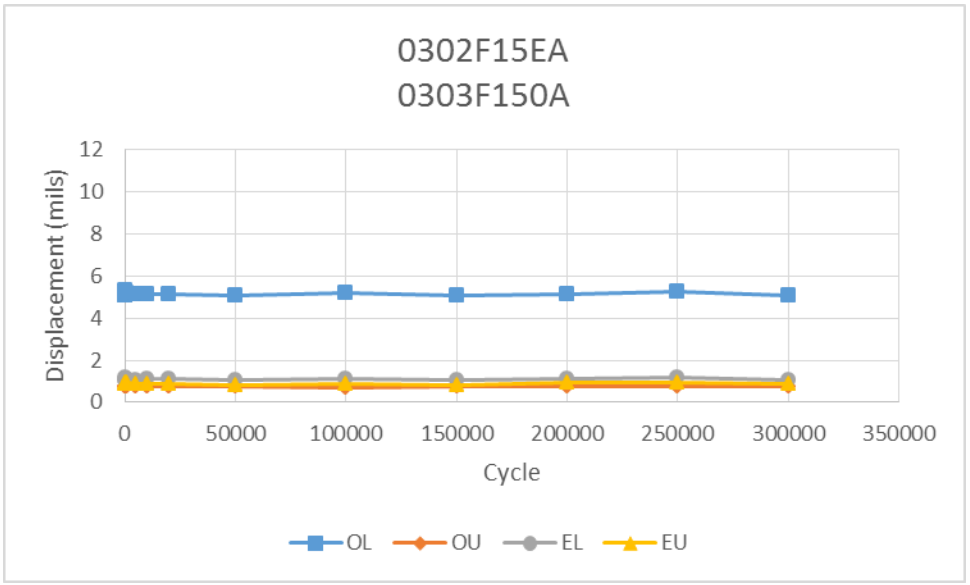

Figure A-A2.3. F15 Displacement vs. Load Cycle (Tested on 4/1/15)

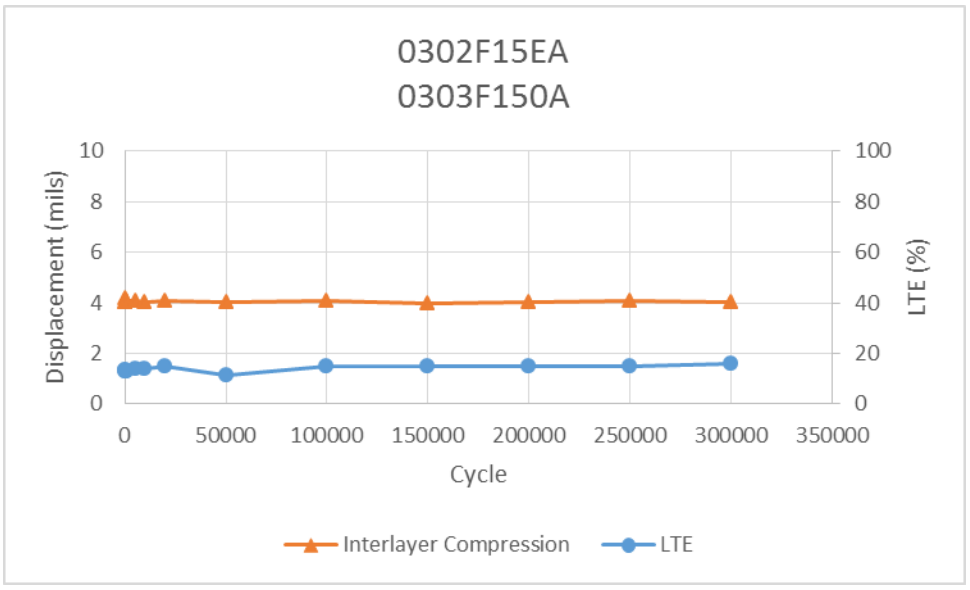

Figure A-A2.4. F15 Interlayer Compression and LTE vs. Load Cycle (Tested on 4/1/15)

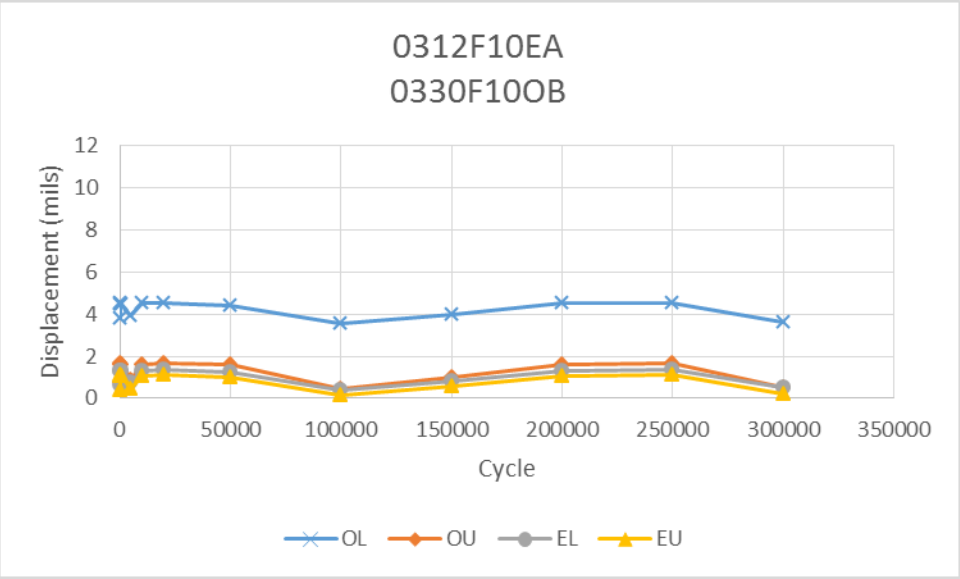

Figure A-A2.5. F10 Displacement vs. Load Cycle (Tested on 4/8/15)

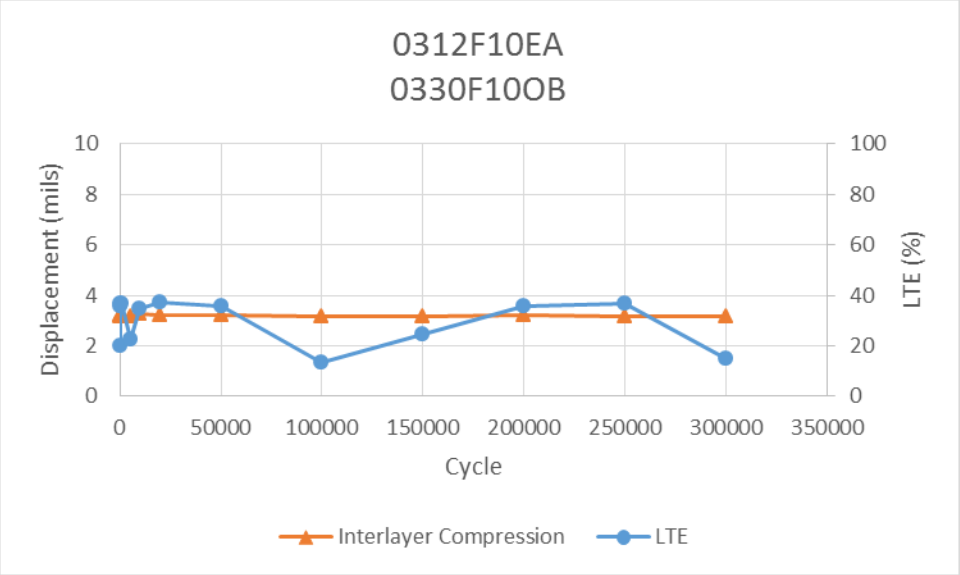

Figure A-A2.6. F10 Interlayer Compression and LTE vs. Load Cycle (Tested on 4/8/15)

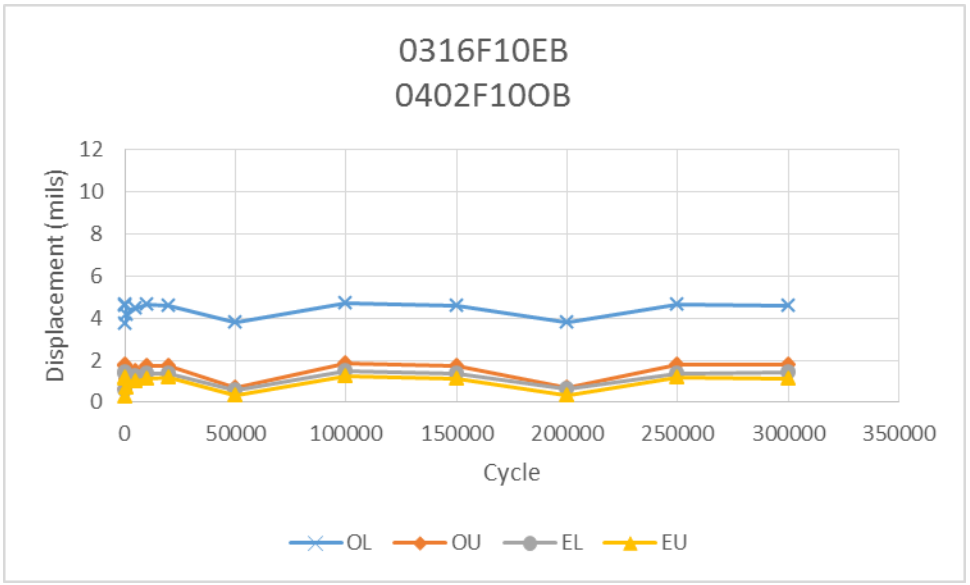

Figure A-A2.7. F10 Displacement vs. Load Cycle (Tested on 4/9/15)

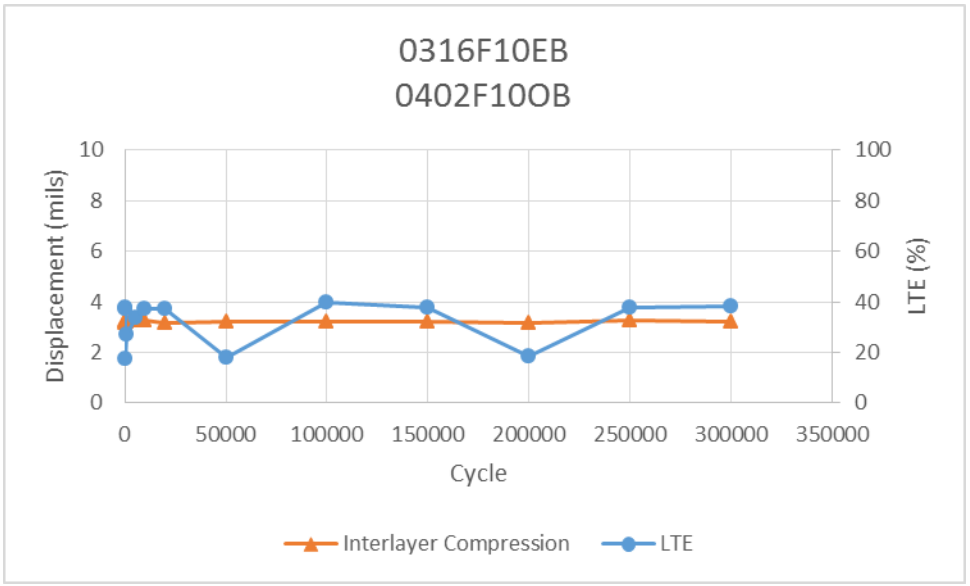

Figure A-A2.8. F10 Interlayer Compression and LTE vs. Load Cycle (Tested on 4/9/15)

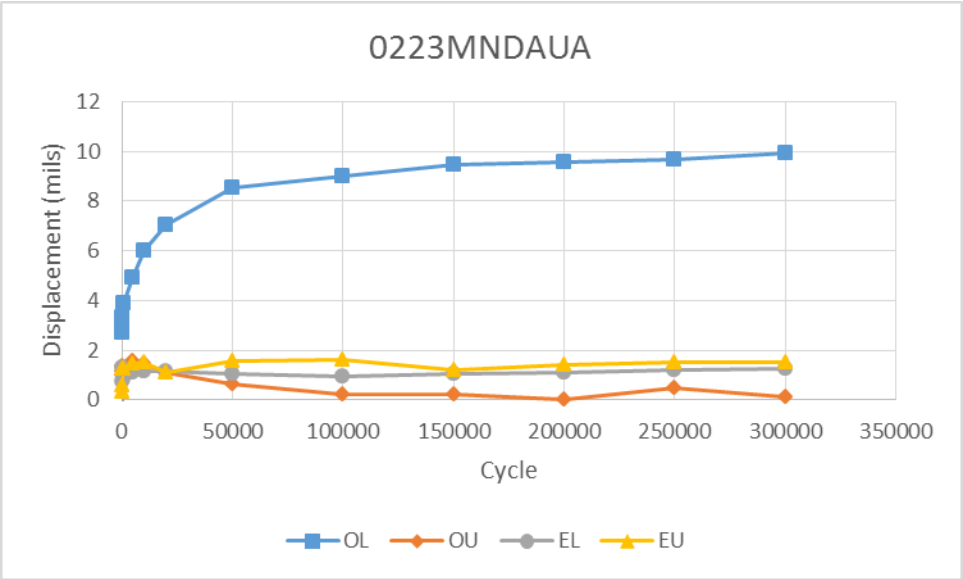

Figure A-A2.9. MNDAU Displacement vs. Load Cycle (Tested on 3/25/15)

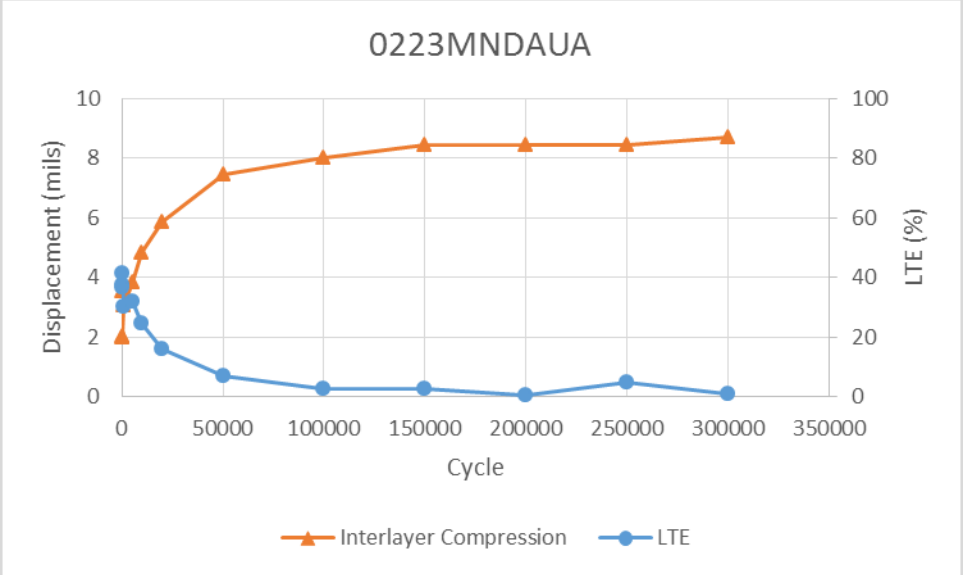

Figure A-A2.10. MNDAU Interlayer Compression and LTE vs. Load Cycle (Tested on 3/25/15)

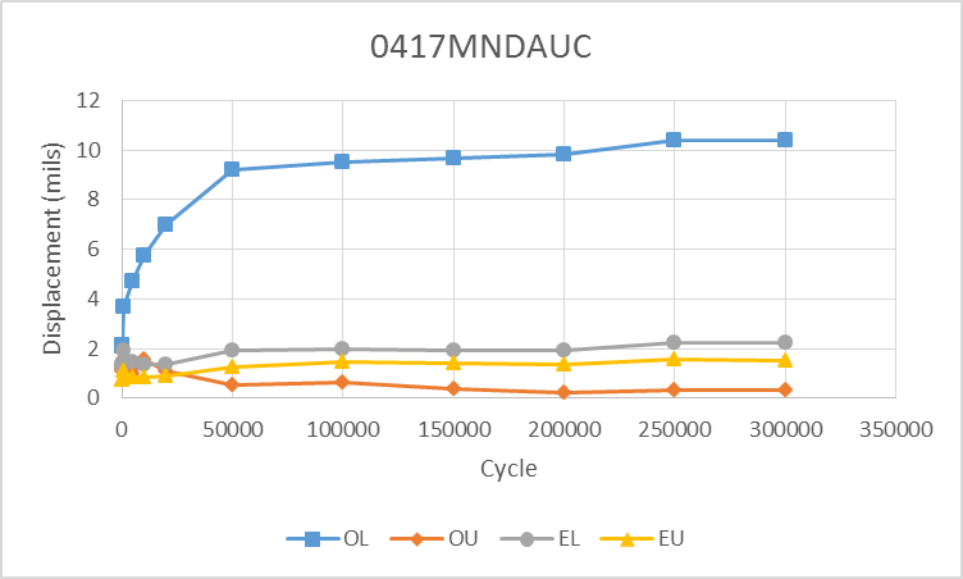

Figure A-A2.11. MNDAU Displacement vs. Load Cycle (Tested on 4/23/15)

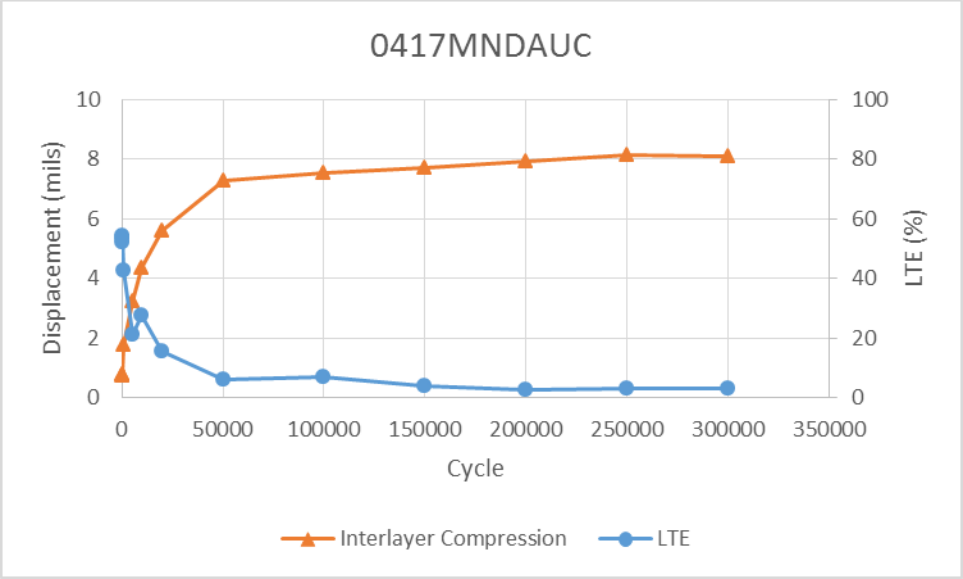

Figure A-A2.12. MNDAU Interlayer Compression and LTE vs. Load Cycle (Tested on 4/23/15)

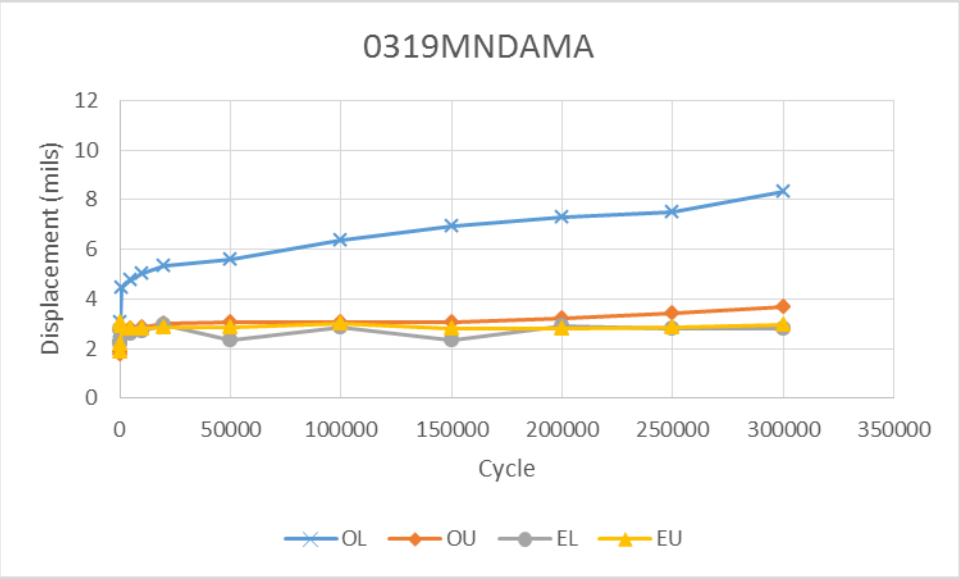

Figure A-A2.13. MNDAM Displacement vs. Load Cycle (Tested on 4/2/15)

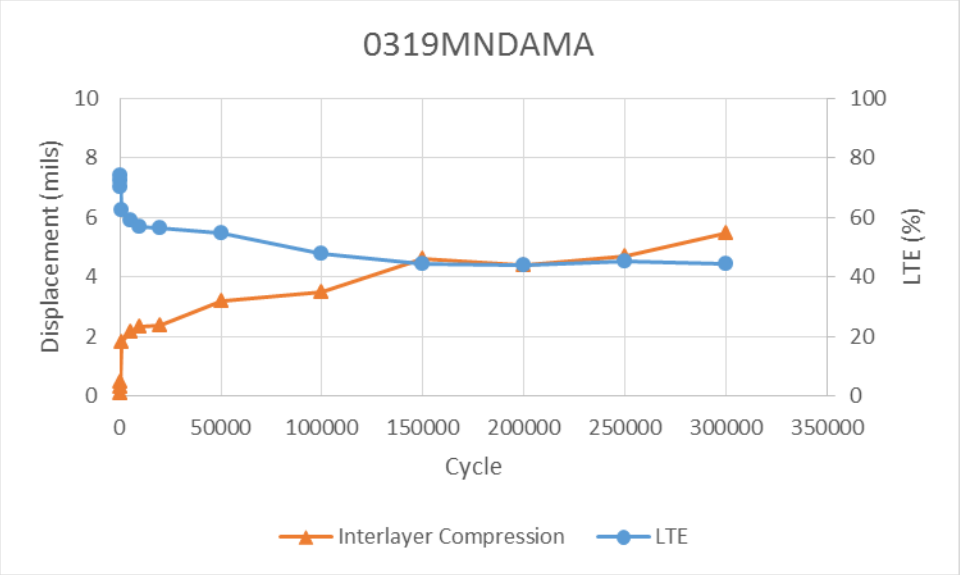

Figure A-A2.14. MNDAM Interlayer Compression and LTE vs. Load Cycle (Tested on 4/2/15)

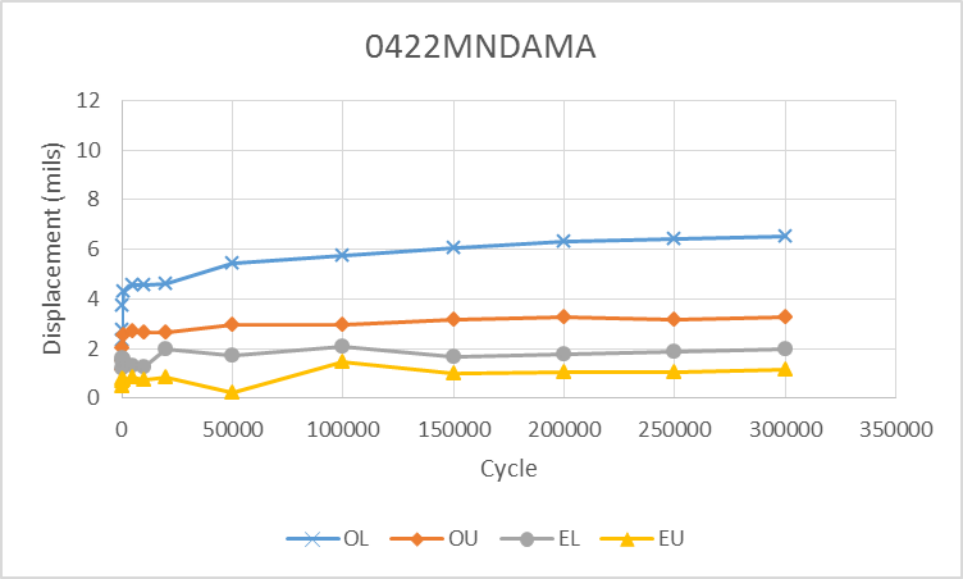

Figure A-A2.15. MNDAM Displacement vs. Load Cycle (Tested on 4/28/15)

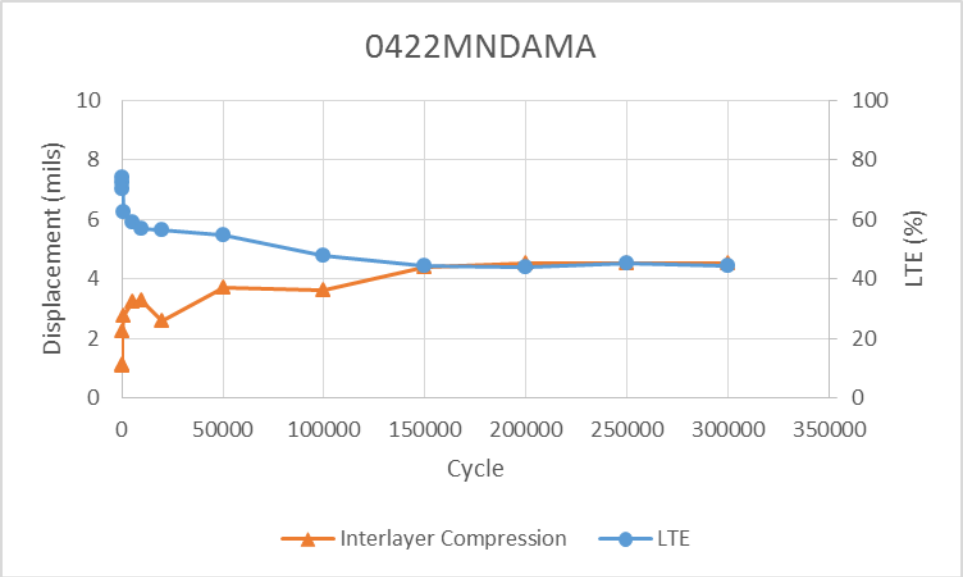

Figure A-A2.16. MNDAM Interlayer Compression and LTE vs. Load Cycle (Tested on 4/28/15)

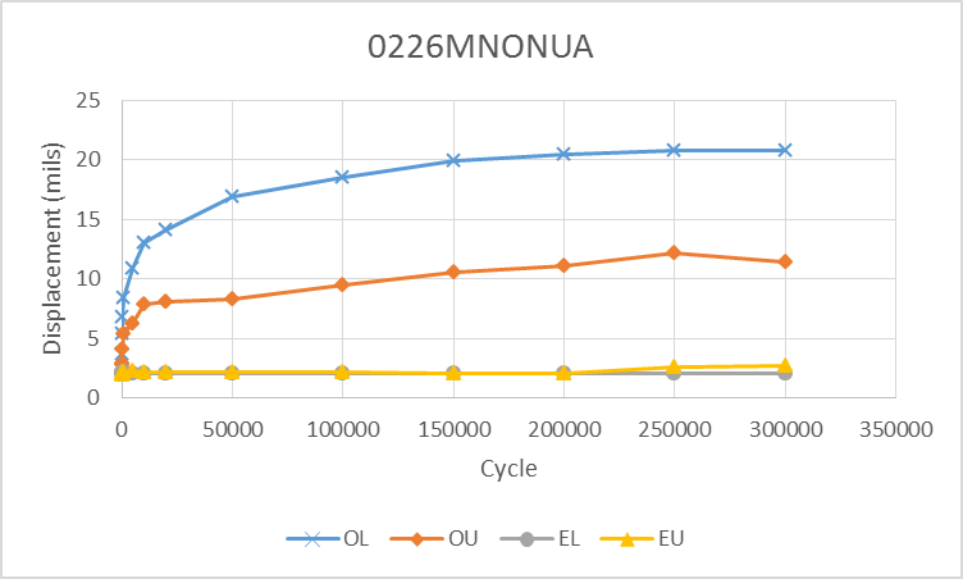

Figure A-A2.17. MNONU Displacement vs. Load Cycle (Tested on 3/27/15)

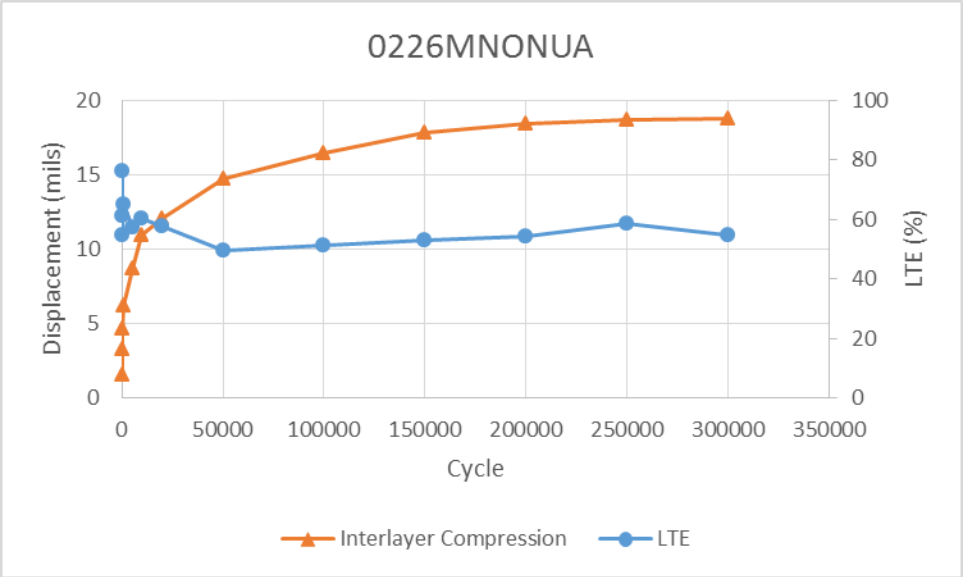

Figure A-A2.18. MNONU Interlayer Compression and LTE vs. Load Cycle (Tested on 3/27/15)

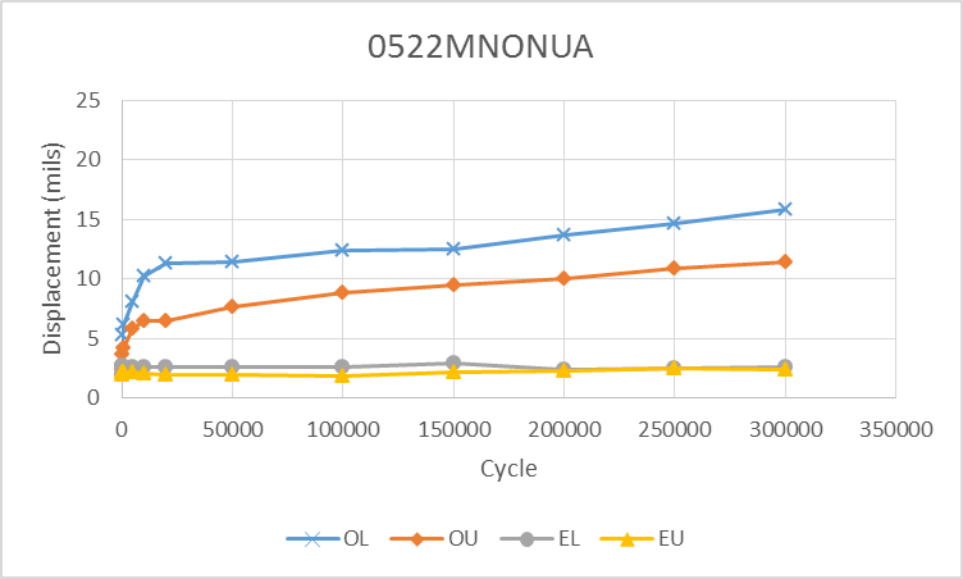

Figure A-A2.19. MNONU Displacement vs. Load Cycle (Tested on 5/27/15)

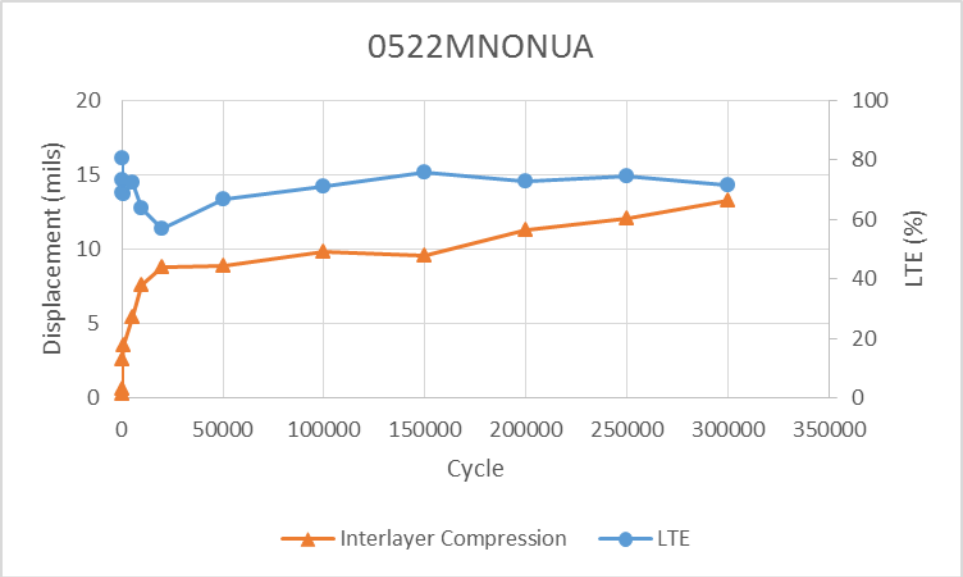

Figure A-A2.20. MNONU Interlayer Compression and LTE vs. Load Cycle (Tested on 5/27/15)

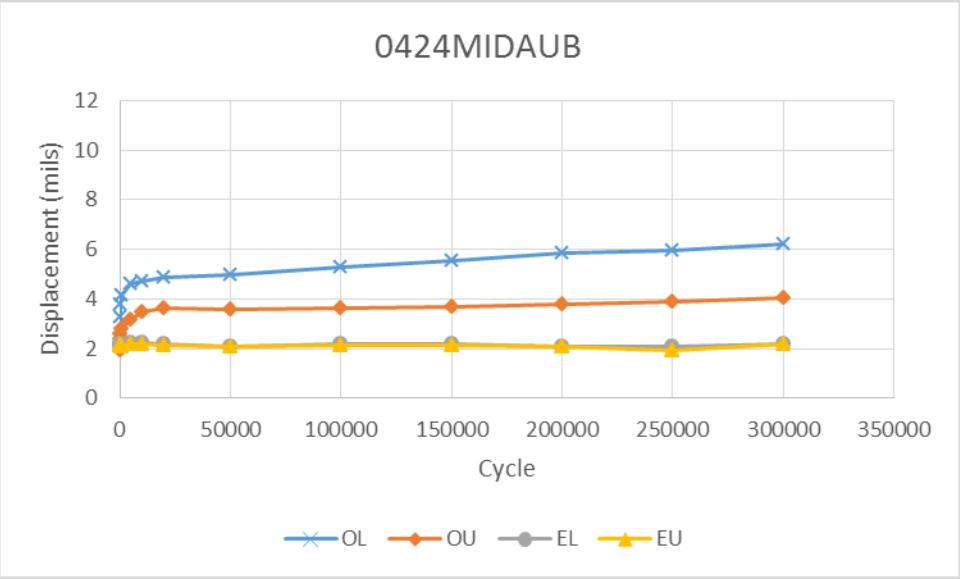

Figure A-A2.21. MIDAU Displacement vs. Load Cycle (Tested on 4/29/15)

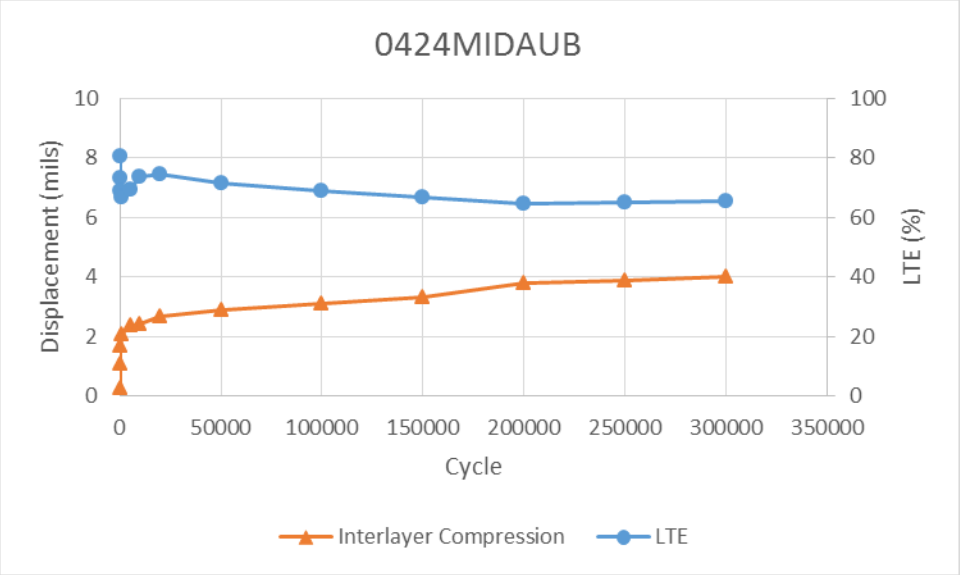

Figure A-A2.22. MIDAU Interlayer Compression and LTE vs. Load Cycle (Tested on 4/29/15)

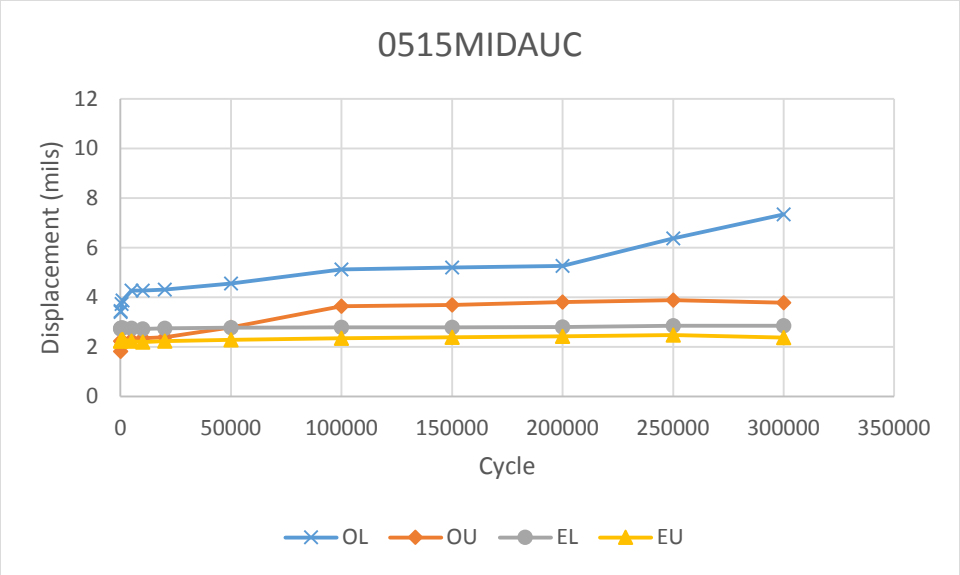

Figure A-A2.23. MIDAU Displacement vs. Load Cycle (Tested on 5/20/15)

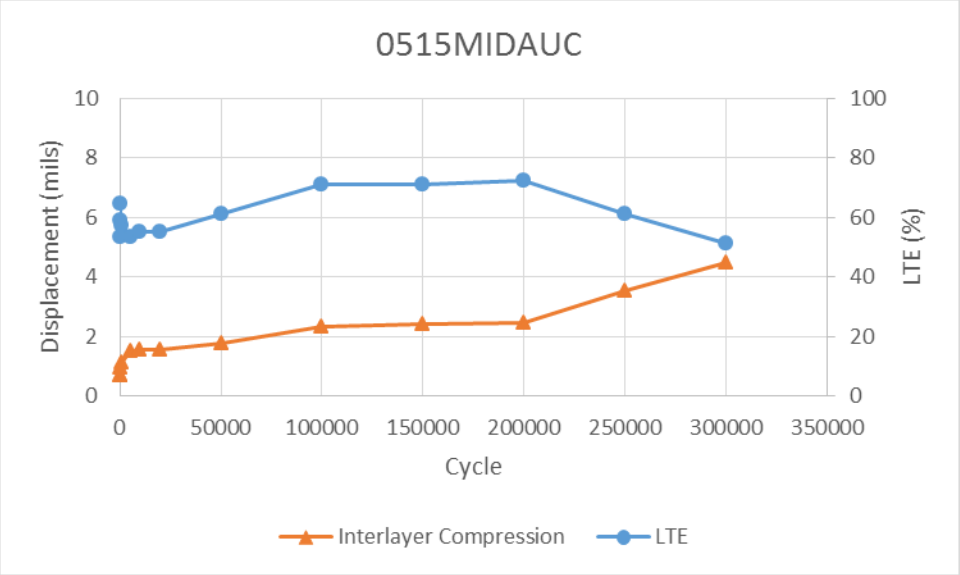

Figure A-A2.24. MIDAU Interlayer Compression and LTE vs. Load Cycle (Tested on 5/20/15)

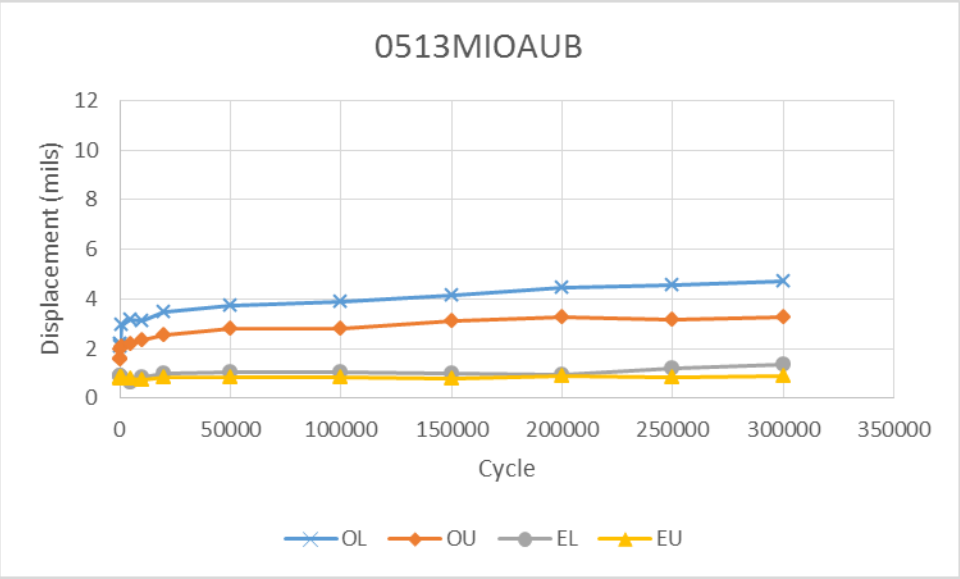

Figure A-A2.25. MIOAU Displacement vs. Load Cycle (Tested on 5/19/15)

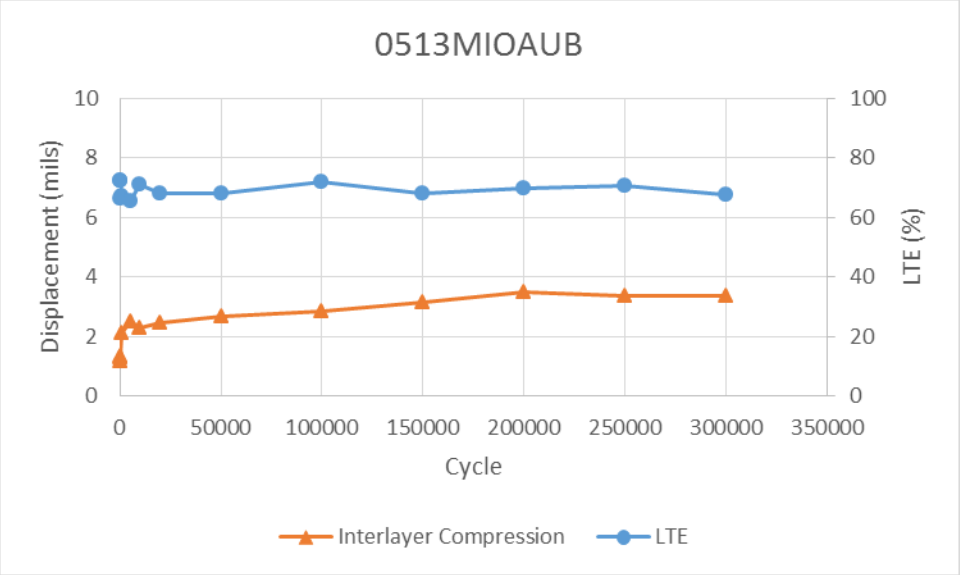

Figure A-A2.26. MIOAU Interlayer Compression and LTE vs. Load Cycle (Tested on 5/19/15)

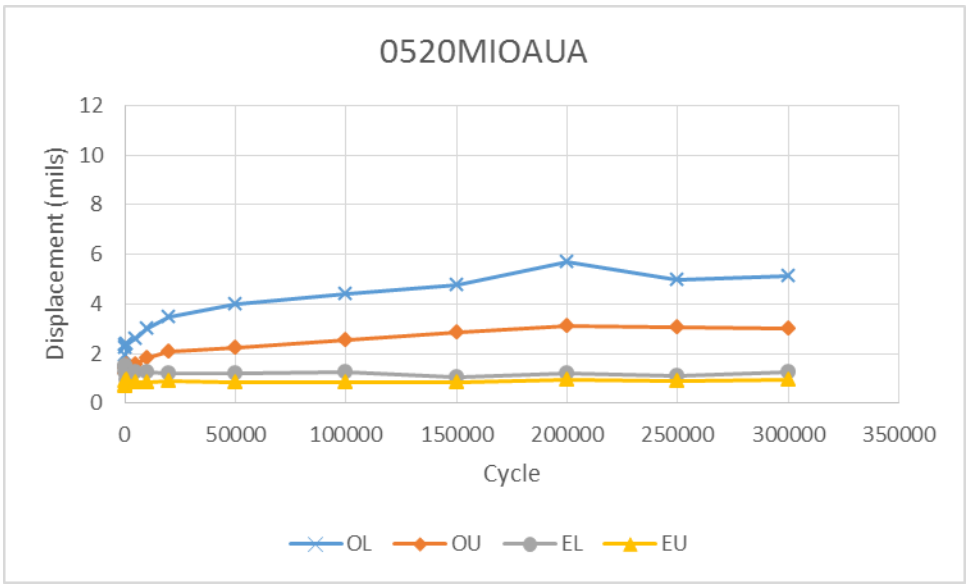

Figure A-A2.27. MIOAU Displacement vs. Load Cycle (Tested on 5/26/15)

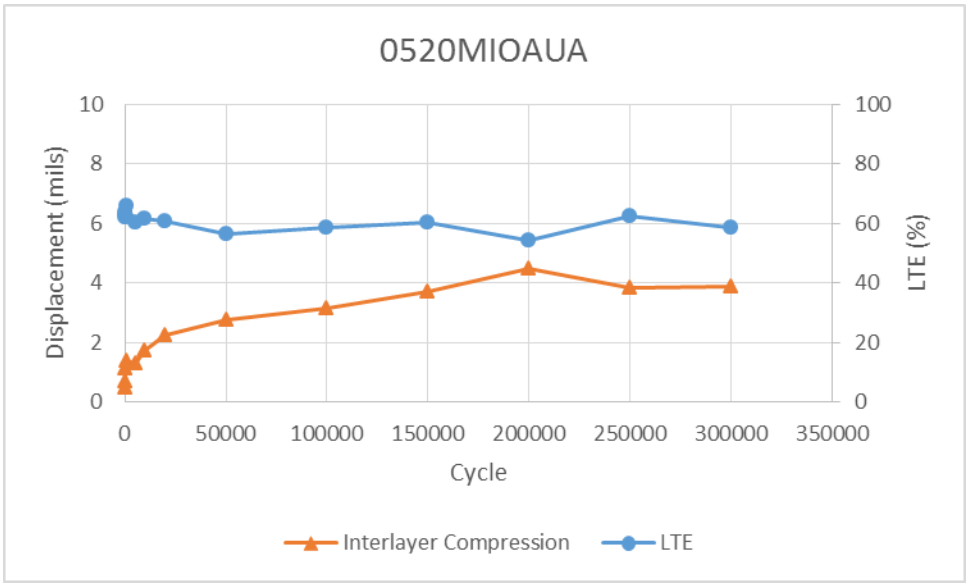

Figure A-A2.28. MIOAU Interlayer Compression and LTE vs. Load Cycle (Tested on 5/26/15)

Appendix 3: Mechanism 2 Plots

This appendix contains two types of plots for the modified push-off test. Each specimen has two plots, one of each type. The first type of plot shows force and displacement versus time. The second plot shows force versus displacement for each load cycle.

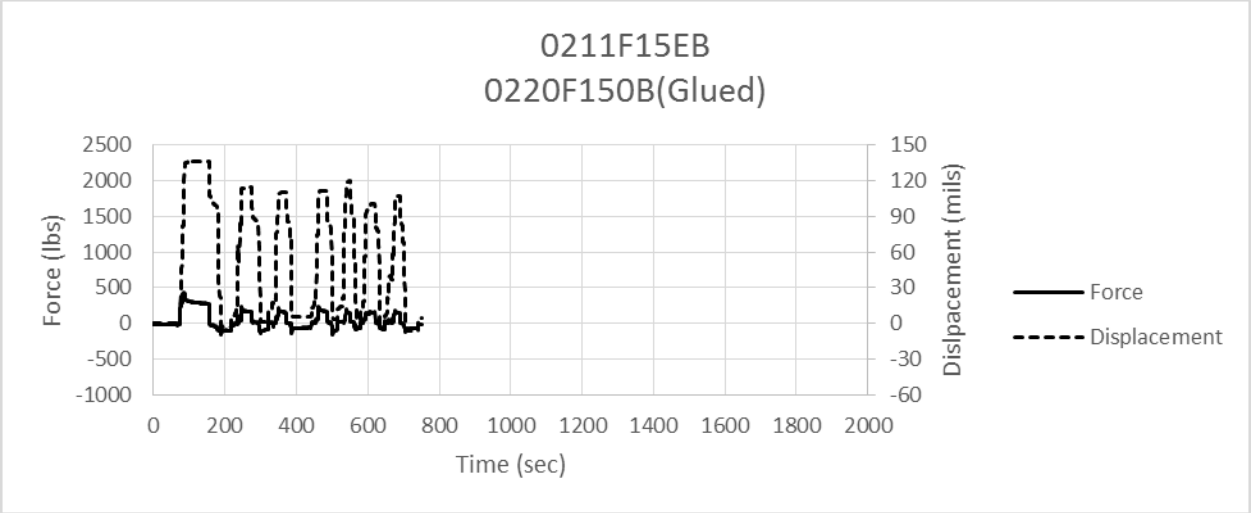

Figure A-A3.1. F15(Glued) Force and Displacement vs. Time (Tested on 3/20/15)

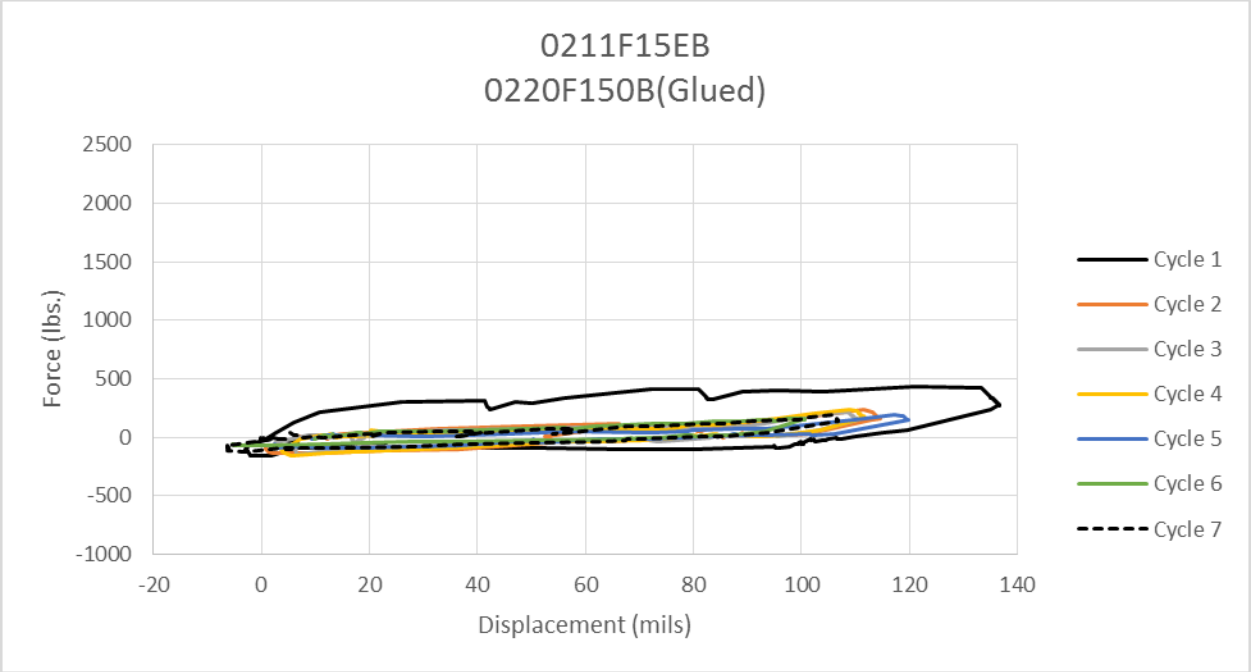

Figure A-A3.2. F15(Glued) Force vs. Displacement (Tested on 3/20/15)

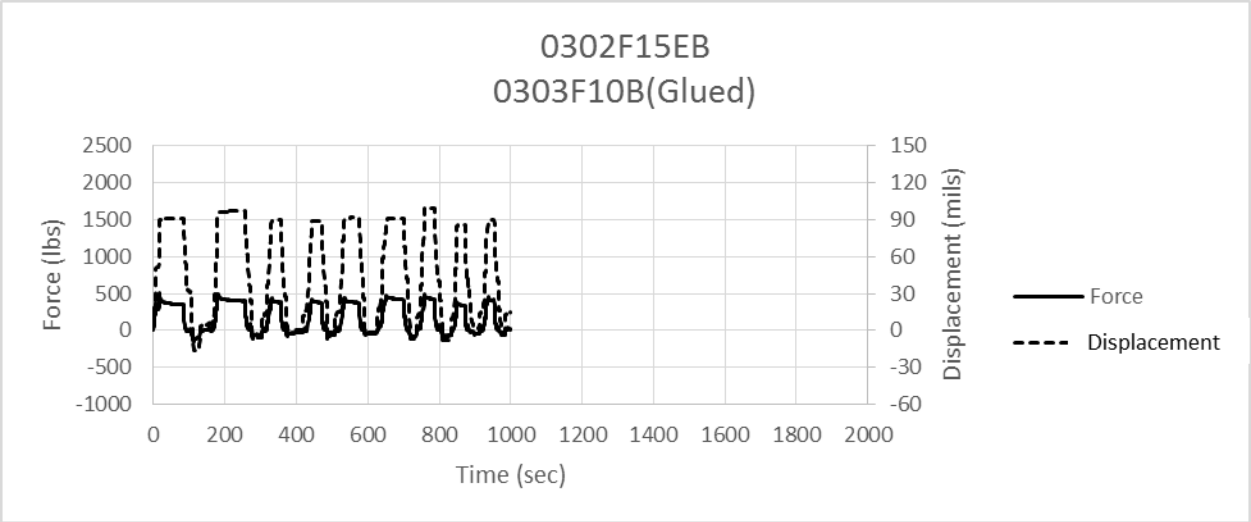

Figure A-A3.3. F15(Glued) Force and Displacement vs. Time (Tested on 4/1/15)

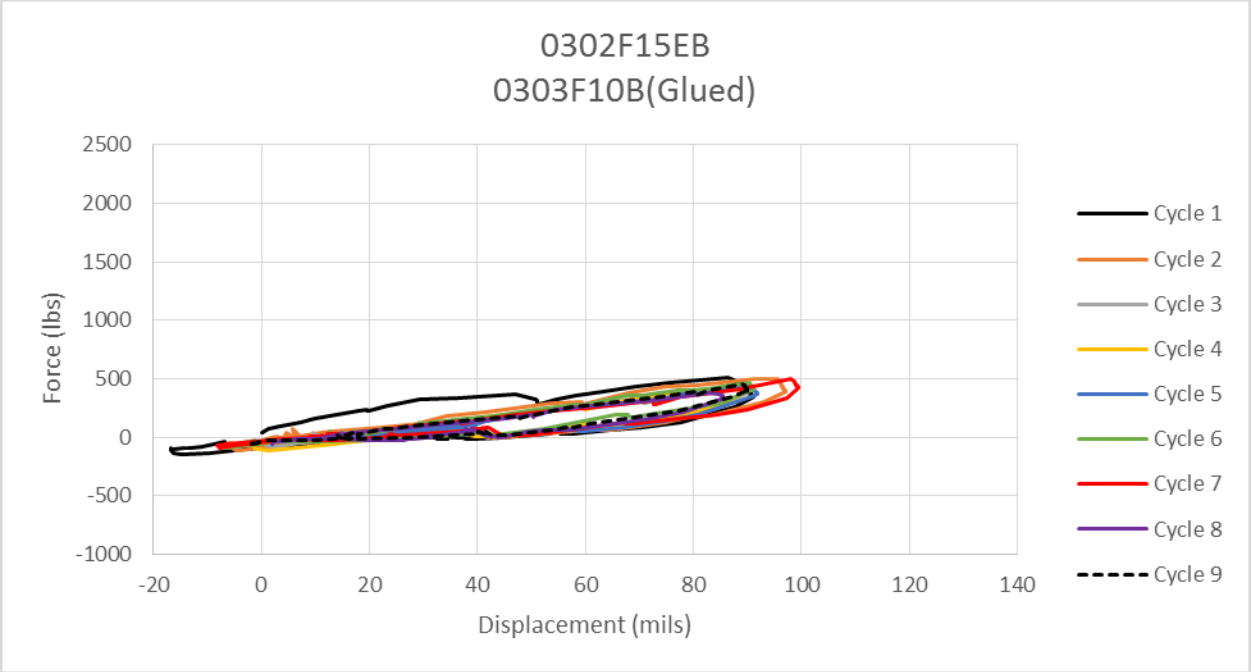

Figure A-A3.4. F15(Glued) Force vs. Displacement (Tested on 4/1/15)

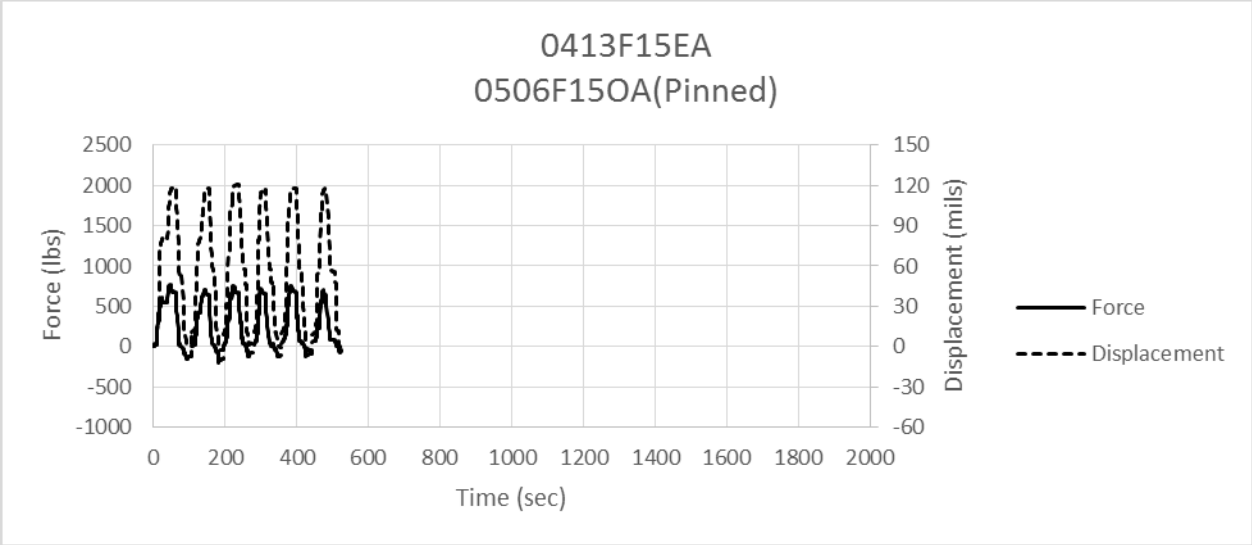

Figure A-A3.5. F15(Pinned) Force and Displacement vs. Time (Tested on 5/11/15)

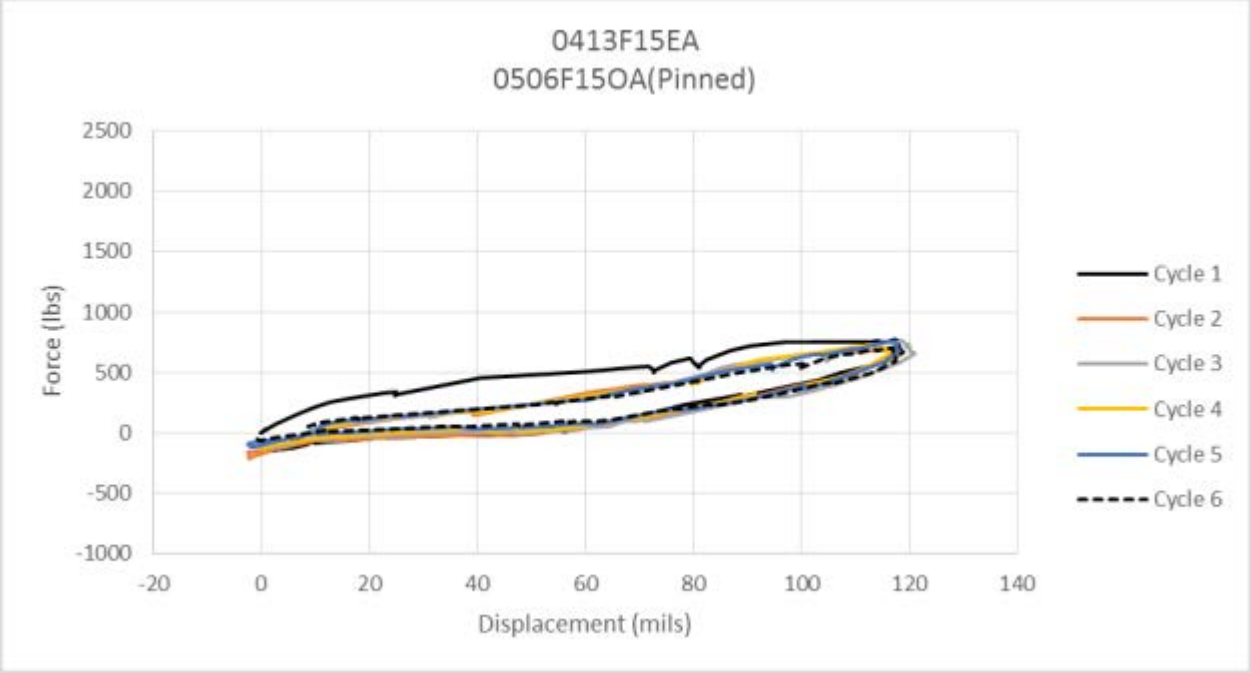

Figure A-A3.6. F15(Pinned) Force vs. Displacement (Tested on 5/11/15)

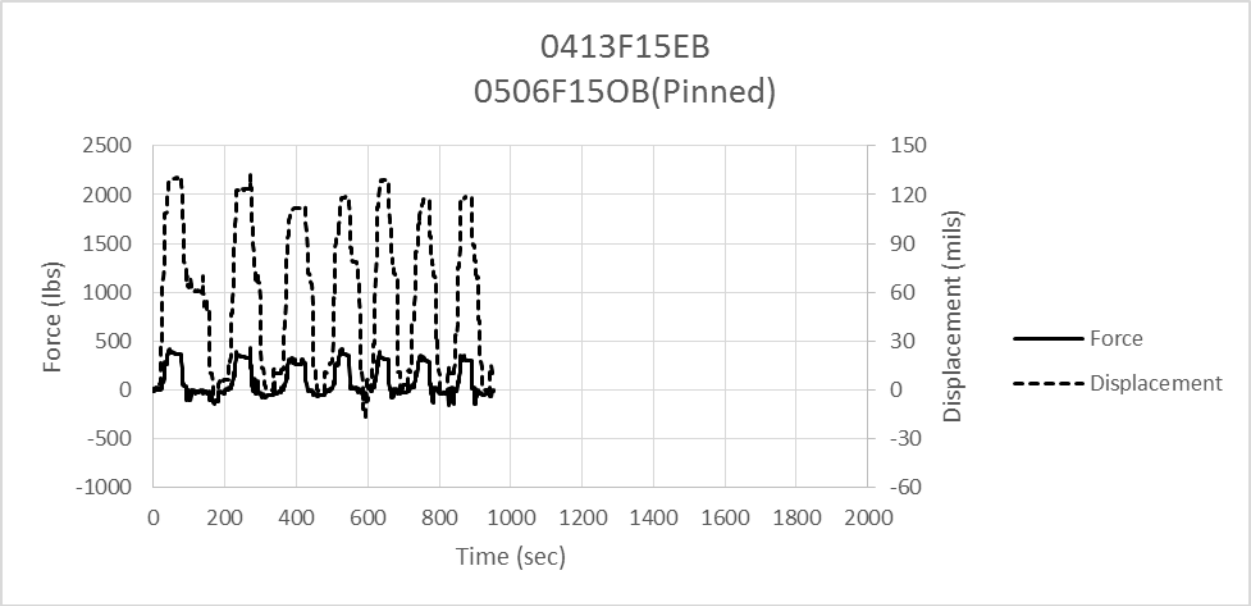

Figure A-A3.7. F15(Pinned) Force and Displacement vs. Time (Tested on 5/12/15)

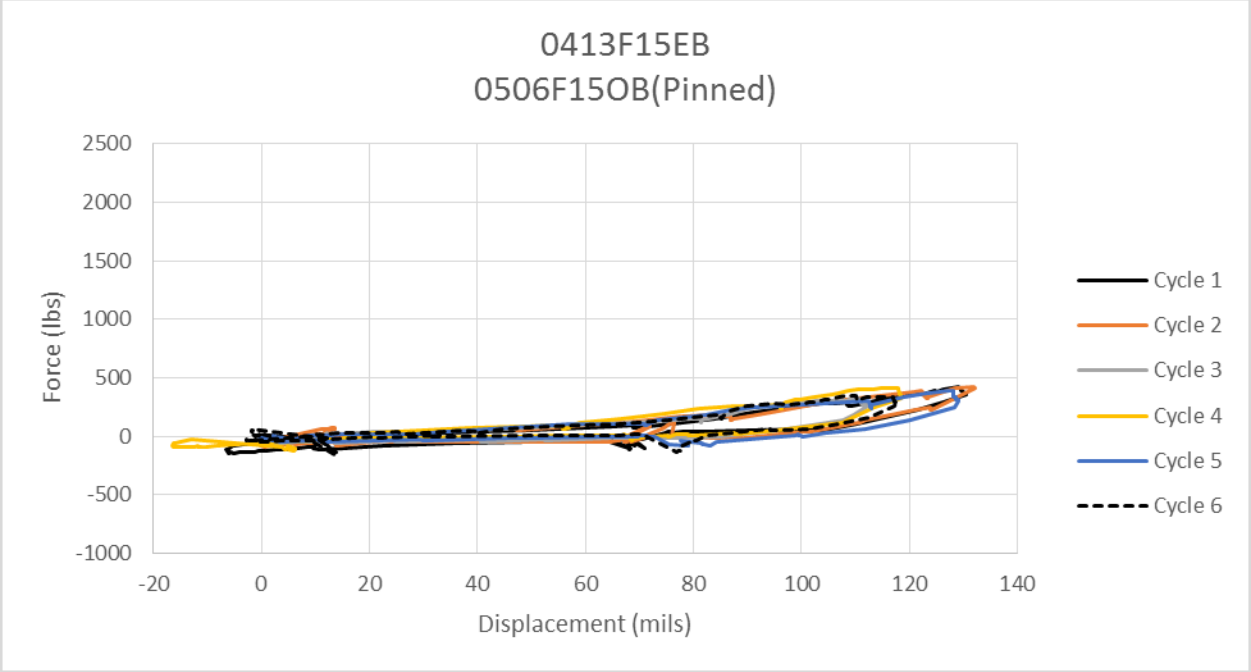

Figure A-A3.8. F15(Pinned) Force vs. Displacement (Tested on 5/12/15)

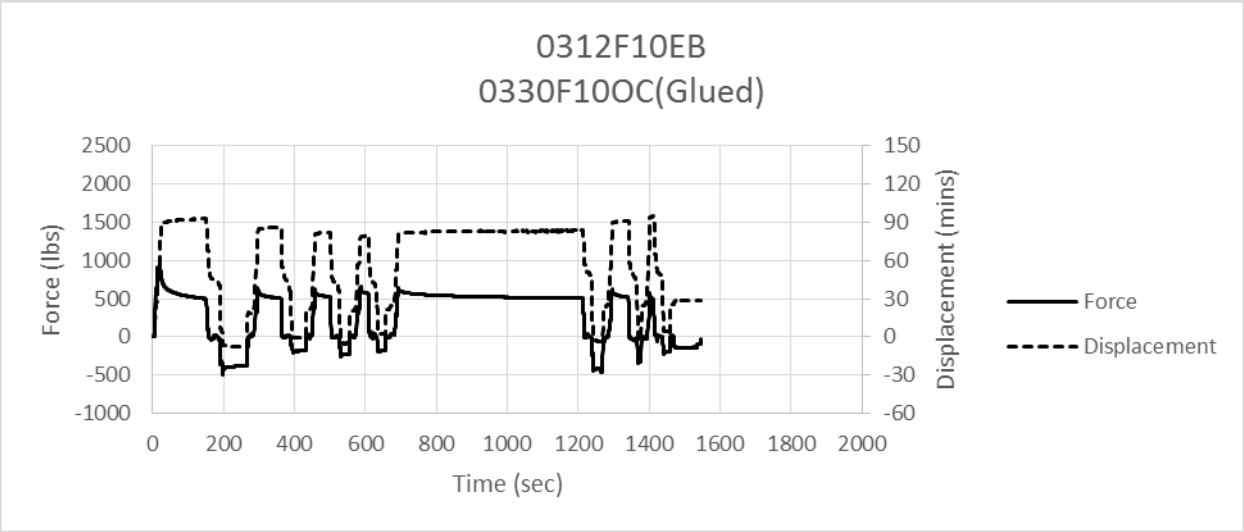

Figure A-A3.9. F10(Glued) Force and Displacement vs. Time (Tested on 4/10/15)

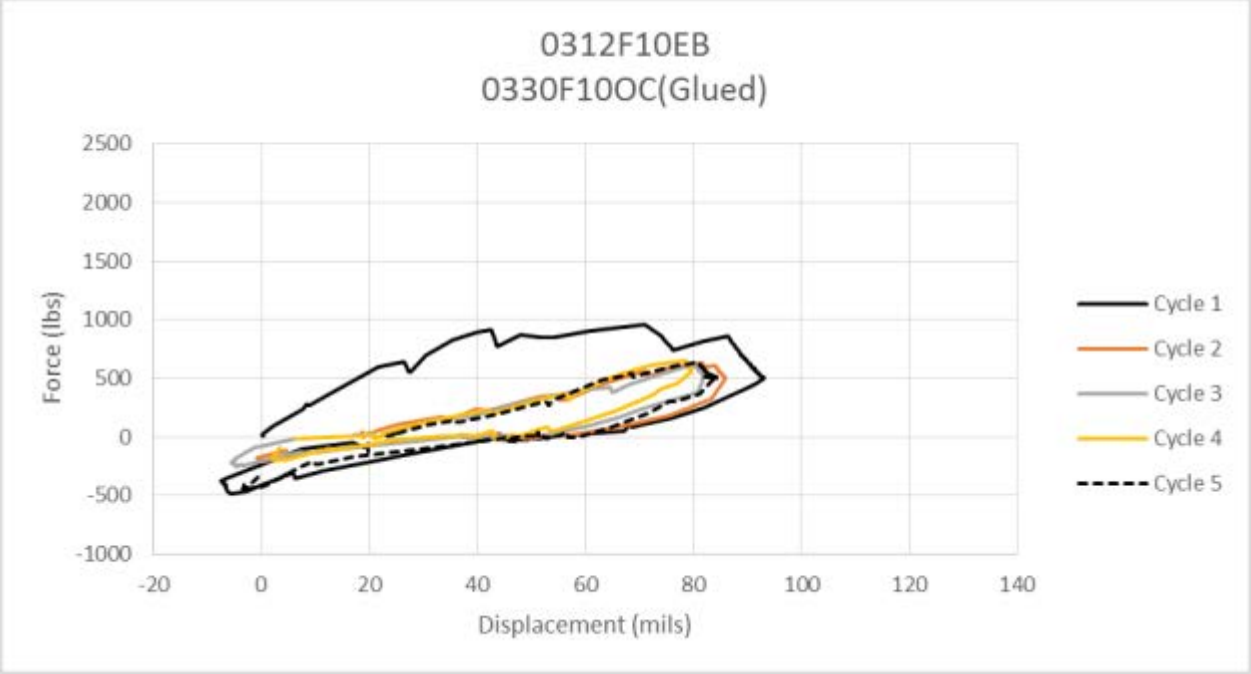

Figure A-A3.10. F10(Glued) Force vs. Displacement (Tested on 4/10/15)

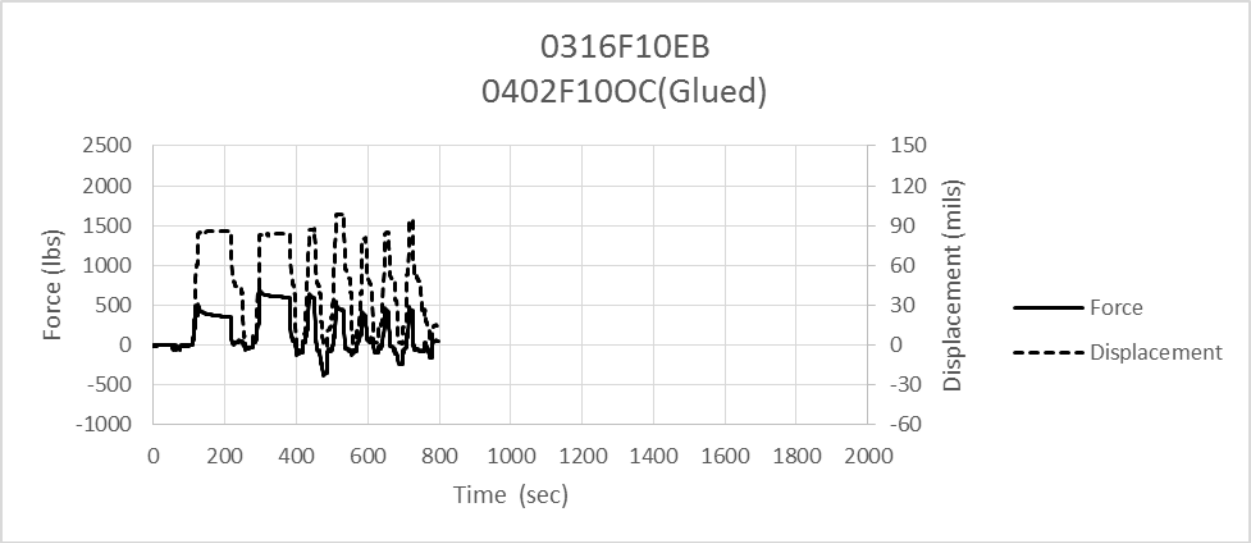

Figure A-A3.11. F10(Glued) Force and Displacement vs. Time (Tested on 4/10/15)

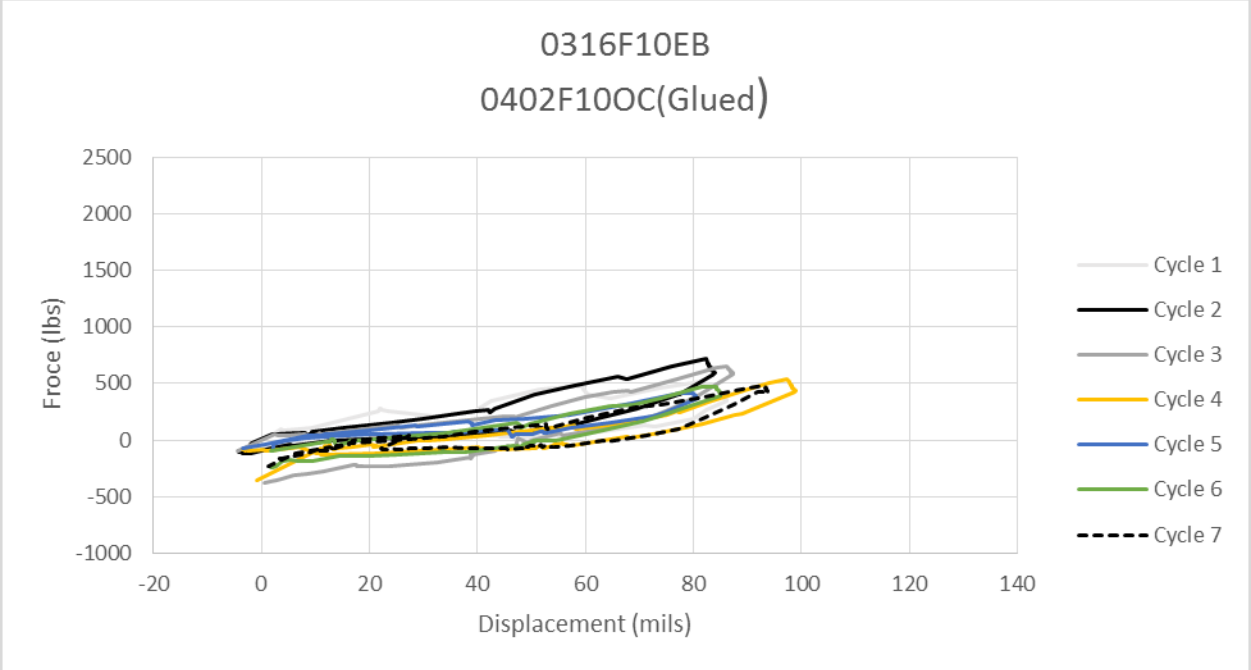

Figure A-A3.12. F10(Glued) Force vs. Displacement (Tested on 4/10/15)

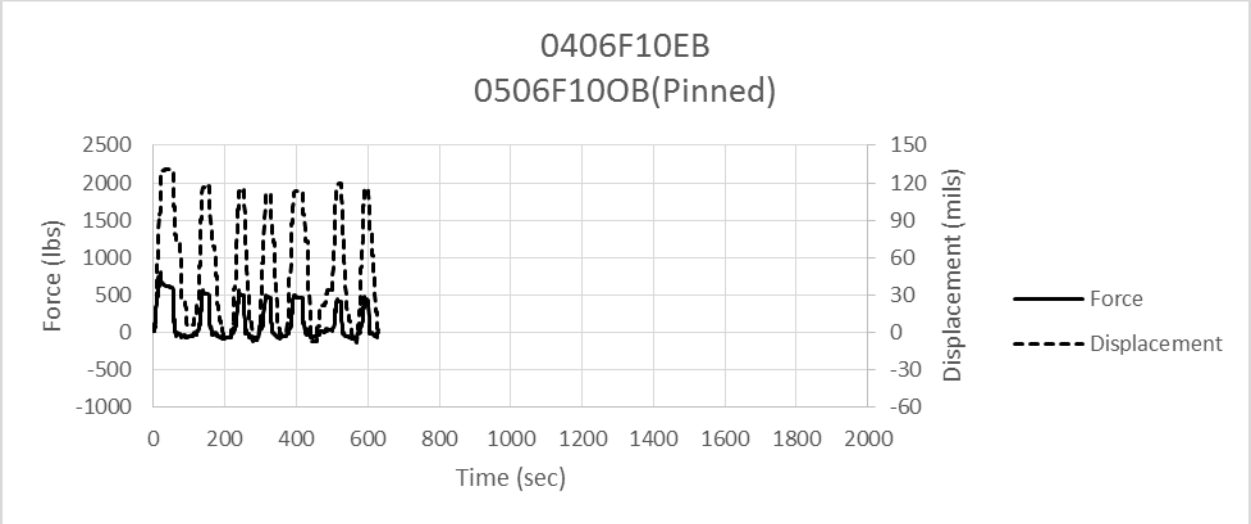

Figure A-A3.13. F10(Pinned) Force and Displacement vs. Time (Tested on 5/11/15)

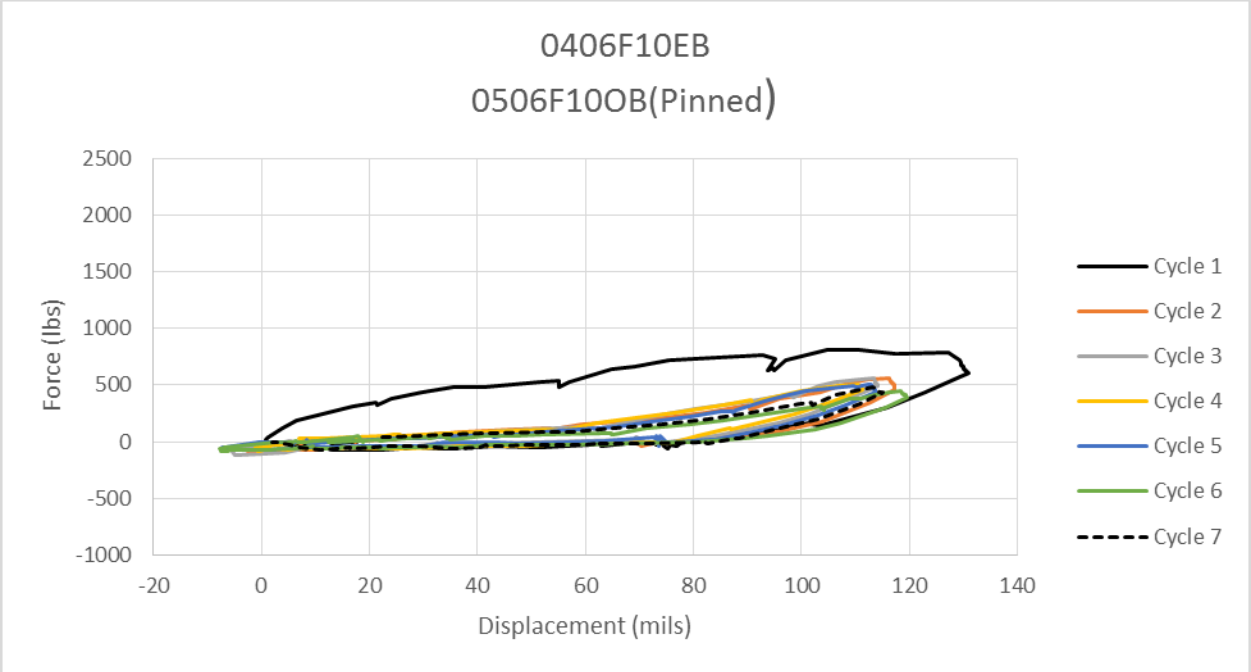

Figure A-A3.14. F10(Pinned) Force vs. Displacement (Tested on 5/11/15)

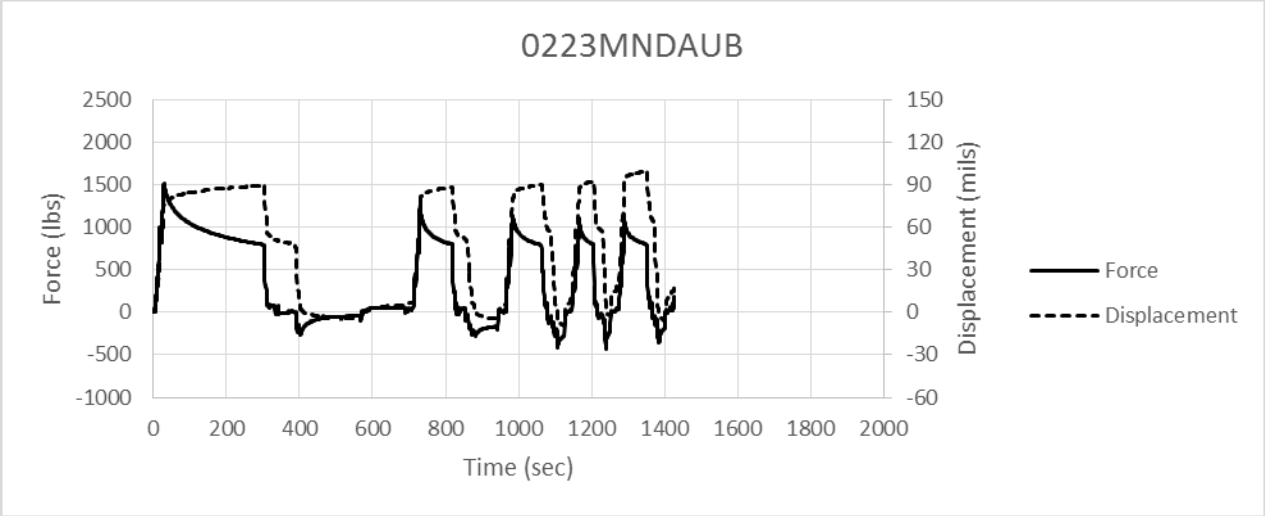

Figure A-A3.15. MNDAU Force and Displacement vs. Time (Tested on 3/24/15)

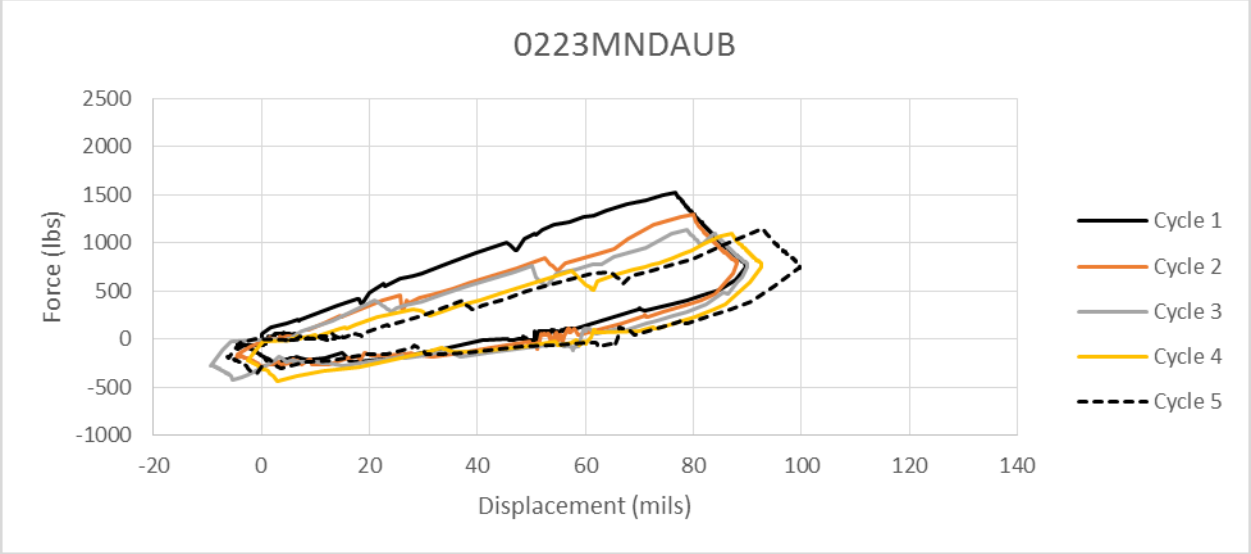

Figure A-A3.16. MNDAU Force vs. Displacement (Tested on 3/24/15)

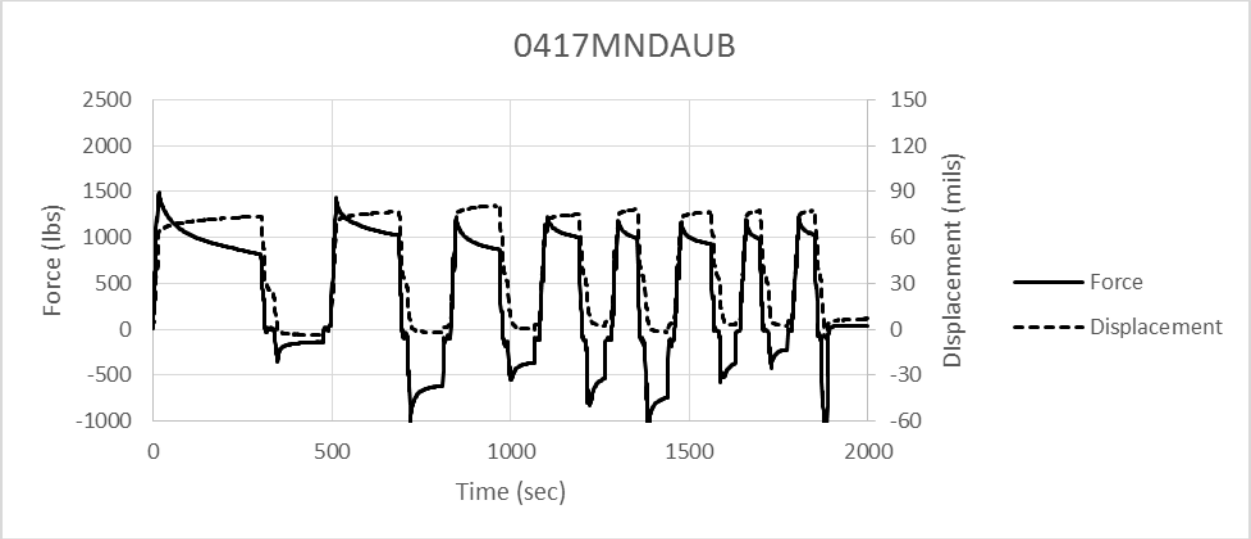

Figure A-A3.17. MNDAU Force and Displacement vs. Time (Tested on 4/23/15)

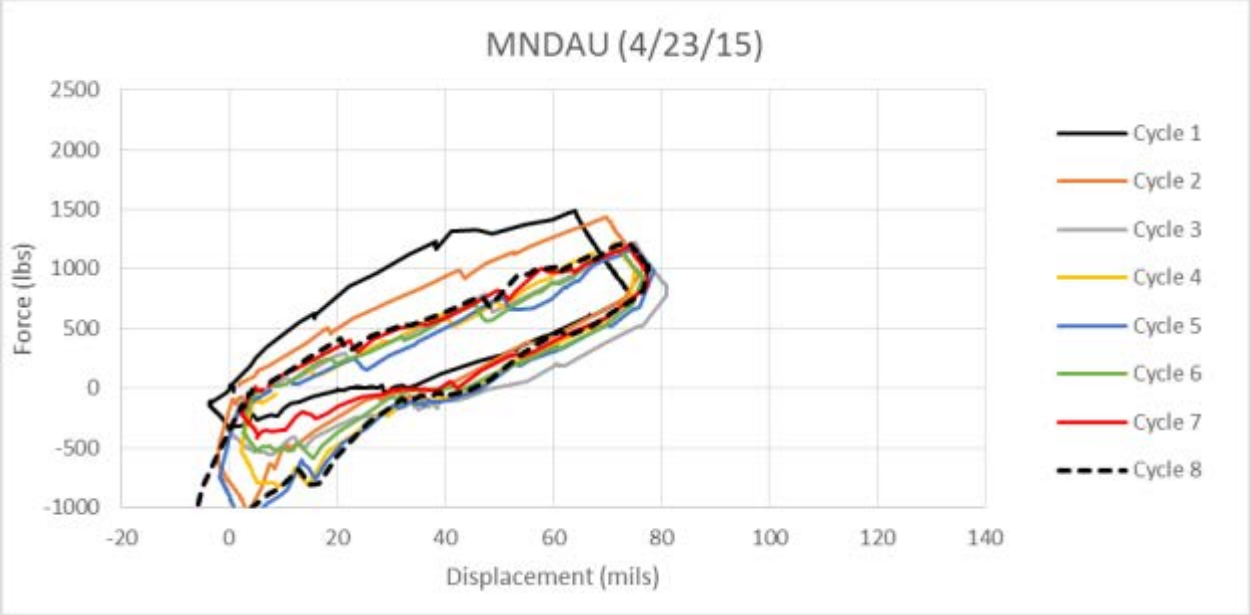

Figure A-A3.18. MNDAU Force vs. Displacement (Tested on 4/23/15)

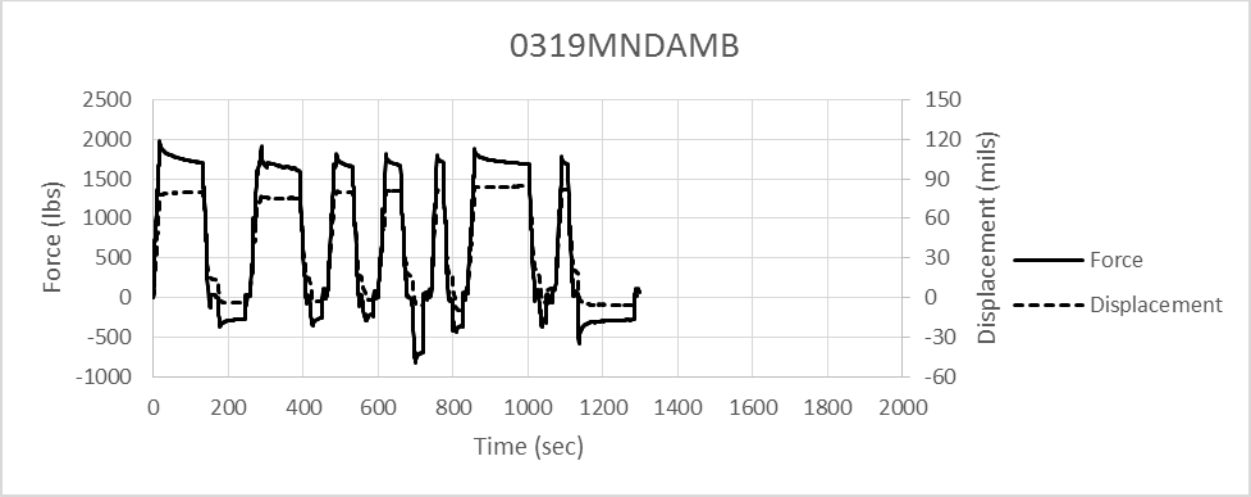

Figure A-A3.19. MNDAM Force and Displacement vs. Time (Tested on 4/3/15)

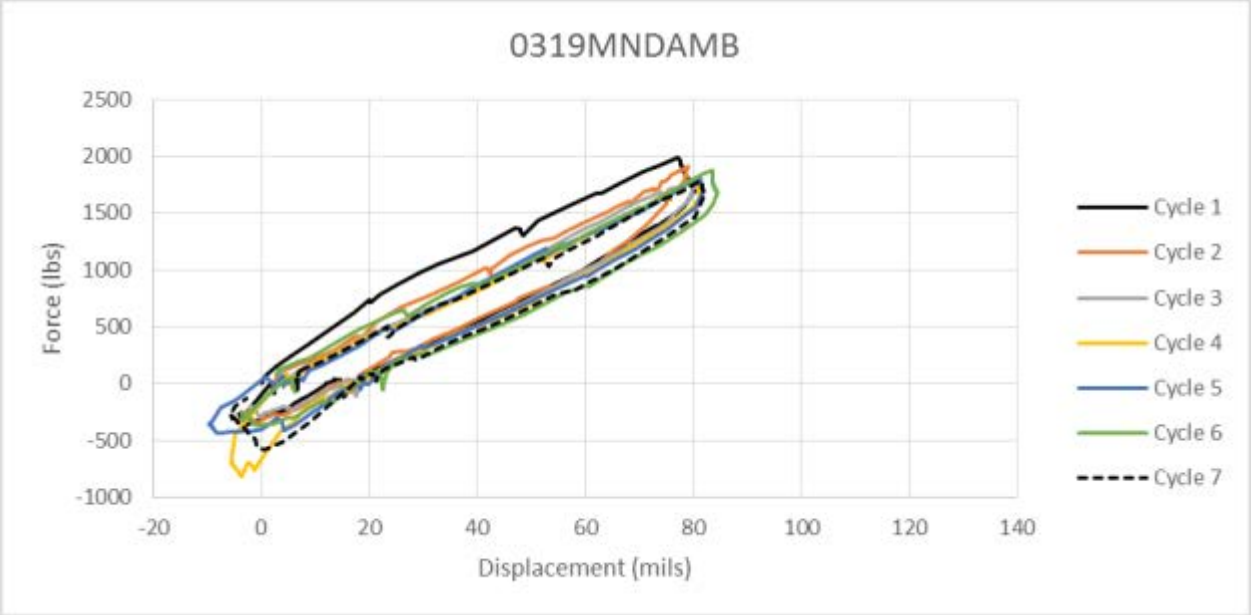

Figure A-A3.20. MNDAM Force vs. Displacement (Tested on 4/3/15)

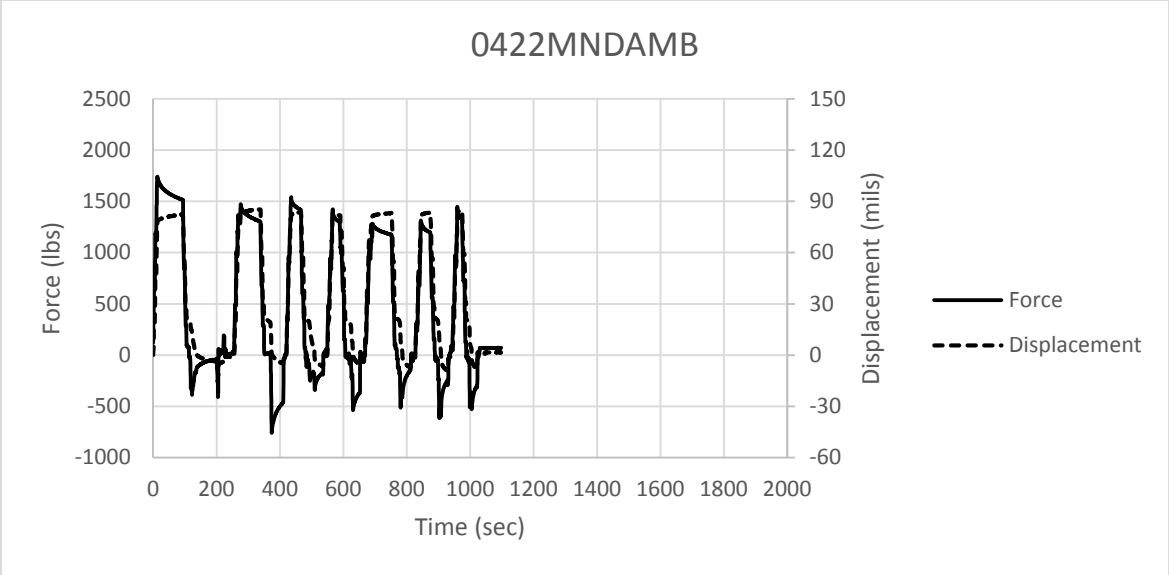

Figure A-A3.21. MNDAM Force and Displacement vs. Time (Tested on 4/27/15)

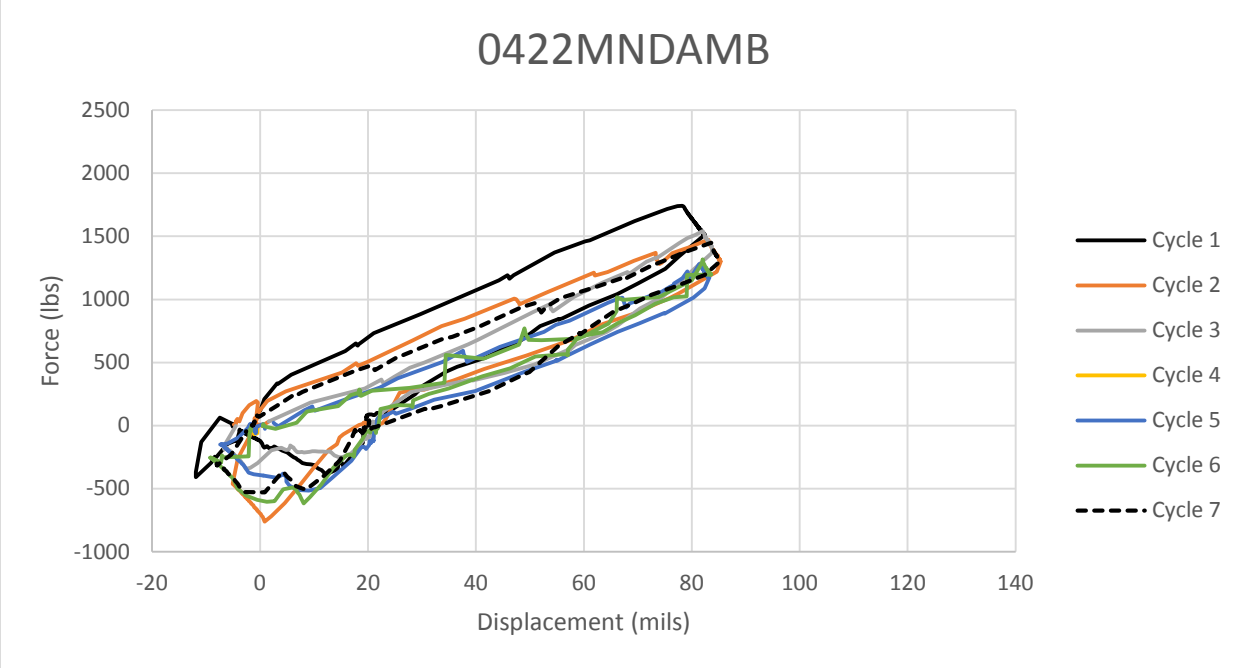

Figure A-A3.22. MNDAM Force vs. Displacement (Tested on 4/27/15)

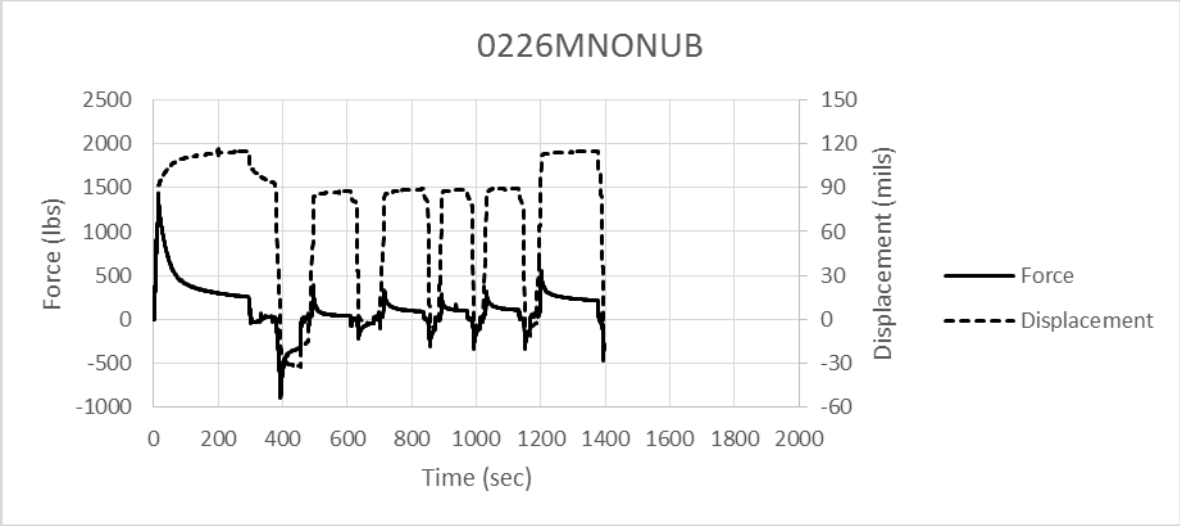

Figure A-A3.23. MNONU Force and Displacement vs. Time (Tested on 3/30/15)

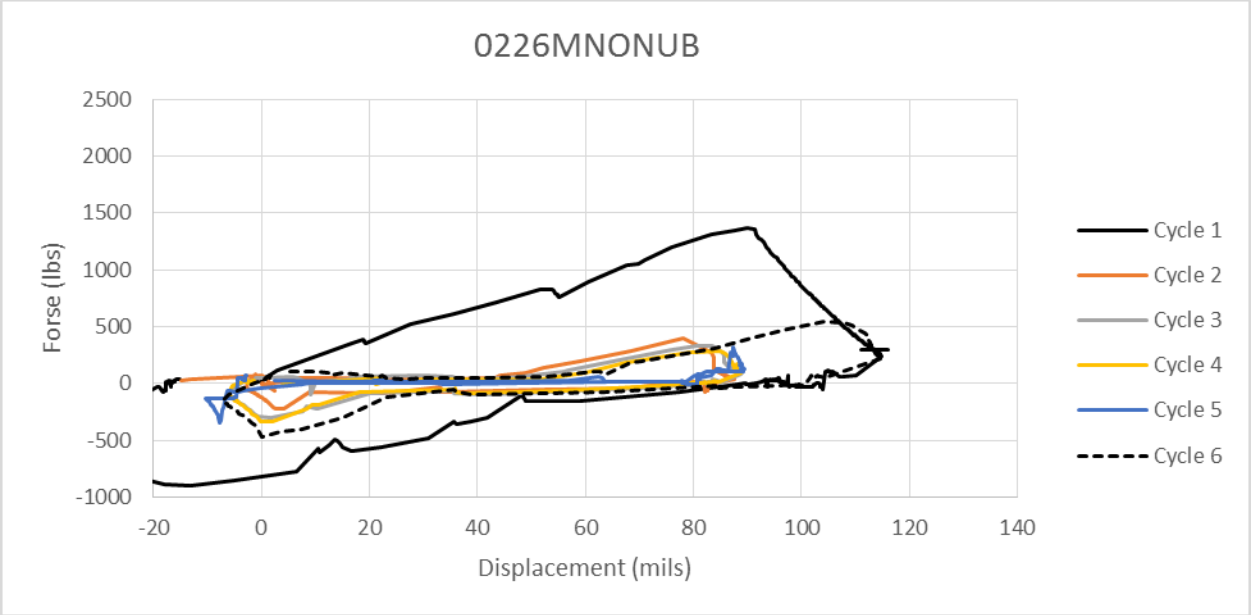

Figure A-A3.24. MNONU Force vs. Displacement (Tested on 3/30/15)

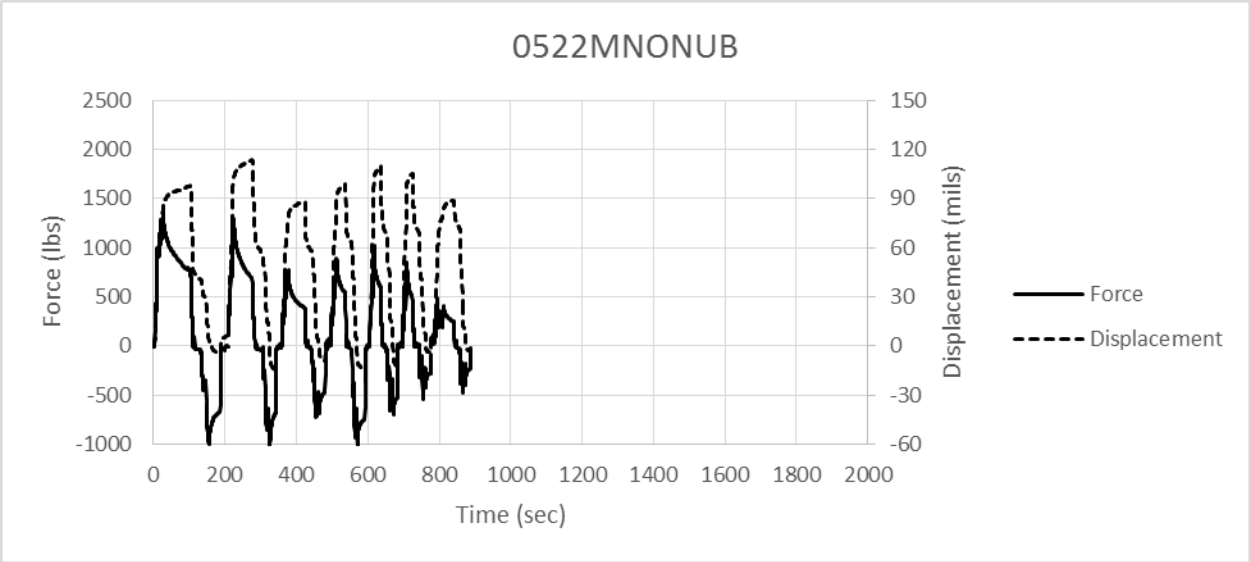

Figure A-A3.25. MNONU Force and Displacement vs. Time (Tested on 5/26/15)

Figure A-A3.26. MNONU Force vs. Displacement (Tested on 5/26/15)

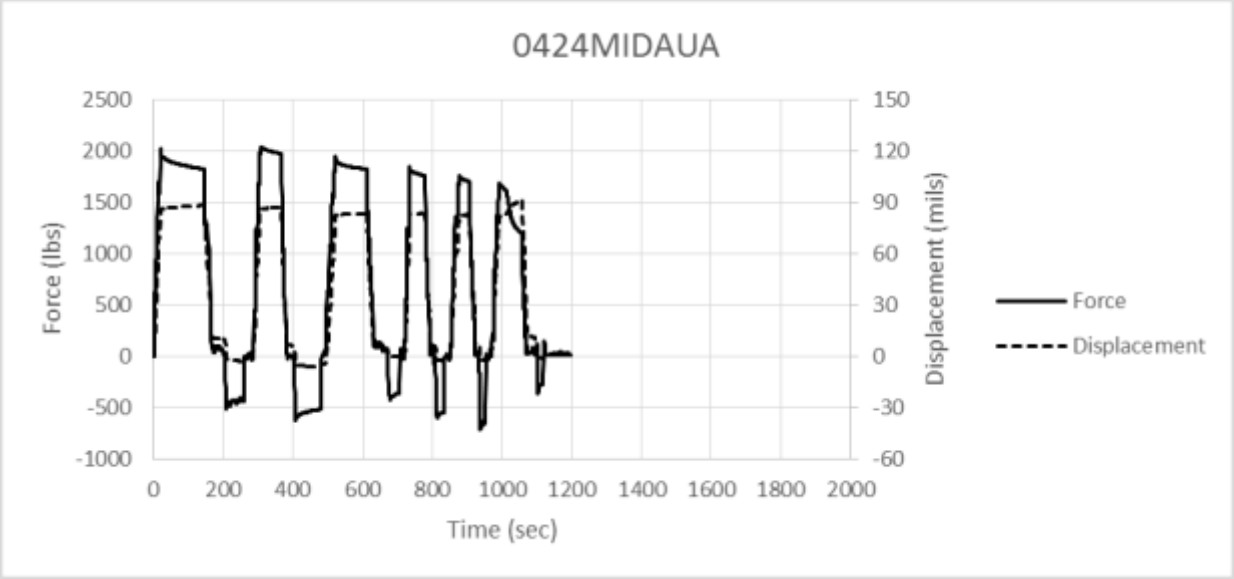

Figure A-A3.27. MIDAU Force and Displacement vs. Time (Tested on 4/29/15)

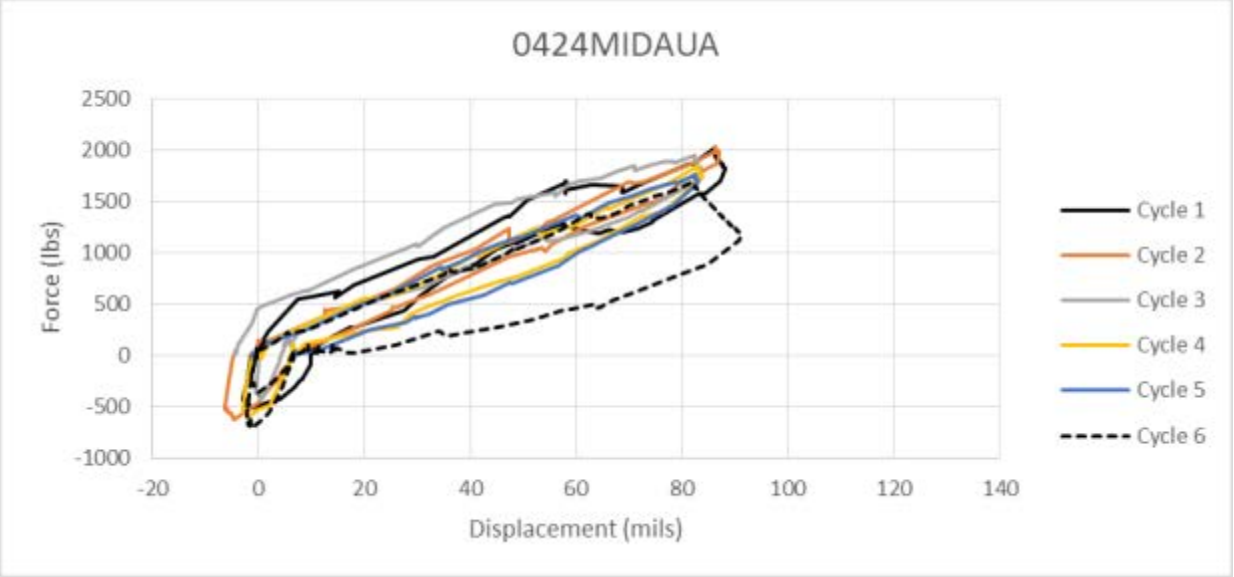

Figure A-A3.28. MIDAU Force vs. Displacement (Tested on 4/29/15)

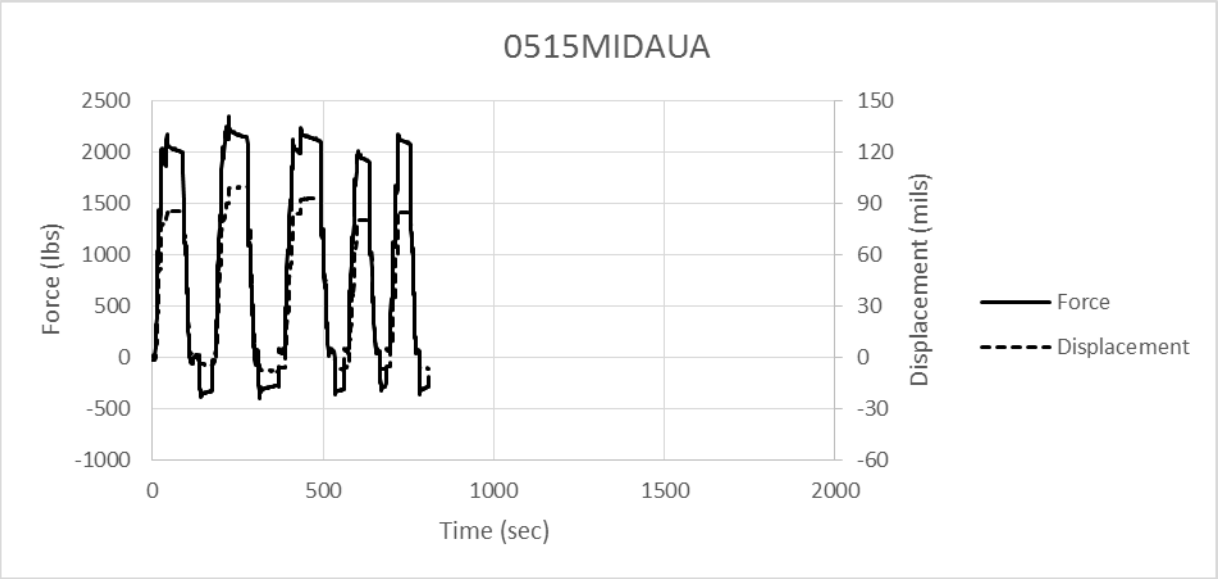

Figure A-A3.29. MIDAU Force and Displacement vs. Time (Tested on 5/20/15)

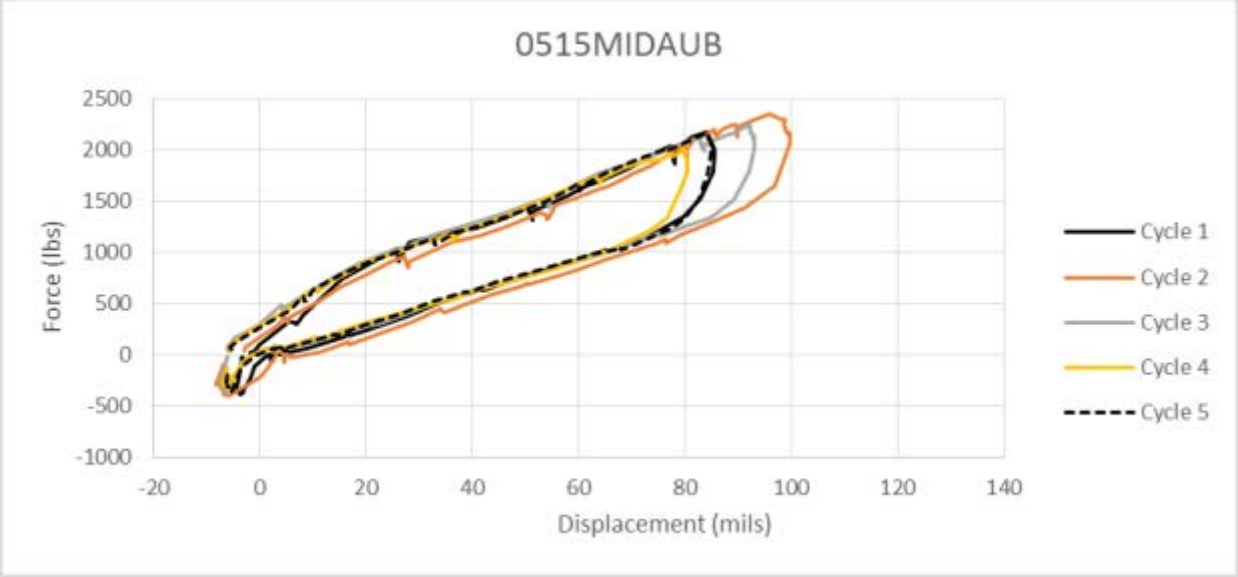

Figure A-A3.30. MIDAU Force vs. Displacement (Tested on 5/20/15)

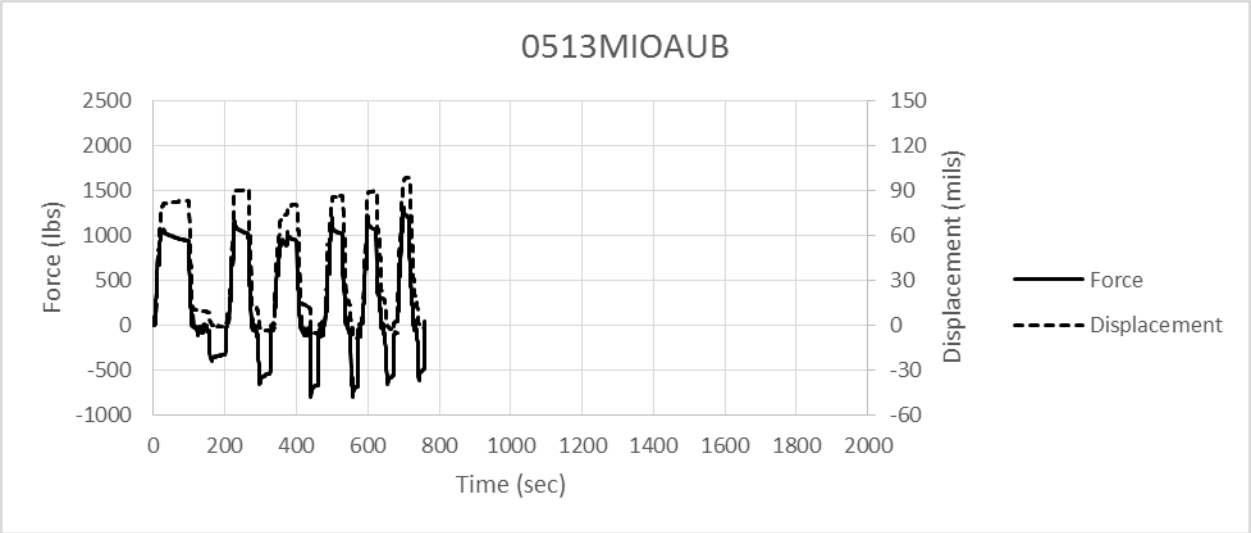

Figure A-A3.31. MIOAU Force and Displacement vs. Time (Tested on 5/18/15)

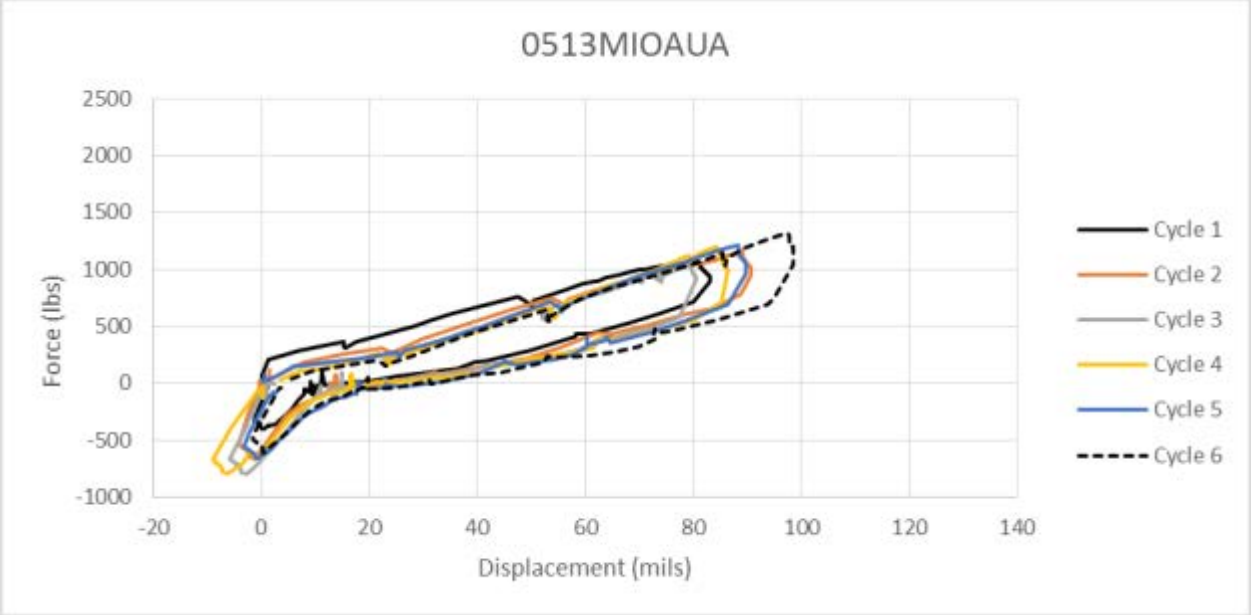

Figure A-A3.32. MIOAU Force vs. Displacement (Tested on 5/18/15)

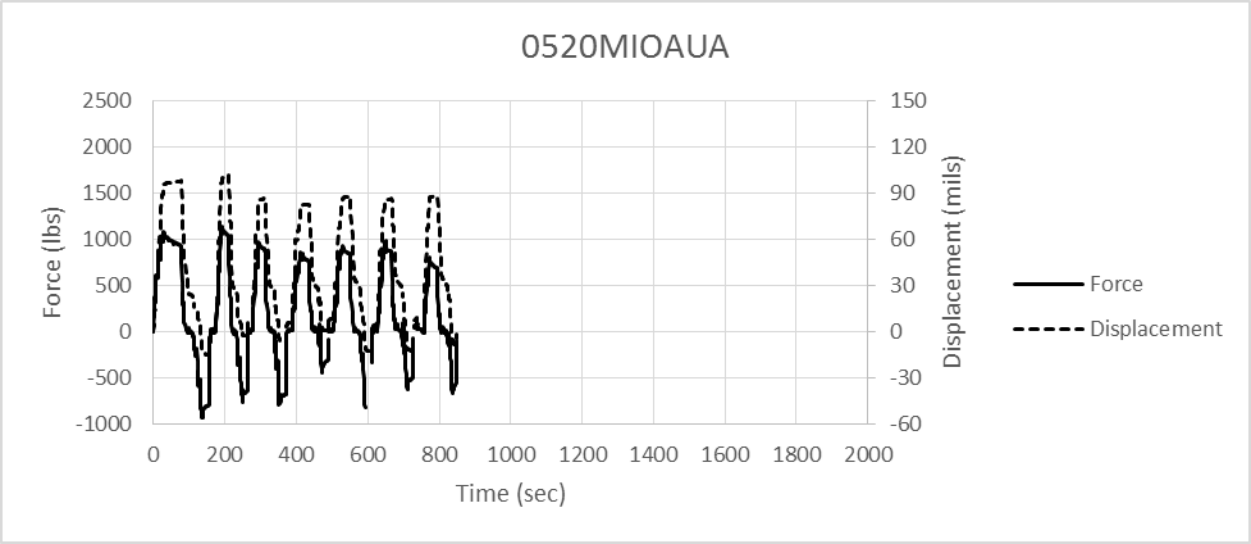

Figure A-A3.33. MIOAU Force and Displacement vs. Time (Tested on 5/26/15)

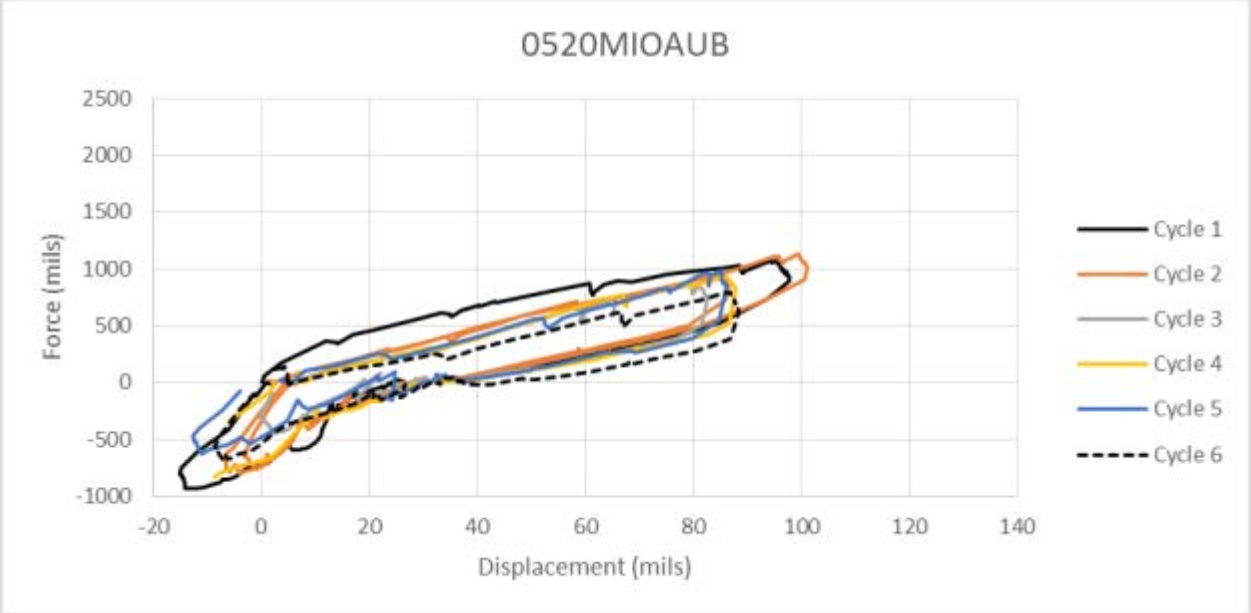

Figure A-A3.34. MIOAU Force vs. Displacement (Tested on 5/26/15)

Appendix 4: Mechanism 3 Data

The following plots, one for each specimen, show measured displacement of the overlay (TOP(OL)) and the existing (BOT(EXIST)) beam versus the force applied to the beam tested for reflective cracking.

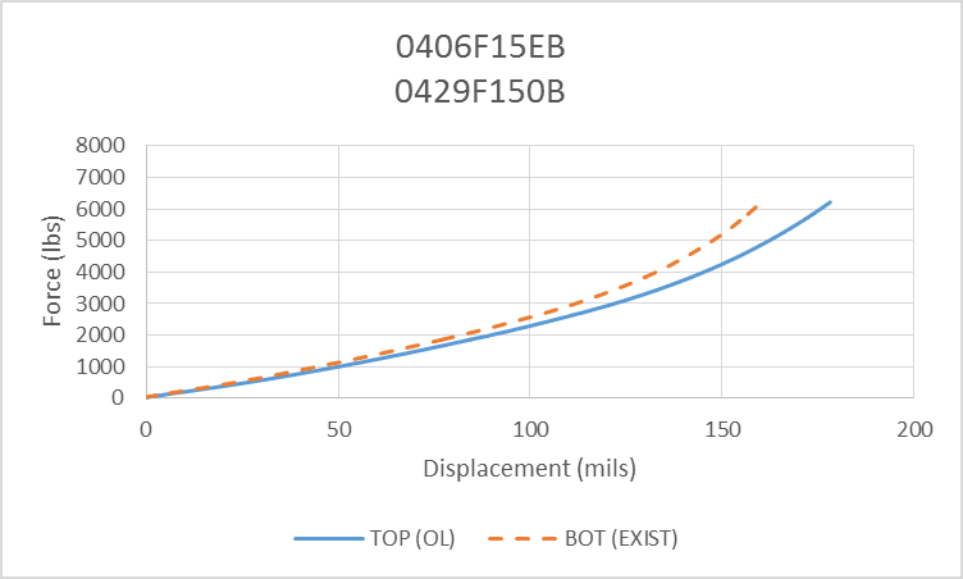

Figure A-A4.1. F15 Force vs. Displacement (Tested on 5/4/15)

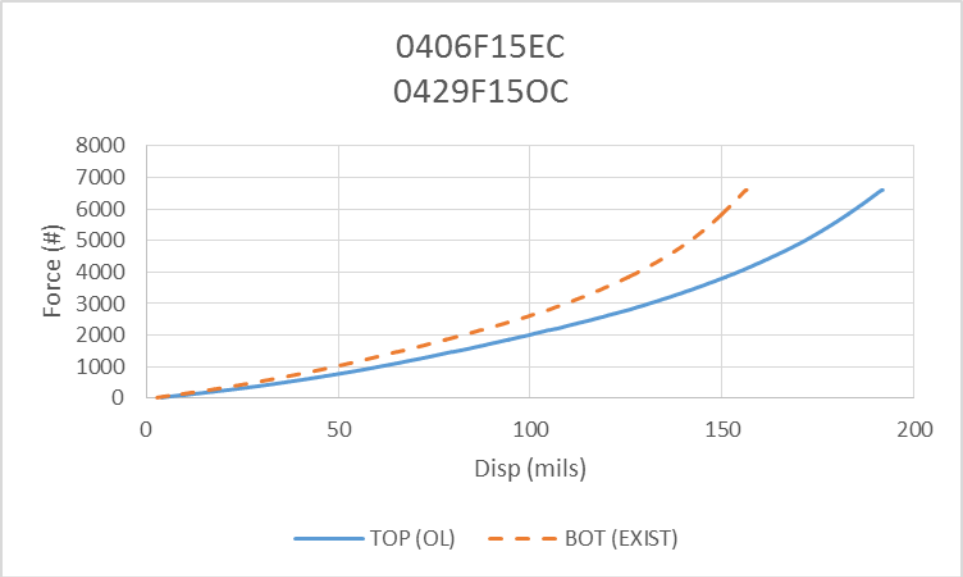

Figure A-A4.2. F15 Force vs. Displacement (Tested on 5/4/15)

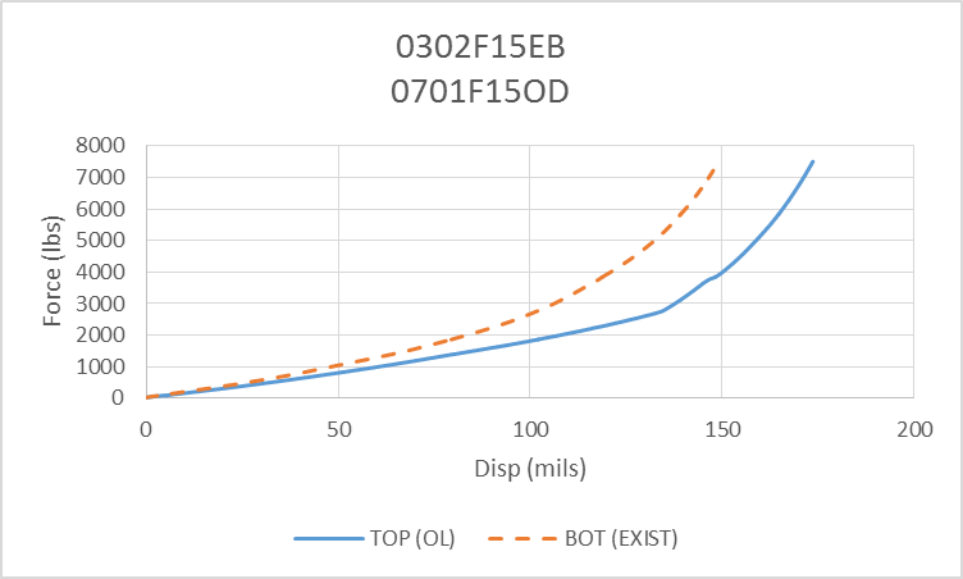

Figure A-A4.3. F15 Force vs. Displacement (Tested on 7/6/15)

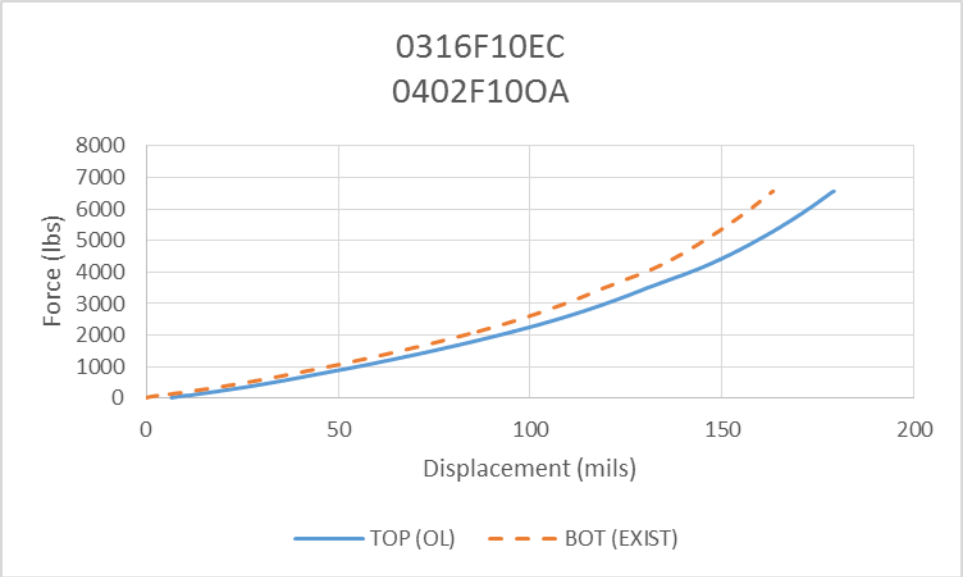

Figure A-A4.4. F10 Force vs. Displacement (Tested on 4/7/15)

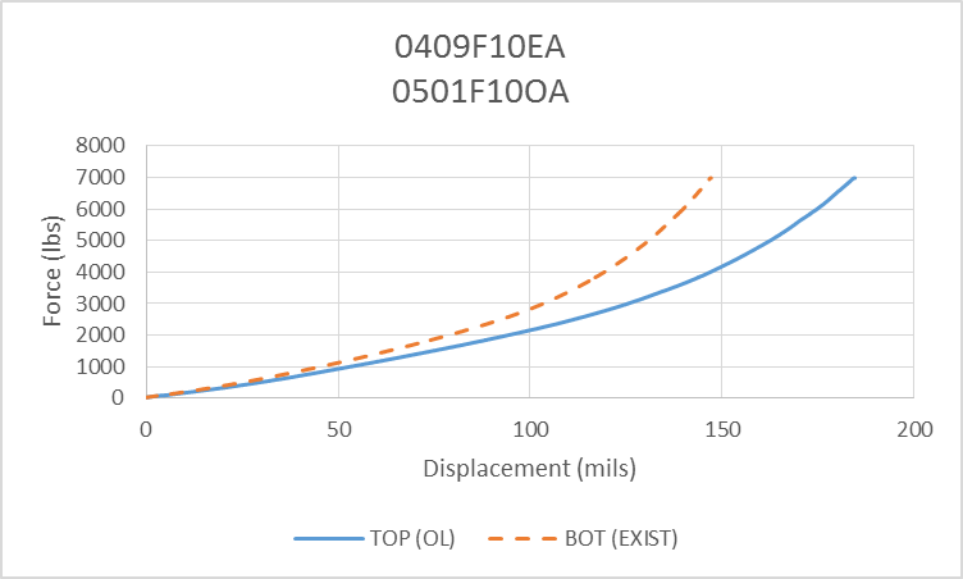

Figure A-A4.5. F10 Force vs. Displacement (Tested on 5/6/15)

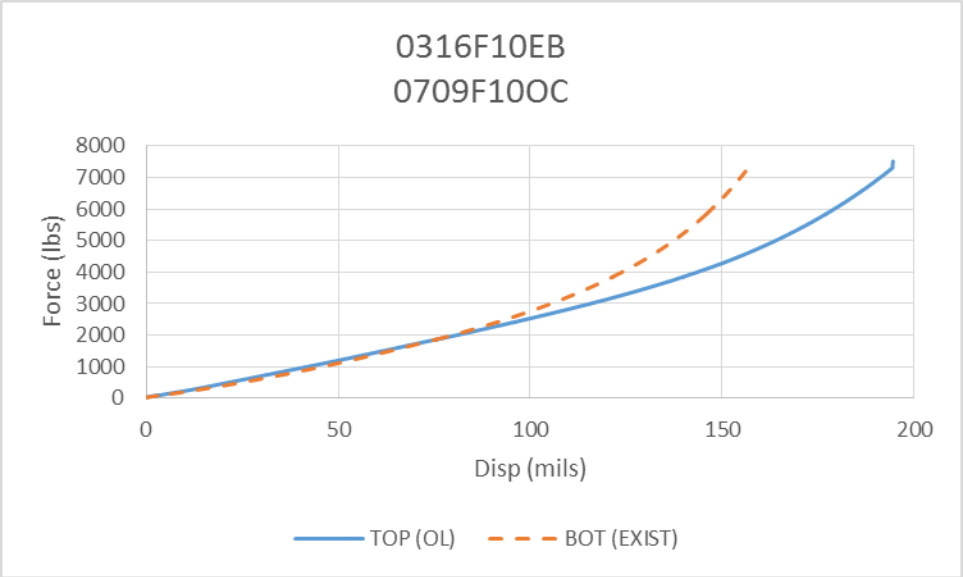

Figure A-A4.6. F10 Force vs. Displacement (Tested on 7/14/15)

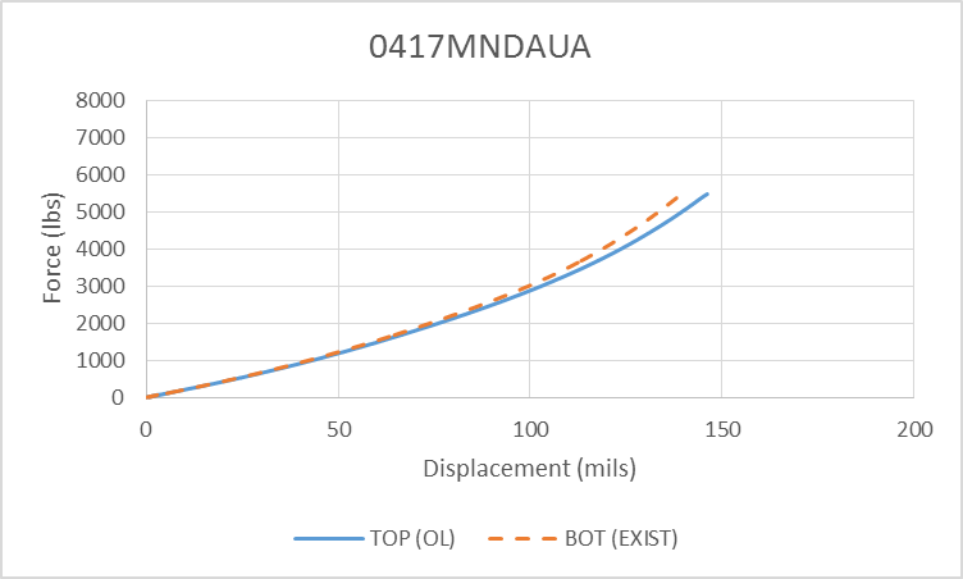

Figure A-A4.7. MNDAU Force vs. Displacement (Tested on 4/22/15)

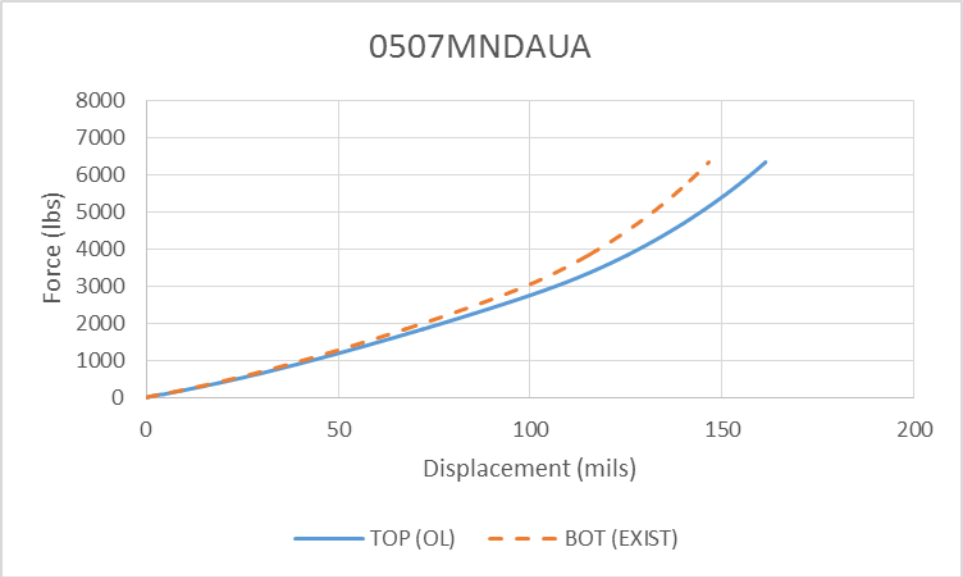

Figure A-A4.8. MNDAU Force vs. Displacement (Tested on 5/12/15)

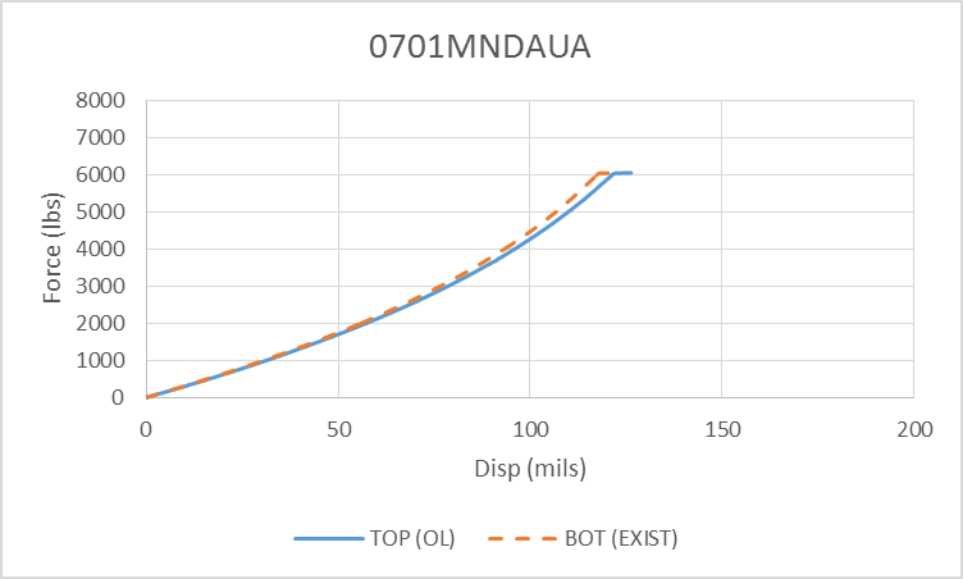

Figure A-A4.9. MNDAU Force vs. Displacement (Tested on 7/6/15)

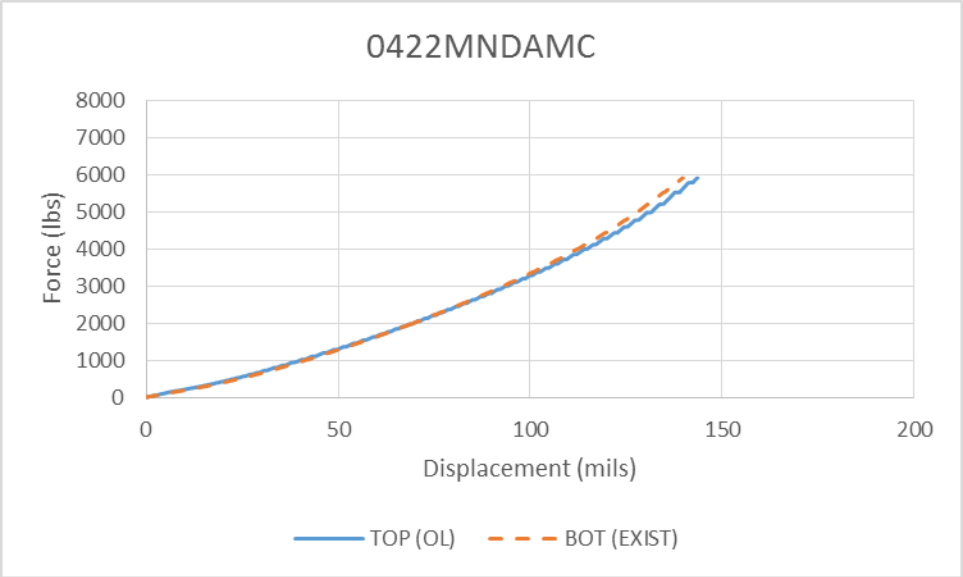

Figure A-A4.10. MNDAM Force vs. Displacement (Tested on 4/27/15)

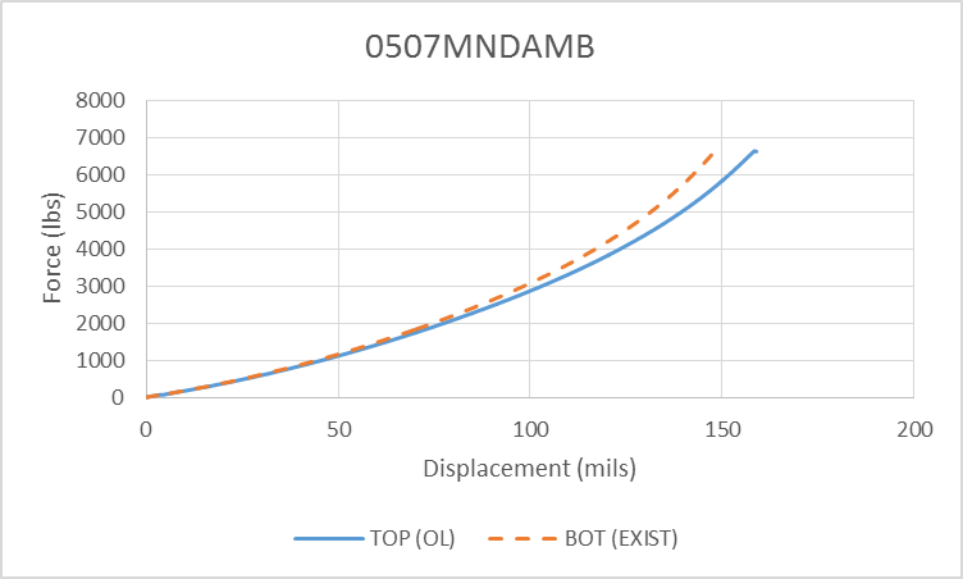

Figure A-A4.11. MNDAM Force vs. Displacement (Tested on 5/12/15)

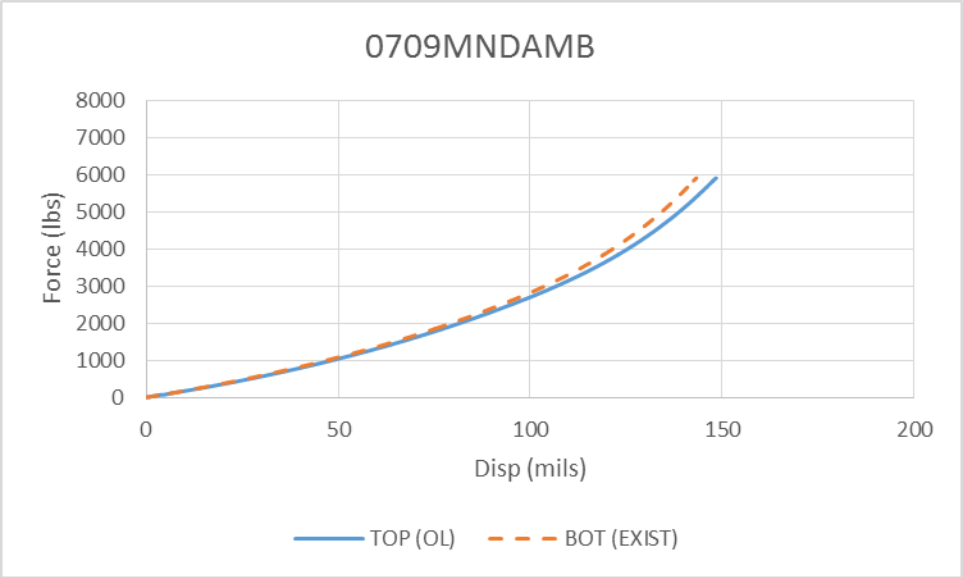

Figure A-A4.12. MNDAM Force vs. Displacement (Tested on 7/14/15)

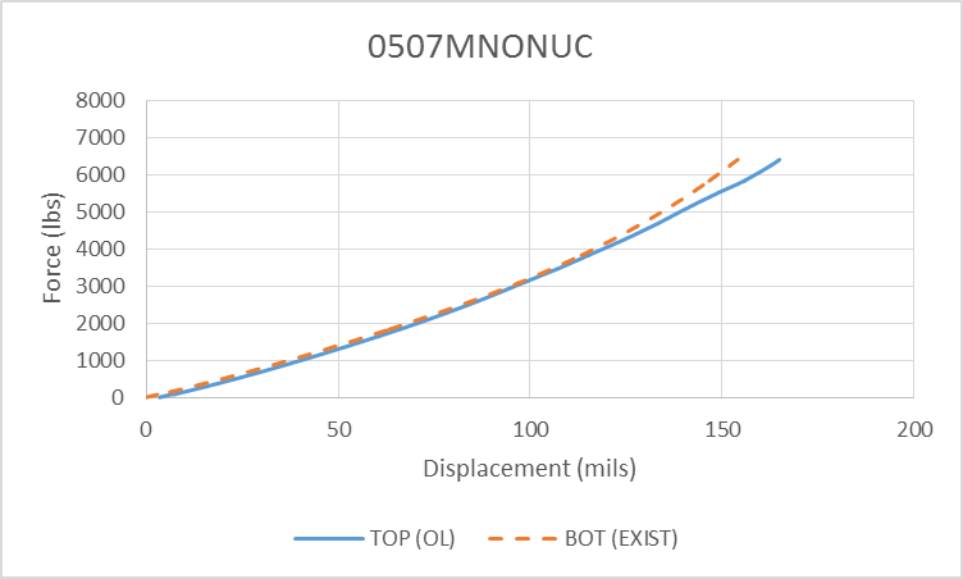

Figure A-A4.13. MNONU Force vs. Displacement (Tested on 5/12/15)

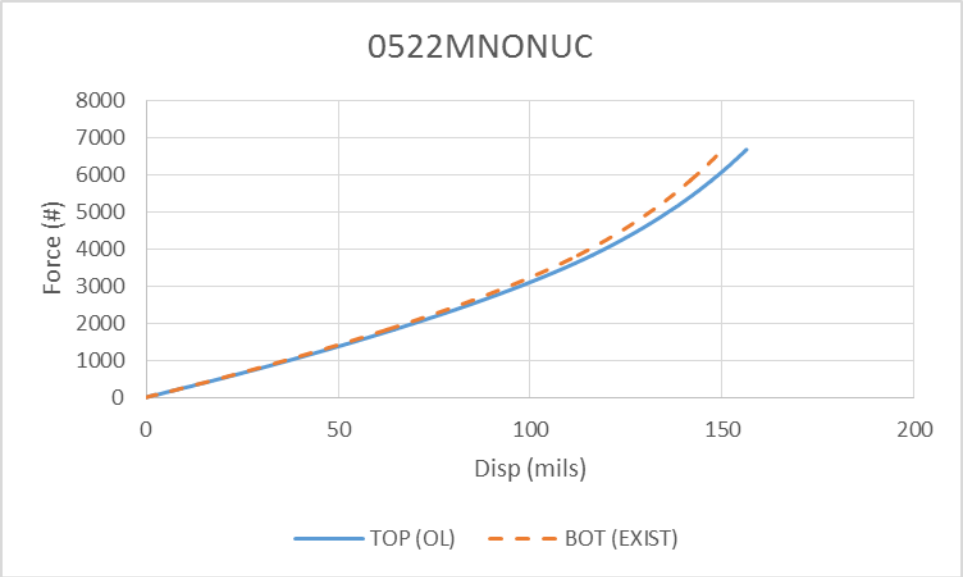

Figure A-A4.14. MNONU Force vs. Displacement (Tested on 5/27/15)

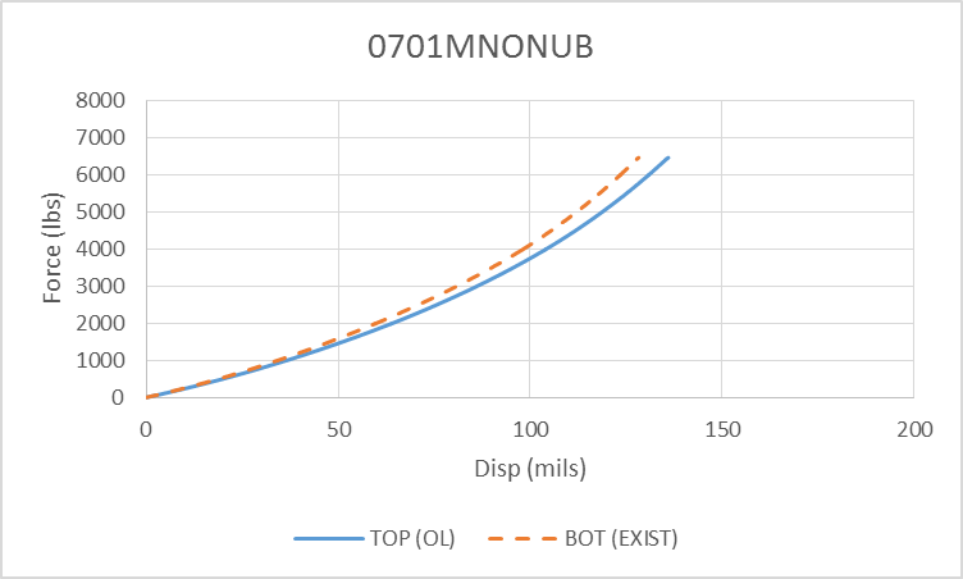

Figure A-A4.15. MNONU Force vs. Displacement (Tested on 7/6/15)

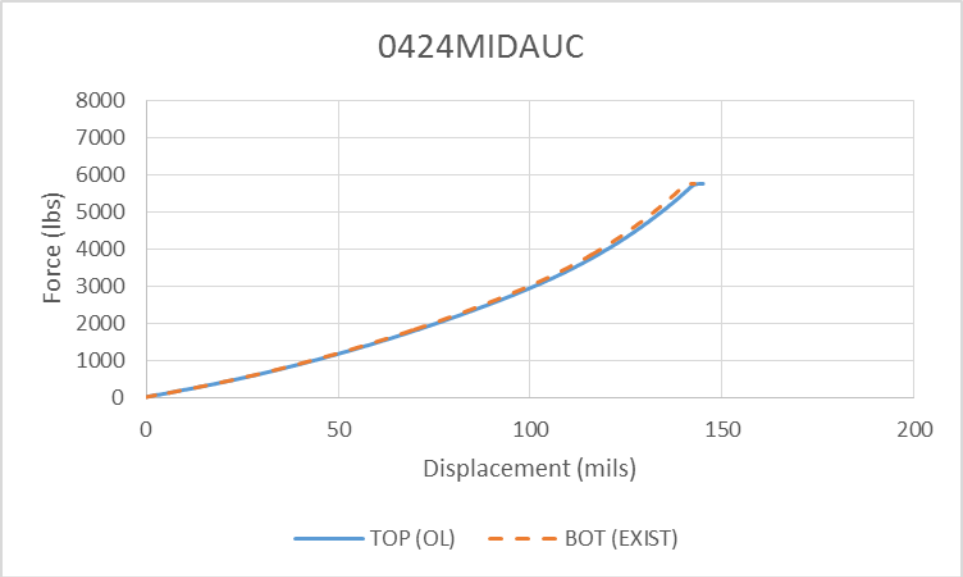

Figure A-A4.16. MIDAU Force vs. Displacement (Tested on 4/29/15)

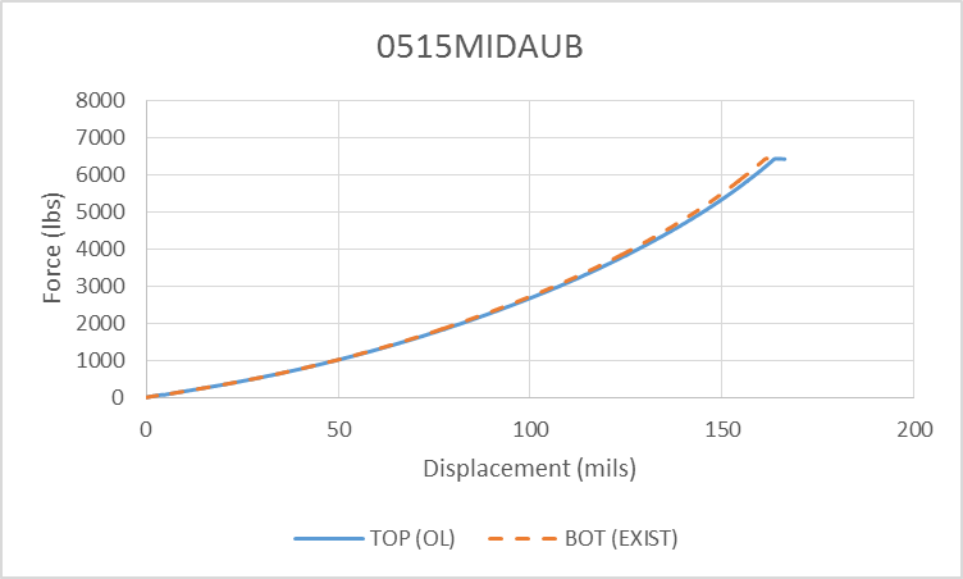

Figure A-A4.17. MIDAU Force vs. Displacement (Tested on 5/20/15)

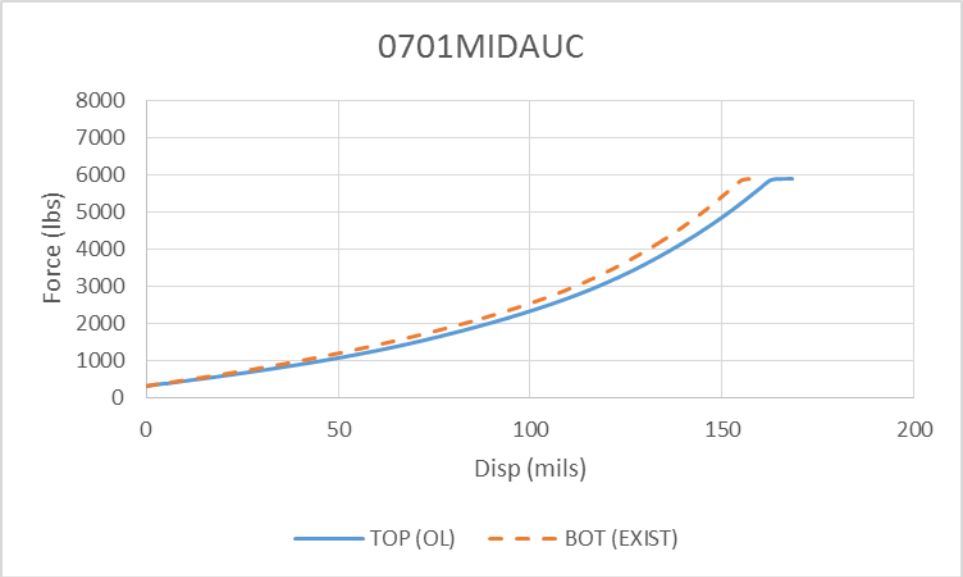

Figure A-A4.18. MIDAU Force vs. Displacement (Tested on 7/6/15)

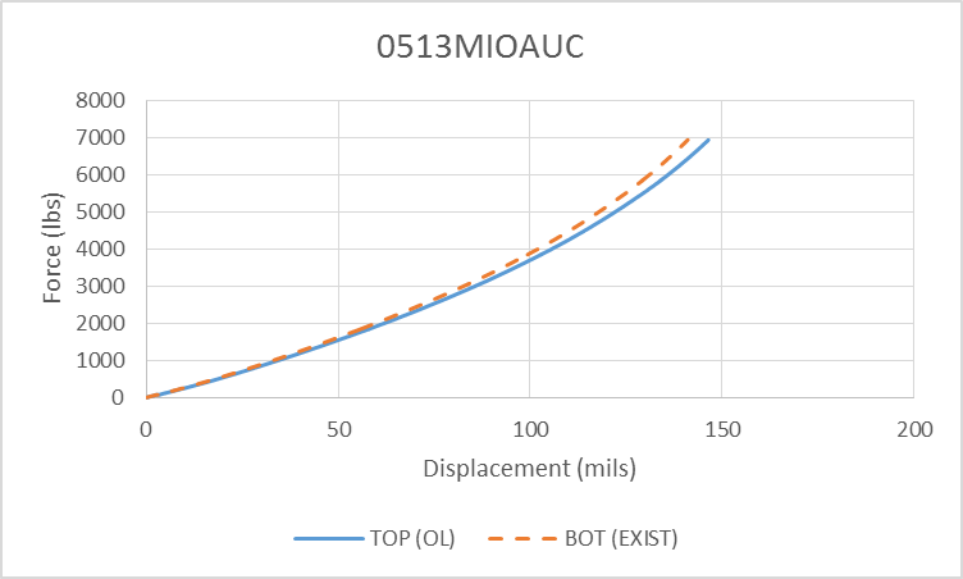

Figure A-A4.19. MIOAU Force vs. Displacement (Tested on 5/18/15)

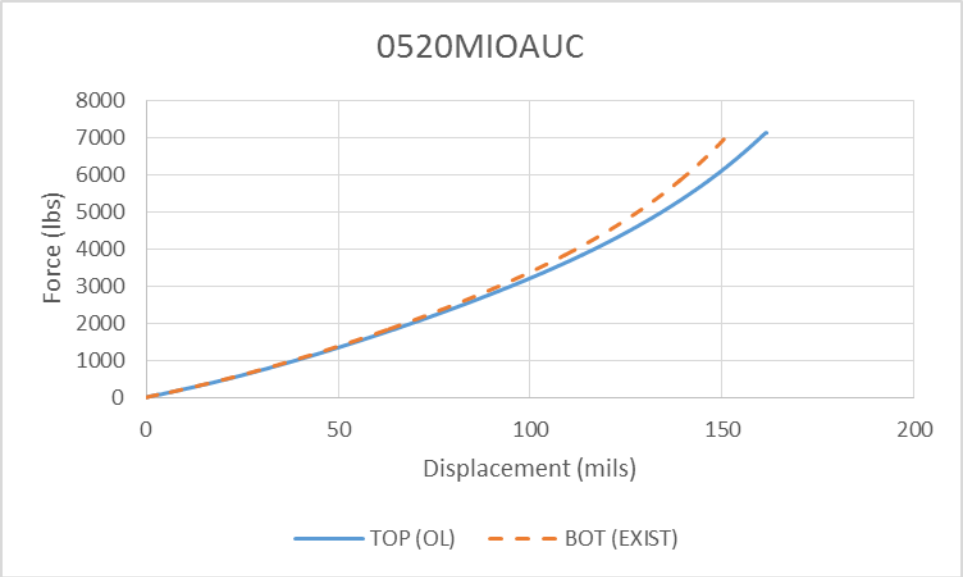

Figure A-A4.20. MIOAU Force vs. Displacement (Tested on 5/25/15)

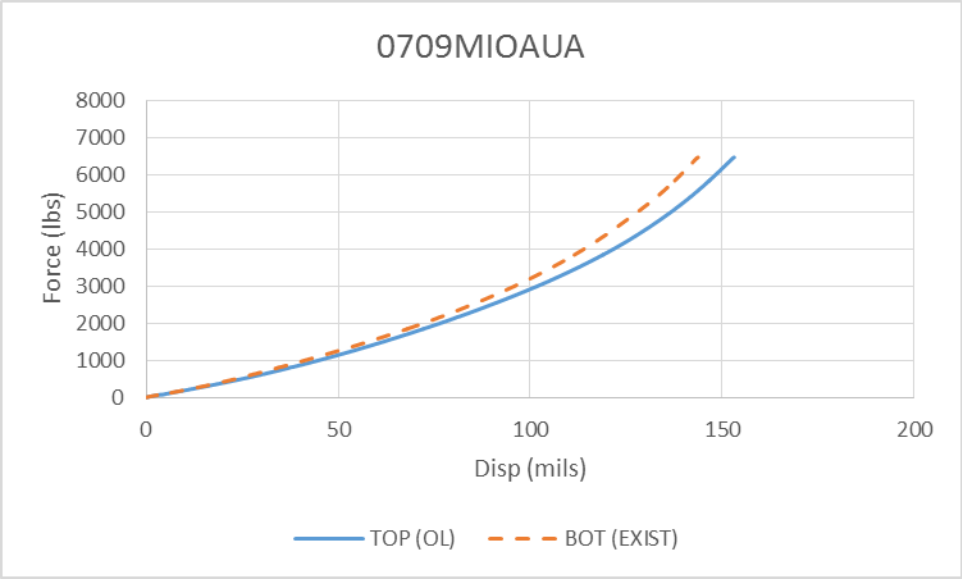

Figure A-A4.21. MIOAU Force vs. Displacement (Tested on 7/14/15)

Appendix 5: Mechanism 4 Data

The following plots, one for each specimen, show force versus displacement for the displacement controlled direct tension test.

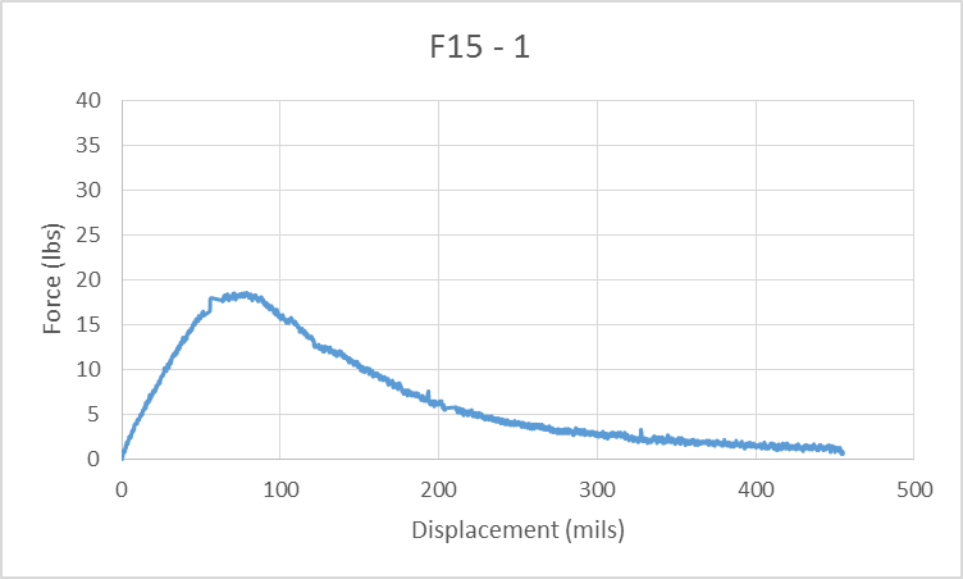

Figure A-A5.1 F15 Specimen 1 Force vs. Displacement (Tested on 5/18/15)

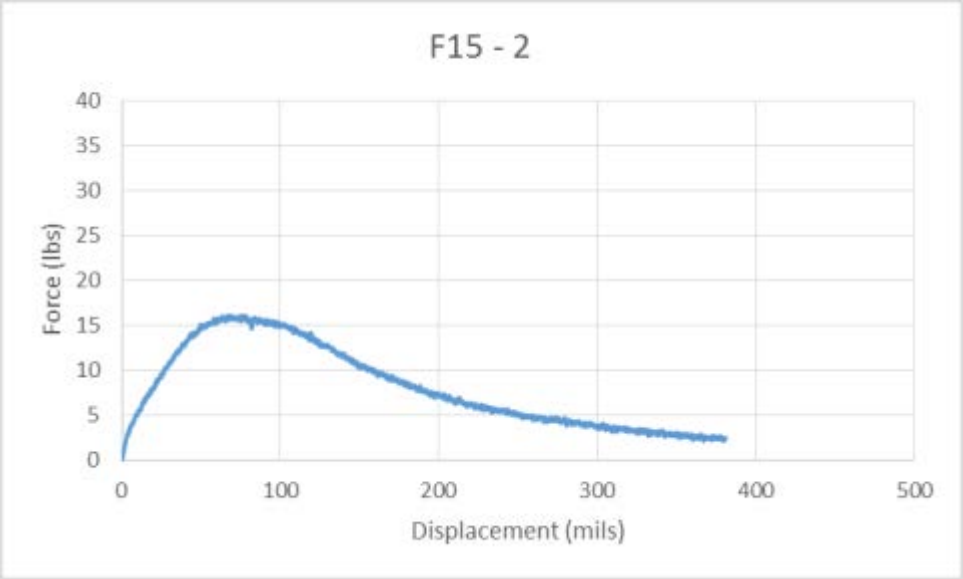

Figure A-A5.2 F15 Specimen 2 Force vs. Displacement (Tested on 5/18/15)

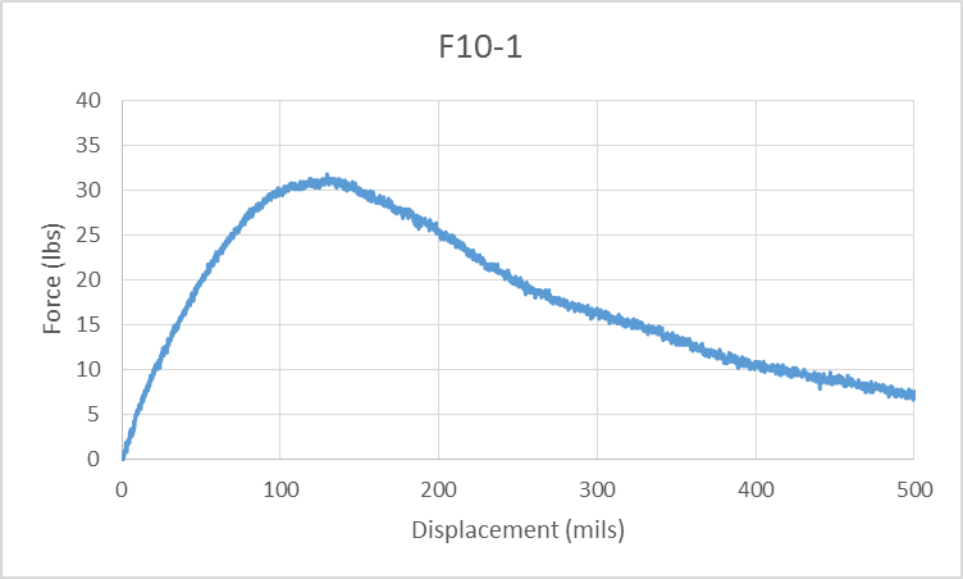

Figure A-A5.3 F10 Specimen 1 Force vs. Displacement (Tested on 5/18/15)

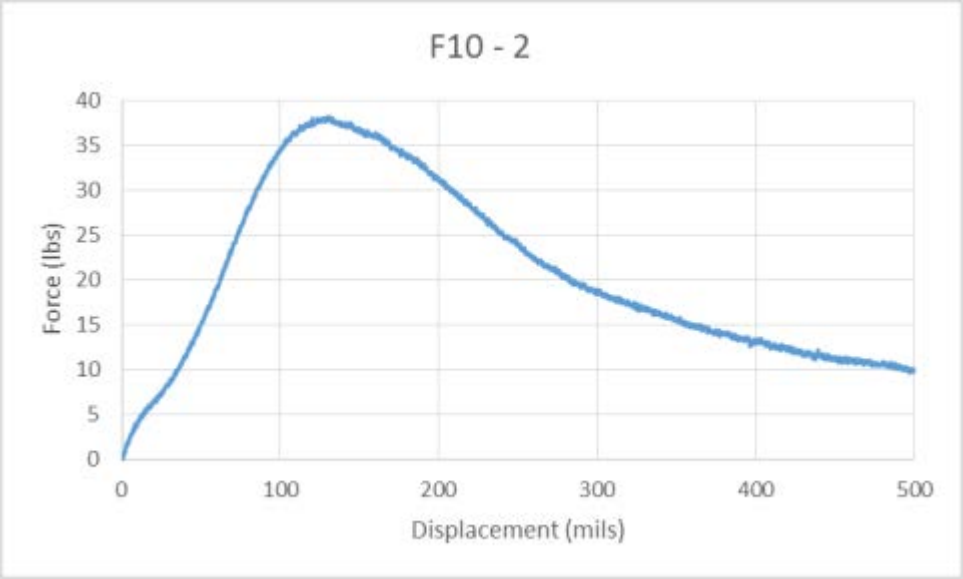

Figure A-A5.4 F10 Specimen 2 Force vs. Displacement (Tested on 5/18/15)

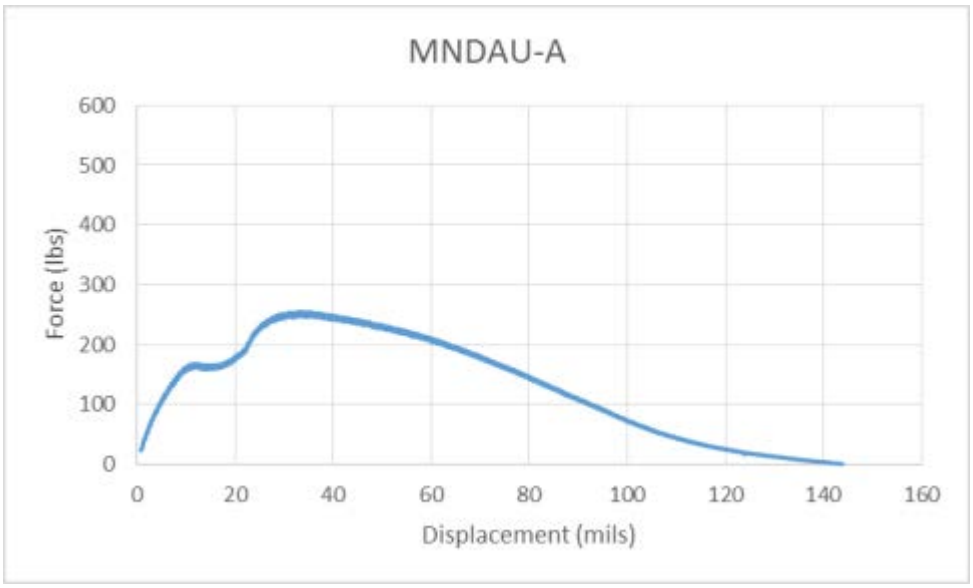

Figure A-A5.5 MNDAU Specimen A Force vs. Displacement (Tested on 6/17/15)

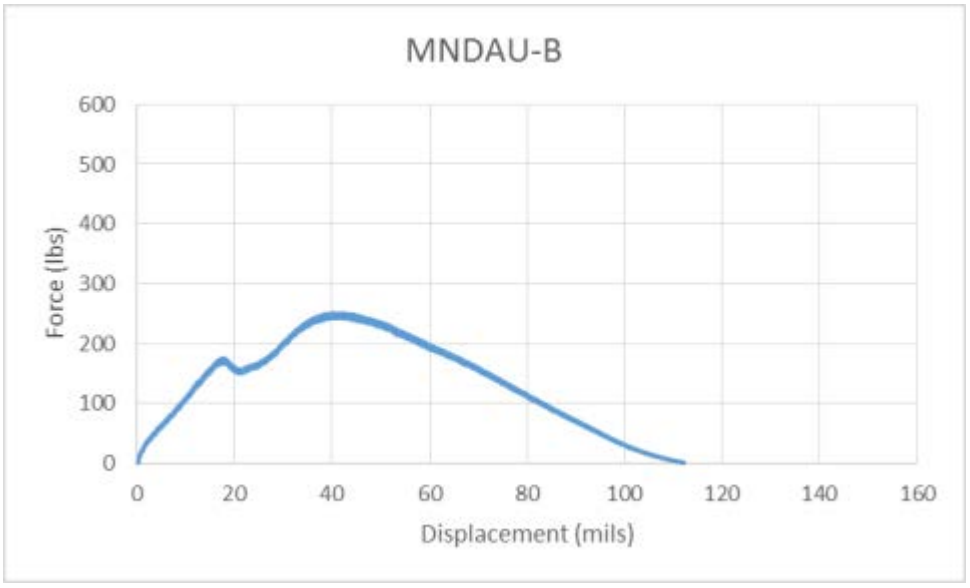

Figure A-A5.6 MNDAU Specimen B Force vs. Displacement (Tested on 6/17/15)

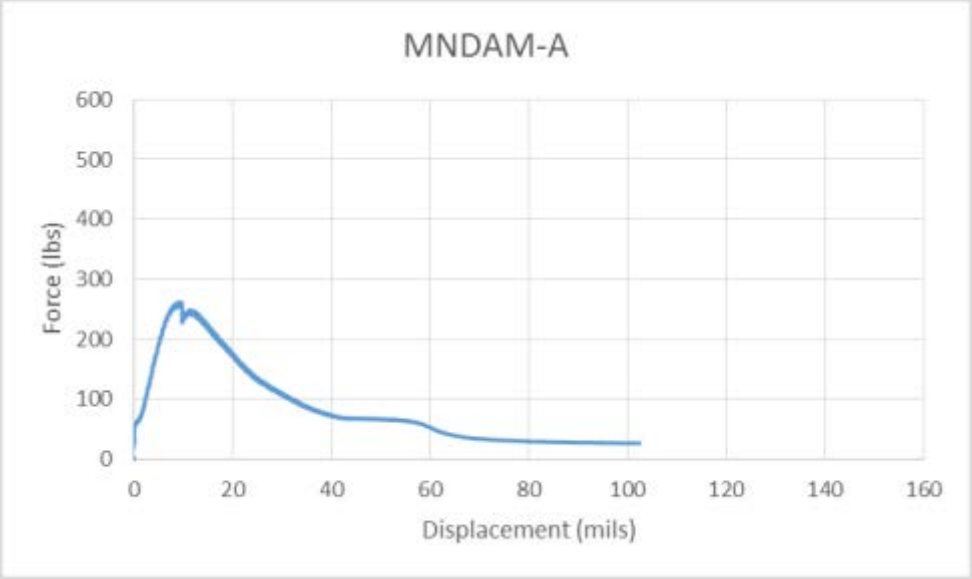

Figure A-A5.7 MNDAM Specimen A Force vs. Displacement (Tested on 6/8/15)

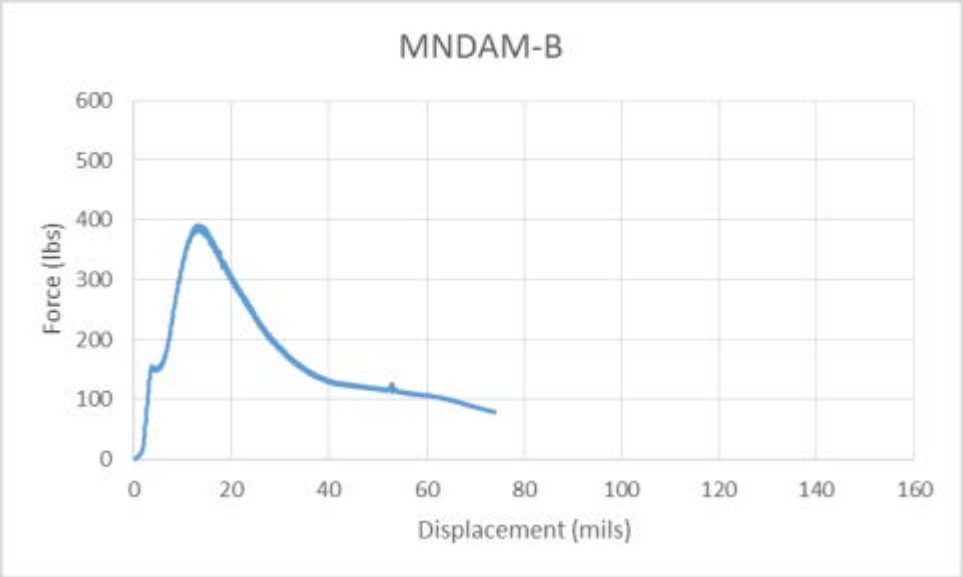

Figure A-A5.8 MNDAM Specimen A Force vs. Displacement (Tested on 6/17/15)

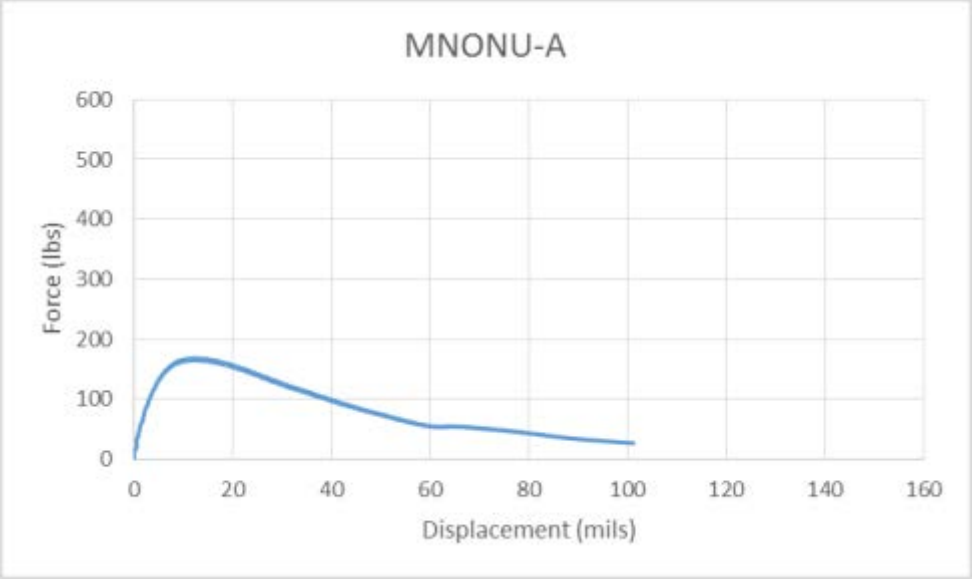

Figure A-A5.9 MNONU Specimen A Force vs. Displacement (Tested on 6/5/15)

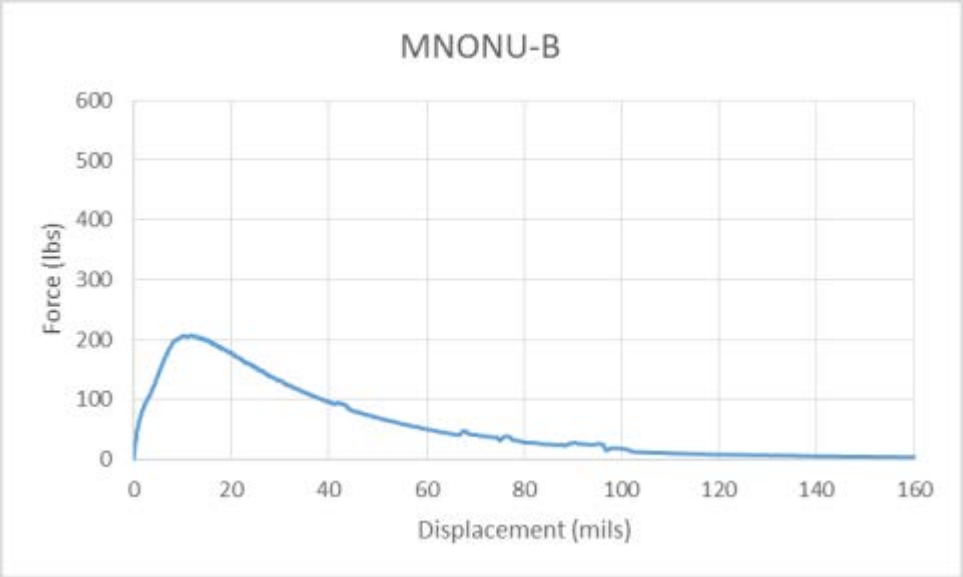

Figure A-A5.10 MNONU Specimen B Force vs. Displacement (Tested on 6/17/15)

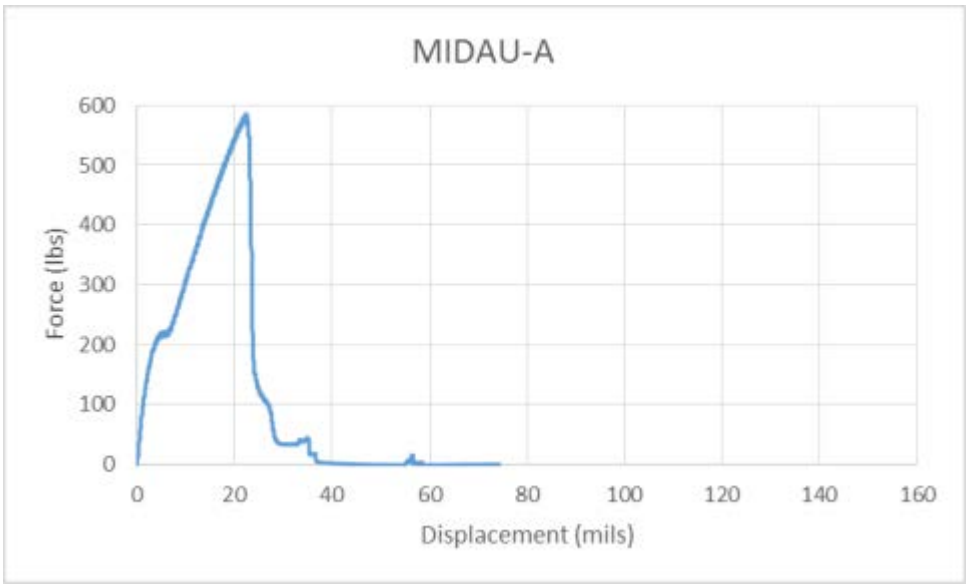

Figure A-A5.11 MIDAU Specimen A Force vs. Displacement (Tested on 6/5/15)

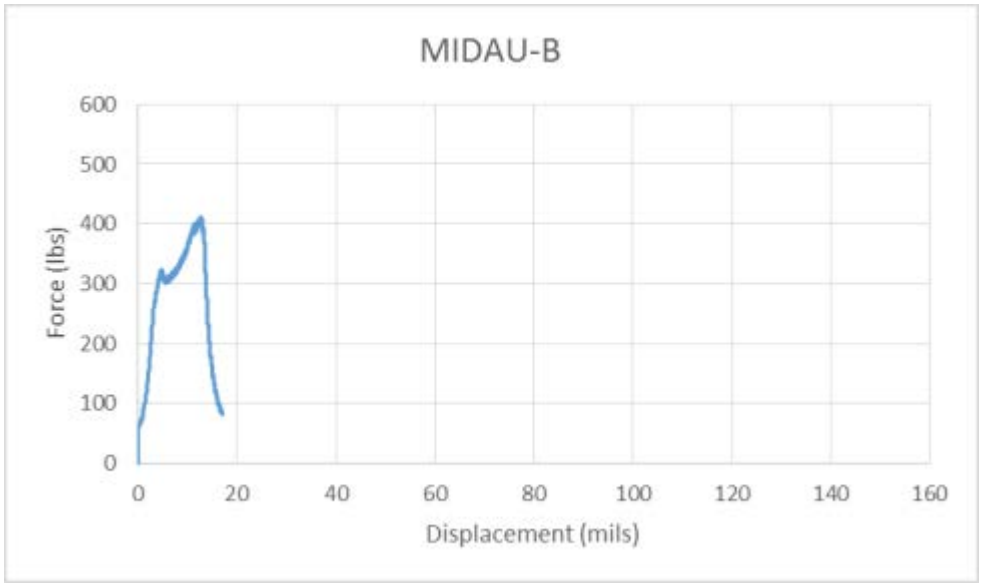

Figure A-A5.12 MIDAU Specimen B Force vs. Displacement (Tested on 6/17/15)

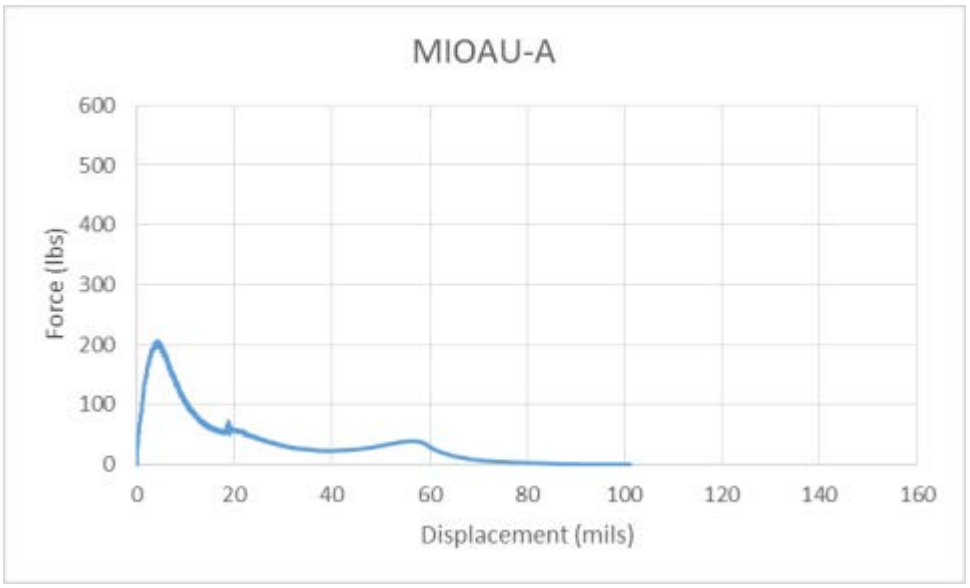

Figure A-A5.13 MIOAU Specimen A Force vs. Displacement (Tested on 6/10/15)

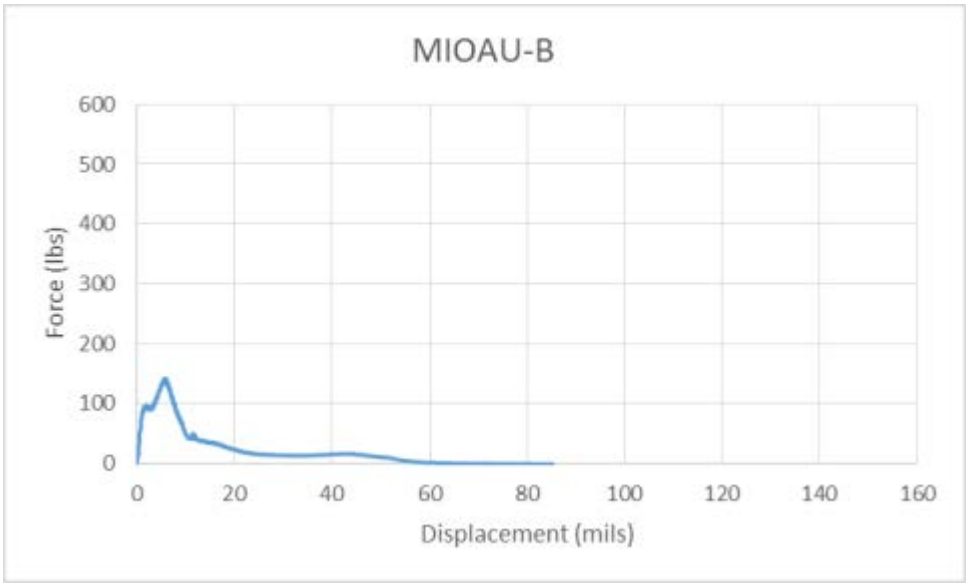

Figure A-A5.14 MIOAU Specimen B Force vs. Displacement (Tested on 6/10/15)

Appendix 6: Beam Measurements and Sand Patch Testing

Sand patch testing was carried at three locations for each beam specimen. The values presented in Table A-A6.2 are the characteristic depth for each of the three locations. The know volume of sand is divided by the average surface area to obtain a characteristic depth. The average lengths, widths, and heights of concrete and asphalt are also reported in Table A-A6.2. The average and standard deviation for each characteristic depth for each asphalt type are reported in Table A-A6.1.

Table A-A6.1. Average Sand Patch Results

	Average (mils)	Std. Dev. (mils)
MNDAU	33.6	6.2
MNDAM	81.3	8.6
MNONU	87.9	6.8
MIDAU	37.8	5.4
MIOAU	62.3	9.0

Table A-A6.2. Measurements and Sand Patch for Each Asphalt Beam

	Sand Patch (Characteristic depth in mils)			Average Dimensions			
Beam	1	2	3	Length	Width	Height (PCC)	Height (HMA)
0223MNDAUC	34.4	31.1	29.6	30.9	6.0	6.1	2.9
0223MNDAUB	34.4	30.8	31.3	30.7	6.2	6.0	2.8
0223MNDAUA	31.9	30.3	31.3	30.3	6.2	6.0	2.8
0226MNONUC	102.7	84.0	91.3	30.1	5.9	6.0	1.6
0226MNONUB	95.4	84.0	94.0	30.2	5.9	5.8	1.6
0226MNONUA	87.5	84.0	91.3	30.6	5.9	6.0	1.7
0319MNDAMC	93.2	82.8	71.4	30.5	5.9	5.8	1.2
0319MNDAMB	76.7	76.7	79.7	30.3	6.1	5.9	1.1
0319MNDAMA	86.0	71.4	76.7	30.3	6.1	6.0	1.0
0417MNDAUC	31.1	29.3	31.1	30.0	5.9	6.1	2.9
0417MNDAUB	29.1	24.9	33.3	30.2	6.3	6.0	2.8
0417MNDAUA	28.2	30.1	25.7	30.3	6.2	6.0	2.9
0422MNDAMC	79.7	71.4	67.7	30.1	6.3	5.8	0.8
0422MNDAMB	89.5	71.4	71.4	30.8	6.0	6.0	0.9
0422MNDAMA	93.2	82.8	93.2	30.1	5.8	6.0	0.9
0424MIDAUC	35.7	38.4	34.4	30.1	5.9	6.0	1.1
0424MIDAUA	35.7	37.7	34.4	30.0	6.0	6.1	1.2
0424MIDAUB	32.1	37.7	34.4	30.3	5.9	5.8	1.1
0507MNDAUA	38.4	40.6	48.6	30.2	6.0	5.9	2.8
0507MNDAMB	79.7	74.0	95.1	30.3	6.2	6.0	1.0
0507MNONUA	91.3	84.0	81.7	30.1	5.8	5.9	1.7
0513MIOAUA	63.4	57.8	57.8	30.1	5.9	5.8	1.8
0513MIOAUB	63.4	52.9	48.6	30.0	6.0	5.9	1.8
0513MIOAUC	73.6	63.4	50.6	30.0	6.1	5.7	1.9
0515MIDAUC	28.2	33.3	32.1	30.5	6.0	6.0	1.1
0515MIDAUB	43.6	46.6	44.8	30.1	5.9	6.0	1.0
0515MIDAUA	31.1	37.0	44.8	29.9	5.9	6.0	1.1
0520MIOAUC	77.5	59.1	49.6	30.0	5.8	6.0	1.9
0520MIOAUB	77.5	54.0	63.4	30.0	5.8	6.0	2.1
0520MIOAUA	60.5	66.6	65.0	30.1	5.9	6.1	2.0
0522MNONUC	77.5	86.3	90.0	30.2	6.1	6.0	2.0
0522MNONUB	86.3	86.3	86.3	29.9	5.8	5.9	1.7
0522MNONUA	102.8	88.8	73.6	30.0	5.9	6.0	1.7
0701MNDAUA	41.4	47.6	41.4	30.2	6.1	6.1	2.8
0701MNONUB	86.3	81.7	91.3	30.0	6.1	5.9	1.8
0701MIDAUC	44.8	44.8	42.2	30.3	6.0	5.9	1.3
0709MIOAUA	63.4	60.5	79.6	30.6	6.1	6.1	1.8
0709MNDAMB	91.0	86.8	89.5	30.1	6.0	5.9	0.8

References

ASTM International. (2009). Standard Test Method for Repetitive Static Plate Load Tests of Soils and Flexible Pavement Components, for Use in Evaluation and Design of Airport and Highway Pavements. ASTM Standard D1195/D1195M. West Conshocken, PA.

ASTM International. (2014). Standard Test Method for Static Modulus of Elasticity and Poisson's Ratio of Concrete in Compression. ASTM Standard C 469. West Conshocken, PA.

ASTM International. (2005). Standard Test Method for Compressive Strength of Cylindrical Concrete Specimens. ASTM Standard C 39. West Conshocken, PA.

ASTM International. (2015). Standard Test Method for Flexural Strength of Concrete (Using Simple Beam with Third-Point Loading). ASTM Standard C 78. West Conshocken, PA.

ASTM International. (2013). Standard Practice for Making and Curing Concrete Test Specimens in the Laboratory. ASTM Standard C 192. West Conshocken, PA.

ASTM International. (2015). Standard Test Method for Measuring Pavement Macrotexture Depth Using a Volumetric Technique. ASTM Standard E 965. West Conshocken, PA.

Harrington, D., Degraaf, D., Riley, R. (2007). Guide to Concrete Overlay Solutions. National Concrete Pavement Technology Center (CP Tech Center), Iowa State University.

Maitra, S. R., Reddy, K. S., & Ramachandra, L. S. (2009). Experimental Evaluation of Interface Friction and Study of. Journal of Transportation Engineering, 135(8), 563–572.

Otto Rasmussen, R., & Rozycki, D. K. (2001). Characterization and modeling of axial slab-support restraint. Transportation Research Record: Journal of the Transportation Research Board, 1778(1), 26–32.

Ruiz, J. M., Kim, P. J., Schindler, A. K., & Rasmussen, R. O. (2001). Validation of HIPERPAV for Prediction of Early-Age Jointed Concrete Pavement. Transportation Research Record: Journal of the Transportation Research Board, 1778(1), 17–25.

Smith, Kurt D., H. Thomas Yu, and David G. Peshkin. (2002). Portland Cement Concrete Overlays: State of the Technology Synthesis: Federal Highway Administration.

APPENDIX B. BACKCALCULATION USING LTPP FWD DATA

Objectives

The main objective of this study is to understand the behavior of UCOCP by analyzing the FWD deflection basins obtained from various test sections and in-service pavements. To this end, the following tasks are currently considered.

- Obtain the time histories of the FWD deflections collected through "GPS 9 - Unbonded PCC Overlay of PCC Pavement (PCC/PCC)" under "the General Pavement Studies (GPS)" as part of the "Long-Term Pavement Performance (LTPP) program."
- Perform dynamic backcalculation based on the generalized Pasternak model proposed by (Khazanovich & Booshehrian, 2015).
- Define different case scenarios to investigate the structural contribution of the existing PCC and the overlay.
- Compare the analyses conducted on the available road sections to examine whether it is possible to make a comprehensive conclusion about the general behavior of UCOCP.

Theory

Consider an infinite, homogeneous, isotropic, and linearly viscoelastic plate on a generalized Pasternak foundation (FIGURE B-1). The viscoelasticity of the plate is simulated using the three-parameter standard linear solid (SLS) model as illustrated in the inset of FIGURE B-1. The generalized Pasternak foundation is a four-parameter model consisted of:

1) linear Winkler springs representing the subgrade coefficient of reaction, *k*,
2) linear dashpots representing the damping coefficient of the foundation, *c*,
3) mass elements representing the mass of the viscoelastic plate and the moving portion of foundation, *m*, under the applied dynamic loads, and
4) an incompressible shear layer representing the shear resistance of the foundation with elastic shear modulus *G*.

In this foundation model, the two-parameter Kelvin-Voigt model is used to capture the viscoelastic behavior of the foundation using a combination of elastic linear springs and dashpots. Self-evidently, if zero values were assigned to mass elements and dashpots, the classic two-parameter Pasternak model would be achieved.

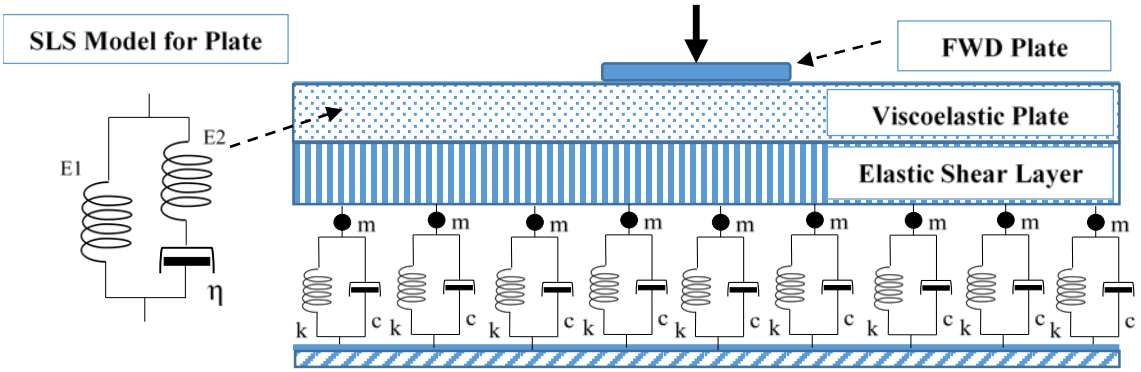

FIGURE B-1 Generalized Pasternak Model

The axisymmetric response of the pavement in terms of plate surface deformation under the FWD circular load plate can be formulated as follows.

$$D\left(\tilde{I}-\tilde{R}\right)\nabla^4 w(r,t)-G\nabla^2 w(r,t)+kw(r,t)+c\frac{\partial w(r,t)}{\partial t}+m\frac{\partial^2 w(r,t)}{\partial t^2}=p(r,t) \quad \textbf{(1)}$$

where $D=Eh^3/12(1-v^2)$ is plate's instantaneous flexural stiffness; and *E*, *h*, and *v* are instantaneous modulus of elasticity, thickness, and Poisson's ratio of the surface layer (plate), respectively. $w(r,t)$ is the surface deflection, $p(r,t)$ is the applied FWD pressure, r is the distance from the center of FWD loading plate, and *t* is the time; ∇^2 is the Laplace operator defined as $\nabla^2=\frac{1}{r}\frac{\partial}{\partial r}+\frac{\partial^2}{\partial r^2}$; $\tilde{I}$ is the identity operator, and $\tilde{R}$ is the relaxation operator found based on the stress-strain relationship (constitutive equation) of the SLS model used for the viscoelastic plate, and is defined as

$$\tilde{R}\epsilon(t)=\frac{{E_2}^2}{\eta(E_1+E_2)}\int_0^t e^{-\tau(t-x)}\epsilon(x)dx \quad \textbf{(2)}$$

where E_1, E_2 are two stiffness parameters of the SLS model. In addition, η is the material viscosity parameter, and therefore, $\tau=\eta/E_2$ is the relaxation time of the viscoelastic plate. The detailed steps for deriving equation (2) can be found in (Khazanovich & Booshehrian, 2015). Therefore, the three parameters used in this study based on SLS model are:

1) the instantaneous modulus of elasticity of the plate, $E=E_1+E_2$,
2) the ratio of $\frac{E_1}{E_2}$, and
3) the plate relaxation time, $\tau=\eta/E_2$.

Equation (1) is solved numerically using a combination of zero order Hankel transform in space and finite difference in time. Then, in order to perform the backcalculation, the normalized sum of squares of errors (SSE) is selected as the error function.

$$SSE=\left(\frac{1}{w_{max}^M}\right)^2\sum_{i=1}^{n}\sum_{j=1}^{m}(w_{ij}^M-w_{ij}^C)^2 \quad \textbf{(3)}$$

The combination of parameters that leads to the minimum error value is the solution to the inverse problem.

Selecting Studied Sections

Initially, the information related to the all the sections studied under GPS 9 were collected from InfoPave™, the online LTPP database. The available time histories of the FWD deflections are:

- Jointed plain concrete pavement (JPCP): 14 sections with 63 visits
- Jointed reinforced concrete pavement (JRCP): 8 sections with 45 visits
- Continuously reinforced concrete pavement (CRCP): 4 sections with 21 visits

A majority of the visits are related to years before year 2000. The quality of the recorded data after year 2000 is relatively better because the of the longer recorded time history (60 ms vs 30

ms) and the shorter time steps (0.1 ms vs 0.2 ms). Therefore, it was tried to focus on the FWD data collected after year 2000.

Also, in order to perform the preliminary study, the structural layers of the available sections were examined and the ones with very thin HMA interlayer were sampled. The main focus was put on JPCP sections, as they are more likely to agree with principles in the plate-on-a-foundation model. The following sections were selected mainly based on the mentioned preferences, and to include the sections related to the pooled fund member states:

- JPCP located at California (ID = 069048)
- JPCP located at Kansas (ID = 209037)
- JPCP located at Minnesota (ID = 279075)
- JRCP located at Michigan (ID = 269029)

The details of the selected pavement sections are described in Table B-1.

TABLE B-1 Detailed Information on the Selected Pavement Sections

Location	ID	OL Layer / Thickness (in)	Interlayer / Thickness (in)	Original PCC / Thickness (in)	Base layer / Thickness (in)	Subbase layer / Thickness (in)	Subgrade Type
California	069048	JPCP / 6.4	Chip Seal / 0.2	JPCP / 8.1	-	-	Coarse-Grained Soil: Silty Sand with Gravel
Kansas	209037	JPCP / 5.8	Open Graded Asphalt / 2.0	JRCP / 8.8	Unbound Granular Sand / 4.0	-	Fine-Grained Soils: Lean Clay with Sand
Minnesota	279075	JPCP / 5.9	Open Graded Asphalt / 0.8	JPCP / 7.8	-	-	Fine-Grained Soils: Sandy Lean Clay
Michigan	269029	JRCP / 7.3	Open Graded Asphalt / 0.8	CRCP / 8.0	Unbound Granular Gravel / 4.0	Unbound Granular Sand / 9.5	Fine-Grained Soils: Sandy Lean Clay

For each studied section, the following information/plots are provided:

1) The section structural layers and their thickness.
2) The year at which the FWD data is obtained and analyzed.
3) A Table B-of the obtained backcalculated pavement parameters for all the different stops tested for the desired road section.
4) For all sections, the backcalculation is performed at multiple load levels for one of the stops (stop 5) to examine whether the studied pavement is load dependent. The results are highlighted in the summary Table B-for each section.
5) Depending on the obtained error values, the plots of the FWD-measured deflections and the model-calculated deflections for the stops with the best and worst error values are presented for each section. These plots are provided to show the ability of the proposed model to capture the behavior of the under-study pavement.

6) For each road section, even though the same FWD load level is considered, the pavement deformations vary at different stops. A plot of the maximum deflections for FWD sensors for each stop is provided to show this phenomenon. This phenomenon clearly shows the variation of structural capacity of the same pavement at different locations, which consequently results in varying backcalculated pavement parameters.
7) In order to find a connection between the maximum deflection and the backcalculated pavement parameters, these parameters are plotted against the maximum deflections recorded at each stop. The following plots are provided for each section:
    a. The backcalculated E- and k-values and the maximum recorded deflections for each stop.
    b. The backcalculated m-value and the maximum recorded deflections for each stop.
    c. The backcalculated c-value and the maximum recorded deflections for each stop.
    d. The backcalculated G-value and the maximum recorded deflections for each stop.

California (ID = 069048)
Located in California and fabricated with JPCP

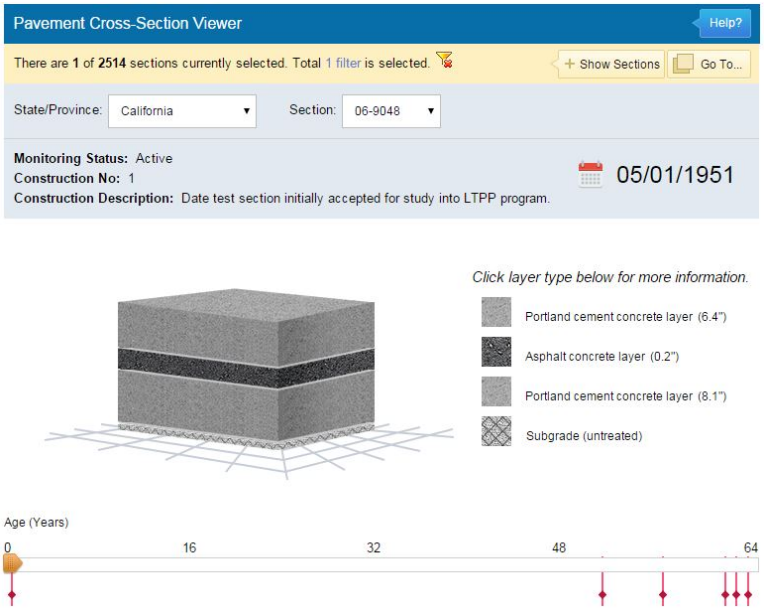

FIGURE B-2 Pavement Structural Layers for JPCP in California

The data used for analyses are related to year 2004.

TABLE B-2 Backcalculated Pavement Structural Parameters for JPCP in California

	E	K	M	C	G	l	Error
Stop	**GPa**	**KPa/mm**	**kg/m^2**	**KPa.s/mm**	**GPa**	**m**	**-**
1	64.98	29.28	3165	0.167	0.179	0.947	9.51
2	62.40	44.00	1240	0.234	0.022	0.847	1.96
3	36.19	56.91	1059	0.189	0.041	0.693	2.87
4	55.40	44.30	1664	0.185	0.066	0.821	3.72
5-L1	83.31	33.22	1020	0.120	0.061	0.976	2.78
5-L2	78.82	32.88	1088	0.114	0.062	0.965	2.39
5-L3	82.23	30.06	1065	0.105	0.061	0.998	2.34
6	29.96	41.98	1321	0.161	0.094	0.713	2.11
7	58.15	30.60	805	0.147	0.092	0.911	4.13
8	34.24	42.49	1336	0.191	0.086	0.735	2.07
9	34.00	42.75	1489	0.205	0.063	0.733	2.89
10	79.92	39.70	1097	0.231	0.053	0.924	1.26
11	47.19	63.29	759	0.263	0.000	0.721	3.19
12	84.59	34.49	1085	0.248	0.060	0.971	1.12
13	87.15	45.56	1120	0.203	0.034	0.912	1.69
14	73.42	40.34	1287	0.265	0.066	0.901	1.54
15	84.10	40.04	1267	0.236	0.022	0.934	1.73

In general, the matches between the measured and calculated deflections were good. The best (stop 12) and the worst (stop 1) cases are depicted here.

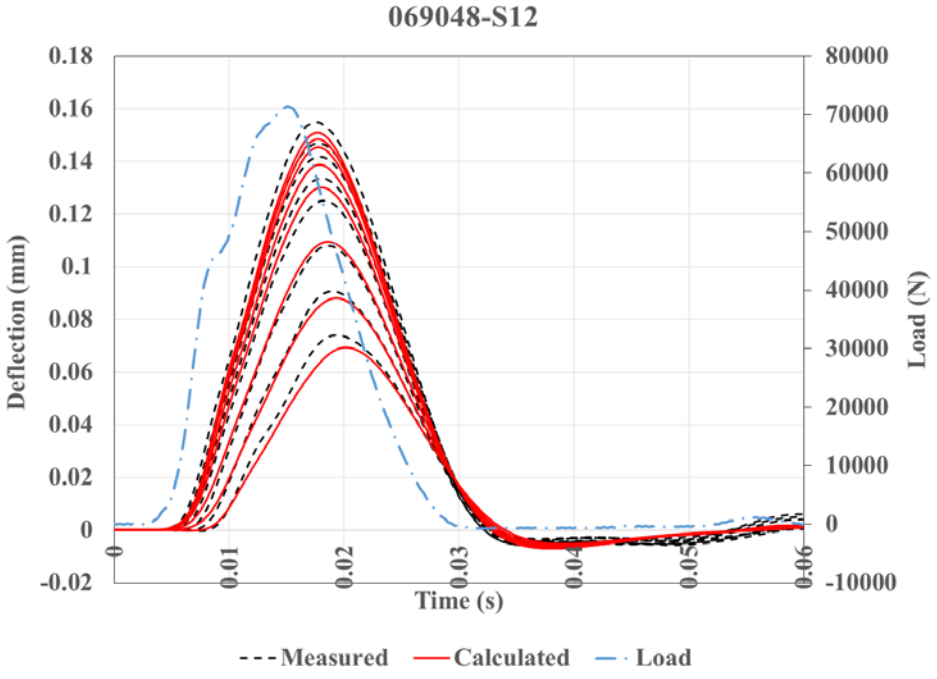

FIGURE B-3 Measured vs Calculated Deflections for Stop with Best Fit

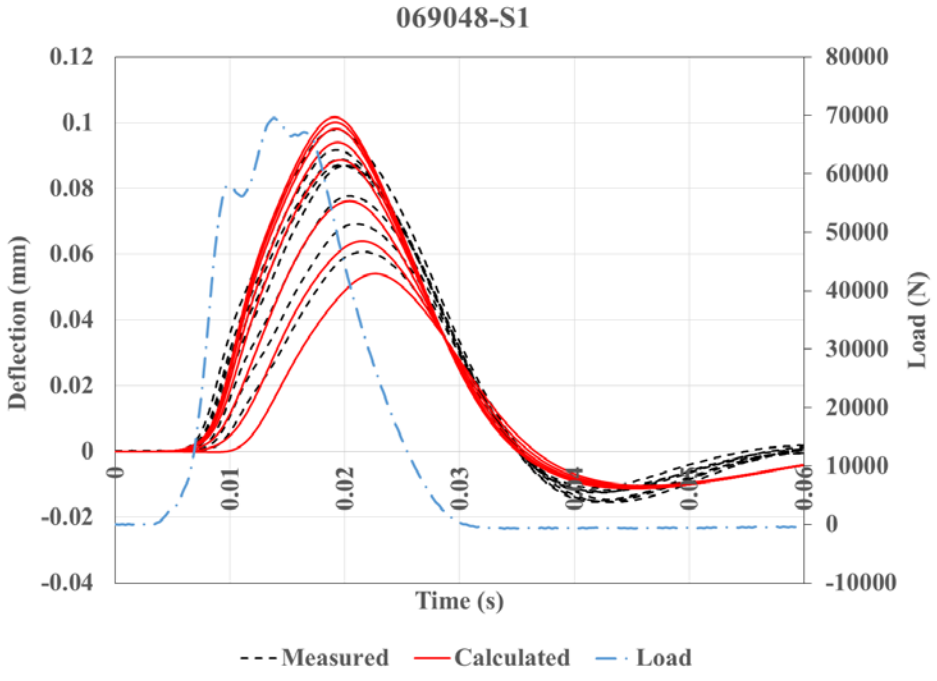

FIGURE B-4 Measured vs Calculated Deflections for Stop with Worst Fit

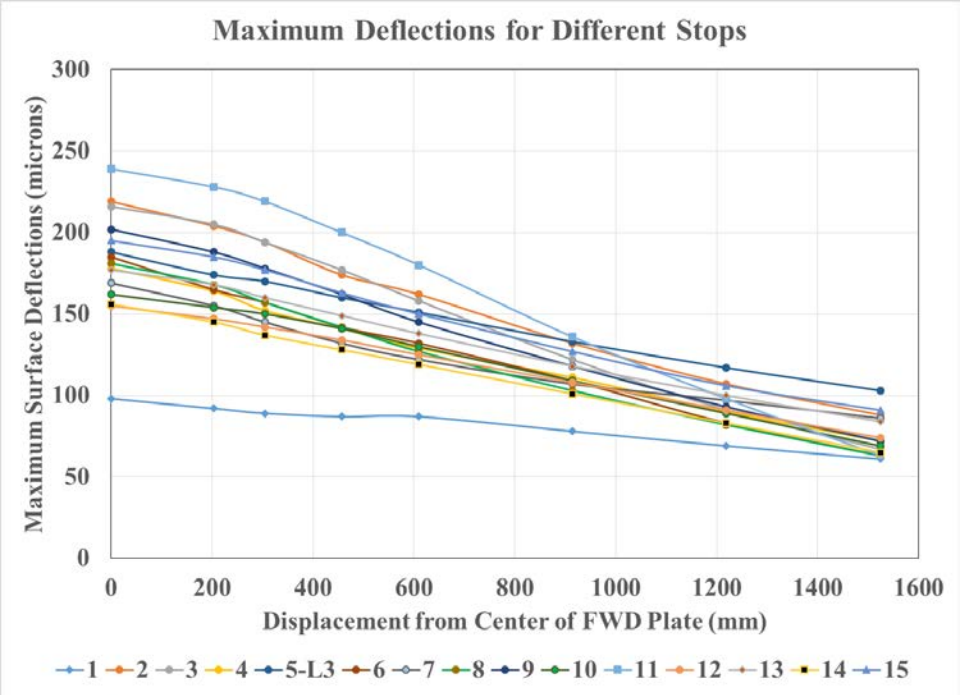

FIGURE B-5 Peak Recorded Deflections at each FWD Sensor Location for Different Stops

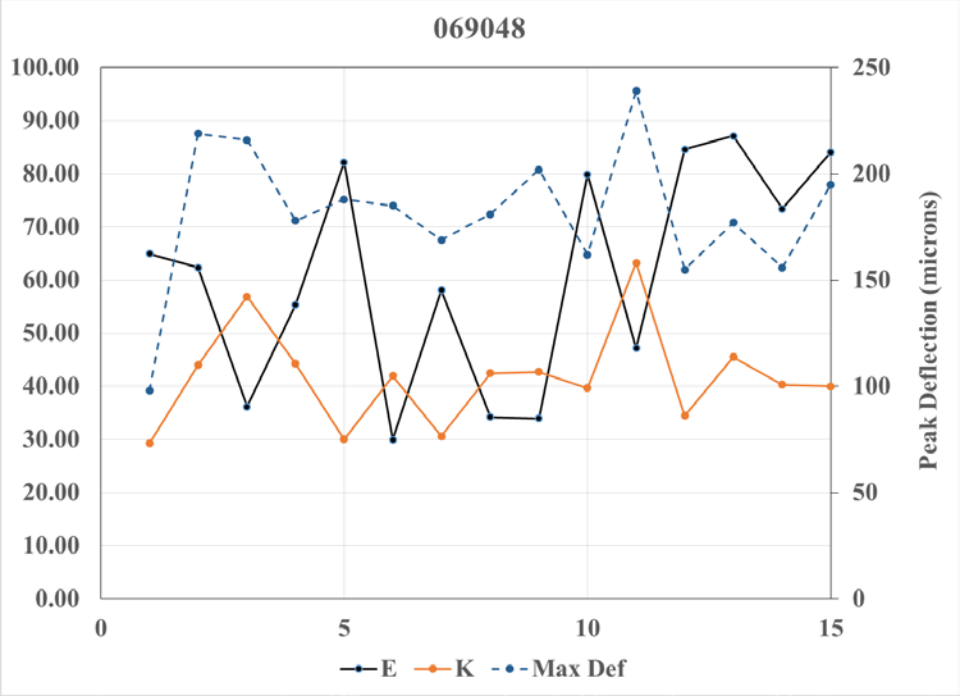

FIGURE B-6 Backcalculated E- and k-Values and Peak Deflections for Different Stops

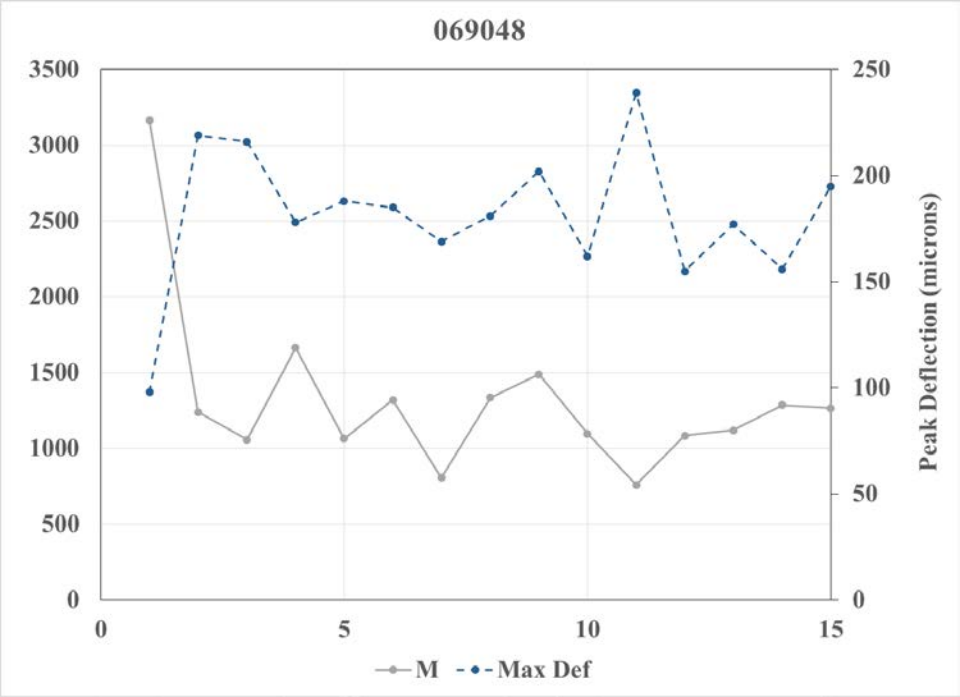

FIGURE B-7 Backcalculated m-Values and Peak Deflections for Different Stops

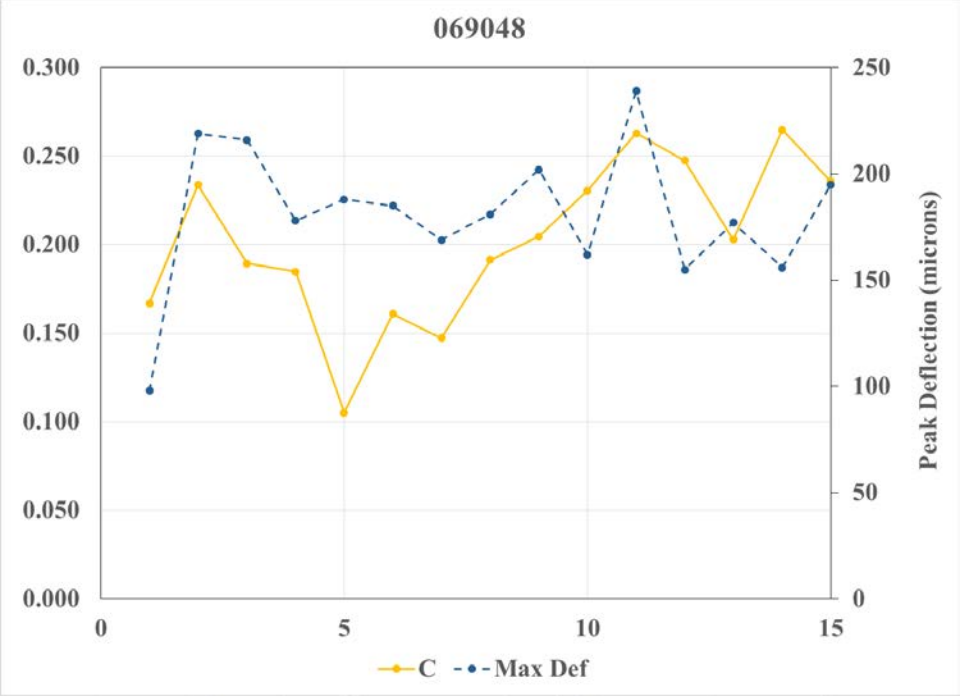

FIGURE B-8 Backcalculated c-Values and Peak Deflections for Different Stops

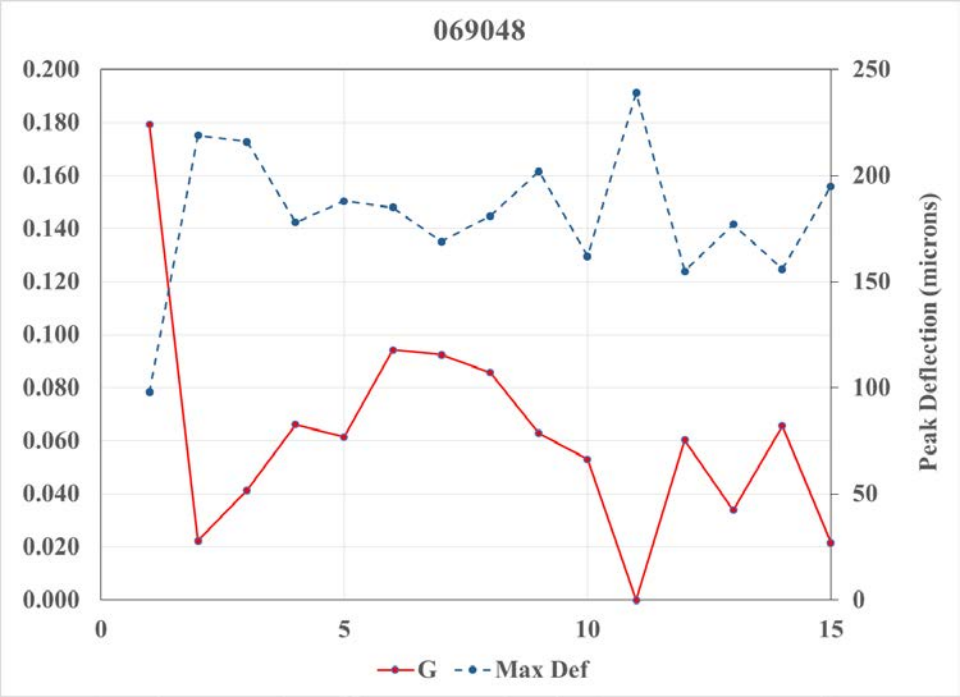

FIGURE B-9 Backcalculated G-Values and Peak Deflections for Different Stops

Kansas (ID = 209037)
Located in Kansas and fabricated with JPCP

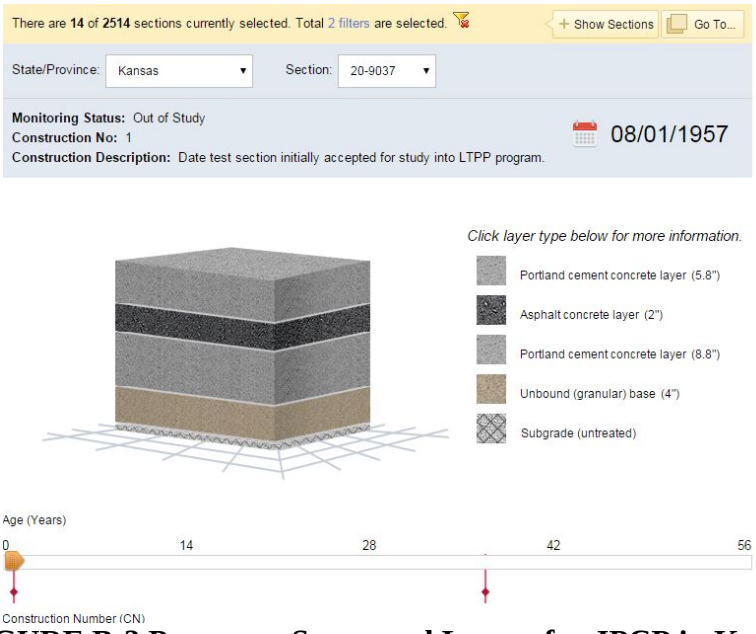

FIGURE B-2 Pavement Structural Layers for JPCP in Kansas

The data used for analyses are related to year 1994.

TABLE B-3 Backcalculated Pavement Structural Parameters for JPCP in Kansas

	E	K	M	C	G	l	Error
Stop	**GPa**	**KPa/mm**	**kg/m2**	**KPa.s/mm**	**GPa**	**m**	**-**
1	100.45	22.10	175.5	0.2182	0.031	1.069	2.13
2	81.39	13.94	231.0	0.2368	0.050	1.138	0.88
3	100.27	21.46	548.2	0.2525	0.056	1.077	1.68
4	101.25	24.46	297.9	0.2423	0.031	1.045	0.61
5-L1	117.31	35.34	169.7	0.2115	0.000	0.989	0.99
5-L2	111.95	33.84	136.1	0.2220	0.000	0.988	0.79
5-L3	108.48	35.38	150.3	0.2279	0.000	0.969	0.83
6	115.99	34.51	188.8	0.2333	0.000	0.992	0.67
7	91.55	39.50	173.9	0.2629	0.000	0.904	1.57
8	102.80	41.86	217.2	0.3041	0.000	0.917	1.50
9	95.71	36.61	183.4	0.2485	0.000	0.931	1.04
10	99.52	38.58	200.0	0.2611	0.000	0.928	1.05
11	63.74	40.87	88.2	0.2444	0.000	0.818	1.79
12	94.46	36.42	238.2	0.2210	0.000	0.929	0.73
13	68.68	28.00	339.1	0.2070	0.031	0.917	1.10
14	95.24	10.00	206.1	0.1090	0.060	1.287	0.36

15	64.74	17.70	360.7	0.1904	0.061	1.013	0.88
16	56.46	19.36	166.8	0.1648	0.047	0.957	0.66
17	75.77	38.83	122.3	0.2098	0.000	0.866	0.80
18	66.58	34.79	50.2	0.1778	0.000	0.861	1.29
19	35.84	23.41	38.3	0.1973	0.019	0.815	1.17
20	79.11	40.94	107.4	0.2657	0.000	0.864	0.98
21	77.36	26.41	166.0	0.2368	0.023	0.958	1.06

In general, the matches between the measured and calculated deflections were good. The best (stop 14) and the worst (stop 1) cases are depicted here.

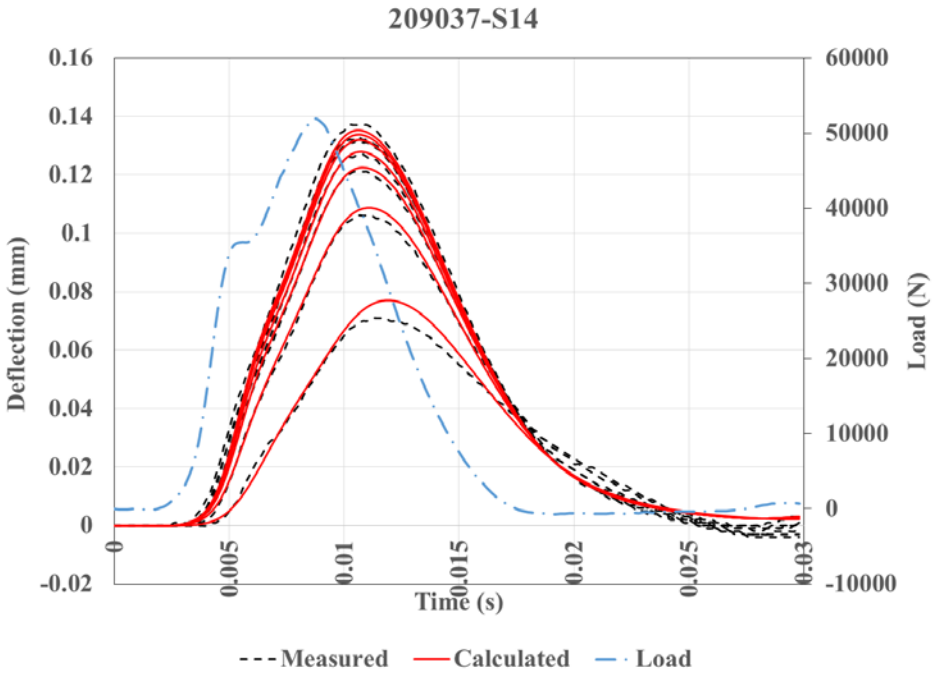

FIGURE B-10 Measured vs Calculated Deflections for Stop with Best Fit

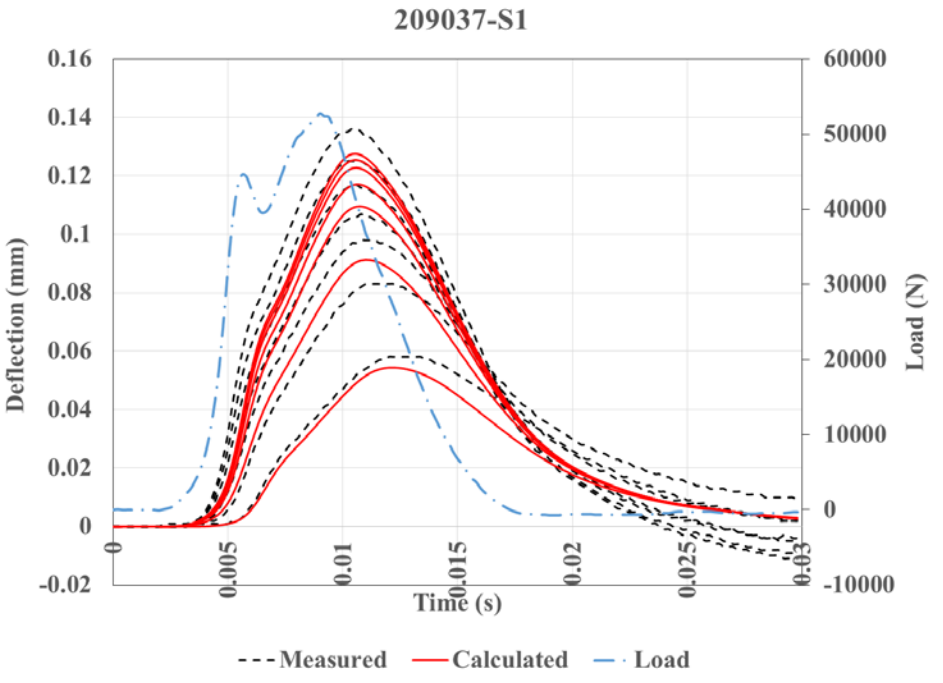

FIGURE B-11 Measured vs Calculated Deflections for Stop with Worst Fit

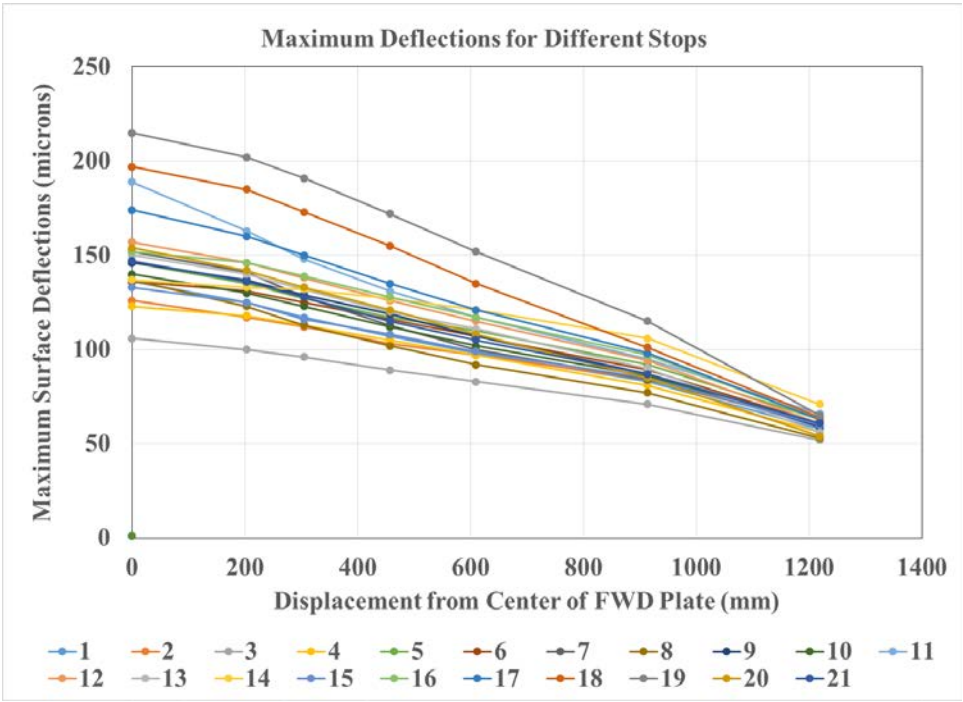

FIGURE B-12 Peak Recorded Deflections at each FWD Sensor Location for Different Stops

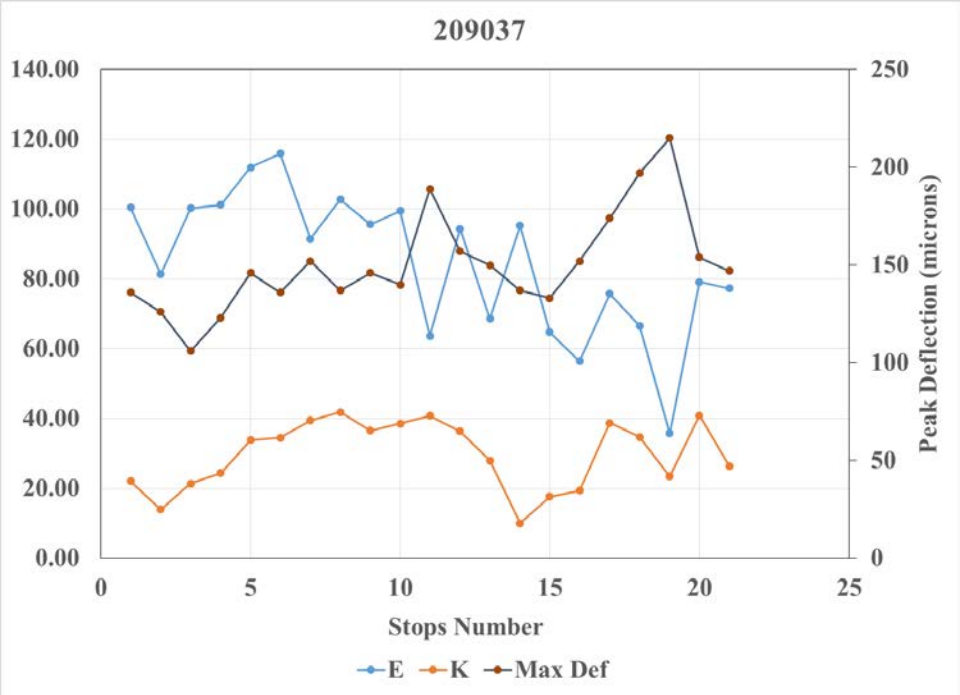

FIGURE B-13 Backcalculated E- and k-Values and Peak Deflections for Different Stops

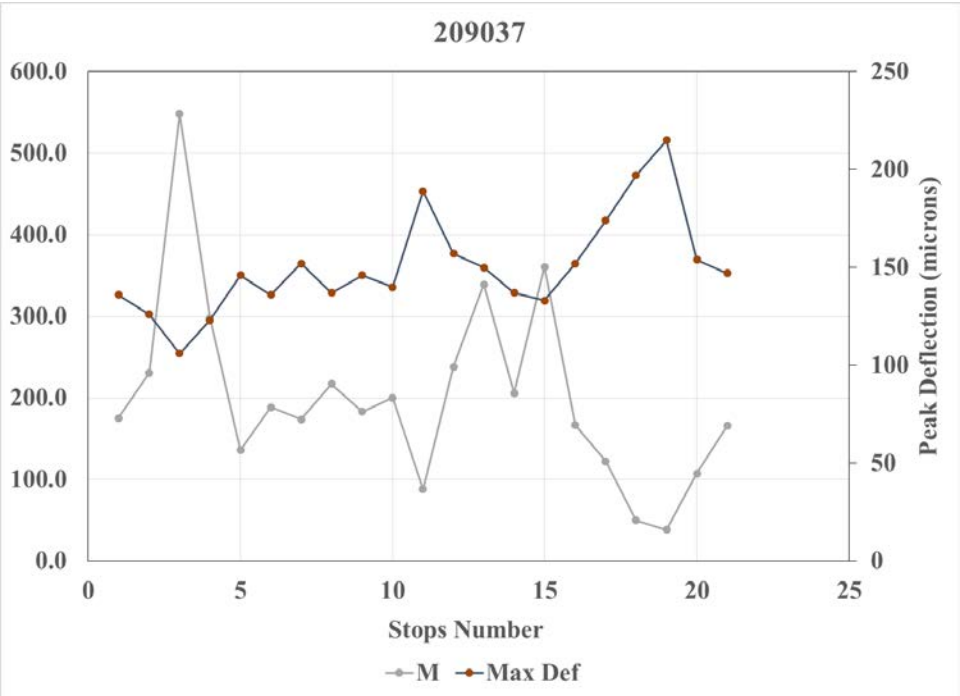

FIGURE B-14 Backcalculated m-Values and Peak Deflections for Different Stops

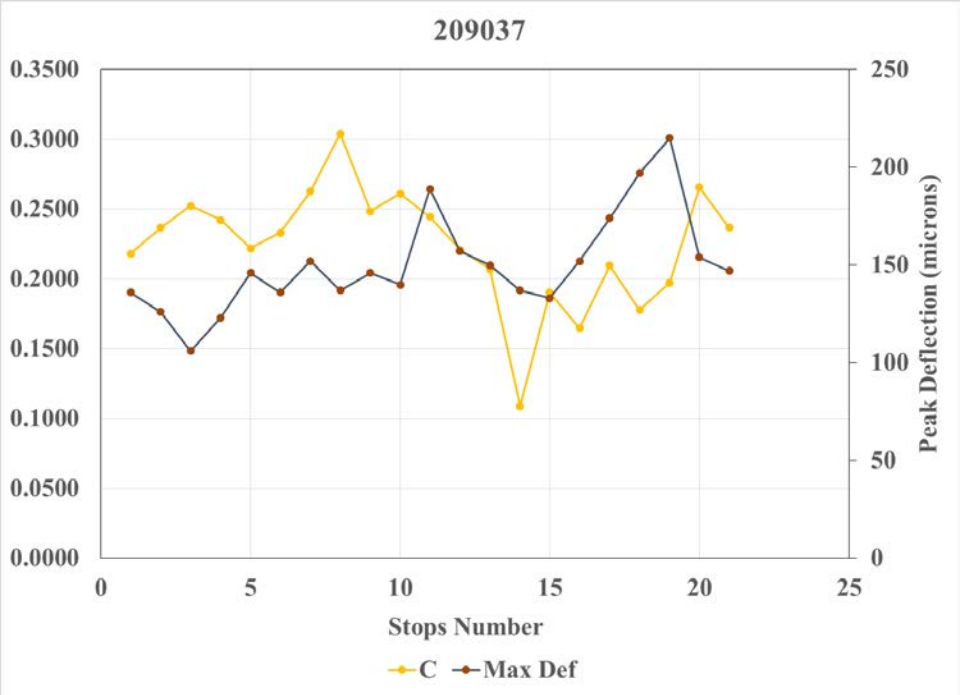

FIGURE B-15 Backcalculated c-Values and Peak Deflections for Different Stops

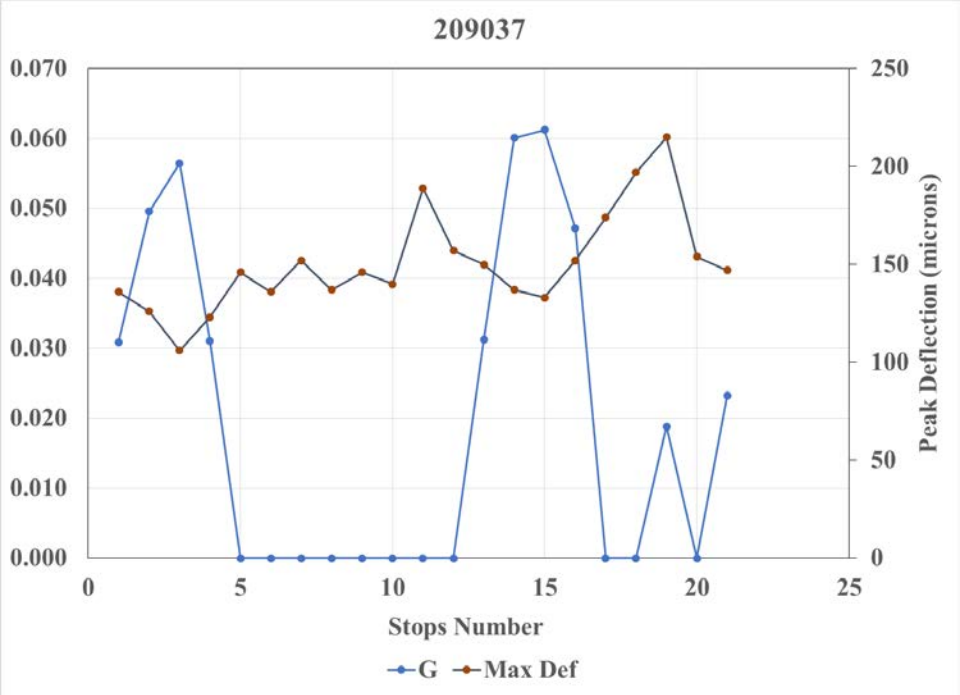

FIGURE B-16 Backcalculated G-Values and Peak Deflections for Different Stops

Minnesota (ID = 279075)
Located in Minnesota and fabricated with JPCP

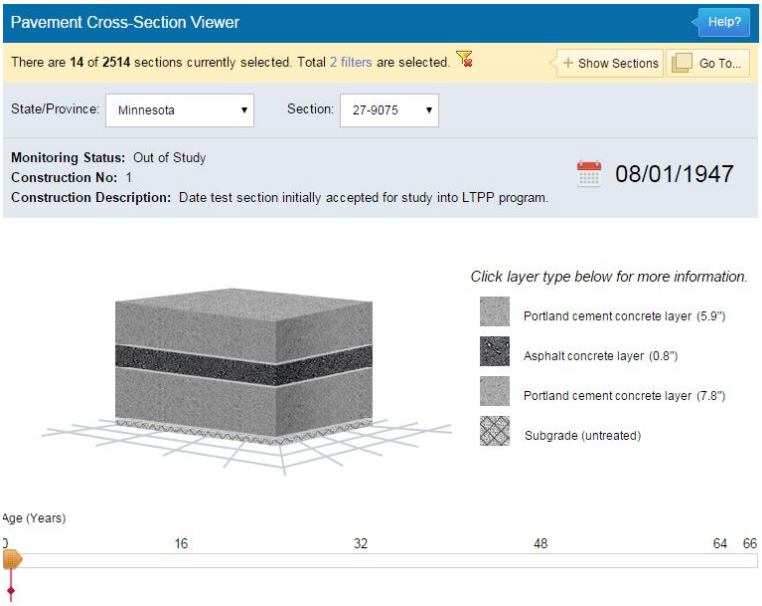

FIGURE B-17 Pavement Structural Layers for JPCP in Minnesota

The data used for analyses are related to year 1994.

TABLE B-4 Backcalculated Pavement Structural Parameters for JPCP in Minnesota

	E	K	M	C	G	l	Error
Stop	**GPa**	**KPa/mm**	**kg/m2**	**KPa.s/mm**	**GPa**	**m**	**-**
1	83.41	10.00	447.5	0.0532	0.018	1.245	0.78
2	83.70	15.57	394.6	0.1005	0.000	1.115	1.06
3	47.81	10.00	42.5	0.0892	0.000	1.083	1.93
4	88.85	11.48	354.1	0.1007	0.000	1.222	1.14
5-L1	94.46	11.81	256.5	0.1708	0.000	1.232	0.58
5-L2	102.02	11.80	266.6	0.1552	0.000	1.256	0.69
5-L3	90.20	12.11	265.7	0.1672	0.000	1.210	0.71
6	90.39	12.75	325.3	0.1411	0.000	1.195	1.04
7	111.33	15.05	602.0	0.0928	0.000	1.208	1.83
8	120.00	13.64	547.5	0.1091	0.000	1.261	1.75
9	103.80	14.15	521.0	0.1523	0.000	1.205	2.23
10	101.82	13.54	416.3	0.1563	0.000	1.213	1.78
11	115.03	13.80	525.7	0.1385	0.000	1.244	1.66
12	101.99	15.57	626.6	0.1558	0.000	1.172	2.11
13	113.70	13.57	554.8	0.1334	0.000	1.246	1.76
14	76.58	13.55	345.6	0.1685	0.000	1.129	2.16
15	102.24	10.00	370.7	0.1571	0.000	1.310	1.29

16	103.77	10.00	425.9	0.2387	0.000	1.315	1.69
17	98.15	11.20	126.3	0.2675	0.000	1.260	1.21
18	101.12	10.00	299.2	0.2174	0.011	1.306	1.28
19	100.84	10.00	264.6	0.2387	0.006	1.305	1.09
20	66.26	10.00	10.1	0.1625	0.000	1.175	0.72
21	101.91	12.67	310.1	0.1732	0.000	1.233	1.74
22	106.32	10.00	474.0	0.1277	0.014	1.322	1.41

In general, the matches between the measured and calculated deflections were good. The best (stop 20) and the worst (stop 9) cases are depicted here.

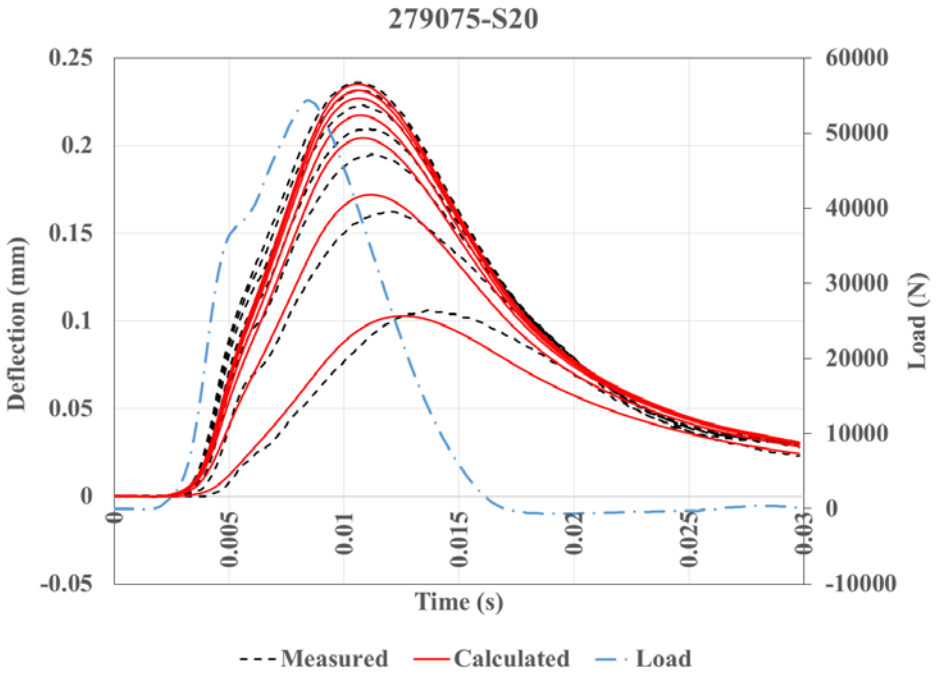

FIGURE B-18 Measured vs Calculated Deflections for Stop with Best Fit

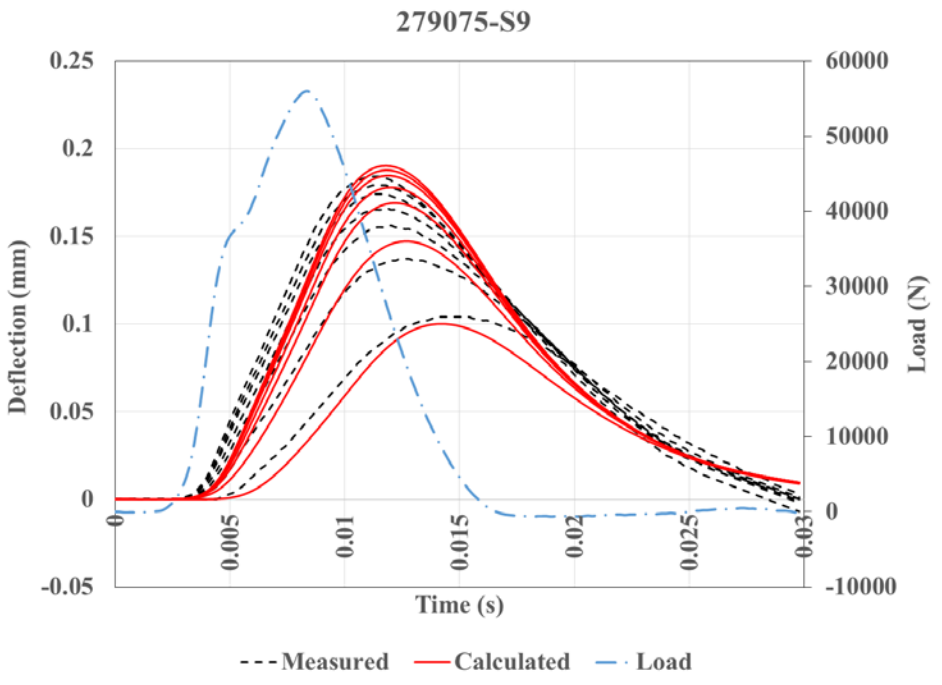

FIGURE B-19 Measured vs Calculated Deflections for Stop with Worst Fit

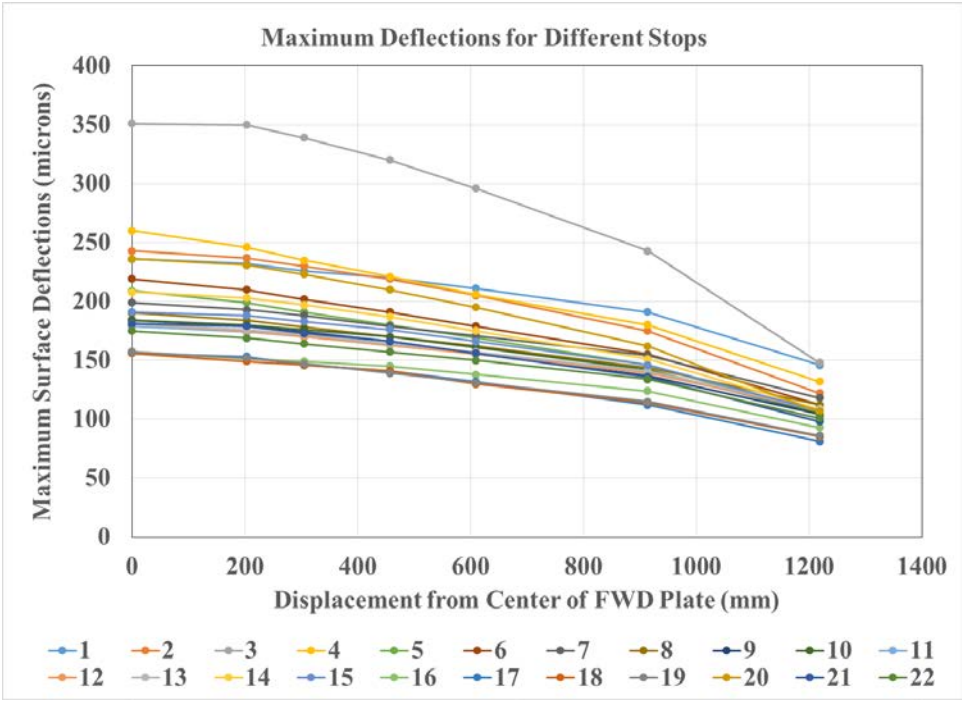

FIGURE B-20 Peak Recorded Deflections at each FWD Sensor Location for Different Stops

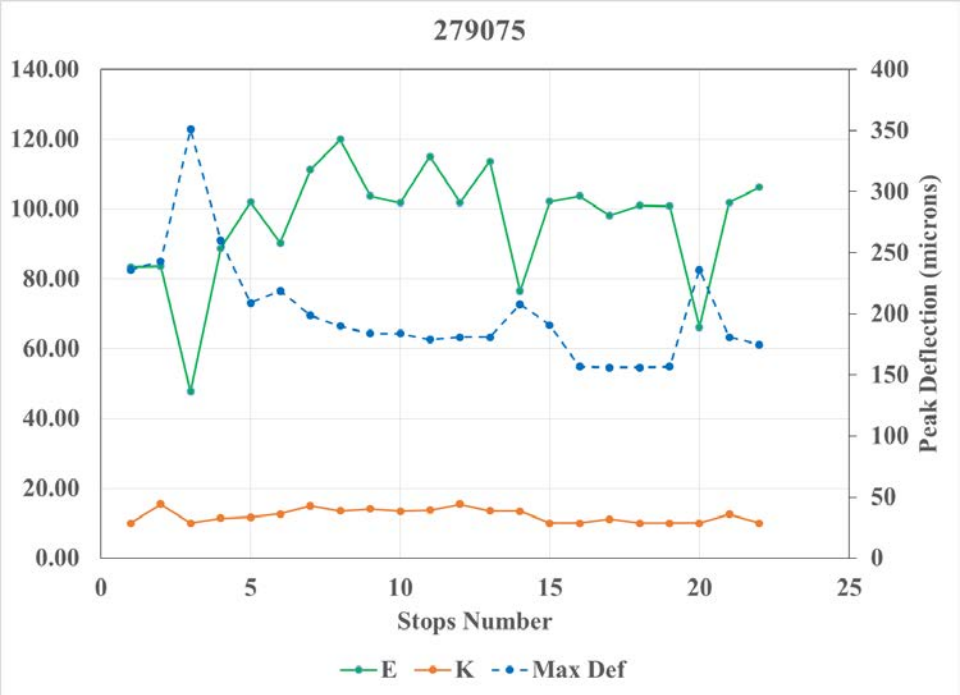

FIGURE B-21 Backcalculated E- and k-Values and Peak Deflections for Different Stops

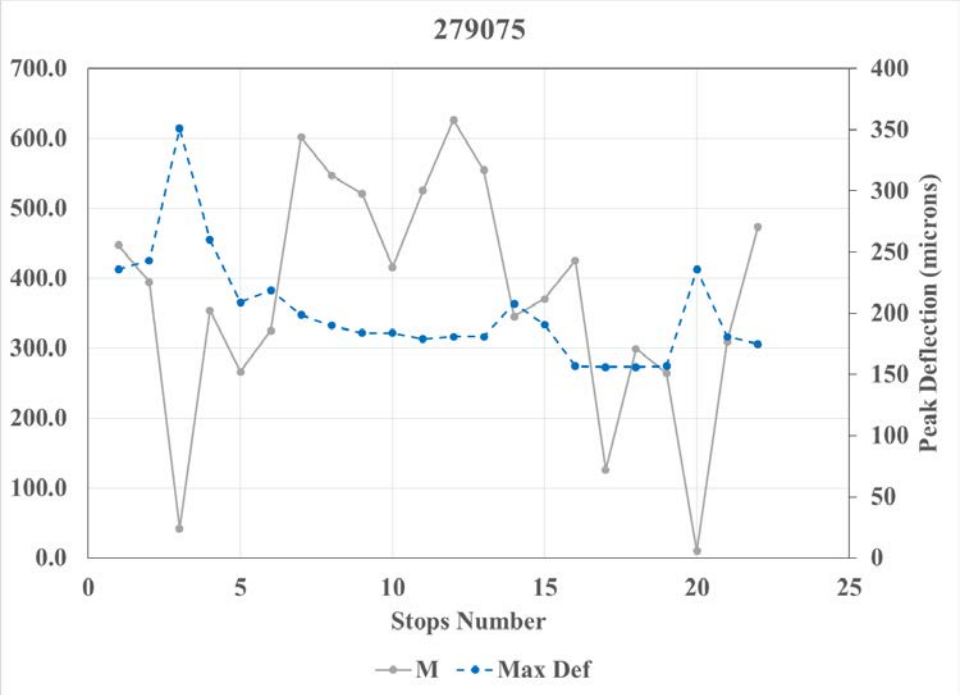

FIGURE B-22 Backcalculated m-Values and Peak Deflections for Different Stops

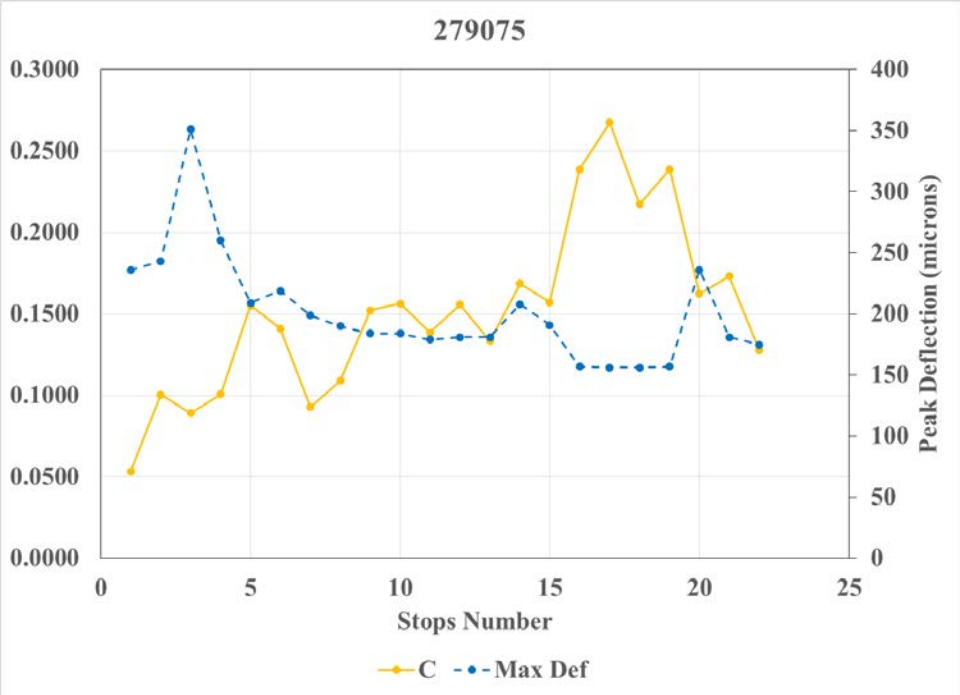

FIGURE B-23 Backcalculated c-Values and Peak Deflections for Different Stops

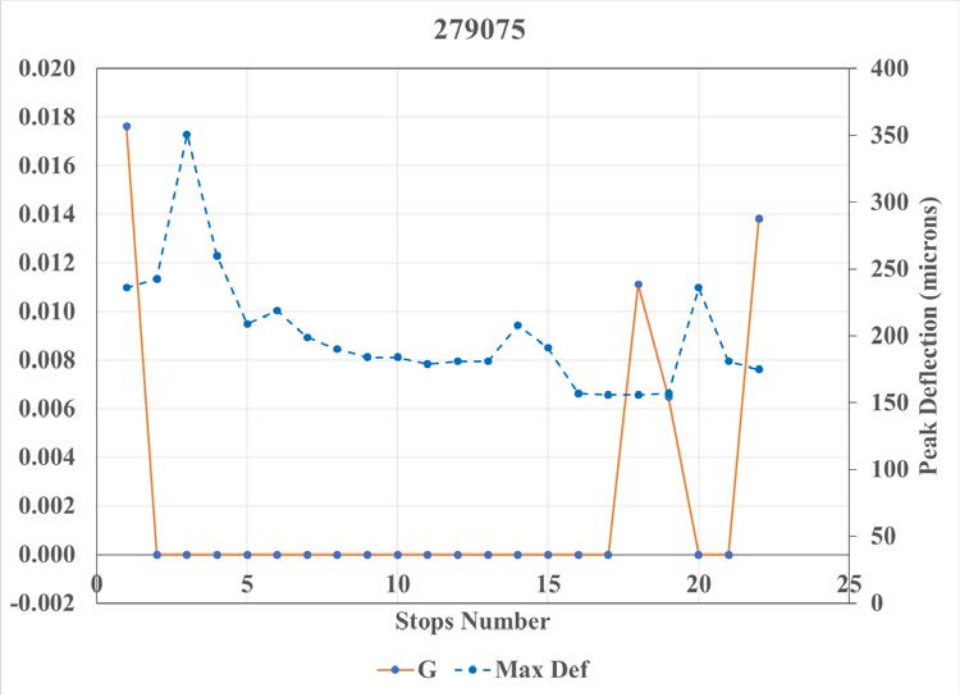

FIGURE B-24 Backcalculated G-Values and Peak Deflections for Different Stops

Michigan (ID = 269029)
Located in Michigan and fabricated with JRCP

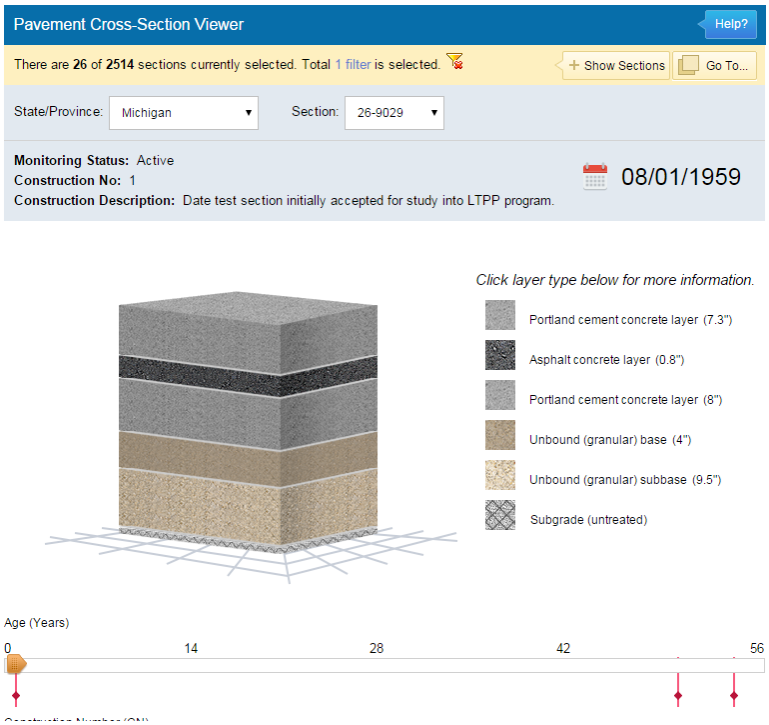

FIGURE B-25 Pavement Structural Layers for JRCP in Michigan

The data used for analyses are related to year 2002.

TABLE B-5 Backcalculated Pavement Structural Parameters for JRCP in Michigan

	E	K	M	C	G	l	Error
Stop	**GPa**	**KPa/mm**	**kg/m2**	**KPa.s/mm**	**GPa**	**m**	**-**
1	49.41	34.61	3165	0.167	0.179	0.938	13.61
2	97.13	48.10	1240	0.234	0.022	1.023	7.00
3	80.66	35.50	1059	0.189	0.041	1.054	19.17
4	61.23	28.00	1664	0.185	0.066	1.044	16.90
5-L1	50.21	29.33	1020	0.120	0.061	0.982	26.82
5-L2	57.93	30.74	1088	0.114	0.062	1.006	26.77
5-L3	57.84	32.46	1065	0.105	0.061	0.992	26.78
6	74.02	59.75	1321	0.161	0.094	0.906	3.60
7	62.89	16.86	805	0.147	0.092	1.193	8.65
8	75.56	21.81	1336	0.191	0.086	1.171	9.26
9	42.71	41.93	1489	0.205	0.063	0.863	6.19
10	67.97	47.04	1097	0.231	0.053	0.941	11.30
11	73.38	61.40	759	0.263	0.000	0.898	8.34
12	60.61	42.21	1085	0.248	0.060	0.940	16.65

In general, the matches between the measured and calculated deflections were decent. The best (stop 6) and the worst (stop 5) cases are depicted here.

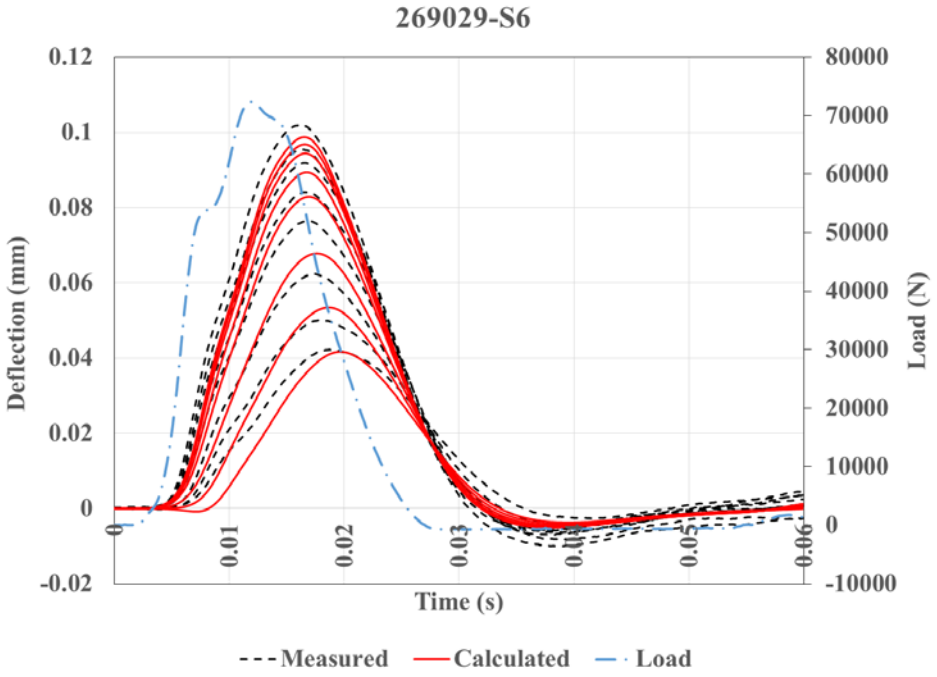

FIGURE B-26 Measured vs Calculated Deflections for Stop with Best Fit

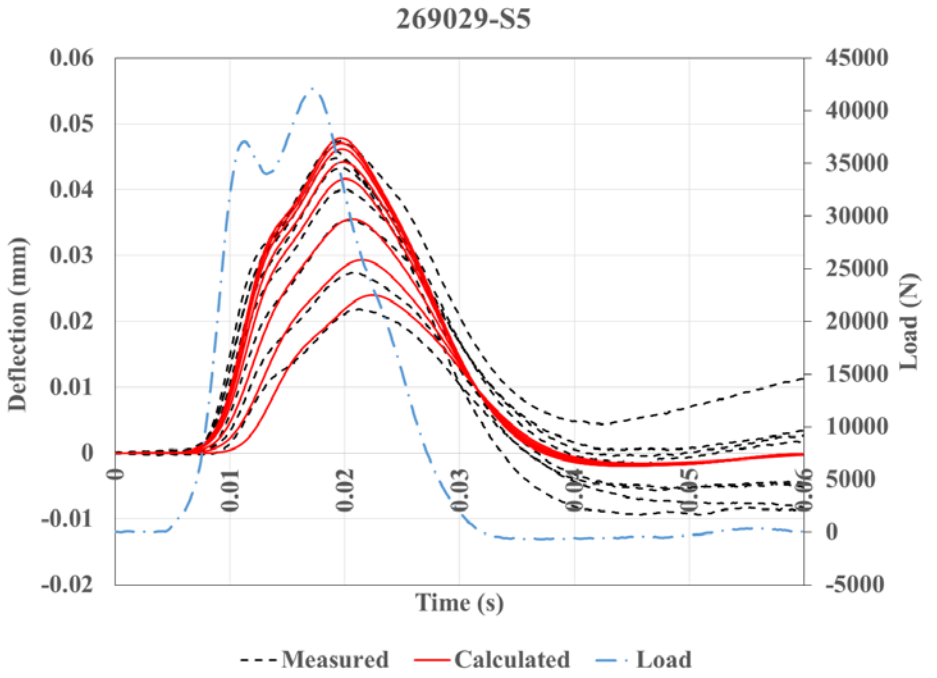

FIGURE B-27 Measured vs Calculated Deflections for Stop with Worst Fit

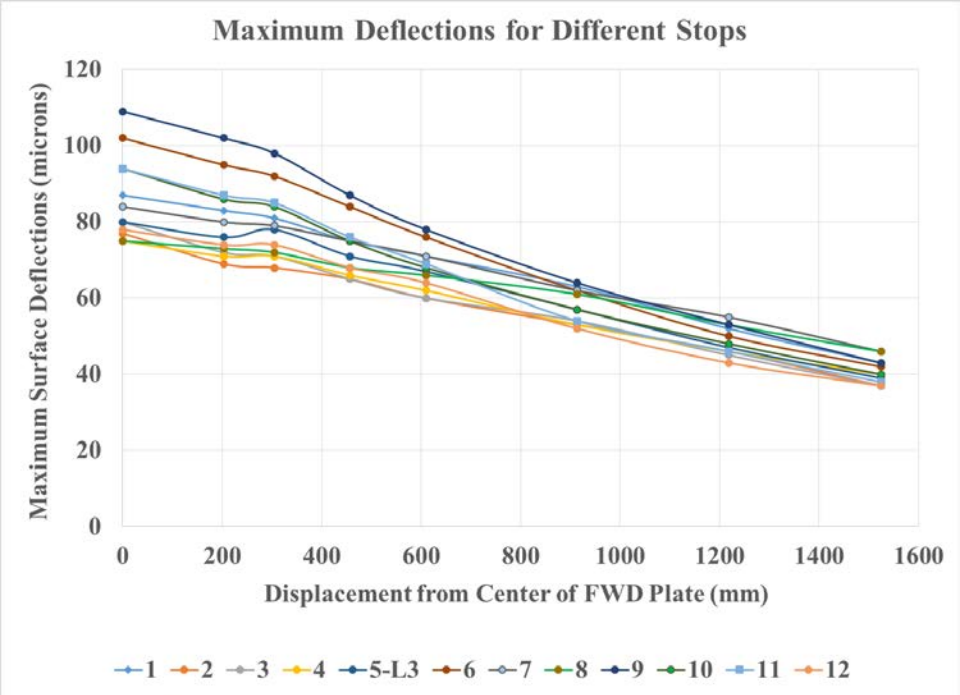

FIGURE B-28 Peak Recorded Deflections at each FWD Sensor Location for Different Stops

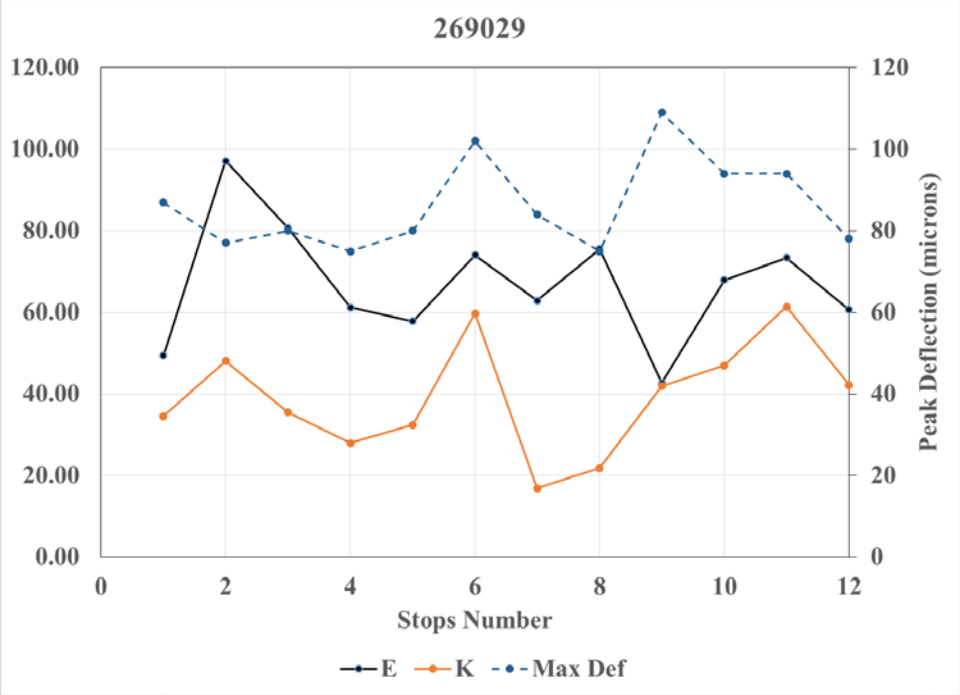

FIGURE B-29 Backcalculated E- and k-Values and Peak Deflections for Different Stops

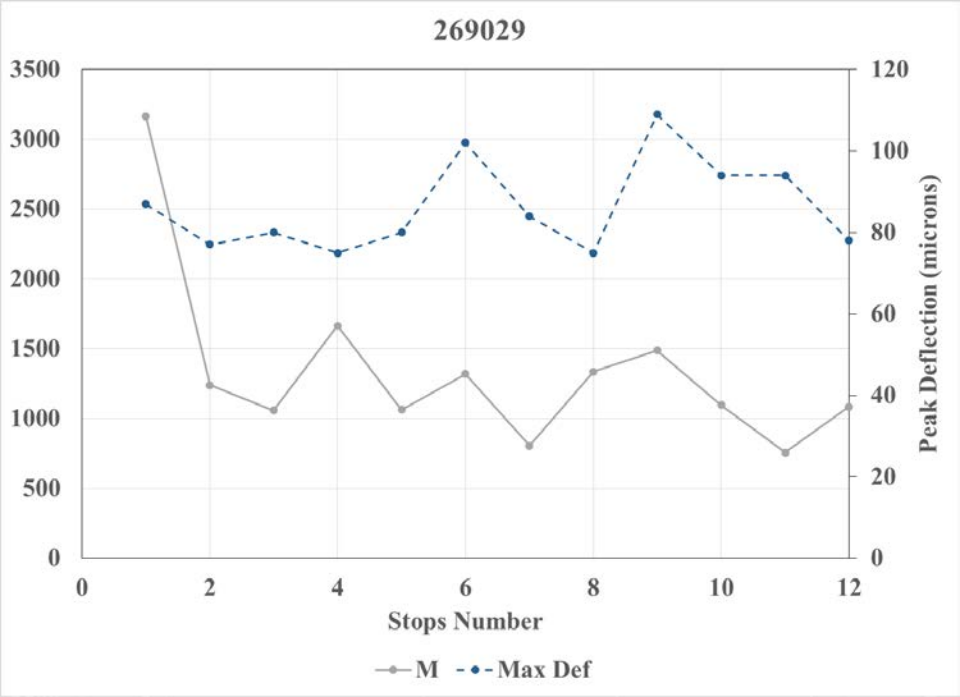

FIGURE B-30 Backcalculated m-Values and Peak Deflections for Different Stops

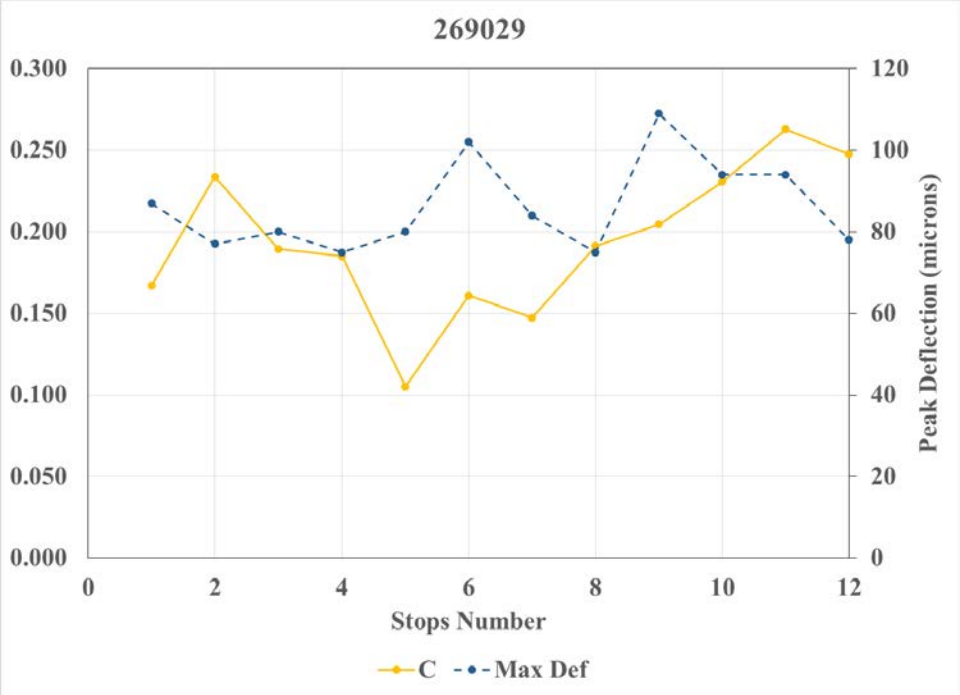

FIGURE B-31 Backcalculated c-Values and Peak Deflections for Different Stops

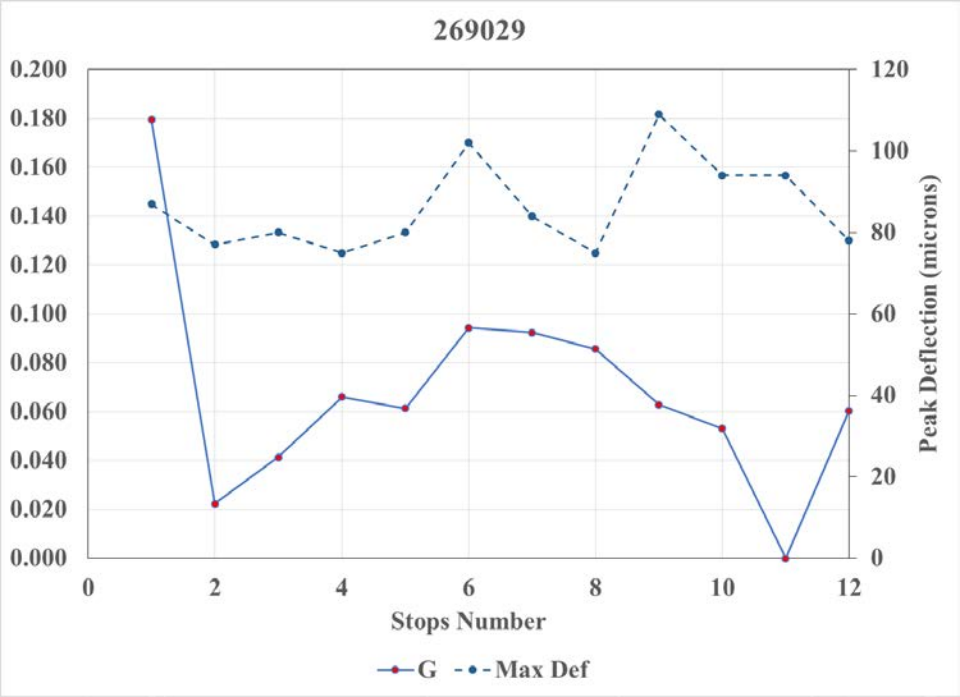

FIGURE B-32 Backcalculated G-Values and Peak Deflections for Different Stops

Preliminary Conclusions

Based on the preliminary study, the following conclusions can be drawn:

- The generalized Pasternak model is capable of capturing the behavior of UCOCP constructed with JPCP and JRCP.
- The existing PCC contributes to the overlay slab rigidity and increases the elastic modulus of the plate in the plate-on-a-foundation model. However, the exact amount of contribution of the existing PCC to the structural capacity of the plate and subgrade is not identifiable yet.
- Performing the dynamic backcalculation at different load level on the same location resulted in very similar structural parameters. This shows that sections under study are not constructed with stress dependent materials (at least for the typical stress ranges applied by FWD).
- Self-evidently, the structural integrity of a road pavement changes at different locations. This was supported by the observed change in maximum deflections under very similar applied FWD loads. It was tried to find a trend based on the changes in maximum deflections and the backcalculated pavement parameters. In spite of existence of connections between the deflections and the pavement parameters for each individual road section, these connections were not consistent for other pavement sections constructed with different materials and exposed to different climatic conditions. Therefore, no generalization could be made with the analyses performed so far.

References

1. Khazanovich, L., and A. Booshehrian. Dynamic visco-elastic analysis of falling weight deflectometer deflections for rigid and flexible pavements. *Accepted for publication in Transportation Research Record: Journal of the Transportation Research Board*, 2015.